Photon Migration in Highly Scattering Media as a Measurement Technique on Automated Cow Milking Systems

A thesis submitted in fulfilment of

the requirements for the degree of

Doctor of Philosophy

at the

University of Waikato

by

GEOFFREY KHOO

The University of Waikato

Te Whare Wānanga o Waikato

University of Waikato,

Hamilton, New Zealand

July, 2005

Abstract

An investigation has been performed on the scattering properties of cow's milk. The main aim of the study has been to determine the usefulness of photon migration techniques in the measurement of milk components, and the extent to which they can be applied. Online applications are also investigated.

The milk components that influence the optical scattering properties the most are the fat content and the protein content. Fat in milk exists in the form of small globules in a range of diameters from under 1 μm to as large as 20 μm. These globules are the major contributor to the light scattering properties of the milk. Milk protein is also a contributor to the scattering, but to a much lesser extent.

Another component of milk that is of interest is the somatic cell concentration. These cells are usually present in milk at a low level, ranging from about 5×10^4 cells mL^{-1} up to 2×10^5 cells mL^{-1}. Their numbers in milk dramatically increase with the onset of a mastitis infection. The *somatic cell count* is one of the primary measurements used in the dairy industry to monitor udder health and mastitis.

Since milk is a highly scattering medium, one needs to choose a suitable mathematical model to characterise it so that quantitative measurements can be made. The diffusion approximation, a simplified version of transport theory, was selected. The derivation and the limitations of the diffusion approximation were discussed and noted in order to ensure that any subsequent measurements made with milk fell within the limits of the theory.

A photon migration instrument (PMI) was built using the principles from the diffusion approximation theory. The instrument was configured to work with multiple-distance measurements. It was tested with a suspension of uniform microspheres and was shown to return results that agreed with Mie theory.

Experiments were performed using the photon migration instrument with homogenised and raw milk. A good correlation was found between the fat content and the reduced-scattering coefficient. Homogenised milk samples of varying fat content were made by mixing trim milk with homogenised cream while raw milk of varying fat content was obtained from a robotic milking system. Both milks were tested with

the photon migration instrument – the homogenised milk was tested off-line, while the raw milk was tested with the instrument beside the robotic milking system.

It was found that the instrument could determine the fat content in homogenised and raw milk with a precision of ±1.0 % and ±2.0 % milk fat content respectively. Protein and somatic cell count had a poor correlation with either the absorption coefficient or the reduced-scattering coefficient at a 670 nm wavelength.

The precision of the raw milk fat content measurements can be increased by separating the milk samples by breed. Grouping milk samples from Friesian cows separately from milk samples from Jersey cows yielded precisions of ±1.6 % and ±1.4 % respectively. Further increases in precision could be obtained by separating out the results per cow, resulting in fat percentage measurements with a precision as high as ±0.8 %. One of the more significant conclusions is that the fat globule particle size distribution is similar within the breed of cow and certainly similar from day-to-day with a single cow.

Fluorescence photon diffusion techniques using the DNA stain ethidium bromide were used to determine somatic cell count. The results of this work showed that high cell-count samples could be quantified, with a lower detection limit of 4×10^5 cells mL^{-1}. The lower detection limit was too high, and during attempts to reduce it, evidence for an ethidium bromide inhibitor was found. This inhibitor appeared to use up free ethidium bromide without changing its fluorescence lifetime. This was shown by experiments where the milk was diluted with IntraLipid to remove the contribution that differences in the absorption and reduced-scattering coefficient would make. The discovery of the ethidium bromide inhibitor was another significant conclusion of this work, but further investigation of the inhibitor was beyond the scope of this dissertation..

The primary conclusion of this thesis is that photon migration techniques can measure some milk components online directly, notably fat content and somatic cell count. Improvements to the instrument are required however, in order to improve the precision of the measurements to the level required by the dairy industry.

Acknowledgements

I would like to express my thanks to several different folks that have helped me throughout the years that I have been involved with this thesis. They are:

The Lord Jesus Christ, for providing me with a stable and solid foundation in life where I could stand up throughout all the trials, tribulations, and successes of this thesis. Without Him, I don't think I could have start this, let alone finish it.

My colleagues at Sensortec Ltd., Hamilton New Zealand. I somehow managed to end up with Sensortec in 2001 when the company was created. Over that time (and throughout the company's expansion), I have met and thoroughly enjoyed the company of all the people there, especially the card games. Thanks to Javier, Paul, Thomas, Pete, Johann, Beth and Rob for a great and productive time.

David Whyte, of Sensortec. Without his help and knowledge of the all things dairy, as well as his mature attitudes, this thesis just would not be the same.

Dr. Rod Claycomb, CEO of Sensortec. A wonderful source of great encouragement throughout the years, in the good and the bad.

Dr. Rainer Künnemeyer, my University supervisor. Also a great source of encouragement and support over the years. The no-nonsense pragmatic attitude towards my work and the great ideas from him helped to define and, work towards my final goals.

Finally, thanks go to Tash, my wonderful wife, who has faithfully and diligently put up with my numerous late nights while I worked on this. I don't know how she put up with it, but I am very grateful for her support.

Table of Contents

List of Tables

List of Figures

1 Introduction

Milk is a major income earner for the Waikato and New Zealand (Work and Income New Zealand, 2000). Because of that, there is a constant search to improve the quality of milk products and to produce them more efficiently and economically.

A large amount of past and present research has been focused on the search for new sensor techniques. However, most of these sensor techniques are focused towards implementations that cannot be used in a live milking situation – that is, in line with the milk flow on a milking machine. The ability to put a sensor in line with the milk flow has become more important now, especially with the introduction of automated milking systems.

Optical techniques are well established in the fields of process and quality control. In particular, near infrared (NIR) spectroscopy is heavily used in the food industry, especially for the production of milk products. The main advantages of optical techniques are they are non-destructive to the sample, and fast. Optical sensors can be easily incorporated into most production systems and can be made to be very robust.

The major problem with milk with regard to optical sensing is the large amount of light scattering, which is the root of most of the problems with the application of standard optical techniques to milk measurement. In addition to the optical scattering, the typical dairy parlour is a wet and electrically noisy environment, which presents additional difficulties with the design of an on-farm, on-line instrument.

Light scattering and fluorescence techniques (as well as spectroscopy) have been used as methods for providing feedback in process control situations that involve highly scattering materials. It is only fairly recently that frequency-domain photon migration and fluorescence methods have been proposed and used to characterise these materials. The main application for frequency-domain photon migration and fluorescence methods to date has been in biomedical applications such as the blood oxygenation monitor. These methods have already been used with milk, but not in an online situation. However, there is a strong possibility that these methods can be adapted to work online and therefore might be useful in that situation. This is based on the hypothesis that photon migration methods will work equally well on a moving milk sample as they do on a static one, since the behaviour of the light scattering will be very similar in both situations.

The advantages mentioned previously for online optical sensors apply to the dairy parlour as well. It is very useful for the farm owner or manager to have quick access to milk component analysis results without having to spend time obtaining milk samples from the main milk lines. Additionally, the concern that an added reagent may make its way back into the milk line is removed. The results of these advantages come in the form of reduced labour and consulting costs due to the lesser amount of manual work required, and also in the form of useful data for which animal management decisions can be made.

With those points in mind, it was the aim of this thesis to investigate:

1. the extent with which photon migration measurement techniques can yield useful information about milk composition,
2. whether photon migration measurement methods can be applied to an online situation (as in a dairy parlour).

The outcome of these objectives has depended on the successful design and implementation of an instrument that can measure the optical properties of cow's milk and return values that can be related to milk component concentrations. Achievement of the first goal has allowed the determination of which milk components are realistically measurable with photon migration methods. Achievement of the second goal is the successful implementation of an online photon migration sensor that can measure to a known accuracy, the milk components from the first goal.

Table 1-1 shows a few parameters of interest that are used to describe the optical characteristics of highly scattering media.

Parameter	Symbol	Description
Absorption coefficient	μ_a (cm^{-1})	Inverse of the mean free path before an absorption event
Scattering coefficient	μ_s (cm^{-1})	Inverse of the mean free path before a scattering event
Scattering anisotropy	g	Average cosine of the scattering angle
Refractive index	n	Ratio of speed of light in vacuum to the speed of light in the medium.

Table 1-1: Parameters of interest in highly scattering media.

These parameters are related to the physical characteristics of the medium. They indirectly describe the chemical and structural properties of the medium. Having knowledge of these parameters as well as the details of the structural properties can allow the discovery of other information about the medium such as its composition.

Note that the units of the absorption and scattering coefficients are reciprocal centimetres. These coefficients represent the average distance a photon travels in the medium before either a scattering or absorption event occurs. These coefficients give an indication of the opacity and the perceived colour of the medium.

Since it is important to understand the medium that will be analysed in this thesis, next section constructs the case for the use of photon migration methods for milk component analysis with a review of the properties of cow's milk. This is followed by an investigation into one of the major problems facing the dairy industry – mastitis.

2 The Dairy Cow and the Nature of Milk

2.1 The Dairy Cow

The dairy cow (*Bos Taurus*) is a large ruminant mammal of the family *Bovidae*. It has been domesticated in many countries around the world where it is used as a milk producer and also as a source of meat. Cows are herbivorous, eating grasses and other low-lying vegetation. In many countries, cows are kept in barns and other similar enclosures while being fed pre-prepared grain mixes and other supplements. The alternative is pastoral-based farming, which is predominant in New Zealand.

In New Zealand, the agricultural industry has a large focus on dairying. On a traditional New Zealand dairy farm, the cows are milked twice a day using manned mechanical milking systems. Cows on such a dairy are fed mostly on pasture with few additional feed supplements.

Figure 2-1: Jersey Cows

The most commonly encountered breeds of dairy cow in New Zealand are the Jersey and the Holstein-Friesian. The Jersey (shown in Figure 2-1) is a smaller cow usually with a light tan colouring. As a breed, it originates from the Channel Islands off the coast of Great Britain. Jersey cows are renowned for the relatively high milk fat

percentages, which was recognised as a large bonus in the cheese and butter industry. Holstein-Friesian cows (commonly called by the last part of their name "Friesian", shown in Figure 2-2) are a cross between the Holstein breed from continental Europe and the Friesian breed from Great Britain. These cows are slightly larger than the Jersey and have a mixture of black and white markings. The Holstein-Friesian was bred for its milk capacity – it delivers more milk volume than a Jersey but its milk fat percentages are lower, the average being 3.7% versus 4.6% for the Jersey.

Figure 2-2: Holstein-Friesian cows.

2.2 Milk

The term "milk" is a generic term used to describe the fluid produced by female mammals for the nutrition of their offspring. They contain, with some exceptions, the nutrients required for the development of the juvenile mammal. Generally, if the development time is short then the milk is dense in nutrients. All milks contain specific components and are designed to be digested easily by the juvenile mammal. In general, milks are opaque and white in colour. They consist mainly of water, with the other components (usually fats, proteins, enzymes, vitamins and sugars) either in

solution or in the form of either emulsified globules coated with a membrane or as a colloidal dispersion of micelles (Jensen, 1995).

2.3 Cows' Milk

Cows' milk is typical of mammalian milk. It is a white liquid that is produced in the mammary gland which is located in the udder. The udder is a relatively large external feature of the cow, situated towards the rear, in between the hind legs. It has four teats, each of which has a milk reservoir (referred to as the teat cistern) that is completely isolated from the others. Above the teat cistern, separated by a teat sphincter is the udder cistern. The structure of the udder is not unlike that of the human lung in that there is a tree-like structure leading from the cistern and terminating in small *alveoli*. It is in these alveoli that the milk-producing cells produce the milk.

Cow's milk is approximately 85% water. The remaining 15% contain fat, protein, lactose, vitamins, minerals, enzymes, hormones, cells and immunoglobulins. These components are either suspended as an emulsion or dissolved in the milk itself. The exact composition of the milk varies depending on cow and breed, as well as environmental factors such as stage of lactation and feed quality or quantity. Table 2-1 shows average percentages of the various cow-milk components. All components are given as a percentage by weight in the milk. The minor components are also known as ash and make up about 0.7% of the milk by weight.

Major Components of Milk	**Quantity**
Fat	3.7%
Protein	3.4%
Casein	2.8%
Lactose	4.6%
Minor Components (Ash)	0.7%

Table 2-1: Total milk components (Jensen, 1995).

The various solid components in milk exist in one of three different basic states – dissolved in solution, as a colloidal suspension, or as an emulsion. The milk carbohydrates and much of the minor components are in solution; the casein and whey

proteins exist as a colloidal suspension. Milk fat exists as an emulsion, with fat globules in suspension.

2.3.1 Milk Components

Milk Fat

Fat in milk is largely composed of triglycerides. Much of the milk lipids are derived from lipids circulating in the cow's blood. The remainder of the milk lipid is directly synthesized inside the lactating mammary cell. A breakdown of the different types of milk lipids is shown in Table 2-2.

Lipid class	Percentage of total lipid by weight
Phospholipid	0.20-1.00
Cholesterol	0.419
Triacylglycerol	97-98
1,2-Diacylglycerol	0.28-0.59
Free fatty acids	0.10-0.44
Monoacylglycerol	0.16-0.38

Table 2-2: Lipids in milk (Jensen & Newberg, 1995).

The milk fat globules are spherical lipid particles coated with a plasma membrane (Patton, 1973). They originate as fat droplets inside the lactating mammary cells, formed in the rough endoplasmic reticulum. The new droplet is gradually added to by the cell and is eventually secreted. At the point of its secretion, the droplet is enveloped by a plasma membrane. The progressive envelopment effectively separates the droplet from the cell. Secretion is complete when the membrane is pinched off, and the droplet is released. The mechanism for the origin of the fat globule is not precisely known (Keenan & Patton, 1995).

The size distribution of milk fat globules falls into three overlapping size distributions: small globules below 1 μm, medium-sized globules from 3-5 μm, and large globules at around 8-10 μm. Some of the large globules approach 20 μm in diameter. However, these large globules are formed by post-secretion aggregation. Thus, the typical milk fat globule falls in the two smaller-diameter groups (Keenan & Patton, 1995).

A surprising number of globules (70 to 90%) fall in the below 1 μm category. However, they only account for less than 5% of the total milk fat. The large-diameter globules account for a further 0.01% of the total globule population while representing 1 to 4% of the total milk fat. That leaves the remainder of the particles in the middle size distribution to make up the remaining 90% or so of the total milk fat while only containing roughly 10-30% of the total globule number.

The Milk Lipid Globule Membrane (MLGM)

Milk fat globules are surrounded by a two-layer plasma membrane. The plasma membrane is composed primarily of proteins, with a small amount of lipids and other compounds. Of particular note are the phospholipids, which aid with the structural integrity of the MLGM.

Some MLGMs have a crescent-shaped bulge attached to them on the side of the fat globule. These are actually a part of the secreting cell, and are thus filled with cytoplasm. They are formed when the closure of the plasma membrane around the pre-secreted fat globule occurs through the cytoplasm instead of around the globule surface. Cytoplasmic crescents add their own distinctive contribution to the composition and properties of milk (Keenan & Patton, 1995).

The MLGM is important in keeping the majority of the lipid content in emulsion. Without the membrane, the lipids would float to the top much like oil in water.

Proteins

Milk proteins are divided up into two main groups – caseins and whey proteins. The caseins make up the majority (82%) of the milk proteins, with the whey proteins making up the remainder. Caseins exist in milk in the form of protein and salt complexes called micelles ranging in size from 30 to 600 nm in diameter.

According to Slattery (1976), there are four different types of caseins that make up the micelles. They are known as alpha-s (α_s), beta (β), gamma (γ) and kappa (κ) caseins. They are all present in milk as the calcium salt (calcium caseinate). All the caseins are classed as glycophosphoproteins due to the presence of carbohydrates and phosphorus in their structures. The formation of the casein micelles is complex involving binding mechanisms that rely on the properties of the four protein fractions.

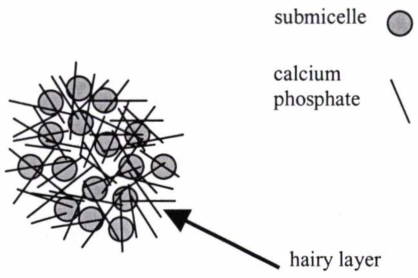

Figure 2-3: Casein micelle structure.

The structure of the casein micelle has been described as that of a "hairy" sphere. Each micelle is made up of many submicelles, which are held together by colloidal calcium phosphate. The submicelles are made of the individual casein protein molecules and can be considered to be truly spherical. The micelle carries a strong negative charge, making them self-repelling in milk.

α_s-casein is the dominant of the fractions in milk. The structure of the α_s-casein molecule is that of a random coil with short isolated helical regions. β-casein is thought to be found in the form of long rod-like strands that can be attached to α_s-casein. κ-casein is a glycoprotein that is vital to the stability of the casein micelle system. Casein micelles require the presence of the calcium ion to form, but in overly high calcium ion concentrations, the casein will precipitate out. The κ-casein is responsible for stopping the other fractions from precipitating when the calcium ion concentration is too high.

Whey proteins make up the remaining 18% of the total milk proteins. The major whey proteins are β-lactoglobulin and α-lactalbumin. These proteins exist in milk in a colloidal form, and form about 88% of the total whey proteins. The remaining minor whey proteins include serum albumin (identical to blood serum albumin) and the immunoglobulins IgM, IgA, IgG1 and IgG2. The immunoglobulins are also significant components of the MLGM, and contribute to the natural bacterial inhibitory properties of milk. Swaisgood (1995) compiled a table containing a complete breakdown of milk proteins.

Other Components

The remaining components in cow's milk are mainly carbohydrates and enzymes. Of the carbohydrates, more than 99% is in the form of lactose (Osborne, 1994). The remaining carbohydrates are found only in trace amounts, and consist of:

- Cerebrosides
- Sugars (glucose, galactose and sucrose)
- Amino sugars
- Oligosaccharides

Lactose comes in two forms that are enantiomers of each other. Their physical properties are slightly different to each other. In solution, α and β lactose undergo mutarotation (where the α and β forms are able to change from one to the other), with the process reaching equilibrium in 24 hours. At that stage, the lactose solution will consist of about 62.25 % β-lactose and 37.75 % α-lactose. It is expected that this will also happen in milk.

Other notable components of milk are enzymes, trace minerals, somatic cells and bacteria. The enzymes are of particular interest as they alter the properties of the milk by changing its chemistry. Milk enzymes fall into four main classifications:

1. *Proteases* (protein splitting) – responsible for the slow decomposition of proteins in milk.
2. *Carbohydrases* (carbohydrate splitting) – includes lactase (breaks down lactose) and amylase (breaks down starch).
3. *Esterases* (split esters) – the most notable of this group is lipase, which splits fat.
4. *Oxidases and Reductases* – enzymes that catalyse oxidation and reduction reactions respectively, such as peroxidase, which aids the splitting of hydrogen peroxide into water and active oxygen.

Minerals and salts tend to exist in small quantities in milk. Most notably present is calcium and phosphorus, which play an important role in the structure of casein micelles, along with citric acid and magnesium.

2.3.2 Physical Properties of Cows' Milk

At a glance, cows' milk appears to be a thin, and rather unremarkable off-white liquid. As described previously however, that is far from the truth. Cows' milk is a highly complex biological fluid with many interacting components. The bulk physical properties of the milk will be dictated by the nature of the individual components themselves, along with any possible interactions that may occur between those components. Table 2-3 shows some of the measured physical properties of cows' milk.

Physical Property	**Value**
Viscosity (centipoise)	1.6314
Surface Tension (dynes/cm^2)	52.8
Specific Gravity	1.030
Electrical Conductivity (Siemens)	0.00465
pH	6.62
Refractive Index	1.34[a]
[a] Measured with surface plasmon resonance instrument. All other values from (Neville & Jensen, 1995).	

Table 2-3: Physical and Chemical properties of milk.

Optical Properties of Milk

The off-white colour of cows' milk is primarily due to the light scattering from the fat globules. There are on average, about 3×10^9 fat globules and about 7×10^{15} casein micelles per millilitre of milk. The high numbers of fat globules and casein micelles indicates that milk has a high attenuation coefficient, and the nearly white colour of milk indicates that it does not have a particularly high absorption of light at any visible wavelength. Due to the highly scattering properties of milk, it is not easy to obtain an accurate spectrometer reading in large volumes of cows' milk. A set of raw spectrometer readings with different depths of milk, and therefore different optical path lengths (sample thicknesses) is shown in Figure 2-4 and 2-5.

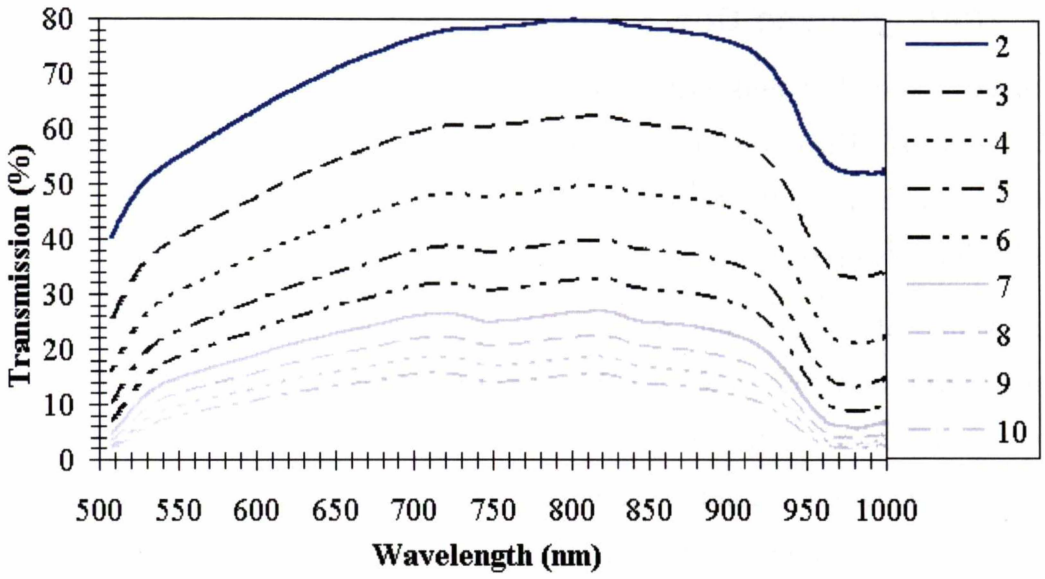

Figure 2-4: Raw milk visible / NIR spectra with path lengths of 2-10mm (Whyte, 1998).

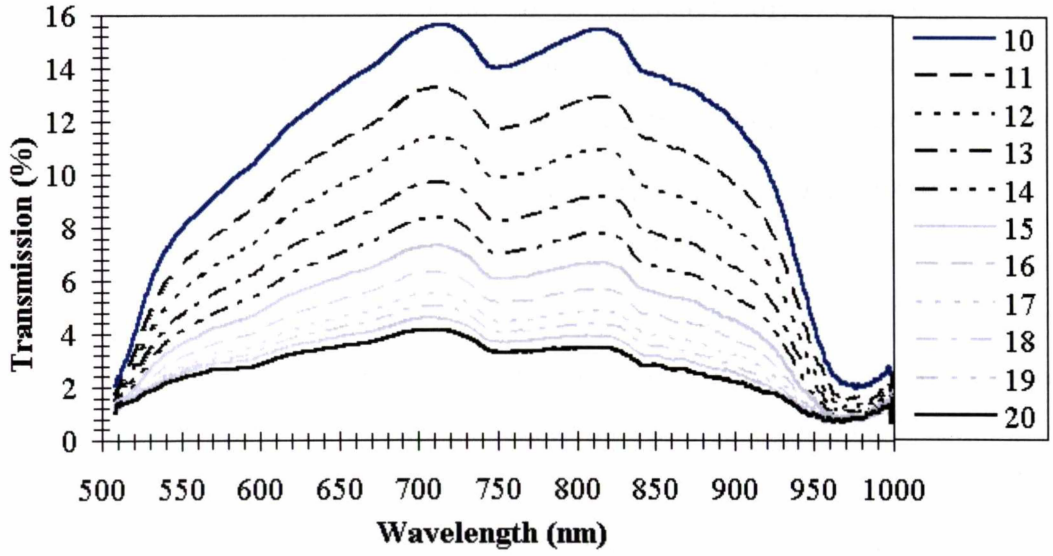

Figure 2-5: Raw milk visible/NIR spectra with path lengths of 10-20mm (Whyte, 1998).

Figure 2-4 and Figure 2-5 show a measurement of the transmission spectrum of milk with different thicknesses of milk between the light source and the detector. Both figures show that the transmission percentage and relative heights of the spectral peaks change as the optical path length through the sample changes. It can be concluded therefore that the use of visible / NIR spectra has limited application in bulk milk since with raw spectrometer readings, it is not possible to determine whether spectra are due to actual absorption or from extinction due to scattering.

2.4 Homogenised Cow's Milk

Homogenised milk is milk that has been processed so that the fat globules are very uniform in size. The development of homogenisation as a method of milk processing dates back to the early 1900s. The earliest and most complete and authoritative review was by Sidersky (1909).

Paul Marix of France was granted two patents in 1892 for the purpose of manufacturing margarine. Both of them were for different applications of the same invention. In order to make margarine, Marix made an emulsion by forcing the liquid mixture of margarine ingredients through a very small orifice. At this stage, nobody had thought of applying it to natural liquids, such as milk. This was patented by Gaulin in 1899, in a procedure designed to stabilise natural emulsions.

The official definition of homogenised milk, according to Trout (1950a), is "milk which has been rendered homogenous by mechanical means." A more practical definition is found in the Illinois State definition of homogenised milk, discussed by Tracy (1941) who defines it as milk which:

a) Shall not show any visible cream after 48 hours storage.
b) Shall not differ by more than 0.2% in fat tests from the top and the bottom of the bottle.

The most notable characteristics of homogenised cow's milk in comparison with raw cow's milk is its consistency and colour. Homogenised milk is whiter than raw milk, and it also appears much less watery. Analyses with a colour analyser have shown that homogenised milk has less colour than raw milk (Trout, 1950c). This colour change is a result of the increased number of fat globules in the milk due to the homogenisation process.

The modern homogeniser pumps milk at high pressures through a valve with a very small clearance. The purpose of this is to break up the fat globules in order to stabilise the emulsion. Several theories have been offered as to what actually happens to the fat globules during homogenisation. These processes are:

1. *Shearing or grinding.* Fat globules are pulled apart by high shear forces due to the high velocities encountered during homogenisation.

2. *Exploding.* The release of pressure when the milk exits the homogenisation orifice causes the fat globule to come apart due to its own high internal pressure.

3. *Splashing, impinging or shattering.* When milk reaches a certain pressure during homogenisation, a valve in the homogeniser opens and allows the pressurised milk to strike a retaining wall with high velocity.

4. *Acceleration and deceleration.* The great acceleration that milk must go through during homogenisation causes the globules to come apart.

5. *Cavitation.* The formation of vapour bubbles in a liquid due to the lowering of pressure.

The most important part about the homogenisation of milk is that the larger fat globules of raw milk are broken up into many small ones. Table 2-4 shows a comparison between raw cow's milk and homogenised milk fat globule populations (a pictorial comparison is shown in Figures 2-6 and 2-7).

Parameter	Raw Milk	Homogenised Milk
Average fat globule diameter	2.9 μm	0.3 μm
Number of fat globules per 100 mL of milk	2.9×10^{11}	3.4×10^{14}

Table 2-4: Milk Fat Globule parameters before and after homogenisation (Trout, 1950b).

2.4.1 Changes in physical and chemical properties of milk due to homogenisation

Very little change is generally found in the physical properties of milk when it is homogenised. The most notable change is the colour and the loss of the apparent watery appearance of raw milk as described previously. Other minor changes are a slight decrease in conductivity and a slight decrease in pH.

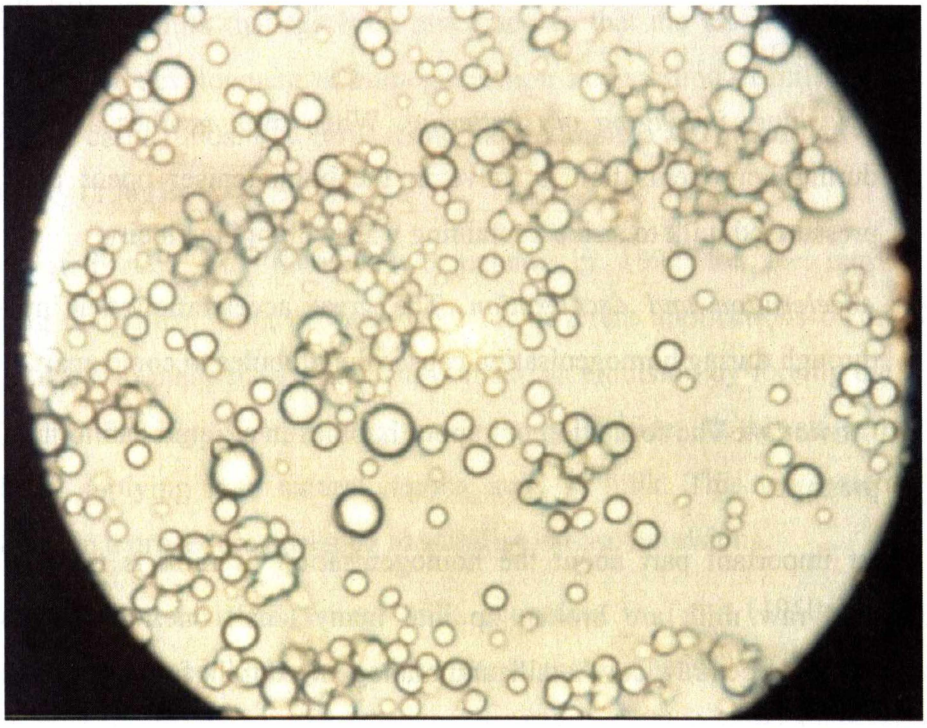

Figure 2-6: Raw milk viewed under a microscope (400x magnification).

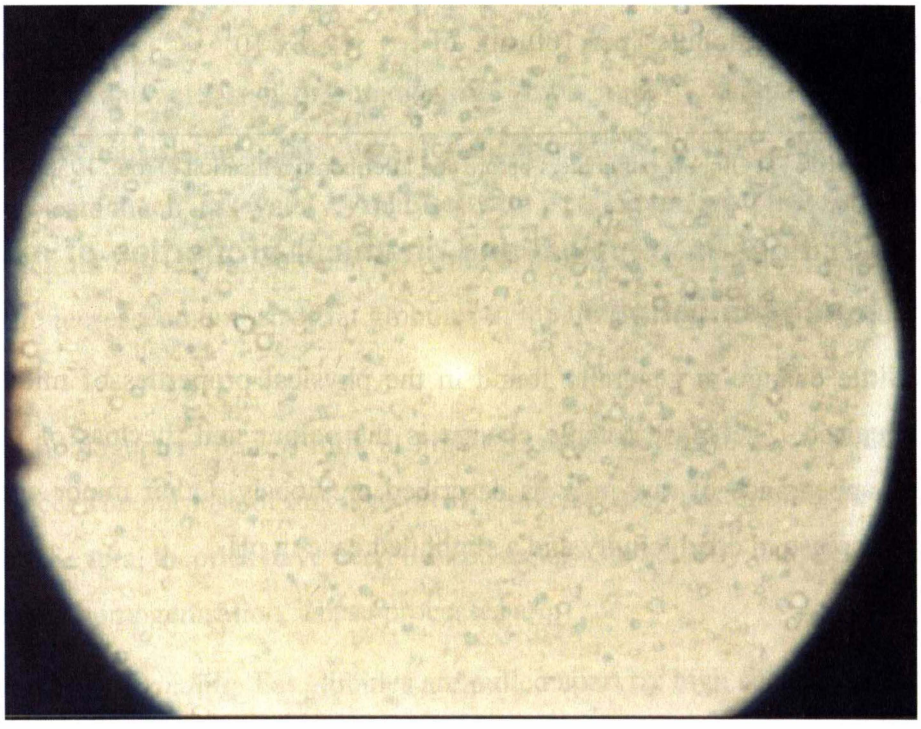

Figure 2-7: Homogenised milk viewed under a microscope (400x magnification).

2.4.2 Changes in fats and proteins of milk due to homogenisation

The main changes in milk due to homogenisation appear to affect the milk fat. The homogenisation process is designed to break up the large fat globules so that there are more of them, but of a smaller average diameter and a smaller size distribution. This is not the only change, however. Creaming in milk occurs when fat globules aggregate and consequently float to the surface. A lack of creaming cannot be attributed to the changes in the size distribution of milk alone.

The lack of the clustering of fat globules in homogenised milk has been linked to three main factors. Firstly, there is the destruction of the natural agglutinin (a protein in milk that causes fat globules to clump) by the homogenisation process. Secondly, there is the resurfacing of the fat globules. This happens primarily from the destruction of the MLGM, which causes the homogenised fat globules form a new membrane by adsorbing suitable milk proteins, usually whey proteins but caseins can also participate in this process. Thirdly, due to the greatly increased percentage of small fat globules, there is much more bulk Brownian movement. All three of these factors appear to be interrelated, as no single one seems to wholly account for the marked lack of interglobule attraction in homogenised milk. However, it has been noted that homogenised milk with a fat percentage greater than the usual 3.3 % still tends to have some degree of fat globule clustering evident.

It has been found that the homogenisation process affects the proteins in milk. For instance, it is known that some of the casein micelles in milk do adsorb onto the fat globules. In raw milk, Wiegner (1914) calculated that the percentage adsorbed is about 2 %. For homogenised milk, that figure rises to 25% (Trout, 1950b). The other proteins in milk are affected differently, in that the homogenisation process appears to destabilise them. Consumer complaints have been recorded regarding the curdling of homogenised milk during cooking, indicating that some adverse effect has occurred.

For the most part, the homogenisation process has changed milk from a highly unpredictable substance to one that is much more stable. This has important consequences regarding its optical properties, which will be discussed in a later chapter.

2.5 Milk Component Measurement

2.5.1 Why measure milk components?

There are many reasons why we should want to measure the different components of cows' milk. The reasons are primarily economic and can be split into two areas – farmer remuneration and food processing costs.

Cow's milk is a product that is widely used in the food industry. The food industry requires a high level of quality control on its products to ensure that they are suitable for human consumption. The fat and protein content of milk affect the yields of products such as cheese and butter, while high somatic cell count will adversely affect the quality (smell, test or texture) of those products.

High somatic cell counts is symptomatic of another problem – how mastitis affects cows. During lactation (milking season) if a cow contracts mastitis, her milk production will decrease. If mastitis is contracted in the first ten weeks of lactation, the average drop in production is 11%; otherwise it is about 6% (Taponen & Myllys, 1995). As a cow can produce up to 9,000 litres of milk or more per lactation, the amount of milk lost can be quite considerable. The lost milk volume manifests as money lost to the farmer. A more in-depth assessment of losses incurred by mastitis infections will be given later.

Thus, there are good reasons for measuring milk component levels, as a dairy farmer or a milk processor. The information in knowing the milk composition is important for making the correct decisions to optimise processes as a milk processor, or for the best possible management of the herd as a dairy farmer. The next section examines the milk components and measurement methods that have been developed previously.

2.5.2 What components of milk can we measure?

The components of milk that are most important to the dairy industry are fat, protein, lactose (and other carbohydrates) and somatic cell count. The other lesser components such as enzymes and low-concentration proteins are important in specific cases, but will not be considered in this investigation.

Fat

As milk fat is the predominant non-water component, it is the easiest to measure. Fat in raw milk is in the form of an emulsion, with globules from 0.5 to 10 μm diameter suspended in the water. The large number of globules in milk has given rise to three distinct types of fat measurement – particle counting and sizing, spectroscopic measurements and laboratory wet tests.

The standard laboratory method for quantitative fat measurement in milk products as defined in the *List of IDF Standards* (International Dairy Federation, 2003) is the Röse-Gottlieb method (although a faster version of it, the Mojonnier method is often used). This is a chemical method that works by dissolving the fat in the milk, separating out the dissolved fat and evaporating the solvent, then weighing the remaining fat (Kim *et al.*, 1984; Matheson & Otten, 1999).

In 1890, Babcock introduced the first convenient method for the estimation of fat in milk (Atherton & Newlander, 1977). It involved the addition of sulphuric acid and then centrifugation to separate out the fat. The fat percentage could then be easily read at a glance off a properly marked centrifuge tube. Haugaard & Pettinati (1959) developed a method for the use of turbidity of milk to measure fat percentage. Their research culminated in the development of a method to predict fat content by determining the globule size distribution from multi-wavelength scattering measurements using a spectrophotometer. Walstra (1965) also managed to predict fat content in milk using a scattering model.

The particle-counting methods for milk fat measurement usually used a Coulter counter to measure the globule size distribution. Obviously, the sum of the population of all globules of all sizes gives the fat content. Cornell & Pallansch (1966) used a Coulter counter to determine the fat globule size distribution change caused by homogenization. Kernohan & Lepherd (1968) used the Coulter counter to determine the average fat globule distribution over the period of a single milking, while Whittlestone (1962) did the same thing several times in one milking. Overall, fat globule size distribution measurement did not seem to be very useful as it did not easily provide a number that corresponded to the fat content of the milk.

The area of spectrophotometry for fat measurement seemed to be the most promising for speed and simplicity of results. In particular, near-infrared analyses yielded very

good correlations as far back as 1964 (Goulden, 1964). Within the next few years, it became the dominant method of milk fat content measurement. However, the Babcock method still is in use today and some argue that the near infra-red spectroscopic analyses under-read compared to the Babcock method (which usually means less pay for the farmer)(Ng-Kwai-Hang. & Moxley, 1987). However, optical scattering methods are once again being used for milk fat content measurement with the arrival of fibre-optic technology (Crofcheck *et al.*, 2000), and of the renewed interest in free fatty acid content as a monitor of rancidity (Fung *et al.*, 1998).

Protein

The milk proteins are relatively constant in percentage over a single milking and do not vary much from cow to cow compared to fat. As the dominant protein in milk is casein, most of the research has focused on that.

The usual laboratory method for the determination of protein is the Kjeldahl method for the estimation of total nitrogen (Jenness & Patton, 1959). This involves digesting the sample with sulphuric acid over a series of catalysts to convert the nitrogen to ammonia, then measuring the amount of the ammonia either directly (in the sample) by Nessler's reagent or by titration.

The importance of protein content is a rather recent development compared to fat. It is interesting to note, that most of the research into protein determination has been optical – that is, using either fluorescence methods or near infra-red spectrophotometric methods. Most research into the optical determination of protein content has been hampered by the fact that the caseins are in suspension in a micellular form, and the fat is also in suspension in a similar form. The major difficulty there has been separating out the effects of the two. However, since spectroscopic methods use the difference in absorption due to the different types of chemical bonds between atoms, they have been used successfully to determine the amount of protein in a sample.

Konev & Kozunin (1959) used a fluorescence technique to measure the amount of protein in a dilute milk sample. A path length of 1 mm was chosen to alleviate the effects of scattering due to fat. They found that the 340-350 nm wavelength fluorescence signals were strongly related to proteins when using an ultraviolet excitation source as milk proteins have an absorption peak at 280 nm.

Haugaard & Damm (1961) used absorption at 180-230 nm and also at 280 nm as a method of protein measurement. Fat compensation was achieved by taking another absorption measurement at a wavelength where proteins did not absorb. Prior to these optical methods of protein determination, nitrogen measurements were the main method of determining the protein content of milk.

Further research in this area focused on spectrophotometric methods. This work increased in intensity in the 1980s. As late as 1990 however, direct nitrogen methods for determining protein were still generally used for the determination of protein in milk (Kamishikiryo-Yamashita *et al.*, 1994). Direct nitrogen methods were not able to differentiate between casein and whey proteins so Sjaunja & Schaar (1984) used a spectrophotometric method and developed a model that allowed the determination of casein only using infra-red absorption measurements.

At present, spectrophotometric methods are the chief industry standard for the determination of proteins (and protein fractions) in milk. Tests on a milk-specific instrument (the Foss Milko-Scan 605) were conducted by Sjaunja & Andersson (1985) and it was shown to be acceptable for use as the measurement standard in the dairy industry.

Multiple Component Analyses

Both fat and protein can be measured simultaneously by a spectrophotometric method as well as by the direct chemistry methods described previously. Most of the milk-related research over the years has concentrated on the determination of the concentrations of fat, protein and lactose.

The predominant spectrophotometric methods used in multicomponent analyses are near infra-red absorption and infra-red absorption measurements. Goulden (1964) discovered that quantitative fat, protein and lactose measurements could be obtained using measurements at 5.73, 6.46 and 9.60 μm wavelengths. Goulden also studied the effects of temperature and pH on the absorption readings and concluded that they had little effect on the fat, protein and lactose results.

Since the proof of the basic technique, near infra-red and infra-red spectroscopy of milk have become increasingly common as the industry standard for measurement of fat, protein and lactose in milk (Grappin & Ribadeau-Dumas, 1992), mostly due to their convenience and ease of automation. Research on milk spectroscopy was limited at first, but since the development of reliable commercial instruments, the amount of work in this area has increased. More recent research has been focusing on the verification of the accuracy of the measurements (Sjaunja & Andersson, 1985) and also towards finding out whether the infra-red and near infra-red techniques can be used to measure any other quantities. Tsenkova *et al.* (1994) used near infra-red spectroscopy as a means of determining udder health and total milk composition. The near infra-red measurements made in this work were compared to the results from the Foss Milko-Scan (Figure 2-8) milk component analyser and the Fossomatic somatic cell counter. The results of these experiments showed that there was a visible correlation between near infra-red spectroscopic measurements and any of the commonly measured milk components, *including* somatic cells (Tsenkova *et al.*, 1994; Tsenkova *et al.*, 2000).

Figure 2-8: Foss Milko-Scan FT6000 Fourier Transform Infra-Red Spectrometer (Foss Electric AS, 2003a).

Somatic Cell Count

This quantity is strongly linked to the incidence of mastitis in a cow. Generally, techniques to measure somatic cell count depend on measuring quantities related to the cells as opposed to measuring the cells themselves. That is due to the fact that there are very few somatic cells in a milk sample, compared to the number of fat globules (which are of a similar size to somatic cells). A detailed review of somatic cell count will be presented in the next chapter.

3 The Somatic Cell Count

A serious problem in today's dairy industry is mastitis. While this is not directly related to the optical properties of milk, it is related to a particular milk component – the somatic cell count.

3.1 Mastitis

3.1.1 What is Mastitis?

Mastitis is the term used to describe the inflammation of mammary tissue. The particular type of mastitis that will be investigated here is mastitis of the bovine udder. Bovine mastitis is a condition that costs the dairy industries around the world billions of dollars every year. The cost of mastitis in the dairy industry in various countries for the year 1998 was studied by Clements (1998) and is shown in Table 5-1.

Country	Loss in millions of US$
US	1 800 – 2 000
Argentina	270.0
Germany	488.5
UK	131.0
Australia	130.0
New Zealand	200.0

Table 3-1: Losses caused by mastitis in selected countries (Clements, 1998)

Mastitis impacts the dairy industry at the farm level. Each case of mastitis on a farm requires treatment in order to either bring the affected cow back from lost productivity or prevent the rest of the herd from being affected. This involves many stages. Firstly, the milk from the affected cow must be discarded during the treatment period in order to avoid contamination. Secondly, the cause of the mastitis must be appropriately dealt with. This is usually bacterially related, so antibiotics are administered. It is at this stage that a decision must be made as to whether to nurse the cow back to a healthy and productive state, or to cull her. All these options cost money. As well as the direct costs due to discarded milk and also due to drugs and veterinary treatment, there are many indirect costs as well. These include:

- Decreased milk yield during the remainder of the lactation period due to udder damage and/or subclinical infection.
- Penalties for high bulk milk somatic cell count results.
- Extra labour for treatment and nursing
- Higher culling and replacement costs, leading to loss of genetic potential.
- Extra cow deaths.

The changes in milk components affect the quality of milk further along the processing chain as well. This obviously affects the profit margins for the processing and milk product manufacturing plants, which in turn further reduces the farmer's income.

Bovine mastitis is divided into two types – clinical and subclinical mastitis. The subclinical form of mastitis is far more prevalent than the clinical form and can be considered a precursor to clinical mastitis.

Subclinical Mastitis

This form of mastitis is not obviously visible on the cow nor in the milk. With a cursory visual inspection, one would not conclude that the cow had an infection – the udder looks normal and the cow is still producing milk. There are signs that can be detected which can indicate the presence of subclinical mastitis, which will be discussed shortly.

Clinical Mastitis

Clinical mastitis is immediately noticeable in comparison to subclinical mastitis. Often, the cow will be visibly uncomfortable and her teats and udder will have visible signs of inflammation. If left untreated, clinical mastitis is capable of destroying most or all of the cow's milk-producing ability, and in many cases, killing the cow. One of the goals of the dairy farmer is to have no cases of clinical mastitis on the farm. Therefore, it is much better to detect mastitis while it is at the subclinical stage.

3.1.2 Causes and Effects of Mastitis

The direct cause of mastitis is usually bacterial. The organisms that cause mastitis are classed into two categories, *contagious* and *environmental*. The categories are indicative of how the infection originates.

Contagious Mastitis Organisms	Environmental Mastitis Organisms
• *staphylococcus aureus* • *streptococcus uberis* • *streptococcus agalactiae* • *streptococcus dysgalactiae* • *corynebacterium bovis* • *mycoplasma* • coagulase negative *staphylococci*	• *Escherichia coli* • *Citrobacter* • *Enterobacter* • *Pseudomonas eruginosa* • *Bacillus cereus* • *Bacillus lichenformis* • *Pasteurella* • *Streptococcus faecalis* • fungi • yeasts

Table 3-2: Examples of mastitis-causing micro-organisms (Blowey & Edmondson, 1995).

These organisms usually enter the udder via the teat canal. They are transferred to the teat by the teats coming in contact with an object that has the organisms on its surface. This can be the ground, a part of the milking machine that comes in contact with the teats, or some other contaminant such as water or infected milk.

The interior of the bovine udder is an ideal incubation area for most of the organisms listed in Table 3-2 as it is warm and rich with nutrients. Upon their arrival in the udder, these organisms increase greatly in number, metabolising the nutrients present and producing damaging toxins. It is these toxins that damage the tissue inside the udder and cause the inflammation. However, before anything visible is noticed, there are changes in milk composition and yield that can be detected. These changes are indicative of a subclinical infection.

Changes in Milk Properties due to Subclinical Mastitis

During a bout of subclinical mastitis, the quality of milk from the cow drops measurably. Many of the useful components of milk decrease or change in character whereas other undesirable components increase. Table 3-3 summarises the changes in milk components during a subclinical mastitis infection.

	Components	*Effect of subclinical mastitis*
Desirable	Total proteins	Decreased slightly
	Casein	Decreased between 6 and 18%
	Lactose	Decreased between 5 and 20%
	Solids not fat (SNF)	Decreased by up to 8%
	Butter fat	Decreased between 4 and 12%
	Calcium	Decreased
	Phosphorous	Decreased
	Potassium	Decreased
	Stability and keeping quality	Decreased
	Taste	Deteriorates and becomes bitter
	Yoghurt starter cultures	Inhibited
Undesirable	Plasmin (degrades casein)	Increased
	Lipase (breaks down fat)	Increased
	Immunoglobulins	Increased
	Sodium	Increased – hence the 'bitter' taste

Table 3-3: Changes in milk components during subclinical mastitis (Blowey & Edmondson, 1995)

It is evident that many of the desirable components of milk are reduced in quantity while at the same time, some of the more undesirable components such as plasmin and lipase are increased. The decrease in casein affects cheese yield, and the increase in lipase and plasmin shorten the shelf life of the milk.

There are other components in milk that change as well, but they are only present in very small amounts compared to the others. These components are the somatic cell count, the serum protein levels (bovine serum albumin, antitrypsin) and certain enzyme concentrations (N-acetyl-β-D-glucosaminidase or NAGase).

With all these different component changes, one would suppose that the detection of subclinical mastitis would be rather straightforward. Many of the component changes in Table 3-3 are individually detectable, but the only widespread method for the non-laboratory detection of subclinical mastitis is the measurement of milk conductivity, and the indirect measurement of somatic cell count.

Measurement of milk components related to mastitis

The reason for the difficulty in the detection of subclinical mastitis is that most of the changes in milk composition are also within the scope of expected changes in the milk components from a cow, over any single milking season. Also, most of these component changes require laboratory tests and therefore are inconvenient for the timely detection of mastitis. Laboratory tests require the transport of a milk sample to a testing site and the results communicated back to the farmer.

The two changes in milk composition that are most frequently used in the detection of mastitis are milk conductivity and milk somatic cell count. It has been shown that milk conductivity, while being a convenient test for use while beside the cow, does not predict mastitis particularly well (Nielen *et al.*, 1991) unless it is kept as a running record, with readings taken for each quarter every milking so that the trends corresponding to mastitis (increased conductivity over the norm) are more easily viewable. Somatic cell count however, enjoys a much better correlation with incidences of mastitis. Currently somatic cell count is the gold standard method of mastitis detection, although technologies to measure other components are under development (Sensortec Ltd., 2003).

3.1.3 The Process and Detection of Mastitis – Somatic Cell Count

Somatic cells are cells from the body of the cow. The name comes from the Latin *soma*, meaning "of the body". These cells are released into the milk either because of damage to the cow's udder due to pathogenic activity, or by the cow's immune response to such pathogenic activity. However, there are always some somatic cells in milk. A healthy cow can have up to 2×10^5 cells mL^{-1} of milk whereas a clinically mastitic cow will have over 10^6 cells mL^{-1}. That number is dependent on many factors, such as the age of the cow, the time of year and of course, the presence of mastitis-causing pathogens. Table 3-4 shows a breakdown of the somatic cell population.

Percentage of cell types in milk and colostrum		
	Mid-lactation	**Colostrum**
Polymorphonuclear leukocytes	3	61
Vacuolated macrophages	65	8
Non-vacuolated macrophages	14	25
Lymphocytes	16	3
Epithelial cells	2	3

Table 3-4: Percentage of somatic cell types in healthy milk at different times during lactation (Blowey & Edmondson, 1995).

The bulk of the somatic cell count in mastitic milk is made up of *polymorphonuclear leukocytes* (PMNs), a major part of the immune response against mastitis. Their main purpose is the destruction of the invading organisms by their envelopment and

digestion by enzymes, a process known as *phagocytosis*. Figures 3-1 to 3-3 show how the somatic cell count increases over the onset of an infection.

Under normal circumstances (Figure 3-1), the epithelial lining of the interior of the udder is in good condition, and the PMNs tend to stay inside the blood vessels. A few of them enter into the milk through the gaps between the cells making up the capillaries and epithelium (PMNs are amorphous and are easily able to flatten themselves sufficiently to fit through the narrow gaps between the cells). At this stage, the PMNs still make up the bulk of the somatic cell count. The normal count in milk is referred to as the *baseline* somatic cell count.

When mastitis-causing organisms manage to invade the interior of the udder and have

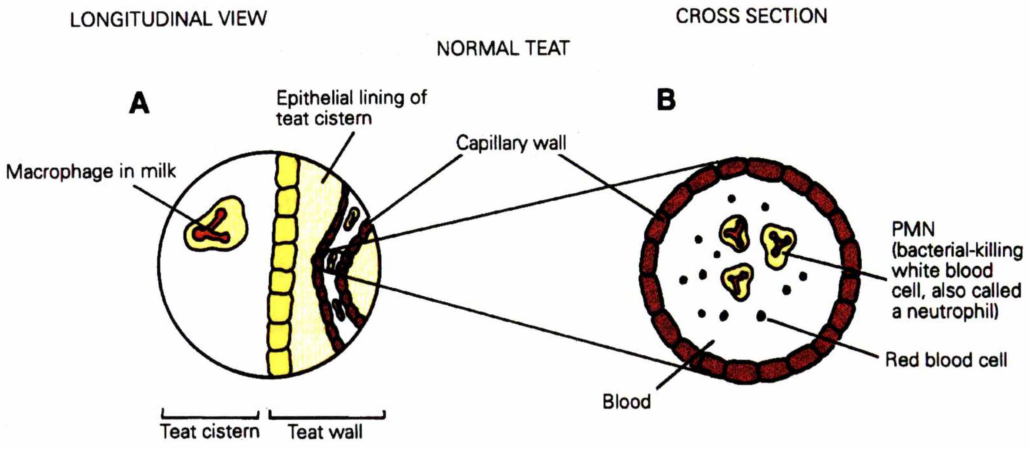

Figure 3-1: Normal circumstances in the bovine udder. (Blowey and Edmondson, 1995).

increased in number to such a level where the toxins they generate are starting to cause damage, PMNs and other white blood cells start to respond to the messages given off by the damaged cells. They start entering the udder cavities in great numbers as shown in Figure 3-2.

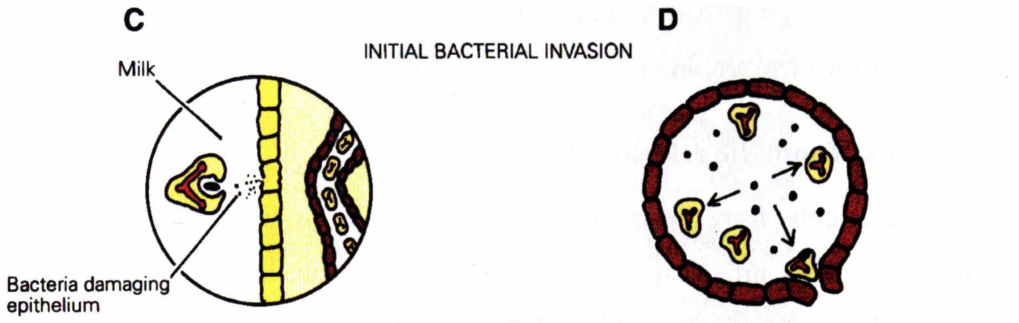

Figure 3-2: At the start of the mastitis infection in the bovine udder (Blowey and Edmondson, 1995).

At this stage, the cow is not yet at subclinical mastitis. The somatic cell count in the milk has only just begun to rise, and it may indeed be that the cow is able to fight off the infection. Should that occur, the somatic cell count would decline back to the baseline level. However, if this does not occur, the somatic cell count will continue to rise as more PMNs travel from the blood vessels to the udder cavities.

Figure 3-3 shows the scenario in the cow's udder once subclinical mastitis is under way. At this point, the somatic cell count is much higher than the baseline, and there may be changes in the quality of milk. If the infection is left unchecked clinical mastitis may develop.

It is clear that if the somatic cell count increase can be detected early enough to administer treatment to the cow (in the form of antibiotics), the adverse effects of

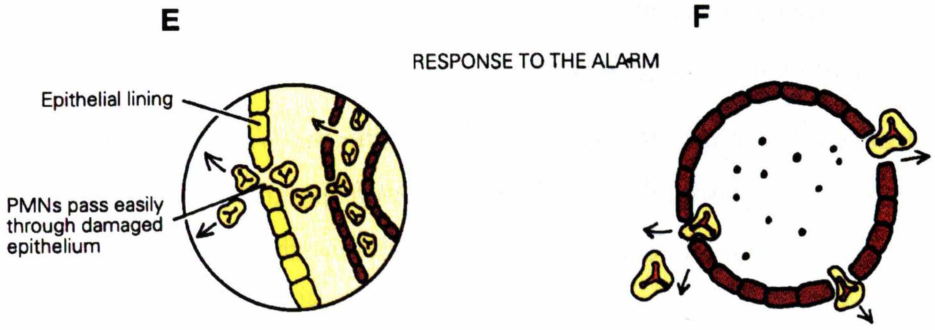

Figure 3-3: Later stages of the mastitis infection in the bovine udder (Blowey and Edmondson, 1995).

mastitis can be greatly minimised. The most valuable improvement is that the downtime of the cow would be reduced as a result of this.

Methods of somatic cell count measurement

Since somatic cells have been shown to be a reliable indicator of the presence of a subclinical mastitis infection, many different ways have been found to measure the somatic cell count (referred to as SCC from now on). Methods are available to measure SCC at the individual cow level, the individual udder quarter level and of course, at the bulk tank level. We will now introduce some of the most commonly used ways of measuring SCC on and off the farm.

Whiteside Test

The Whiteside test is a laboratory-based test in which somatic cells react with sodium hydroxide. The milk / sodium hydroxide mixture coagulates when the SCC is above 5×10^5 cells mL^{-1}. The mechanism behind this test involves lysing the cells and causing the fat globules to aggregate and form shreds and clumps (Schalm & Noorlander, 1957). The action of the sodium hydroxide also has the effect of creating a gel using the DNA from the lysed cells – an action which led to the California Mastitis Test.

California Mastitis Test

The California Mastitis Test (or CMT – also known as the Rapid Mastitis Test or RMT) is a simple test that can be performed beside the cow during milking. All four quarters can be tested relatively quickly and easily. The CMT is a crude estimation of SCC – it does not give a quantitative value for the actual count but more an indication as to whether the cell count is high or low.

This test was developed in the 1950s as a means to bring the Whiteside test to the cow at the farm (Schalm & Noorlander, 1957). Its mode of operation is dependent on the action of detergent on somatic cells. The detergent lyses the cells and depending on the number of cells in the milk, a gel is formed. The more cells there are in the milk, the thicker the gel is. It has been concluded that the gel is formed from at least a part of the DNA-protein complex that is present in the nuclei of somatic cells (Nageswarao & Derbyshire, 1969). DNA from other sources such as bacteria do not appreciably

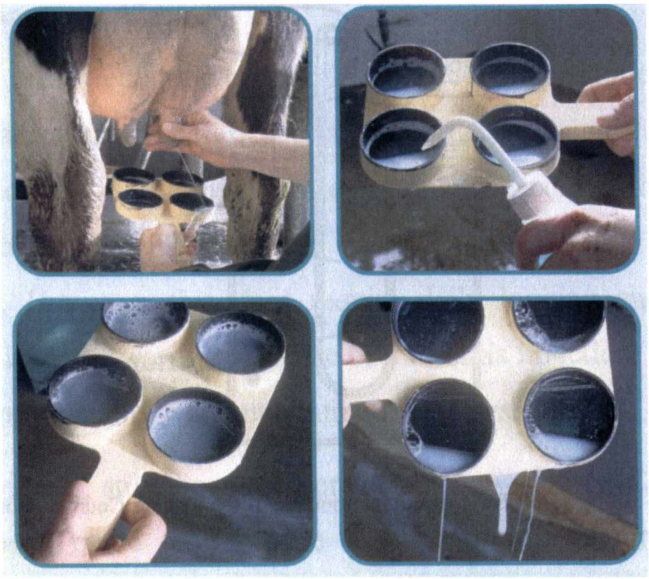

Figure 3-4: The four steps of the CMT (Livestock Improvement Corporation, 2001).

From top left heading clockwise:

1. Before milking, obtain about 2mL of milk from each quarter into each of the different trays. Discard first squirts from each quarter.
2. Add an equal volume of reagent (detergent).
3. Swirl the mixture vigorously.
4. Assess the gelling in each sample. Tilting the tray may make it more visible.

affect the gel formation as there is simply not enough of it, compared to the amount of DNA from somatic cells. Figure 3-4 shows the four steps in the CMT.

There is a quantitative version of this test known as the *Wisconsin Mastitis Test* or WMT. The WMT assigns a number to the viscosity of the gel depending on the time it takes to flow out of an orifice of known dimensions (Thompson & Postle, 1964).

Coulter Counters

The Coulter Counter is a general laboratory bench-top particle sizing and counting device that was the first accepted automated method for measuring SCC. Samples require treatment before measurement to remove the fat (which has a particle size distribution all of its own). The samples are usually centrifuged, with cells being resuspended before counting.

The basic principle of the Coulter Counter is shown in Figure 3-5. The sample is placed in the centre tube, with the outside beaker filled with an electrolyte. A measured amount of the sample is pumped through a small aperture of known size. The two electrodes, one in the sample and one in the electrolyte measure the

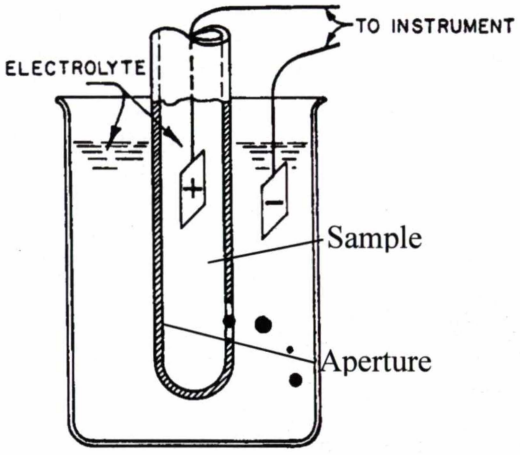

Figure 3-5: Operational principle of the Coulter Counter (Cornell & Pallansch, 1966)

resistance through the aperture. A particle moving through the aperture will change the resistance through the aperture while it is travelling through it. The number of changes in the sample's resistance is counted, giving the total number of particles of the aperture's size. It is possible to use many different aperture sizes concurrently to obtain a particle size distribution.

Foss Somatic Cell counter

Figure 3-6: The Fossomatic 5000 (Foss Electric AS, 2003b).

The Foss Somatic Cell Counter (Fossomatic 5000) has completely replaced the Coulter Counter as the instrument of choice worldwide for SCC measurement. Foss of Denmark makes these laboratory-based instruments, which are high volume fully automated flow cytometers. They operate by staining the somatic cells with ethidium bromide and then passing the stained cells through a very narrow passage containing a laser light source and then measuring the fluorescence from the ethidium bromide. The Fossomatic 5000 is capable of analysing up to 500 samples per hour with a repeatability as good as 4% (Foss Electric AS, 2003c). Most herd testing stations in countries around the world, including New Zealand use these machines or earlier versions of them. It is in these machines that bulk tank somatic cell count tests (BTSCC) are performed.

What can be improved?

Currently, SCC is measured at the bulk tank. Very few opportunities have been taken to measure SCC at any stage before the tank, apart from using the CMT. The ease with which conductivity can be implemented means that most of the mastitis sensing systems built into milking machines are based on the relative milk conductivity between quarters. However, this does require daily logging and viewing of the conductivity data to determine the presence of a mastitis infection. There are ways of automating this, most notably with automatic milking systems.

The CMT is obviously still the most convenient cow-side SCC test to this date. Attempts have been made to automate it for use as a commercial laboratory instrument (Whittlestone & Allen, 1966) but this was abandoned in favour of newer and faster technologies such as the Fossomatic flow cytometers. However, the Fossomatic is not a cow-side SCC measurement device, and there is some interest again in using the CMT as an automated cow-side test (Whyte *et al.*, 2002).

When SCC can be conveniently and reliably measured on-line at the farm with a device that could be attached to a milking system, the detection of subclinical mastitis would be much faster. This could reduce costs for the farmer and for the milking industry as a whole.

Having now reviewed the properties of milk and one of the major problems affecting the dairy industry (mastitis), the current optical and mathematical models available that can be used to characterise milk will be presented, with the aim of creating a set of measurable parameters that relate to milk component concentrations.

4 Optical Theory

Photon migration is a term used to describe the way that photons travel through a highly scattering medium. It has been thoroughly studied in recent years and many theoretical models have been developed.

4.1 The effects of medium composition on light transmission

As photons travel through a medium, there are two possible events that can alter their final destination. The first is an absorption event and the second is a scattering event. Both these events alter the linear trajectory of the photon in different ways.

Absorption is the process where a photon encounters an object in the medium of interest and thereafter does not exist any longer. The presence or absence of absorption is strongly dependent on the wavelength (and hence the energy) of the photon. The energy in the photon is transferred to the object (atom, molecule or solid), whose energy is temporarily increased from its current state. Absorption has the effect of reducing the total number of photons reaching an observer.

Scattering is the process where a photon encounters an object in the medium of interest and is deflected from its original direction by that object. The direction of the deflection is difficult to determine but in many cases, the angular distribution is broadly in the original direction of the photon. The scattering direction is also highly dependent on the nature of the medium. Scattering does not reduce the number of photons, and usually does not alter the wavelength of the scattered photon. However, the exception in this case is *Raman scattering*, where the interaction of the photon with the scatterer can cause the transfer of energy to or from the scattered photon, causing a change in wavelength. This often occurs via the photon exciting the vibrational modes of scattering molecules.

An important side effect of scattering is that the length of the path that is travelled through the medium may be greatly increased, leading to a greater chance of absorption. Figure 4-1 illustrates the difference between absorption and scattering.

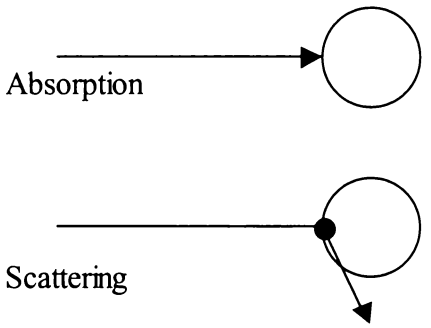

Figure 4-1: Difference between absorption and scattering.

Collectively, absorption and scattering can be referred to as *extinction*. Note that there is no requirement for the presence of any detectable objects separate to the medium to observe photon absorption – the medium itself may be capable of absorbing photons at the wavelength of interest. An example of this is a food colouring and water mixture – any absorption is simply caused by the photons being absorbed by the mixture itself, which in this case is the medium, which contains no discernable objects.

4.2 Measuring the behaviour of photons in scattering media

Given these three definitions (absorption, scattering and extinction), all may yield useful information about a participating medium. The nature of the information is reliant on exactly which of these three quantities are measured. Absorption measurements can yield chemical composition and molecular structure of a medium (or any constituents). Scattering measurements can yield information about the particles in the medium. A highly scattering medium can be defined as a non-scattering (transparent) matrix with multiple objects suspended in it causing the scattering, or it could be defined as a matrix that by its very nature is turbid and does not allow light to proceed through it without being scattered. From this point on, the second definition for highly scattering media will be used – that is, it is a matrix that is inherently scattering by nature.

The easiest one of the three quantities to measure is absorption. Given a purely absorbing medium, one only has to inject photons into one side and assuming that the medium is linear, homogeneous and isotropic, a simple photon detector at the other side will yield a result. Given that the number of photons injected into the medium is known, (or a relative measurement to a known standard is taken) the number of

emitted photons will correlate with the amount of absorption in that medium. The most obvious application of this technique is the estimation of the concentration of an absorbing substance in a solution. The Beer-Lambert Law is an equation relating the concentration of an absorber in solution to the amount of light attenuation. It was discovered (in its various forms) by Johann Lambert in 1760 and August Beer in 1852, and it is written:

$$\frac{I}{I_0} = \exp(-\alpha l c) \qquad [4\text{-}1]$$

where:

I is the detected light intensity

I_0 is the incident light intensity

α is the absorption coefficient (cm^{-1})

l is the optical path length (cm)

c is the concentration of the absorber in solution (molar)

The absorption coefficient is a number that is inherent to the absorber and is defined as the reciprocal of the distance a photon travels in that medium before it is absorbed. The absorption coefficient will be further explored later on.

If we take a closer look at the Beer-Lambert Law, we notice that there are terms to account for the properties of the absorber, the concentration of the absorber, and also the length that photons have to travel through the medium. It is well known that this law is not applicable with highly scattering media, due to a lack of provision for scattering in the equation. In highly scattering media, the *extinction* is greater than the *absorption*. Including wavelength dependence in our analysis, and investigating the medium with multiple wavelengths is the basis of spectroscopy. However, that does not solve the problem of the extinction outweighing the absorption. Still, one cannot tell whether the extinction (in particular, the scattering component) has wavelength dependence.

Thus, the use of the Beer-Lambert law at different wavelengths is adequate for describing the absorption properties of a medium, *as long as the medium does not scatter appreciably.* There are many highly scattering media of great interest that need a superior model. In order to achieve this, the scattering needs to characterised in the media of interest so that the problem of scattering can be eliminated. Another option

is to characterise scattering, which could yield information about the medium in question. In both cases, a model accounting for optical scattering in a turbid medium must be found. A review of suitable models for the description of photon migration in a highly scattering medium follows.

4.3 The behaviour of bulk photons in scattering media

In order to simulate any bulk photon propagation through a medium, or quantify any measurements of bulk photon propagation in a highly scattering medium, a mathematical description of the photon propagation must be found.

Of all the photons entering the medium, some of them will do one of the following (Mobley & Vo-Dinh, 2003):

1. travel through the medium and not be scattered (ballistic photons)
2. be scattered once in the medium and then not be affected by scattering subsequently (singly-scattered photons)
3. be scattered through the medium in such a way that their incident direction is not lost (snake photons)
4. be scattered through the medium in such a way that their incident direction is completely lost (multiply-scattered photons)
5. be absorbed after any (or no) amount of scattering has occurred

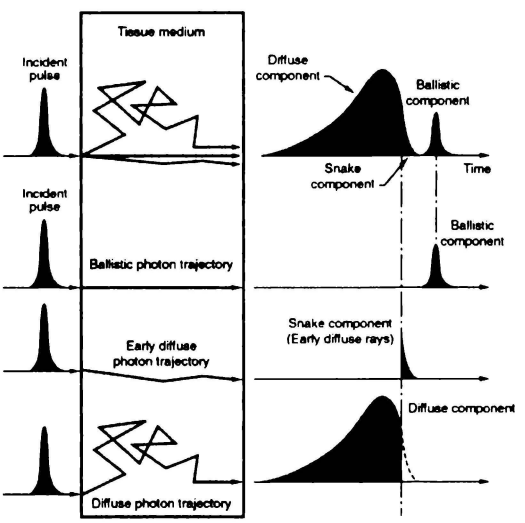

Figure 4-2: Paths taken by photons undergoing different processes in a medium (Mobley & Vo-Dinh, 2003).

Figure 4-2 shows the different types of paths that photons can follow once they enter a turbid medium. Whether photons tend to be more diffusive or ballistic depends entirely on the concentration of the scatterers in the medium. The greater the concentration, the more diffusive the photons will become. With highly scattering media, the bulk of the photons within will be diffusive.

Most of the research regarding photon migration applications has concentrated on the use of the more abundant diffusive photons. These photons have been scattered multiple times, and therefore will arrive at the detector long after the much smaller number of ballistic, single-scattered and snake photons. Unfortunately, these photons contain little information about their journey through the medium. These photons therefore, have little imaging ability. However, recent research has shown that with the correct models and processing, useful imaging and non-imaging data can be obtained. The next sections discuss the history and the theory of the non-imaging models to date.

4.3.1 Simple Models

In general, the simpler models of light propagation in highly scattering media tend to be used for ballistic, single-scattered or snake photons. The paths that these photons take are easily understood and a simple model can account for their behaviour.

Ballistic photons contain information about the spatial characteristics of the medium that they have just passed through. However, it was found that for successful imaging, a sample had to be sufficiently thin so that a useful proportion of the photons arriving at the detector would be ballistic photons. Ballistic photon imaging is not commonly used in the study of highly scattering media, due to the very small number of ballistic photons that pass through the sample.

Singly scattered and snake photons are treated differently. The Beer-Lambert Law has been modified on many occasions to account for scattering media. One such modification is given by Tuchin (2000), and deals with continuous-wave spectrophotometry in tissue samples. It is stated as:

$$\frac{I}{I_0} = \exp\left(-\varepsilon_{ab} \cdot c_{ab} \cdot r_{sd} \cdot DPF - G_S\right) \qquad [4\text{-}2]$$

where:

ε_{ab} is the absorption coefficient of the medium

c_{ab} is the absorber concentration

r_{sd} is the source-detector separation

DPF is the differential path length factor, and

G_S is the attenuation factor

DPF accounts for the increase in photon migration paths due to scattering, and G_S accounts for attenuation due to scattering and the geometry of the medium.

However, the main problem with using any relationships derived from the Beer-Lambert law is that only photons scattered out of the light path are accounted for (Sevick-Muraca *et al.*, 2003). Photons scattered into the light path, and consequently into the light detector are ignored and can be a source of error. However, this has not stopped variants of the Beer-Lambert law from being used in more recent research though. Tsuchiya & Urakami (1996) use a microscopic Beer-Lambert law (a variant of the Beer-Lambert law that works on the scale of a single photon absorption path length) to determine the concentration of an absorber in a tissue-like medium, with the assumption that the medium is homogeneous.

Zhang *et al.* (1999) also use a modified Beer-Lambert law in their work as it does not require a large volume of sample material which other theories require, such as those based on the diffusion equation.

All versions of the Beer-Lambert law do not discriminate between the ballistic, snake and diffusive photons. Studies using snake photons alone have been done in the field of tissue optics. Das *et al.* (1993) managed to use snake photons to resolve the location of the fat layer in a 4 cm thick piece of chicken breast. However the relative lack of snake photons compared to diffusive photons has much reduced the use of snake photons in general photon migration applications.

4.3.2 Kubelka-Munk Theory

The Kubelka-Munk model of light transport is one of the earlier quantitative models of light transport in scattering media. It relates the propagation of opposing light fluxes to the scattering and absorption properties of a medium via a set of coupled differential equations.

The simplest form of this theory is the two-flux version. This assumes two opposing diffuse light fluxes. A number of other conditions must also be fulfilled for this theory to be valid. They are (Mobley & Vo-Dinh, 2003):

- both fluxes contain only diffuse light,
- the sample is infinitely thick and
- the sample is planar and homogeneous.

Another condition sometimes stipulated especially with the measurement of transmittance rather than reflectance is that the sample be divisible into slices of identical thickness (Ishimaru, 1978).

The Kubelka-Munk model is derived from a model of light propagation originated by Schuster (Mobley & Vo-Dinh, 2003), which was used to describe photon propagation in stellar atmospheres. This was further developed by Kubelka and Munk, with the full statement of the differential equations by Kubelka (1948). Their equations were one of many similar sets of coupled differential equations developed to describe the same problem. The Kubelka-Munk equations however, were a more general solution compared to the others (Kubelka, 1948).

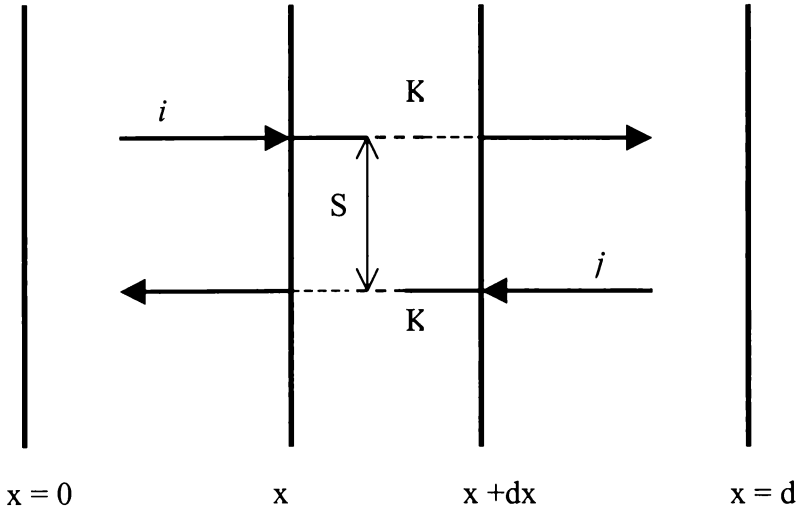

Figure 4-3: The geometry for the Kubelka-Munk two-flux model (Cerussi, 1999).

The geometry of the Kubelka-Munk model is shown in Figure 4-3. The actual equations that describe the light fluxes are:

$$-di = -(S + K)idx + Sjdx \qquad [4\text{-}3]$$

$$dj = -(S + K)jdx + Sidx \qquad [4\text{-}4]$$

with $-di$ being the flux in the positive x direction and dj being the flux in the negative x direction.

The two coefficients K and S are related to the absorption and scattering in the medium. They are similar in concept to the absorption and scattering coefficients discussed in the radiative transfer theory section. However, they are not directly related to any of the physical properties of the medium and their values must be determined by experiment (Ishimaru, 1978).

The two-flux model shown in Figure 4-3 is insufficient for describing a collimated beam of light passing through a turbid medium. The four-flux model gets around this limitation by introducing a set of collimated forward and backward fluxes in addition to the contributions from the diffuse fluxes (Tonon *et al.*, 2001; Tuchin, 2000). Light from the collimated fluxes can attenuate due to absorption and scattering only. Similarly, light from the diffuse fluxes can attenuate from scattering and absorption, but it can also increase due to light scattering from the collimated flux into the diffuse flux.

Patterson *et al.* (1991b) studied the application of the two flux Kubelka-Munk model as a way to describe the propagation of optical radiation through tissue. It was found that the expressions derived for the diffuse reflectance and transmittance were relatively simple and in theory could be used to calculate the absorption and scattering coefficients of the medium. However, the underlying assumptions used had a strong possibility of being incorrect. Patterson also describes other researchers modifying the Kubelka-Munk theory to include more fluxes (up to seven) but there has been no real agreement on how the coefficients, K and S, match up to real-world measurable quantities such as the absorption coefficient. The seven-flux model represents a three-dimensional space with six opposing diffuse fluxes and a single collimated flux (Tuchin, 2000). The Kubelka-Munk theory is not obsolete and is quite capable of modelling the propagation of light in tissue if a direct correlation to real-life parameters such as absorption and scattering coefficients is not required.

Durkin *et al.* (1994) used a Kubelka-Munk model to help characterize the absorption and scattering on human aorta samples. This, in conjunction with an extended rank-annihilation-factor analysis (a method used in fluorescence spectroscopy but modified

so that it could be used in turbid media), allowed them to obtain absolute intensity data as opposed to simply the line shape information of the fluorescence spectrum of the sample. Most of the available literature on fluorescence work rely on the normalised fluorescence intensity without scattering correction to distinguish changes between healthy and abnormal tissue (Alfano *et al.*, 1989).

Vargas (1998) builds a generalised one-dimensional four-flux model that is similar to Kubelka-Munk theory using a collimated and diffuse flux. Their model took into account the average photon path length and the forward scattering ratio. They assume a symmetry condition, where the forward diffuse flux is equal in magnitude to the backwards-diffuse flux. This led to a new set of differential equations and a new solution.

In summary, Kubelka-Munk models were widely used in the early stages of tissue optics research. They have proven to be valuable for the qualitative understanding of scattering in tissue, but the coefficients, K and S, have not yielded quantitative results for the optical coefficients of tissues, possibly due to the one-dimensional nature of the theory (Cerussi, 1999). Ishimaru (1989) considers Kubelka-Munk theory only useful for an approximate estimate of the optical properties of a sample. From this, it can be concluded that Kubelka-Munk theory is not suitable for the accurate characterisation of scattering and absorption in a scattering medium due to the lack of a well-defined relationship between its coefficients, K and S, and measurable parameters such as the absorption and scattering coefficients.

4.3.3 Monte Carlo Modelling

Monte Carlo modelling is a stochastic method based on modelling the path that individual photons take in a highly scattering medium. Monte Carlo methods allow one to visualise what happens to light in a scattering medium. Photon trajectories are simulated individually in a characterised medium. Once a sufficient number of photons have been simulated, an overall picture of how light behaves in the medium is gained. Alexandrakis *et al.* (2000) in their hybrid diffusion model noted that they had to increase the number of photons from 20,000 to 800,000 to bring the accuracy of their results for skin-on-muscle simulations to acceptable levels. Thus, Monte Carlo simulations are limited by their inherent need for large amounts of computing power.

Monte Carlo simulations are used mostly in the generation of alternative data that is used to confirm calculated or experimental results. Several researchers have done this, especially in the tissue optics field. Hasegawa *et al.* (1991) used it to model the effects of light through different types of scattering media to obtain results that would help describe the fundamental characteristics of light travelling through tissues. Zijp & ten Bosch (1997) used it to determine the characteristics of the light recovered by the small-numerical aperture fibre-optic probes typically used for photon migration studies on tissue samples. However, some researchers have used Monte Carlo simulations in different ways. Spott & Svaasand (2000) used it to supplement photon diffusion theory at small source-detector, distances and Alexandrakis *et al.* (2001) apply the theory in a similar way, supplementing photon diffusion theory in a two-layer medium where the first layer is very thin.

It should be noted that Monte Carlo simulations are not applicable in general for the inverse problem in photon migration (the recovery of optical coefficients from calculated or measured data) due to the way in which it works. Since the basis of Monte Carlo modelling is to simulate the trajectory of individual photons in the medium it is easy to see that if you already have a set of recorded trajectories, reconstructing the exact nature of the medium is impractical at the least. There has been at least one success at using Monte Carlo in this way (Nilsson *et al.*, 1995) which shows that it is possible. Nevertheless, the difficulty involved with this in comparison to the use of other techniques limits the usefulness of Monte Carlo simulations for the analysis of experimental results.

4.3.4 Mie Theory

Mie theory is an exact solution to the general problem of light scattering by an isotropic sphere in a homogeneous medium. It is based on the solution to Maxwell's equations when applied to the intersection of a plane electromagnetic wave with a spherical particle. An incident wave, with wave vector **k** strikes a sphere of radius a. The sphere has a refractive index of n' and the medium has an index of n. Once the incident wave strikes the particle, an internal wave is set up, with wave vector **k'**, along with a scattered wave that radiates away from the particle. Figure 4-4 shows a simplified geometry of the Mie problem.

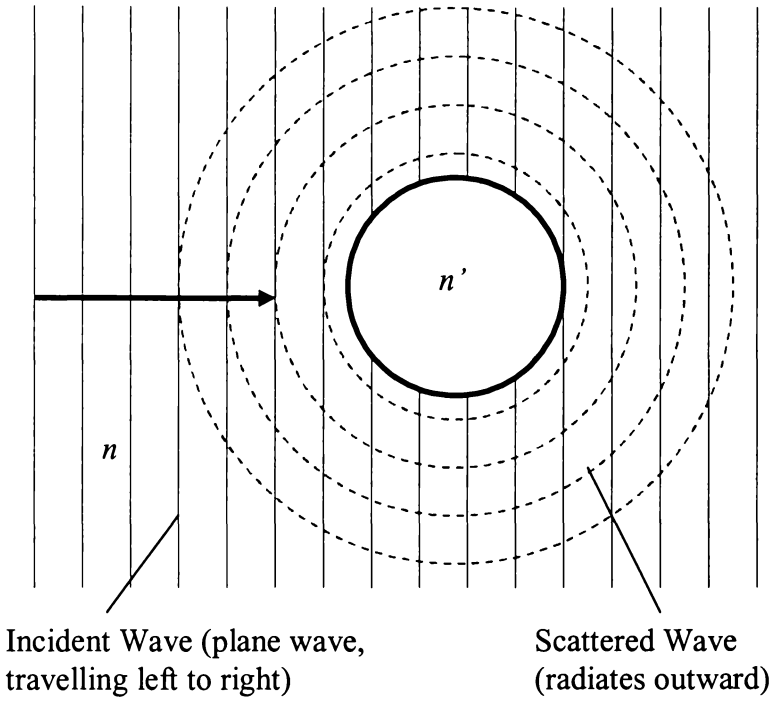

Figure 4-4: Simplified geometry of Mie scattering problem (Mobley & Vo-Dinh, 2003).

This problem has been extensively studied since its original solution by Mie in 1949 and the solutions are well known. The solution of the internal and the scattered waves are an infinite series of spherical harmonics that are weighted by a set of coefficients (Bohren & Huffman, 1983). Two key parameters in Mie theory that affect the weighting coefficients are the *size parameter*, which is written as:

$$x = |\mathbf{k}|a = \frac{2\pi n'a}{\lambda} \qquad [4\text{-}5a]$$

and the relative complex refractive index:

$$m = \frac{n'}{n} \qquad [4\text{-}5b]$$

Given these two parameters, it is a straightforward exercise to retrieve useful coefficients from Mie-calculated data using these formulae (Van de Hulst, 1957):

$$Q_{ext} = \frac{2}{x^2}\sum_{n=1}^{N}(2n+1)\,\mathrm{Re}(a_n + b_n) \qquad [4\text{-}6a]$$

$$Q_{sca} = \frac{2}{x^2}\sum_{n=1}^{N}(2n+1)\cdot(|a_n|^2 + |b_n|^2) \qquad [4\text{-}6b]$$

$$g = \frac{4}{x^2 Q_{sca}} \sum_{n=1}^{N} \left[\frac{n(n+2)}{n+1} \mathrm{Re}(a_n a_{n+1}^* + b_n b_{n+1}^*) + \frac{2n+1}{n(n+1)} \mathrm{Re}(a_n b_n^*) \right] \qquad [4\text{-}6c]$$

where Q_{ext} is the extinction efficiency, Q_{sca} is the scattering efficiency and g is the scattering anisotropy. The values a_n and b_n are complex Mie coefficients from the solution of the scattered wave.

Since Mie theory is a complete and general theory for optical scattering from spherical particles, it is common for the expressions for other types of scattering (such as Rayleigh scattering) to be a special case of Mie scattering. In this case, $|m|x$ is much less than 1. This occurs when the size of the particles is much smaller than the incident wavelength, or $a << \lambda$.

Another well-known case is when the relative refractive indices of the medium and the particle are similar to the refractive index of free space. Cerussi (1999) describes it as the situation where $|m\text{-}1| << 1$, $|\mathbf{k}|.a.|m\text{-}1| << 1$, and that the internal wave inside the particle is approximately the same as the external, scattered wave. This situation is known as *Rayleigh-Gans* scattering. It has been used in the study of tissue optics. Maier *et al.*, (1994) developed a method using Rayleigh-Gans scattering of measuring glucose concentration in tissues by measuring their scattering coefficient. The change in glucose concentration (and therefore refractive index) in the extracellular fluid influences the value of the reduced-scattering coefficients of the tissue by a small, but detectable amount.

If interparticle interactions are considered to be negligible, and the volume fraction of the spherical particles is known, the reduced-scattering coefficient of a collection of particles in a suspension may be found using the following expression (Richter *et al.*, 1998):

$$\mu_s'(\lambda) = \frac{3}{2} \frac{Q_{scat}(n, x, \lambda)(1 - g(n, x, \lambda))\phi}{x} \qquad [4\text{-}7]$$

Here, x is the particle diameter and ϕ is the volume fraction. From this, one can see that Mie theory could be useful in multiple-scattering cases and in the area of particle sizing, due to the strong dependence of μ_s' on x and ϕ. (Jiang *et al.*, 1997).

Mie scattering theory is still often used to verify the values of the optical properties of samples that have been tested using other methods. Coquoz *et al.* (2001) verified their

measurements of the optical properties of small volume samples with predictions made using Mie theory. Ghosh *et al.* (2001) also used Mie theory to help estimate the size of scatterers in human breast tissue. The usefulness of Mie scattering lies in the verification of other models since extending it to include the general multiple-scattering case increases the complexity of the mathematics to the point where finding an accurate solution is an impractical exercise.

4.3.5 Exact Electric and Magnetic Field Simulations

One way to solve the scattering problem in general for all particles and scattering conditions is to model Maxwell's equations for the propagation of electromagnetic radiation directly, along with the proper boundary conditions. This was not a possibility before the existence of computers with sufficient memory capacity. A common approach is to use a numerical approximation to the equations in question. There are several different ways of modelling the relevant differential equations in a quantised form. Examples of this are the forward-time centered-space schemes and Crank-Nicolson algorithms (Garcia, 1994). They have far fewer restrictions on model parameters such as the choice of wavelength or geometry, because the simulation accounts for them itself (Cerussi, 1999). However, one must consider the amount of memory required for a reasonably good simulation of a multiple-scattering medium. If the model has a resolution of one micrometer and used two bytes per unit volume (one for the electric field and one for the magnetic field), it would require 2000 gigabytes of storage capacity to model a single cubic centimetre of space. Clearly, memory space is the limiting factor with this approach.

Yee (1966) developed a finite difference numerical model for Maxwell's equations. He showed that if one chooses the field points appropriately, this model would work for perfectly conducting boundary conditions. His example was the scattering of an electromagnetic pulse by a perfectly conducting cylinder.

Taflove & Brodwin (1975) later extended Yee's method to arbitrary dielectric scatterers and outlined a way to further extend the finite-difference model to three dimensions. They were able to predict the location of the field maxima and minima within a scatterer with less than 10% error after a one-minute program execution time.

Work on finite-difference time-domain models continued with Mur (1981) developing two- and three-dimensional models for absorbing boundary conditions. Umashankar

& Taflove (1982) subsequently devised a general finite-difference time-domain model in three dimensions that could simulate arbitrarily shaped dielectric and conducting objects. Their results of near and far field magnitudes were within 2.5% of those methods predicted by the method of moments.

As powerful as they may be, direct electric and magnetic field models are still not suitable for general multiple-scattering problems as it is still difficult to solve the inverse problem – the recovery of the optical properties of a medium. Another difficulty is the large amount of computing time and power required. This does not preclude their use altogether, as a finite-difference model was used by Drezek *et al.*, (1999) to predict light scattering from cells. More recently, Pogue *et al.* (2001) developed a numerical image reconstruction algorithm based on diffusion theory. They found that while testing data from human breast tissue, a model made up of a 3-D mesh in the shape of a cylinder had very similar results to a more detailed model that accurately resembled a human breast shape. However, this algorithm does require some experimental measurements before the image reconstruction can be started.

4.3.6 Transport Theory

With multiple-scattering media, the evolution of mathematical models that can deal with real-world quantities has tended towards two distinct branches – analytical theory and transport theory. Mie theory is an example of an analytical theory.

Unlike direct electric and magnetic field simulations and Mie theory, radiative transport theory is not an exact model. It is not derived from the electromagnetic wave equations and thus is not directly attributable to the electric or magnetic fields of the incident, internal or scattered waves. The multiple-scattering effects of a turbid medium (and the consequent decoherence effects) effectively suppress the wave nature of light (Mobley & Vo-Dinh, 2003). Instead, transport theory tracks the passage of energy through the medium in the form of photon density. As it is assumed that there is no correlation between any of the fields, the addition of powers at any point rather than the addition of fields is valid (Ishimaru, 1978). Transport theory, therefore, is a *heuristic* model of photon propagation.

The basic equation in transport theory is called the Boltzmann transport equation, which is functionally identical to the equation used by Boltzmann in the kinetic theory of gases. A major similarity to the kinetic theory of gases is that like the atoms (or

molecules) of a gas, the photons are regarded as identical, distinguishable and non-interacting.

Transport theory can be likened to a book-keeping scheme (Haskell *et al.*, 1994), where the number of photons in any particular area in the medium is tracked. Thus, with such a scheme, terms are needed that add to the photon count and that subtract from the photon count. One important feature is that all photons in this scheme must be accounted for. This is required so that the law of conservation of energy is upheld.

Before assembling the Boltzmann equation before one must understand the physical processes that each part of the equation represents. There have been numerous publications explaining the use of transport theory in photon migration. Cerussi (1999), provides a good description of transport theory, as well as a derivation of the diffusion equation that is clear and easy to understand. The following derivations will be based upon that work.

What follows are definitions of the principal quantities of interest in the transport equation They are:

1. $u(\mathbf{r},\hat{\Omega},t)$ is the *angular photon density*, whose units are measured in photons×cm^{-3}×sr^{-1}. Centimetres are used here instead of metres, as it is a convention in tissue optics. It is defined such that $u(\mathbf{r},\hat{\Omega},t)d^3rd\hat{\Omega}$ is the expected number of photons inside the volume element d^3r at $\mathbf{r}$ whose velocity directions are located within the solid angle element $d\hat{\Omega}$ in the direction $\hat{\Omega}$ at time t. The volume element d^3r in conjunction with the solid angle $d\hat{\Omega}$ is what is rederred to as the *region of interest.*

2. $\mathbf{j}(\mathbf{r},\hat{\Omega},t)$ is the *angular photon current*, a vector quantity related to the angular photon density by the photon speed v; that is, $\mathbf{j}(\mathbf{r},\hat{\Omega},t) = v\hat{\Omega}u(\mathbf{r},\hat{\Omega},t)$. Its units are photons×cm^{-2}×s^{-1}×sr^{-1}. It describes the flow of the photon density in the direction $\hat{\Omega}$. $\mathbf{j}(\mathbf{r},\hat{\Omega},t)\cdot d\mathbf{A}$ is therefore the expected number of photons per unit time that pass through the area element $d\mathbf{A}$.

3. $\mathbf{q}(\mathbf{r},\hat{\Omega},t)$ is the *angular source density*, which is the number of photons per unit time that is injected into the medium at $\mathbf{r}$. It has units of photons×cm^{-3}×s^{-1}×sr^{-1}.

Four assumptions that are used in this assembly of the transport equation. They are:

1. The medium is *macroscopically homogeneous*. This implies that the scattering phase function $f(\hat{\Omega}' \rightarrow \hat{\Omega})$ depends only on the cosine of the scattering angle (Kaltenbach & Kaschke, 1993) and that the optical properties are invariant throughout the medium. In the case of a volume of milk approximating an infinite medium, this is a reasonable assumption.
2. Photon scattering by the medium is *elastic* and *homogeneous*. With the assumption that n is constant, all photons in the medium will propagate at the same speed. As milk is predominantly water, it is assumed that the background refractive index is that of water, i.e. n = 1.33. Inelastic scattering processes such as Raman scattering can occur in strongly scattering media, but the problems caused by this can be avoided by reducing the source intensity.
3. Photon-photon interactions are negligible. However, the collective properties of the photon density do show interference effects.
4. The boundary of the medium is non re-entrant. Once a photon has exited the medium, it no longer contributes.

Taking the assumptions into account, the Boltzmann transport equation can now be assembled. As Figure 4-5 shows, a photon can undergo five different processes inside the medium. This is described by Cerussi (1999) and Mobley & Vo-Dinh (2003). The five processes are:

Physical Process	Mathematical Description
Source emits photon into volume	$+q(\mathbf{r},\hat{\Omega},t)d^3r\ d\hat{\Omega}$
Photon absorbed within volume	$-(v\mu_a)\,u(\mathbf{r},\hat{\Omega},t)d^3r\ d\hat{\Omega}$
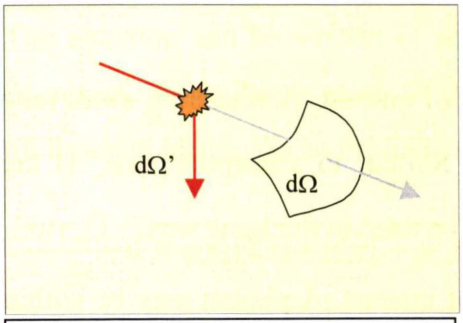 Photon scatters out of solid angle	$-(v\mu_s)\,u(\mathbf{r},\hat{\Omega},t)d^3r\ d\hat{\Omega}$
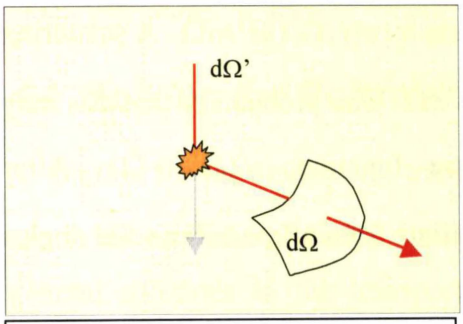 Photon scatters into solid angle	$+\left[\int_{4\pi} d\hat{\Omega}(v\mu_s)f(\hat{\Omega}'\rightarrow\hat{\Omega})u(\mathbf{r},\hat{\Omega},t)\right]d^3r d\hat{\Omega}$
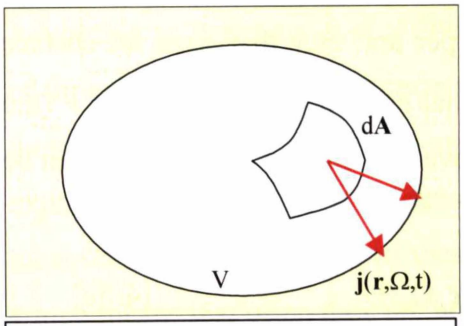 Photon leaves volume	$OUT-IN=\left[\int_A d\mathbf{A}\cdot\mathbf{j}(\mathbf{r},\hat{\Omega},t)\right]d\hat{\Omega}$

Figure 4-5: Physical Processes included in the Boltzmann Transport Equation (Cerussi, 1999).

1. Photons are injected into the medium from the source. The angular source density should be a known quantity as the source is usually controlled.
2. Photons may be absorbed by the medium. The absorption probability per unit time is given by $v\mu_a$ so that the product $(v\mu_a)\cdot u(\mathbf{r},\hat{\Omega},t)d^3rd\hat{\Omega}$ describes the probability per unit time that the angular photon density will decrease due to absorption in the medium.
3. Photons may be scattered out of the region of interest. A scattering event may push a photon out of $d\hat{\Omega}$ or out of d^3r. Similar to absorption, $v\mu_s$ is the scattering probability per unit time and can be used in the same way.
4. Photons may be scattered into the region of interest. A photon may be within the same volume element as the region of interest but have its velocity vector in the wrong direction – it does not contribute to $u(\mathbf{r},\hat{\Omega},t)d^3rd\hat{\Omega}$. A scattering event may push this photon from $d\hat{\Omega}'$ into $d\hat{\Omega}$. The probability that this may happen is given by the scattering-phase function, $f(\hat{\Omega}'\rightarrow\hat{\Omega})$. After integrating over $d\hat{\Omega}'$, all possible contributions from all possible solid angles are accounted for.
5. Photons may simply leak in and out of the region of interest. Since $\mathbf{j}(\mathbf{r},\hat{\Omega},t)\cdot d\mathbf{A}d\hat{\Omega}$ is the number of photons per unit time that cross the surface element d**A**, the total number of photons that enter or exit the volume V (the medium) can be calculated by integrating over the surface area A. This can be expressed as:

$$\text{photons}\times\text{s}^{-1}(\text{OUT-IN}) = d\hat{\Omega}\int_A d\mathbf{A}\cdot\mathbf{j}(\mathbf{r},\hat{\Omega},t) \qquad [4\text{-}8a]$$

The divergence theorem can be used to convert the surface integral to a volume integral, giving:

$$\text{photons}\times\text{s}^{-1}(\text{OUT-IN}) = d\hat{\Omega}\int_V d^3r\vec{\nabla}\cdot\mathbf{j}(\mathbf{r},\hat{\Omega},t) \qquad [4\text{-}8b]$$

A conservation-of-energy equation combining all these terms into a single equation gives:

$$d\hat{\Omega}\int_V d^3r\left\{\begin{array}{l}\dfrac{\partial u(\mathbf{r},\hat{\Omega},t)}{\partial t}-q(\mathbf{r},\hat{\Omega},t)+v(\mu_a+\mu_s)u(\mathbf{r},\hat{\Omega},t)\\ \quad -v\mu_s\int_{4\pi}d\hat{\Omega}'u(\mathbf{r},\hat{\Omega},t)f(\hat{\Omega}'\rightarrow\hat{\Omega})+\vec{\nabla}\cdot\mathbf{j}(\mathbf{r},\hat{\Omega},t)\end{array}\right\}=0 \qquad [4\text{-}9]$$

This equation must be satisfied in order to make sure that energy conservation is not violated. Thus, the integrand of equation 4-9 gives the Boltzmann transport equation. The equation can be written in several different ways (Yoon *et al.*, 1989; Spott & Svaasand, 2000; Pogue *et al.*, 2001). However, despite their differing notation, they all function identically to the Cerussi-derived equation shown (equation 4-10).

$$\frac{\partial u(\mathbf{r},\hat{\Omega},t)}{\partial t}=q(\mathbf{r},\hat{\Omega},t)-v(\mu_a+\mu_s)u(\mathbf{r},\hat{\Omega},t)$$

$$+v\mu_s\int_{4\pi}d\hat{\Omega}'u(\mathbf{r},\hat{\Omega},t)f(\hat{\Omega}'\rightarrow\hat{\Omega})-\vec{\nabla}\cdot\mathbf{j}(\mathbf{r},\hat{\Omega},t) \qquad [4\text{-}10]$$

4.4 Solving the Boltzmann Transport Equation

A solution for the Boltzmann transport equation in terms of $u(\mathbf{r},\hat{\Omega},t)$ is required for use in the analysis of highly scattering media. One major problem, however, is that general solutions to the transport equation do not exist (Kaltenbach & Kaschke, 1993).

According to Patterson *et al.* (1991b) and Spott & Svaasand (2000), formal solutions of the transport equation for certain situations exist. They are analytical solutions, but they are not 'exact' solutions in that the expression for the *radiance* (alternative expression for angular photon density) requires the evaluation of complex integrals. In many cases, the evaluation of these integrals requires the use of numerical methods, which means that often they are no more accurate than the use of an approximation to the transport equation.

In this case, using an approximation is more efficient because it can provide a sufficiently accurate expression of the transport equation, as well as potentially simplify the mathematics.

There are three different ways of approximating the Boltzmann transport equation (Patterson *et al.*, 1991b):

1. **Invariance method**

   The basic idea is to consider the changes in radiance when an infinitesimally thin layer is added to one of the surfaces of the medium. With a thin layer, the scattering contribution by that layer is minimised. However, the emphasis is placed on calculating the radiance outside the medium.

2. **Discrete Ordinates Methods**

   This scheme converts the radiative transfer equation to a set of linear algebraic equations, which can then be solved. One example of this method is the Kubelka-Munk model. This approach is used by Vargas (1998) to develop a generalized four-flux model.

3. **Functional Expansion Methods**

   This is similar in style to the discrete ordinates methods except that instead of developing a set of linear algebraic equations, a set of coupled differential equations are developed. This method is the one most commonly used in tissue optics studies and is the method used in this derivation of the diffusion equation.

4.5 The Diffusion Approximation

The diffusion approximation to the Boltzmann transport equation is the simplest model of photon migration available (Boas *et al.*, 1995). It is the standard model for photon migration in recent work (Alexandrakis *et al.*, 2000), especially in the field of tissue optics. It has been extensively studied, and there are several papers validating it as a viable theory for the study of turbid media. Kim & Ishimaru (1998) determined the validity of the diffusion equation for imaging biological media. Arridge *et al.* (1992) justified the use of the diffusion equation in tissue optics by studying the behaviour and accuracy of the diffusion equation in describing various parameters of photon propagation such as mean time, differential path length and phase shift.

There are several publications that include the derivation of the diffusion equation from the Boltzmann Transport equation. All of them follow the same basic principles in their derivation of the diffusion equation (Ishimaru, 1978; Haskell *et al.*, 1994). Cerussi (1999) has a similar derivation but from a different point of view. Please note that it is intentional that some of the resulting equations presented in this derivation are identical to Cerussi's.

The diffusion equation will now be derived from the Boltzmann transport equation, using the functional expansion method. Equation 4-10 is restated for ease of reference.

$$\frac{\partial u(\mathbf{r},\hat{\Omega},t)}{\partial t} = q(\mathbf{r},\hat{\Omega},t) - v(\mu_a + \mu_s)u(\mathbf{r},\hat{\Omega},t)$$

$$+ v\mu_s \int_{4\pi} d\hat{\Omega}' u(\mathbf{r},\hat{\Omega},t) f(\hat{\Omega}' \rightarrow \hat{\Omega}) - \vec{\nabla} \cdot \mathbf{j}(\mathbf{r},\hat{\Omega},t) \qquad [4\text{-}10]$$

Before going any further, three new quantities need to be defined that will be used for the photon "book-keeping" (Haskell *et al.*, 1994):

$$U(\mathbf{r},t) = \Phi^{(0)} = \int_{4\pi} u(\mathbf{r},\hat{\Omega},t) d^2\hat{\Omega} \qquad [4\text{-}11a]$$

$$\mathbf{J}(\mathbf{r},t) = \Phi^{(1)} = \int_{4\pi} u(\mathbf{r},\hat{\Omega},t)\hat{\Omega} d^2\hat{\Omega} \qquad [4\text{-}11b]$$

$$Q(\mathbf{r},t) = \int_{4\pi} q(\mathbf{r},\hat{\Omega},t) d^2\hat{\Omega} \qquad [4\text{-}11c]$$

Equation 4-11a is the *photon density* or *photon fluence rate*, and has units of photons×cm^{-3}. Equation 4-11b is the *photon current* and has units of photons×cm^{-3}×s^{-1}. The last term in equation 4-11c is the *source photon density*, and has the same units as the photon density.

Integrating equation 4-10 over all angles and taking the zeroth moment results in the *photon continuity equation* (Pogue *et al.*, 2001):

$$\frac{\partial U(\mathbf{r},t)}{\partial t} = Q(\mathbf{r},t) - v\mu_a U(\mathbf{r},t) - \vec{\nabla} \cdot \mathbf{J}(\mathbf{r},t) \qquad [4\text{-}12]$$

One point to take note of is that since all angles have been integrated over, none of the components of the equation have any angular dependence. Instead of the angular photon density being the quantity of interest, there is now the photon density, often referred to as the *fluence rate*. This substitution is valid, as long as the magnitude of the angular photon density is not strongly dependent on its direction (Patterson *et al.*, 1991a).

The photon continuity equation, while appearing simpler than the transport equation, is not any easier to solve. This is due to the $\vec{\nabla} \cdot \mathbf{J}(\mathbf{r},t)$ term. While taking the zeroth

moment of the transport equation has removed the scattering term, it has introduced the photon current as a new unknown.

Cerussi (1999) goes on further to take the first order moment of the photon continuity equation to derive the *photon-current continuity equation*. This does not solve anything as yet another unknown has been introduced. Cerussi concludes with the statement "*it is not possible to obtain a set of closed equations* since *m* moments of the Boltzmann transport equation will always introduce *m*+1 unknowns." It should be noted that this extra unknown has an angular dependence, and to effectively deal with it, this dependence requires removal.

The way this is generally done for the transport equation is to firstly assume that the angular photon density is isotropic, with a small directional (linearly anisotropic) component (Pogue *et al.*, 2001). This usually occurs in scattering media where scattering strongly dominates absorption ($\mu_s' >> \mu_a$). With that, one can now re-write the angular photon density, the source angular photon density and the scattering phase function in terms of an infinite series of spherical harmonics (Star, 1989):

$$u(\mathbf{r},\hat{\Omega},t) = \frac{1}{4\pi}\sum_{i=0}^{N}(2i+1)u_i(\mathbf{r},\hat{\Omega},t)P_i(\cos\theta) \qquad [4\text{-}13]$$

where P_i are Legendre polynomials (the spherical harmonic terms) and cos θ is the scattering angle. The approximation improves with the addition of more terms. However with each additional term, the possible anisotropy of the angular photon density increases. Since isotropic scattering has been assumed, and also that expansions with even *N* do not contribute anything meaningful, *N* shall be restricted to low values, the most common ones being *N*=1 and *N*=3. These are referred to as the P_1 and P_3 approximations.

The P_3 approximation is more accurate than the P_1 approximation. Its strengths are that it can handle collimated light sources and absorbing media (Spott & Svaasand, 2000). It has been studied and has been found to be a useful model for tissue optics where a laser beam is incident directly on tissue (Star, 1989).

The P_1 approximation for the angular photon density, and the source angular photon density, is as follows:

$$u(\mathbf{r},\hat{\Omega},t) \approx \frac{1}{4\pi}U(\mathbf{r},t) + \frac{3}{4\pi\nu}\mathbf{J}(\mathbf{r},\hat{\Omega},t) \qquad [4\text{-}14a]$$

$$q(\mathbf{r},\hat{\Omega},t) \approx \frac{1}{4\pi}Q(\mathbf{r},t) + \frac{3}{4\pi}\mathbf{Q}_1(\mathbf{r},\hat{\Omega},t) \qquad [4\text{-}14b]$$

The scattering phase function needs to be approximated in the same way in order to complete the approximation. This is difficult mainly due to a lack of knowledge of the exact form of the function. However, even if exact functions do not exist, approximate ones certainly do. One commonly used scattering phase function is the Henyey-Greenstein scattering phase function. It was first used by Henyey & Greenstein (1940) in their studies of diffuse radiation in space.

The Henyey-Greenstein scattering phase function has been shown to approximate biological scattering (Van de Hulst, 1957). Madsen *et al.* (1991) assumed its suitability as a scattering phase function in their study of the use of India ink as an absorber in tissue-simulating phantoms. Star (1989) used this in his models for the human dermis, and also extended this further by adding a delta function to the scattering phase function (known as the delta-Eddington approximation), which helped to simulate the highly forward scattering nature of tissues.

The expansion of the Henyey-Greenstein function in terms of Legendre polynomials (similar to the angular photon density) was given by Spott & Svaasand (2000) as:

$$p_{HG}(\hat{\Omega}',\hat{\Omega}) = \frac{1}{4\pi}\frac{1-g^2}{\left[1+g^2-2g(\hat{\Omega}',\hat{\Omega})\right]^{3/2}}$$

$$= \sum_k \frac{2k+1}{4\pi} g^k P_k(\hat{\Omega}',\hat{\Omega}) \qquad [4\text{-}15]$$

where $g = \int_{4\pi} p(\hat{\Omega}',\hat{\Omega})\hat{\Omega}d\Omega$ is the average cosine of the scattering angle, commonly referred to as the *scattering anisotropy*.

Substituting all these approximations back into equation 4-10 gives:

$$\frac{1}{\nu}\frac{\partial \mathbf{J}(\mathbf{r},t)}{\partial t} + (\mu_a + (1-g)\mu_s)\mathbf{J}(\mathbf{r},t) + \frac{\nu}{3}\vec{\nabla}\cdot U(\mathbf{r},t) = \mathbf{Q}_1(\mathbf{r},\hat{\Omega},t) \qquad [4\text{-}16]$$

The term $(1-g)\mu_s$ is from this point replaced with a new quantity, μ_s'. This is known as the *reduced-scattering coefficient* and represents the order of length in which

scattering is isotropic. The effect of the isotropic scattering over the scale of μ_s' is effectively the same as that of anisotropic scattering over μ_s.

Equation 4-12 and 4-16 make up our coupled pair of differential equations that one can use to approximate the Boltzmann transport equation. There are two ways to continue on this particular course of approximation. The first is to notice that there aew two equations and two unknowns, and then solve the pair in terms of the photon density. The equation obtained is referred to as the *telegrapher's equation* (Aronson & Corngold, 1999), or the P_1 equation (Kaltenbach & Kaschke, 1993) and is written:

$$vD\left[\frac{3}{v^2}\frac{\partial U(\mathbf{r},t)}{\partial t}-\nabla^2 U(\mathbf{r},t)\right]+(1+3\mu_a D)\frac{\partial U(\mathbf{r},t)}{\partial t}+v\mu_a U(\mathbf{r},t)=$$

$$Q(\mathbf{r},t)+\frac{3D}{v}\frac{\partial Q(\mathbf{r},t)}{\partial t}-3D\vec{\nabla}\cdot\mathbf{Q}_1(\mathbf{r},\hat{\Omega},t) \qquad [4\text{-}17]$$

Note that D in equation 4-17 is the diffusion coefficient, which will be defined subsequently. The second approach is to consider equation 4-16 a little more closely, and apply two more assumptions:

1. Time variations in the photon current are negligible compared to changes in the photon density (Aronson & Corngold, 1999).
2. The source photon density has little or no angular dependence, and can be treated as a point source (Fantini *et al.*, 1997).

Mathematically, that means that the first term can be dropped and equation 4-16 set equal to zero, so that:

$$(\mu_a+(1-g)\mu_s)\mathbf{J}(\mathbf{r},t)+\frac{v}{3}\vec{\nabla}\cdot U(\mathbf{r},t)=0 \qquad [4\text{-}18]$$

Re-arranging and solving for the photon current gives (bearing in mind that this is an approximation):

$$\mathbf{J}(\mathbf{r},t)\approx-\frac{v}{3(\mu_a+\mu_s')}\vec{\nabla}U(\mathbf{r},t)=-vD\vec{\nabla}U(\mathbf{r},t) \qquad [4\text{-}19]$$

This is the statement of Fick's Law. It is generally valid for steady-state situations and time-varying fluxes where the frequency is less than about 1 GHz (Pogue *et al.*, 2001).

In essence, these last two approximations have allowed the expression of the photon current simply in terms of the gradient of the photon density. We can substitute equation 4-19 into equation 4-12, noting that $D = \frac{1}{3(\mu_{s'} + \mu_a)}$ to obtain the diffusion equation:

$$\frac{\partial U(\mathbf{r},t)}{\partial t} - vD\nabla^2 U(\mathbf{r},t) + v\mu_a U(\mathbf{r},t) = Q(\mathbf{r},t) \qquad [4\text{-}20]$$

Having now derived the diffusion equation and being aware of the assumptions in its derivation and therefore its limitations, a solution for it can now be found. However before that is done, it would be prudent to examine its limitations.

4.6 Limitations of the Diffusion Approximation

There are two limitations that must be adhered to before the diffusion approximation can be used successfully (Boas *et al.*, 1995; Pogue *et al.*, 2001). They are:

1. Scattering must dominate absorption ($\mu_a << \mu_s'$).
2. If frequency domain methods are used, the source modulation frequency must be less than the scattering rate.

Limitation (1) comes from the assumption in the derivation of equation 4-19 that the source is isotropic and has little angular contribution. Given that, and also that the medium is macroscopically homogeneous, it follows that the photon densities in the medium should also be isotropic. However, this only occurs when scattering greatly dominates absorption. The large amount of scattering is required to sufficiently randomise the individual photon vectors so that at any point in the medium, photons may be converging on it from all directions in equal numbers. If scattering does not greatly dominate absorption, the photon density will be attenuated before isotropic conditions are reached.

Haskell *et al.* (1994) justified limitation (2) from a the point of view that the ratio of the fluence rate to the photon current term must be much greater than unity, as a result of Fick's Law. Cerussi (1999) also verified this.

In equation 4-19, there is no frequency dependent term as these equations have been derived in the time domain. If one works in the frequency domain, one can re-write

$\mathbf{J}(\mathbf{r},t)$ as $\mathbf{J}(\mathbf{r},\omega)\exp(-i\omega t)$. The time derivative in equation 4-11b then becomes $(-i\omega)\mathbf{J}(\mathbf{r},\omega)$. If $D = \frac{1}{3(\mu_s' + \mu_a)}$ is substituted into equation 4-11b the result is:

$$\mathbf{J}(\mathbf{r},\omega) = -vD\frac{1 + i(3\omega Dv^{-1})}{1 + (3\omega Dv^{-1})^2}\vec{\nabla}U(\mathbf{r},\omega) \qquad [4\text{-}21]$$

To transform this into the Fick's Law, $3\omega Dv^{-1}$ must be much less than 1. What this means in practical terms is that because $3\omega Dv^{-1}$ has units of time, the modulation period $\frac{2\pi}{\omega}$ must not approach the photon collision period Dv^{-1} in order to keep this approximation valid. Setting $\frac{2\pi}{\omega} \approx 0.01Dv^{-1}$ should prove to be sufficient. Since the reduced-scattering coefficient for cow's milk is in the range of 15 to 60 cm^{-1}, the source modulation frequency should be kept below about 3.4 GHz to ensure that the modulation period does not approach the photon collision period. This is a different limitation to the 1 GHz restriction mentioned previously.

4.7 Solution of the Diffusion Equation

The diffusion equation can be solved using a Green's function. The solution in the time domain for a source pulse of unit energy at time t = t' is given by (Haskell *et al.*, 1994):

$$U_G(\mathbf{r},t-t') = \frac{c}{[4\pi Dc(t-t')]^{3/2}} \times \exp\left[-\frac{r^2}{4Dc(t-t')} - \mu_a c(t-t')\right] \qquad [4\text{-}22]$$

Equation 4-22 simplifies to a form of the Beer-Lambert law in the presence of negligible scattering. However, this expression does not allow the separation of the effects of absorption from scattering (Cerussi & Tromberg, 2003). The remaining option open at this stage is to work in the frequency domain, if the diffusion equation is still to be used.

Haskell *et al.* (1994) also provided a solution in the frequency domain. They started by placing a harmonic source at the origin emitting power $P \times \exp(i\omega t)$ and solving:

$$U(\mathbf{r},t) = \int_{-\infty} U_G(\mathbf{r},t-t')P \times \exp(i\omega t')dt'$$

$$= \frac{P \times \exp(i\omega t)}{4\pi D} \frac{\exp(-kr)}{r}$$

$$= \frac{P}{4\pi D} \exp(-k_{real} r) \frac{\exp\left[-i(k_{imag} r - \omega t)\right]}{r} \qquad [4\text{-}23]$$

where:

$$k = k_{real} + ik_{imag} = \sqrt{\frac{\mu_a c + i\omega}{Dc}} \qquad \text{and} \qquad \tau \equiv \frac{1}{\mu_a c} \qquad [4\text{-}24]$$

so that:

$$k_{real} = \sqrt{\frac{3}{2}\mu_a(\mu_s' + \mu_a)\left[\sqrt{1+(\omega\tau)^2} + 1\right]}^{1/2} \qquad [4\text{-}25a]$$

$$k_{imag} = \sqrt{\frac{3}{2}\mu_a(\mu_s' + \mu_a)\left[\sqrt{1+(\omega\tau)^2} - 1\right]}^{1/2} \qquad [4\text{-}25b]$$

Equation 4-23 is a form of the Fourier transform of equation 4-22 (Fishkin & Gratton, 1993). It is identical to the frequency-domain solution derived by Cerussi (1999), which is shown in equation 4-26.

$$U(r,\omega) = \frac{P(\omega)\exp(-i\phi_0(\omega))}{4\pi v D} \frac{1}{r} \exp\left[-k(\omega)r\right] \qquad [4\text{-}26]$$

with:

$$k^2(\omega) \equiv \frac{\mu_a}{D}\left(1 - i\frac{\omega}{v\mu_a}\right) \qquad [4\text{-}27]$$

Equation 4-26 represents a spherical photon density wave propagating from the source (Fishkin & Gratton, 1993). Photon density waves are coherent scalar fields representing the local photon density at a certain point in time. The wave attenuates (even in the case of no absorption) exponentially with r. The phase velocity of the wave front is proportional to the source modulation frequency, and the wavelength is dependent on the modulation frequency and the scattering properties of the medium.

Increasing the scattering of the medium will actually decrease the wavelength of the photon density wave (Fishkin *et al.*, 1991). This is useful for using photon density waves to perform imaging in scattering media. The more highly scattering the medium, the greater the spatial resolution of the photon density wave. There has been

a lot of work recently on the use of photon density waves for imaging in scattering media (Boas *et al.*, 1997; Wabnitz & Rinneberg, 1997; Sevick-Muraca *et al.*, 1997).

4.8 Boundary conditions

The exact solution of the diffusion equation depends on the form of the boundary conditions applied to it. The solution shown previously assumed the *infinite medium* boundary condition. This is a situation where the scattering medium extends in all directions indefinitely. The proper choice of boundary condition is important with the use of the diffusion equation in photon migration studies, especially as one starts modelling scattering media with multiple layers (Martelli *et al.*, 2002).

The infinite-medium boundary condition is the simplest and easiest to work with. However as with all simple cases, its usefulness is limited as there are few real-world situations where a scattering medium extends indefinitely. Note that since the photon density wave attenuates exponentially with the distance from the source, a medium that extends at least several tens of mean free paths from the source in all directions should be adequate. Most researchers using the infinite medium geometry tend to use large volumes of medium to ensure the validity of the diffusion equation in this regime.

The infinite-medium boundary condition has been successfully used in this way to measure the optical properties of liquids such as raw milk (Cerussi, 1999), skim milk and India ink mixtures (Fishkin *et al.*, 1991), Liposyn intravenous fat emulsion (Fantini *et al.*, 1994) and a mixture of acrylic-styrene hollow spheres and water (Gerken & Faris, 1999).

A more useful geometry is the *semi-infinite medium*. Like the infinite-medium geometry, it also has a general solution. The semi-infinite medium geometry differs to the infinite medium only in that it has a single boundary – that is, it is a scattering medium that extends in all dimensions except one.

There are three recognised boundary conditions that have been used for the semi-infinite medium (Patterson *et al.*, 1991a). They are the partial-current boundary condition, the zero-fluence boundary condition and the extrapolated boundary condition. These will be only briefly covered along with some of the newer multi-layer geometries, since the infinite medium will be our geometry of choice due to the ease of obtaining large volumes of milk.

4.8.1 Partial Current Boundary Condition

According to Keijzer *et al.* (1988), the most correct way to model an interface is to use the *partial current* boundary condition.

The partial-current boundary condition takes into account the reflection at an index-mismatched boundary. This adds an extra condition to the treatment of boundaries that was discussed when constructing the Boltzmann transport equation. Once photons have left the volume of interest, they are lost forever. In this case, not all photons are lost.

Since the angular photon density at all points in the medium is deemed to be isotropic, it is valid to state that the flux exiting the medium at the boundary is simply equal to the photon density at the boundary. The Fresnel reflection coefficient determines the amount of energy reflected back into the medium.

(Haskell *et al.*, 1994) show that the reflected photon density is:

$$U_{reflected} = R_{eff} U_{emitted} = R_{eff} \iint_{\hat{\Omega}\cdot\hat{n}>0} u(\hat{\Omega})\hat{\Omega}\cdot\hat{n}d\Omega = R_{eff}\left(\frac{U}{4} - \frac{j_z}{2}\right) \qquad [4\text{-}28]$$

where $\hat{n}$ is the outward-bound normal vector to the boundary in the $-z$ direction and j_z is the outward-going flux. They went on further to evaluate the ratio of photon density to the magnitude of the photon current, and found that for perfectly transmitting boundaries, the ratio is 0.7, indicating that the diffusion equation may be inaccurate at modelling photon migration. However, an air-tissue interface showed a ratio of approximately 2.0, which they referred to as marginal. Compared to the infinite medium, where the ratio is close to 7, using the partial-current boundary condition with a small difference in refractive index can lead to problems. Conversely, boundary conditions that have a high index mismatch (or $R_{eff} > 0.95$) appear to mimic infinite-medium conditions. In fact, if the partial-current boundary condition is solved using the method of images, the solution returned for a perfectly reflecting boundary is that of the infinite medium (Haskell *et al.*, 1994).

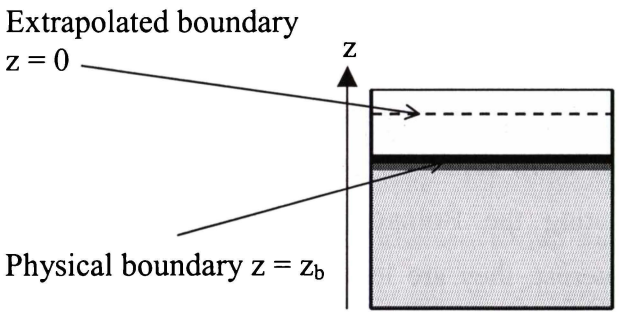

$U(0) = 0, \frac{dU(z)}{dz} = 0$ at $z = z_b$ for the extrapolated boundary condition

$U(z_b) = 0$: zero fluence boundary condition

Figure 4-6: Zero fluence and extrapolated boundary conditions

4.8.2 Zero Fluence Boundary Condition

The zero-fluence boundary condition shown in Figure 4-6 is analogous to having a strongly absorbing container for the medium. Haskell *et al.* (1994) have shown that this can cause errors of up to 15% in the recovery of the optical coefficients. Most importantly in terms of practical application is that if the photon density is zero at the boundary (which for biological tissues could be skin), a detector placed there will not measure anything.

This boundary condition is unphysical, and violates the diffusion approximation in that the photon density is highly anisotropic at the boundary. However, this condition allows for the solution of the diffusion equation via the method of images (Patterson *et al.*, 1991a).

4.8.3 Extrapolated Boundary Condition

The extrapolated-boundary condition (also shown in Figure 4-6) is a compromise between accuracy and correctness. It is a physically possible situation, which can also be solved by the method of images (Patterson *et al.*, 1991a).

In this case, the photon density becomes zero at a point $z = 0$ outside the physical boundary $z = z_b$. Haskell *et al.* (1994) found this model to be almost indistinguishable from the partial current model, so due to its relative simplicity, it is the semi-infinite geometry model of choice.

4.8.4 Other boundary conditions

Various extensions of the basic semi-infinite geometry have been presented in the literature. The first is the slab geometry, which is a simlar to the semi-infinite medium but with a finite thickness. Star (1989) compared a higher (P_3) transport approximation against the diffusion approximation using this geometry. Kaltenbach and Kaschke (1993) have also studied the slab geometry and shown that it has good agreement for a detector placed on the surface.

Later studies have extended the boundary conditions with the introduction of two-layer semi-infinite models. Franceschini *et al.* (1998) found that for a semi-infinite medium when the top layer was less than 0.4 cm thick, the measured optical coefficients were representative of the underlying layer. If the layer was more than 1.3 cm thick however, the optical coefficients were more representative of the top "superficial" layer. Alexandrakis *et al.* (2001) further studied two-layer diffusion boundary conditions. One of the key principles behind their work was that these superficial layers may be thin enough so that diffusion theory may not apply. Their solution was a hybrid model, diffusion theory combined with Monte Carlo simulations. The Monte Carlo technique successfully modelled the thin top section accurately with the diffusion theory model accounting for the underlying layer.

4.9 Problems with the use of the diffusion approximation

There have been studies in the literature that point to the diffusion approximation as an unsuitable model for highly scattering media under certain circumstances. Apart from the limitations presented in the previous section, studies have shown that the theory itself may have fundamental problems. These problems will now be reviewed and whether or not they could pose any significant issues for the work in this thesis examined.

The first question is general – when does the diffusion approximation no longer accurately describe photon migration in a highly scattering medium? A study by Yoo *et al.* (1990) showed that diffusion theory is only accurate when the thickness (z) of the medium divided by the transport mean free path length (l_t) is much greater than unity ($z/l_t >> 1$) for a transmission measurement where the source and detector are facing each other through the sample. When z/l_t decreased below 10, diffusion theory predicted photon arrival times that were slower than what was observed, leading to

the conclusion that there may be ballistic transport involved. However in an infinite medium situation, z/l_t is much greater than 10 in all cases.

Fantini *et al.* (1997) showed that the Green's function solution of the diffusion equation did not describe accurately the phase and steady-state ($\omega = 0$) amplitudes at small source-detector distances. The reason for this was partially due to the non-ideal nature of a real photon source. Changing the model of the source did not help much. However, they state that the effective photon source dimension in this case was of the order of the diffusion length, or the distance after which photon migration becomes diffusive. This is important because the Green's function solution to the diffusion equation is accurate at distances greater than the effective photon source dimension. In an infinite medium geometry, setting up the detector so that this condition is met is trivial.

Another question raised in the literature is whether the diffusion coefficient D has any dependence on absorption or whether they are truly independent. The formal definition of D from diffusion theory is $D = \frac{1}{3(\mu_s' + \mu_a)}$, so it would appear that there is a dependence on absorption. However, recalling that one of the conditions for the use of the diffusion equation is that scattering must dominate absorption, or $\mu_s' >> \mu_a$. Durduran *et al.* (1997) concluded that removing the dependence on the absorption coefficient from D could increase the accuracy of the diffusion equation from approximately 10% to better than 1%. However, several other researchers (Chen *et al.*, 2001) have since shown that Durduran's approach was flawed, and that the diffusion coefficient does have some dependence on absorption. Since the absorption coefficient of milk (in the visible red and near infra-red parts of the spectrum) is at least two orders of magnitude lower than the scattering coefficient, it is not a relevant question.

The final question is whether diffusion theory can satisfactorily cope with all the situations that are presented to it. Hielscher *et al.* (1998) concluded that diffusion theory is insufficient in highly absorbing regions and also in regions where there are *both* low scattering and low absorption coefficients. That research involved a comparison between finite-difference simulations of pure transport theory versus diffusion. A similar study by Chen *et al.* (2001) added the condition that the refractive

indices at the boundaries of the medium and the source and detector must be matched for accurate and predictable results. The refractive index condition is not an issue with cow's milk as the infinite-medium conditions can be used, and thus refractive index mismatches will not affect the results. However, the case of low scattering *and* low absorption could possibly cause problems with photon migration measurements in milk.

4.10 Diffusion Theory and Fluorescence

A highly scattering medium that satisfies the requirements for the valid use of the diffusion equation may also contain fluorophores. A fluorophore will absorb a photon at a wavelength λ_x and after a certain delay (referred to as the *fluorescence lifetime*)

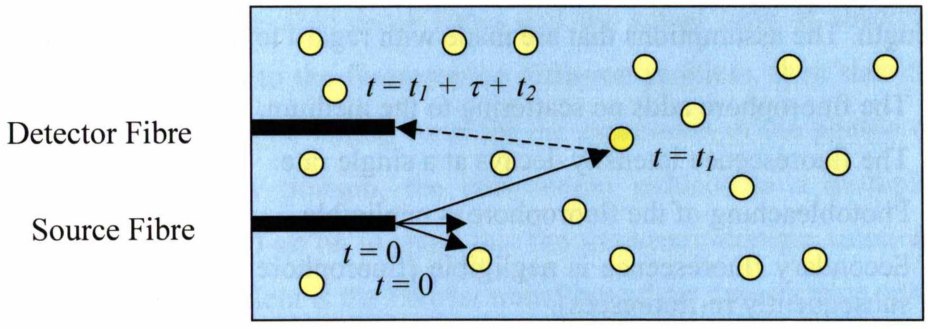

○ Fluorophore – each one of these can emit light at λ_x.

Figure 4-7: Fluorophores distributed throughout a scattering medium

will emit a photon at a wavelength λ_m. Note that the optical coefficients may have different values for different wavelengths (Cerussi *et al.*, 2001).

Assuming that the fluorophores are evenly distributed throughout the medium, it is clear that there will be multiple light sources – one for the excitation light source and the rest due to the fluorophores distributed throughout the medium. Figure 4-7 shows this.

At $t = 0$, a photon at wavelength λ_x emerges from the source fibre. After travelling t_1, the photon is absorbed by a fluorophore. After a time delay τ, a photon of wavelength λ_m is emitted and makes its way back to the detector after a transit time ot t_2. The total time taken for this trip is $t_1 + \tau + t_2$.

There will be at least two photon density waves in a medium with fluorophores. The first is the normal photon density wave from the excitation source and the second wave is from the distributed fluorophores. There will be N+1 waves for N fluorophores in the medium. In order to model this at the detector (so that we know what we are detecting), the terms in the standard diffusion equation require some modification.

Cerussi (1999) contains a derivation of the fluorescence photon migration theory based on uniformly distributed fluorophores in a scattering medium. The main points of this derivation will be reviewed here, with the similar notation used throughout. This theory is basis of the experimental work described in chapter 6.

A good start is to review the definition of the absorption coefficient. Since we are now adding a fluorophore to the medium, it will have an absorption peak at its excitation wavelength. The assumptions that are made with regard to the fluorophore are:

1. The fluorophore adds no scattering to the medium.
2. The fluorescence intensity decays at a single rate.
3. Photobleaching of the fluorophore is negligible.
4. Secondary fluorescence is negligible (fluorophore absorbs emission light and subsequently re-fluoresces).

The new absorption coefficients for N fluorophores at the excitation wavelength (subscript x) can be written as:

$$\mu_{ax} = \mu_{abx} + \sum_{n=1}^{N} \mu_{afxn} \qquad [4\text{-}29]$$

The new absorption at the excitation wavelength is a combination of the absorption by the medium (subscript b) and the fluorophores (subscript f). The emission wavelength undergoes a similar treatment, but with the subscript m for emission:

$$\mu_{ax} = \mu_{abm} + \sum_{n=1}^{N} \mu_{afmn} \qquad [4\text{-}30]$$

The excitation source for the fluorophores will be the photon density wave from the original source. That means that the source term for the *fluorescence photon density wave* will be the solution to the single-source diffusion equation, or equation 4-26:

$$U(r,\omega) = \frac{P(\omega)\exp(-i\phi_0(\omega))}{4\pi vD}\frac{1}{r}\exp[-k(\omega)r]. \qquad [4\text{-}26]$$

The emission source distribution for the fluorophore will be proportional to the excitation photon density at r and t, and also to the quantum yield (Λ_j). Since the probability per unit time for an absorption event to occur in the medium containing fluorescent species j is $v\mu_{afx_j}$, the emission strength must scale according to $v\mu_{afx_j}\Lambda_j U(r,\omega,t)$. The emission strength at any wavelength influences the emission spectrum. Since fluorescence emission is not strictly monochromatic, another quantity known as *emission spectral efficiency* $\varphi_{m_j}(\lambda)$ shall be introduced here. This is written as a probability density normalised to unity. If the fluorophore is going to radiate, it must do it at some wavelength.

The lifetime τ_j of the fluorophore causes a temporal delay in the fluorescence emission. According to Patterson & Pogue (1994), this delay manifests as a convolution between all possible decay times and the actual time of absorption. In their time-domain solution to the fluorescence diffusion problem, they state that due to this convolution, there is no closed form for the expression of the photon density. However in the frequency domain, the convolution reduces to a multiplication. Patterson and Pogue (1994) go on to show that the frequency-domain solution to the fluorescence diffusion problem is the Fourier transform of the time-domain solution.

With all that in mind, the emission photon source within a wavelength range $d\lambda$ is (Cerussi *et al.*, 1997):

$$dQ_{m_j}(r,\omega,t) = d\lambda\varphi_{m_j}(\lambda)\int_0^\infty d(t-t')\Lambda_j v\mu_{afx_j}U_x(r,\omega,t')\frac{1}{\tau_j}\exp\left[-\frac{t-t'}{\tau_j}\right] \qquad [4\text{-}31]$$

Substituting $\Delta t = t - t'$ and then evaluating the integral gives:

$$dQ_{m_j}(r,\omega) = d\lambda\varphi_{m_j}(\lambda)\Lambda_j v\mu_{afx_j}U_x(r,\omega)\frac{1+i\omega\tau_j}{1+(\omega\tau_j)^2} \qquad [4\text{-}32]$$

With this source term for the fluorescence photon density wave, one can now evaluate the total emission photon density for a given fluorophore by the spatial convolution of the source term with the Green's function solution of the diffusion equation (equation 4-26), which eventually gives:

$$dU_{m_j}(r,\omega) = d\lambda\ \Lambda_j\ \mu_{afx_j}\varphi_{m_j}(\lambda)\frac{P_x(\omega)\exp[-i\phi_{x0}(\omega)]}{4\pi D_m D_x}\left(\frac{1+i\omega\tau_j}{1+(\omega\tau_j)^2}\right)\times$$

$$\frac{1}{r}\frac{\exp[-k_x(\omega)r]-\exp[-k_m(\omega)r]}{k_m^2(\omega)-k_x^2(\omega)} \qquad [4\text{-}33]$$

Jiang (1998) writes his solution to the fluorescence photon migration problem (using Cerussi's notation) as:

$$\nabla\cdot[D_m\nabla U_m(r,\omega)]-\left[\mu_{afm}-\frac{i\omega}{c}\right]\phi_m(r,\omega)=-\Lambda_j\mu_{afx}\phi_x(r,\omega)\frac{1+i\omega\tau}{1+\omega^2\tau^2} \qquad [4\text{-}34]$$

This shows that if it is assumed (or make sure) that our distribution of excitation wavelengths is narrow, with an identical condition for the emission wavelengths, then it can be treated in the same way as a non-fluorescent photon density wave. Taking the real and imaginary parts of the right hand side of equation 4-34 give expressions for the detected amplitude and phase, respectively.

If there is more than one fluorophore in the medium and it is assumed that both fluorophores do not interact with each other, then one can linearly add the contributions of the different fluorophores together. The wave vectors k_m and k_x depend only on the total absorption characteristics of the medium. The homogeneous distribution of the flurophores throughout the medium also ensures no dependence on r. Thus, the photon density waves from each of the fluorescent species in the medium can be simply added together.

4.11 The Detected Photon Density

Cerussi goes on to consider the contribution that the photon detector makes to the measured result. Thus, if there is a detector with a spectral response of $\gamma(\lambda)$, then at any point r, the photon density as measured by the detector will be:

$$U_m(r,\omega)=\int_{\lambda_m-\frac{\Delta\lambda}{2}}^{\lambda_m+\frac{\Delta\lambda}{2}} dU_m(r,\omega)\gamma(\lambda) \qquad [4\text{-}34]$$

Evaluating this integral yields the total detected photon density:

$$U(r,\omega)=\frac{P_x(\omega)\exp[-i\phi_{x0}(\omega)]}{4\pi v D_x D_m}\frac{1}{r}\frac{\exp[-k_x(\omega)r]-\exp[-k_m(\omega)r]}{k_m^2(\omega)-k_x^2(\omega)}\times$$

$$\sum_{j=1}^{N}\left(\frac{1+i\omega\tau_j}{1+(\omega\tau_j)^2}\right)\Lambda_j\mu_{afx_j}\phi_{m_j} \qquad [4\text{-}35]$$

This equation can be easily split into its three constituent parts – a *spatial* term (contains r dependence), a *lifetime* term (contains all appearances of τ) and a *yield and source* term (contains source terms and Λ).

Since the emission photon density is a convolution between the emission and excitation photon density waves, the phases associated with each of the emission photon density waves *do not add linearly*. The signal from the detector will be the emission photon density wave(s) plus the excitation photon density wave. As there will not often be much interest in the excitation photon density wave for fluorescence work, a method of removing the contribution from the excitation photon density wave will be required. An example of such a method is to use an optical filter whose pass band is outside the range of the excitation wavelength.

Fluorescence photon migration has been used extensively in the biomedical optics field, especially for the location of tumours. Paithankar *et al.* (1997) demonstrated the ability to recover the fluorescence lifetime and bulk optical properties of tissue using fluorescence frequency-domain photon migration methods. Roy & Sevick-Muraca (2001) used a fluorescence diffusion model to locate fluorescent inhomogeneities in a turbid medium. The fluorescence in this case is used as a contrast agent for locating the inhomogeneities. Nair *et al.* (2002) also performed measurements on human breast tissue using fluorescence diffusion methods to obtain the optical properties of the tissue.

4.12 Summary

In this chapter, different ways of modelling bulk photon propagation in highly scattering media have investigated. Their suitability for our work has been examined and the diffusion approximation to the Boltzmann transport equation has been chosen due to its ability to provide an analytical solution (even though it is approximate) and its convenience. The nature of milk allows that theory to be used extensively.

One important result from the choice of this theory is that the scattering and absorption components of a medium can be resolved *independently* of each other.

5 Experimental Materials and Method

The purpose of this chapter is to introduce the methods and materials involved in the measurements that will be presented in the next chapter. First, a review of how the diffusion equation has been used by other researchers (and consequently by ourselves) to recover the scattering and absorption coefficients from a highly scattering medium will be shown. An explanation of the materials used and the construction of the experimental equipment, as well as a description of the methods used to obtain milk samples follow this.

5.1 Measurement Theory and Practice

5.1.1 Obtaining results using the Diffusion Equation

In the previous chapter, the diffusion approximation to the Boltzmann Transport Equation was derived and solved using a Green's function. As stated, the Green's function solution to the diffusion equation is of the form of a wave, and has wave characteristics. The purpose of this section is to show exactly how to use that solution to obtain measurable parameters than can be related to the optical coefficients of the medium in question.

The solution given in equation 4-26 is repeated here for clarity:

$$U(r,\omega) = \frac{P(\omega)\exp(-i\phi_0(\omega))}{4\pi vD}\frac{1}{r}\exp[-k(\omega)r] \qquad [4\text{-}26]$$

The right hand side of this equation can be split up into two parts – one that includes the source terms (strength and phase), and the other with the frequency and distance terms. Equation 4-27 (the expression for the wave vector) is:

$$k^2(\omega) \equiv \frac{\mu_a}{D}\left(1 - i\frac{\omega}{v\mu_a}\right) \qquad [4\text{-}27]$$

The amplitude of the wave represented by equation 4-26 can be found by taking the modulus, while the phase of the wave is its argument. There is a third parameter of the wave that can be measured which is DC intensity or offset, which can give the same results (Fantini *et al.*, 1994). However for this work, only using AC amplitude and phase will be used as the DC intensity can be affected greatly by and background light that is present.

In order to show how the absorption and scattering coefficients are obtained, the notation and definitions used by Cerussi (1999) will continue being used. Derivations for the expressions for the phase and amplitude of the photon density wave that Cerussi used will also be shown. Substituting equation 4-27 into equation 4-26, and expanding gives:

$$U(r,\omega) = \frac{P(\omega)}{4\pi v D}\frac{1}{r}\exp\left(-r\sqrt{\frac{\mu_a}{D}\left(1 - i\frac{\omega}{v\mu_a}\right)}\right) \qquad [5\text{-}1]$$

The initial phase ϕ_0 is defined to be zero and so it is not included in the equation. The modulus and argument of equation 5-1 are:

$$|U(r,\omega)| = \frac{P(\omega)}{4\pi D v}\frac{1}{r}\exp\left(-r\left(\sqrt{1+\left(\frac{\omega}{v\mu_a}\right)^2}+1\right)^{1/2}\cdot\sqrt{\frac{\mu_a}{2D}}\right) \qquad [5\text{-}2a]$$

$$\arg[U(r,\omega)] = r\left(\sqrt{1+\left(\frac{\omega}{v\mu_a}\right)^2}-1\right)^{1/2}\cdot\sqrt{\frac{\mu_a}{2D}} + \phi_0(\omega) \qquad [5\text{-}2b]$$

To simplify the equation, it can be defined that:

$$V_{\pm} = \left(\sqrt{1+\left(\frac{\omega}{v\mu_a}\right)^2}\pm 1\right)^{1/2} \qquad [5\text{-}3]$$

From that, we can re-write equations 5-2a and 5-2b to get:

$$AC = |U(r,\omega)| = \frac{P(\omega)}{4\pi D v}\frac{1}{r}\exp\left(-rV_{+}\cdot\sqrt{\frac{\mu_a}{2D}}\right) \qquad [5\text{-}4a]$$

$$\phi = \arg[U(r,\omega)] = rV_{-}\cdot\sqrt{\frac{\mu_a}{2D}} + \phi_0(\omega) \qquad [5\text{-}4b]$$

Equation 5-4b is a linear equation in r. That means that the phase (ϕ) of the photon density wave can be measured against the source-detector separation distance. This is not quite so clear for the AC amplitude however, but it is relatively simple to transform. By multiplying the detected AC amplitude with the source-detector separation distance and then taking the logarithm, one can transform equation 5-4a into a linear equation in r as well:

$$\ln\left[r\cdot|U(r,\omega)|\right]=\ln\left(\frac{P(\omega)}{4\pi Dv}\right)-rV_{+}\cdot\sqrt{\frac{\mu_a}{2D}} \qquad [5\text{-}4c]$$

The DC intensity is the AC amplitude at zero modulation frequency. The entire factor $\frac{P(\omega)}{4\pi Dv}$ is the total DC contribution of the photon density wave and is ignored in the measurements performed in this work. The use of the AC amplitude and phase measurements at multiple source-detector distances allows for relative measurements normalised to the values of the first measurement. That is, the phase and amplitude measurement at the smallest source-detector distance is assumed to be unity, with subsequent measurements regarded as smaller fractions.

An intuitive view of how the changes in scattering and absorption will affect the values of phase and AC amplitude at the detector can be reached by examining the following points. Consider the case of increasing μ_s' while keeping μ_a constant. Increasing μ_s' increases the number of scattering events per distance travelled. This will increase the path length of the photons, and since the probability of absorption $v\mu_a$ is still the same per unit distance, the detected intensity will decrease. The increased path length of the photons will increase the phase lag at any point, thus causing an increased phase measurement.

The case of increasing μ_a while holding μ_s' constant is slightly different. Attenuation will increase, as before but the phase will decrease. Increasing μ_a increases the number of absorption events per distance travelled. Therefore, the longer path length photons that will cause an increased phase reading will have a higher probability of being absorbed, and are more likely not to be detected. Only the shorter path length photons will get to the detector, thus explaining the decrease in measured phase.

Measurement Method

In order to recover the optical coefficients, expressions for the absorption and the reduced-scattering coefficients need to be derived. To do that, equations 5-4c and 5-4b can be rewritten in a gradient-intercept form:

$$\ln\left[r\cdot|U(r,\omega)|\right]=-r\,M_{AC}(\mu_a,\mu_s',\omega)+\ln\left(\frac{P(\omega)}{4\pi vD}\right) \qquad [5\text{-}5a]$$

$$\phi = r M_{PH}(\mu_a, \mu_s', \omega) + \phi_0(\omega) \qquad [5\text{-}5b]$$

M_{AC} and M_{PH} are the amplitude and phase gradients. They contain expressions for μ_s' and μ_a, the desired optical coefficients. The most useful feature of these equations is that the source terms (source phase and intensity) are only in the intercept terms. This will allow the recovery of the optical coefficients with *relative measurements* only.

Solving equations 5-5a and 5-5b for μ_a and μ_s' gives (Fantini *et al.*,1994):

$$\mu_a = \frac{\omega}{2v}\left[\frac{M_{PH}}{M_{AC}} - \frac{M_{AC}}{M_{PH}}\right] \qquad [5\text{-}6a]$$

$$\mu_s' = \frac{(M_{AC})^2 - (M_{PH})^2}{3\mu_a} \qquad [5\text{-}6b]$$

These are expressions for the absorption and reduced-scattering coefficients of a scattering medium, obtainable by measurements at multiple source-detector distances. The optical coefficients are also recoverable by a multiple-frequency measurement (Madsen *et al.*, 1994). However the multiple-frequency fit is non-linear (Cerussi, 1999) which leads to the multiple-distance method being preferable.

The errors in the absorption and reduced-scattering coefficients can be calculated using the expressions given by (Fantini *et al.*, 1994):

$$\frac{\Delta\mu_a}{\mu_a} = \frac{\alpha^2 + \varphi^2}{\alpha^2 - \varphi^2}\left[\frac{(\Delta\varphi)^2}{\varphi^2} + \frac{(\Delta\alpha)^2}{\alpha^2}\right]^{1/2} \qquad [6\text{-}1]$$

$$\frac{\Delta\mu_s'}{\mu_s'} = 2\left\{\frac{\alpha^2(\Delta\alpha)^2 + \varphi^2(\Delta\varphi)^2}{2\left(\alpha^2 - \varphi^2\right)^2} + \frac{(\Delta\rho)^2}{\rho^2} + \left[\frac{\alpha^2 - \varphi^2 + 3\mu_a{}^2\rho^2}{2\left(\alpha^2 - \varphi^2\right)}\right]^2 \frac{(\Delta\mu_a)^2}{\mu_a{}^2}\right\}^{1/2} \qquad [6\text{-}2]$$

where α is the slope of the amplitudes at different source-detector distances, φ is the slope of the phase readings at different source-detector distances, and ρ is the source-detector interval distance (the distance between successive source-detector positions).

5.2 Equipment Used

The equipment for the experimentation was designed with the following objectives in mind. Firstly, the equipment had to be able to make the multiple-distance measurement. Secondly, the equipment had to have been built with with low

component cost in mind. Thirdly, simplicity and versatility were important factors in the design.

The first choice is whether to make an instrument based on time-domain measurements or frequency-domain measurements. The time-domain measurement methods are easier to visualise and understand in terms of our intuitive understanding of how photons travel through highly scattering media. The time-domain solution for the diffusion equation for an infinitely short pulse is:

$$U(r,t) = (4\pi vDt)^{-3/2} \exp\left[-\frac{r^2}{4Dvt} - \mu_a vt\right] \qquad [5\text{-}7]$$

This is equivalent to the Fourier transform of the frequency-domain solution to the diffusion equation (Patterson *et al.*, 1989).

Recovery of the optical coefficients of a medium is achieved by fitting equation 5-7 to the detected pulse after it has been injected into the medium. Figure 5-1 shows the expected distribution of the different types of photons at a detector after a very short pulse has been fired into the medium.

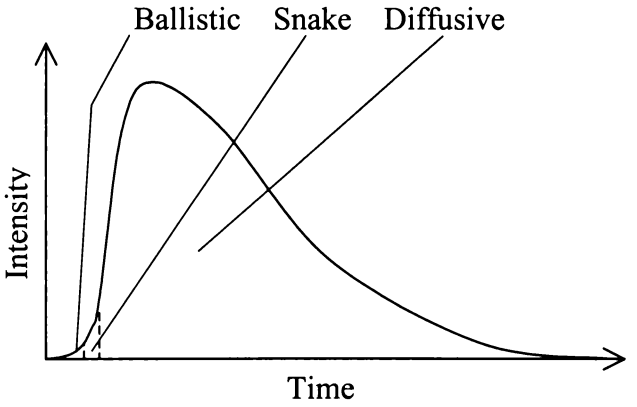

Figure 5-1: Temporal profile the detected photons from a very short pulse fired into a highly scattering medium.

The time scale represented in Figure 5-1 is of the order of nanoseconds. Therefore the equipment required for time-domain measurement must be capable of operating at high speeds. The light pulse source must be able to generate intense sub-nanosecond light pulses to approximate an infinitely short pulse. The detector must be able to clearly resolve light pulses at sub-nanosecond timing in order to resolve the shape of the curve properly. Equipment like this is expensive, making measurements in the

time-domain un suitable for the incorporation into a low-cost and portable instrument for use on a farm.

With cost constraints ruling out the use of time-domain measurements, frequency-domain measurements must be considered. The equipment for frequency-domain measurements is less expensive mainly due to the lower bandwidth. The upper limitation to the modulation frequency is due to the limitations of the diffusion equation. That frequency is in the 1 GHz region and depends on the exact characteristics of the medium, as mentioned in chapter 4.

Modulation frequencies as low as 40 MHz have been used (Fishkin *et al.*, 1991). Equipment capable of generating 40 MHz signals and optical detectors capable of responding to 40 MHz modulation frequencies are relatively inexpensive and common. In particular, this low bandwidth requirement has opened up the use of light emitting diodes (LEDs), with their wide range of wavelengths, as a light source.

Other advantages of a frequency-domain instrument are:

- Rapid (and continuous) measurements may be performed as there is sufficient information in a single modulation frequency to obtain the optical coefficients.
- The time-domain approach does not have an analytical solution to the fluorescence-diffusion problem (Patterson & Pogue, 1994). This is important for fluorescence lifetime measurements.
- The diffusion equation does not properly predict the characteristics or the arrival times of ballistic and snake photons. In the frequency-domain, this information is not important. The contribution of these early photons in time-domain experiments could skew the recovery of the optical coefficients.

The choice of operating in the frequency-domain is clear in this case. The next thing one can do, is to look at how a frequency-domain instrument is set up.

Figure 5-2 shows a block diagram of the two different types of basic photon migration instrument – *homodyne* and *heterodyne* types.

A homodyne instrument modulates and receives at the same frequency, without an intermediate frequency. A heterodyne instrument introduces a second modulation frequency, and at some stage in the instrument, the two frequencies are mixed. This mixing produces an output that is the difference of the two frequencies, thus relaxing the requirements of the signal processing side of the instrument. Mixing the two waves is the same as multiplying them together, so the signal can written this as:

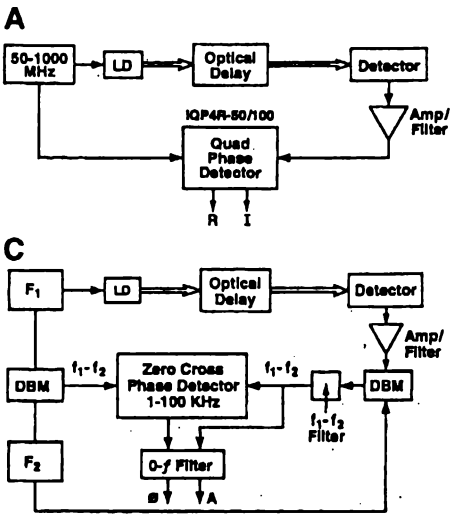

Figure 5-2: Block diagrams of homodyne and heterodyne photon migration instruments. (A) is a homodyne system with quadrature outputs R and I while (C) is a heterodyne system with phase and amplitude outputs (Chance *et al.*, 1998).

$$A_1 \sin(\omega_1 t + \phi_1) \times A_2 \sin(\omega_2 t + \phi_2) =$$

$$\frac{1}{2} A_1 A_2 [\cos((\omega_1 - \omega_2)t + (\phi_1 - \phi_2)) - \cos((\omega_1 + \omega_2)t + (\phi_1 + \phi_2))] \qquad [5\text{-}8]$$

Equation 5-8 shows that there are two sections in the expression on the right hand side of the equation. The term on the left is the difference term and contains the *difference* between the two frequencies and also the difference between their *phases*. The term on the right contains the sums of the phases and the frequencies. If both modulation frequencies are close in value to each other, the contribution from the right hand side can be removed by careful filtering. This mixing allows the use of higher precision recording equipment with a slower response. This includes the use of digital-to-analogue converters with sampling rates in the kHz range and up to 16 bits of precision for further digital signal processing to recover the phase and intensity values.

Typical values chosen for the difference in modulation frequencies are in the range of about 1 kHz or less per 100 MHz. Shinde *et al.* (1999) used a difference in frequency

of 100 Hz. The mixing of two frequencies was achieved by modulating the gain of the photomultiplier tube used in their experiment. Cerussi (1999) used a modulation frequency of 76.2 MHz and a frequency difference of 400 Hz. Mixing of the two frequencies was also achieved by the gain modulation of the photomultiplier tubes used as detectors.

The homodyne system is much simpler in concept and in implementation, but suffers from crosstalk between the source frequency generator and the detector. This will be discussed later on. Despite the crosstalk problem, homodyne frequency domain photon migration systems are still being used (Alexandrakis *et al.*, 2001).

The heterodyne system has the advantage of easier use with digital sampling equipment due to the lowering of the output frequency signal from the mixing. Increased accuracy is another advantage, due to the lower detector bandwidth required (Chance *et al.*, 1998). However, heterodyne instruments are more complex and require a greater number of components, which leads to greater cost.

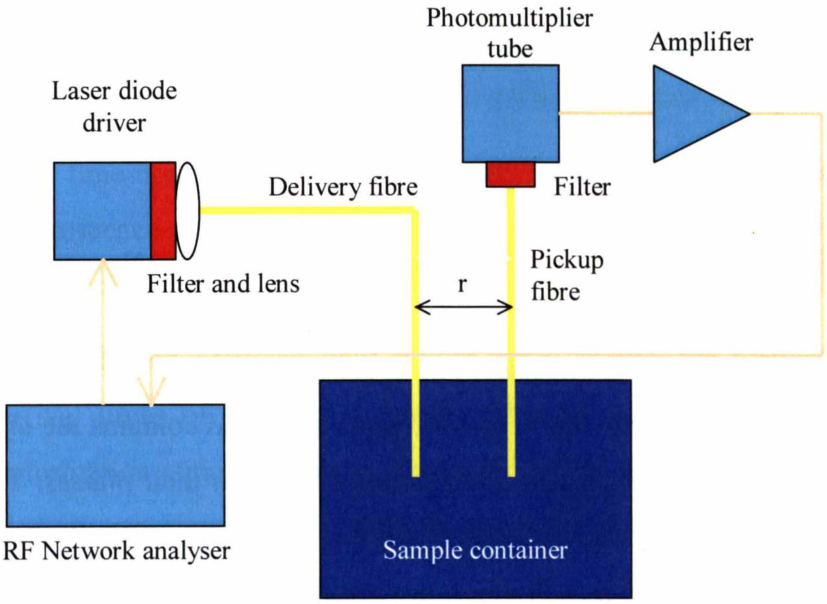

Figure 5-3: Photon migration instrument design.

The instrument type chosen for the experimental work here was the homodyne instrument for its simplicity, relative low cost compared to a heterodyne instrument, and ease of construction. Figure 5-3 shows the overall concept of the instrument used in this work and the details of how signals flow to and from each component.

With reference to Figure 5-3, one can now go through the individual components that make up the photon migration instrument. As noted previously, the homodyne photon migration instrument has a certain number of disadvantages to it. These disadvantages and how they have been overcome will be addressed later in this chapter.

5.2.1 Signal source and processing

The signal source used in our experiments was a radiofrequency (RF) network analyser (8712ET, Agilent, Palo Alto, California, USA). This bench-top instrument is capable of a frequency range from 300 kHz up to 1.3 GHz and an output power range from -2.00 dBm to 23.00 dBm.

As well as having a signal output, this instrument has a signal input. Typically, the RF network analyser is used to measure the RF performance characteristics of a device. This is done by connecting the device under test to the output terminal of the RF network analyser and then connecting its output to the input terminal of the RF network analyser, as shown in Figure 5-4.

The RF network analyser is capable of measuring amplitude, phase, delay and frequency response characteristics of the device under test. The quantities of most

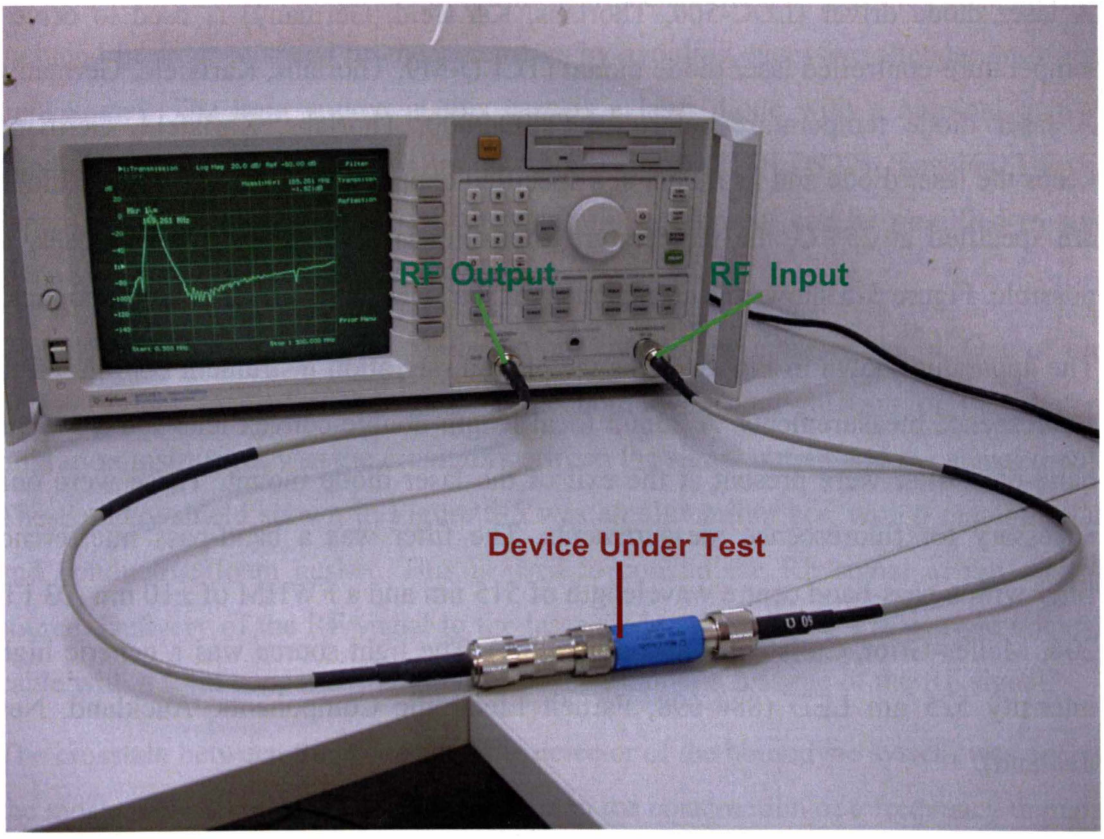

Figure 5-4: Agilent 8712ET example usage.

interested were the amplitude and phase. Error values for the RF network analyser are 0.03 dB peak-to-peak and 0.2 degrees peak-to-peak for amplitude and phase respectively (Agilent Technologies, 2000).

In Figure 5-4, the device under test is a filter and the display is showing its frequency response curve. The photon migration instrument built for these experiments was of the same basic form, except that the light source, sample and detector have replaced the device under test.

The RF network analyser can also perform post-processing of the received signal. As mentioned, it is capable of measuring the phase and amplitude of the signal presented at its input. Before the final phase and amplitude signals are displayed, the signal is averaged over 64 samples. The averaging allows for greatly increased accuracy and precision at the cost of increased sampling time. Due to the averaging, intermittent bursts of interference will not adversely affect the measured results. This is helpful for the use of the photon migration instrument in electrically noisy environments such as a dairy parlour.

5.2.2 Light source and delivery

A laser diode driver (LDC-500, Thorlabs, Karlsfeld, Germany) is used to drive a temperature-controlled laser diode mount (TCLD-M9, Thorlabs, Karlsfeld, Germany). A laser diode temperature controller (TEC-2000, Thorlabs, Karlsfeld, Germany) keeps the laser diode and its mount at a specified temperature. Since most laser diodes are specified at 25° C, the temperature controller is set to keep that as closely as possible. Figure 5-5 shows the arrangement of the laser diode driver and other optics.

The apparatus shown in Figure 5-5 is the photon migration instrument configured for fluorescence measurements. A 25mm focal length double-convex lens and a 515 nm band-pass filter were present at the exit of the laser diode mount. These were only necessary for fluorescence measurements. The filter was a band-pass interference filter with a pass-band centre wavelength of 515 nm and a FWHM of ±10 nm (03 FIL 204, Melles-Griot, Carlsbad, California, USA). The light source was a generic high-intensity 525 nm LED (884-698, Farnell Electronic Components, Auckland, New Zealand).

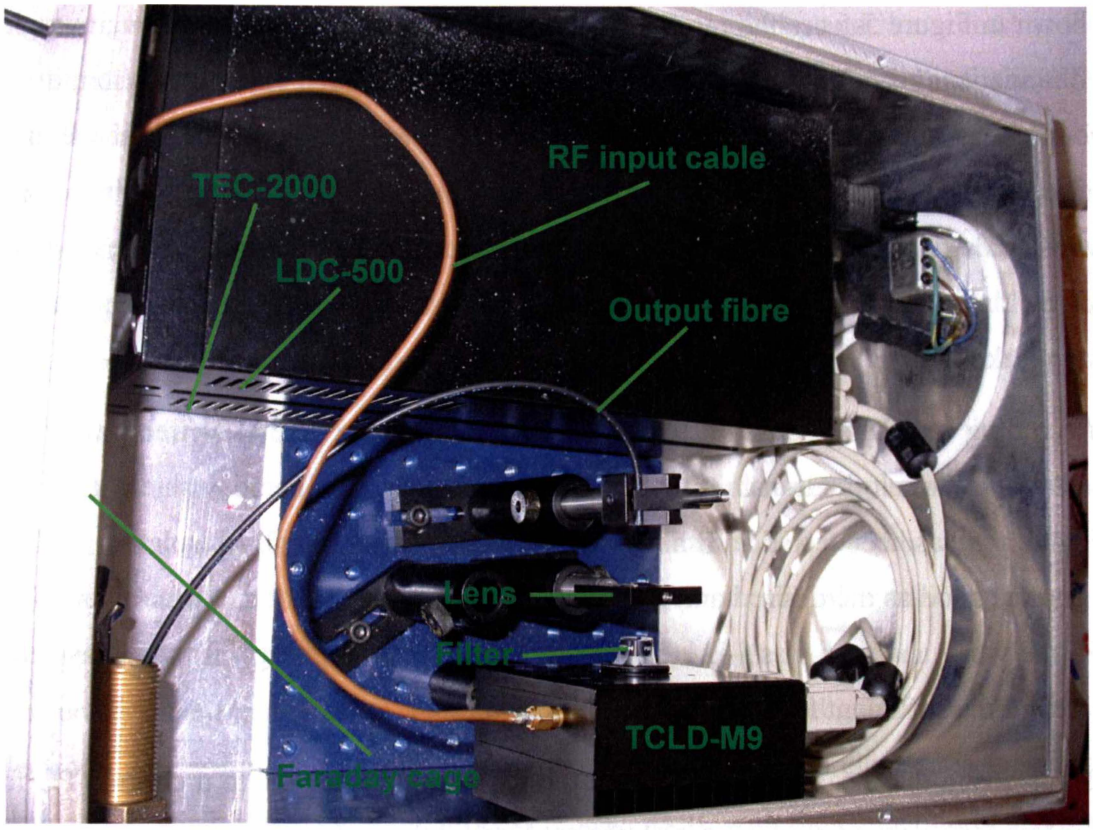

Figure 5-5: Light source assembly (refer Figure 5-3 for schematic).

For non-fluorescence photon migration measurements, the lens and the filters are not included in order to speed up measurements by avoiding excessive attenuation of the light signal. The light source in this case is a laser diode with a nominal 5 mW maximum power output and 670 nm output wavelength (TOLD9221, Toshiba, Tokyo, Japan). This highlights the ease with which the equipment can be modified to suit different types of experiments.

One striking feature of Figure 5-5 is the presence of the Faraday shield. One of the biggest issues to deal with regarding the homodyne configuration of the photon migration instrument was the crosstalk between the signal output and the signal input. The Faraday shield shown in Figure 5-5 was an aluminium box with a matching lid and conductive foam gasket. This is used to contain the RF signal at the optical source. Delivery of the RF signal to the laser diode mount is via a semi-rigid coaxial cable with a solid copper sheath, thus ensuring minimum leakage of the RF signal.

The crosstalk between the source and the detector of the homodyne system was one of the most challenging problems to overcome in the construction of a frequency domain photon migration instrument. The Faraday shield and semi-rigid coaxial cable that are

shown in Figure 5-5 are the result of several generations of evolution through various combinations of different types of shielded cable. After much experimentation, it was found that a solid metal shield with a single opening for cables was the only acceptable shielding solution. The single opening had to be fitted with a metal waveguide to make sure that no radiation from inside the Faraday shield leaked out. Using a waveguide is a well-known method employed in RF communications arena to stop leakage.

According to Chance *et al.* (1998), 120 dB of shielding is the desired amount of isolation between the transmitting and receiving stages. The Faraday shield shown in Figure 5-5 has been tested and shown to have greater than 100 dB of isolation – which is not as good as the desired amount. However, considering that the noise floor of the RF network analyser was –111 dB at its most selective settings, it was considered likely to be sufficient for the purposes of this work.

Transferring the measured results from the RF network analyser to a desktop PC for further data processing was straightforward using the in-built 3 ½ inch floppy disk drive. The RF network analyser exports its data as a set of comma delimited (CSV) files, which can be imported into a spreadsheet for analysis.

5.2.3 Detector

There are two types of detectors that would have been suitable for the photon

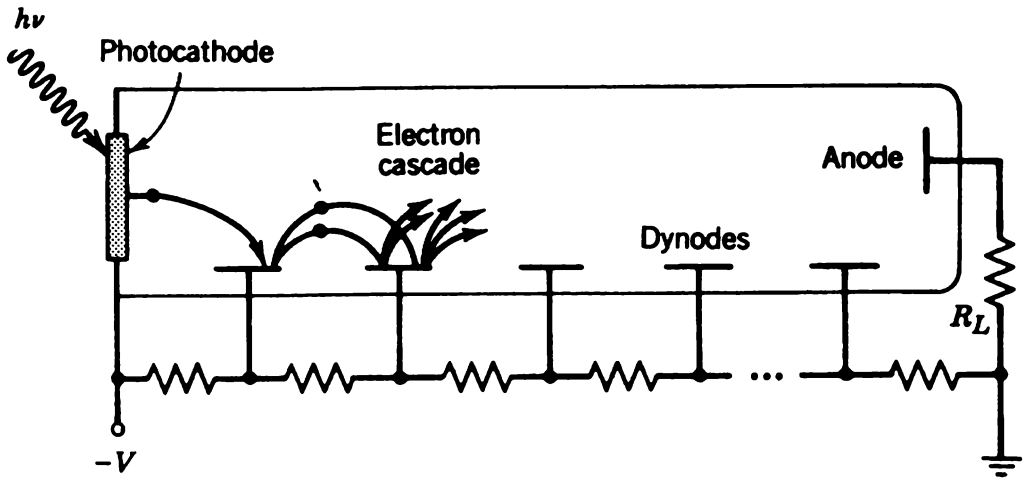

Figure 5-6: Principles of operation of a photomultiplier tube (Saleh & Teich, 1991).

migration experiments. The first is the avalanche photodiode, and the second is the photomultiplier tube. The avalanche photodiode is a device based on the PIN photodiode, but is made so that it can use much larger bias voltages to increase the gain of the photodiode. When a hole-electron pair is formed due to the absorption of a photon, the increased voltage accelerates them to the point that they cause other hole-electron pairs to be formed due to their kinetic energy. Typical gains obtainable from avalanche photodiodes are from between 50 and 200.

The photomultiplier tube works in a different way. Figure 5-6 shows the typical structure of a photomultiplier tube. Light is collected by the metal photocathode. The light striking the photocathode causes an electron to be ejected due to the photoelectric effect. One of the key features of the photomultiplier tube is the large voltage that must be supplied to it for it to achieve its high gain. This voltage accelerates the ejected electron, increasing its kinetic energy and guiding it to the next electrode, referred to as a *dynode*. The impact of the accelerated electron is sufficient to eject multiple electrons and the process repeats itself, with the collection of a single electron resulting in a cascade of up to several million electrons. The photomultiplier tube is capable of gains of more than 10^6. However, it is susceptible to damage from too much light.

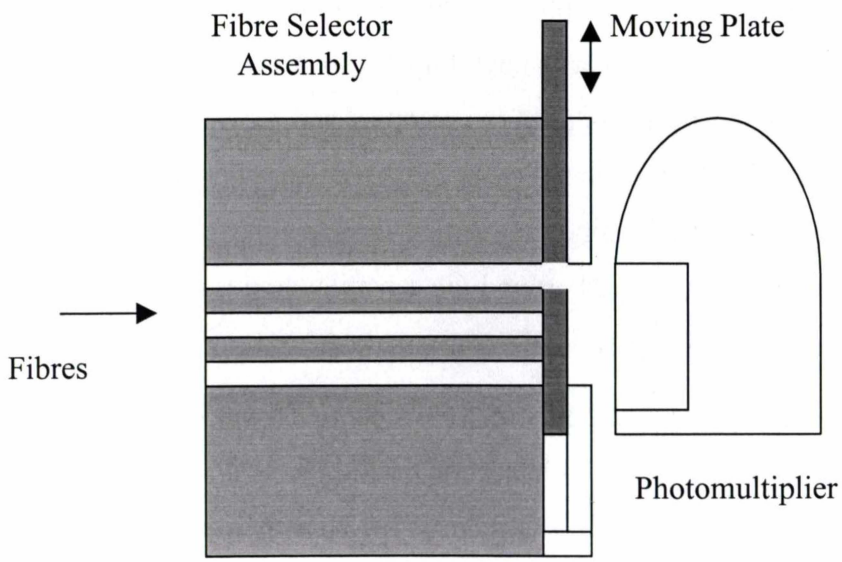

Figure 5-7: Photon migration instrument photomultiplier tube assembly.

The main aim of the detector was to produce the best signal possible for the amount of light that impinges on the detector. In photon migration problems, the amount of light available for detection is usually quite low. Due to this, the photomultiplier tube was the detector of choice in this case.

A photomultiplier tube was chosen for the photon migration instrument (R928, Hamamatsu, Hamamatsu City, Japan). Its main features are a gain of 10^7 and an effective wavelength range from 185 nm to 900 nm. At the wavelengths of interest for this work (600 to 700 nm), the quantum efficiency is between 4.5 and 9%. This equates to an anode sensitivity of approximately 4×10^5 A/W, which is sufficient. Several people have used this photomultiplier for photon migration experimentation, notably Ramanujam *et al.* (1998) and Cerussi (1999).

The photomultiplier is shown with its full working assembly in Figure 5-7. Up to three detector fibres were mounted on one side into a small block, allowing measurements at three different source-detector distances. A sliding panel on the other side ensured that only one fibre delivers light to the photomultiplier. This arrangement allowed the light to fall into the 8 mm × 24 mm light-sensitive area on the photomultiplier tube.

The output of the photomultiplier tube was fed into a current-to-voltage amplifier (HCA-100M-50K-C, Femto Messtechnik GmbH, Berlin, Germany). This was a shielded amplifier designed for photodiode or photomultiplier inputs. As suggested in its model designation, it has a bandwidth of 100 MHz, and a gain of 5×10^4. The physical construction of the amplifier is compact and robust. It has the appearance of a small rectangular block of metal, with the connectors for the signal and the power supply at the ends. This is important in that it means the amplifier is fully shielded, and since the shielding is solid around the sensitive amplification electronics, it does not need to reside inside an external Faraday shield.

The 5×10^4 gain was required so that sufficient signal level is seen at the input of the network analyser. However, with a gain of that magnitude, and the fact that the amplifier's frequency response was relatively constant from DC to 100 MHz meant that a strong DC light signal could have overpowered the small AC modulation signal. There are several ways to overcome this problem, usually by terminating the input into the amplifier with a 50 Ω resistor to ground. This has the disadvantage of halving

the amplitude of the measured signal as the amplifier will often also have a 50 Ω input impedance.

The best solution is one suggested by the manufacturer in one of their application notes. This involves the use of a 50 Ω termination resistor in series with a small inductor. The inductor allows the DC to pass through while blocking the AC component, which enters the amplifier unaffected. This solution is what the manufacturer refer to in their application notes (Femto Messtechnik GmbH, 1999) as the Bias-T configuration. Many of their amplifiers have the Bias-T incorporated into their design, but the HCA-100M-50K-C does not include it. For the instrument used, a Bias-T circuit similar to the manufacturer's one was designed and incorporated into the input stage of the amplifier.

5.2.4 Sample containers

The body of the sample container was from a commercial piece of milking equipment (Teat Cup Remover (TCR), Waikato Milking Systems, Hamilton, New Zealand) as shown in Figure 5-8. It holds approximately 250 mL of milk when totally full, with 200 mL in its lower two-thirds (below the bottom of the upper collar). Figure 5-9 shows a cut-away view of the sample container and details its mode of operation.

Milk flow through the container is as follows. The milk line from the cow is connected into the top of the container while the milk line going to the bulk tank is

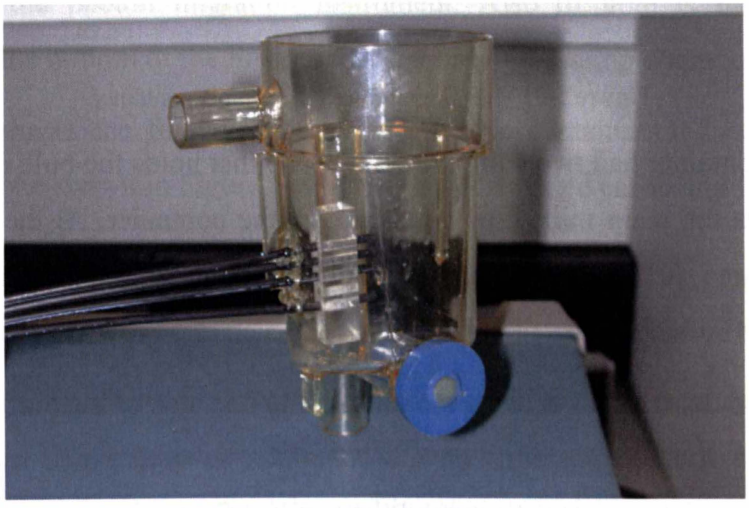

Figure 5-8: Photon Migration Instrument sample flask.

connected into the bottom side outlet. The container has a sealing lid enabling the interior to be under milking vacuum.

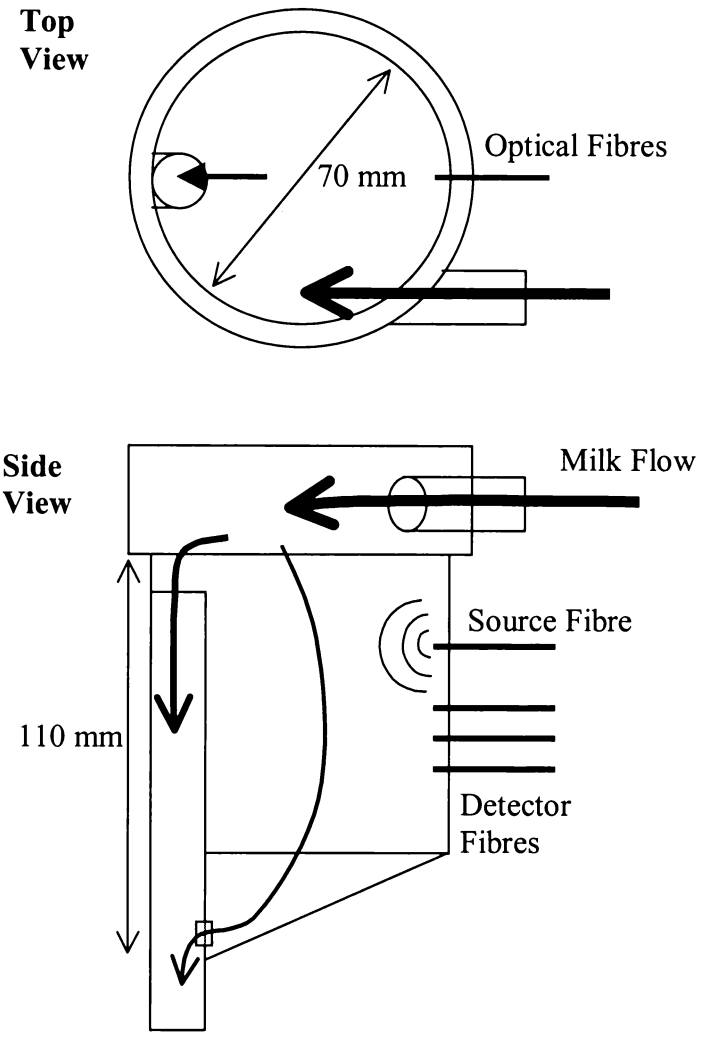

Figure 5-9: Milk flow through the sample container.

The sample container had two compartments – one that holds the bulk of the milk and one that forms the main milk flow path through the container. At the bottom of the bulk storage area there is a small orifice leading into the main flow path. This allows the milk in the bulk area to gradually drain out, and change slowly over time.

The source and detector fibres were mounted off to one side of the outflow pipe. They were mounted at fixed positions on the container, as determined by the limits of diffusion theory, detector sensitivity and the results of experimental trials designed to find the best source-detector distances. The source fibre was designated as the origin, with the three detector fibres mounted at fixed offsets. The source-detector distances

initially used were 1.5, 2.0 and 2.5 cm. Further details of the measurements involved in determining the optimum distances is described in chapter 6, section 4.1.

Field tests with the sample container revealed excessive foaming and poor flow through the container system. It was decided at first not to put the sample container in-line, but to have it off line, close enough to the milking system so that the travel time of the milk from the milking system to the container was under thirty seconds. The reason for that was to simplify the design of the system while both allowing for

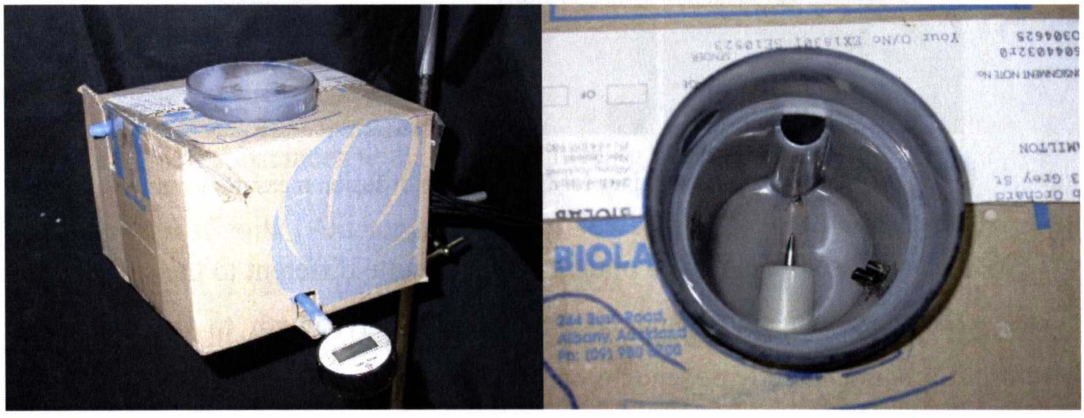

Figure 5-10: Final version of the sample container.

future attachment of the container to the milking system and also a short elapsed time from sampling to analysis for the milk.

Moderate shielding from ambient light was also required in order to obtain the best results from the photon migration instrument. Also of note is the thermometer embedded in the bottom of the flask used to record of the sample temperature.

Figure 5-10 shows the final version of the sample container. It is of an identical design to the one shown in Figure 5-8 but with a corrugated cardboard light shield and a thermometer added.

5.2.5 Modifications for Fluorescence Measurements

Fluorescence-diffusion measurements do not require a multi-distance measurement configuration. Therefore, the sample container did not need to be as complex as the one in Figure 5-10. Only a single detector fibre was required in this case, which meant that the number of fibres required was cut from four to two. The fibre selector mechanism in Figure 5-8 was also no longer needed. Figure 5-11 shows the much simpler sample container for the fluorescence diffusion measurements.

This container was 100 mL in capacity and had the source fibre in the centre with the detector fibre 5 mm away. The close proximity of the detector fibre to the source fibre

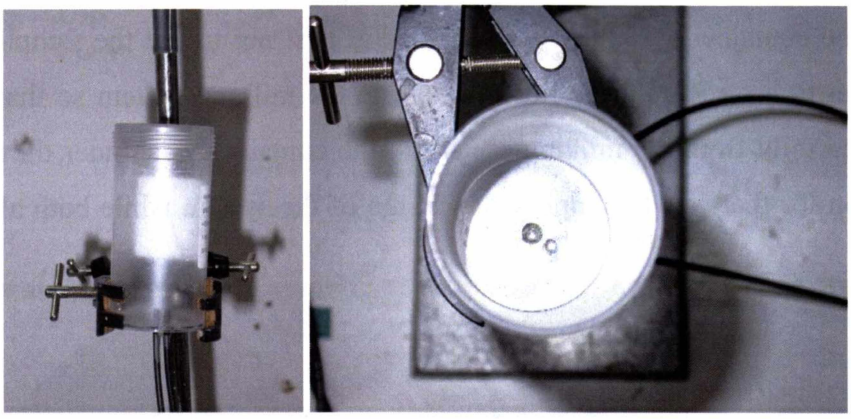

Figure 5-11: Sample container for fluorescence diffusion measurements.

was possible because the expected optical signal is quite different to the source signal. It was a fluorescence signal and had a different wavelength to the source, and therefore it was not directly dependent on the source signal.

The fluorescence diffusion experiments were not performed in-line, but were performed on milk samples collected and brought back to the laboratory.

5.2.6 Testing the Equipment

The photon migration instrument was tested and evaluated throughout its evolution. During testing two limitations were discovered that affected the way methodology of the experiments. The first limitation was in the range of modulation frequencies that can be used. The current amplifier used was capable of operating at up to 100 MHz. A 200 MHz model was available, but the trade-off was the gain, which was at 2×10^4 for frequencies up to 200 MHz. This was a factor of 2.5 lower than the gain for the 100 MHz amplifiers. Combined with the fact that the amplitude of a photon density wave attenuates faster with increased frequency, it was decided that an upper limit of 100 MHz would be sufficient.

The second limitation was discovered when the first tests with milk were performed. It appeared that modulation frequencies above 80 MHz did not return consistent results for both phase and amplitude. The results returned were noisy and any optical properties calculated from them gave results that did not make sense. Therefore, it was decided to impose an upper limit of 80 MHz on any measurements made, to

ensure the accuracy of the results. Other researchers (Fishkin *et al.*, 1991) have used modulation frequencies higher than 100 MHz successfully, with results being similar to those at 40 MHz so it was clear that nothing would be gained anything by using the higher frequencies.

5.3 Sample Supply and Makeup

Three different types of samples were required for the photon migration / fluorescence diffusion work:

- Homogenised milk
- Raw milk
- Milk-like substances with similar scattering properties as milk

The homogenised milk (Anchor, Auckland, New Zealand) was purchased in 1 L and 2 L bottles from a range of local supermarkets. Four grades of milk were used – standard homogenised ("Blue Top", 3.3% fat), reduced-fat homogenised ("Lite Blue", 1.5% fat), trim milk ("Green Top", 0.5% fat) and super-trim milk ("Lite Green", 0.1% fat).

Raw milk was obtained from a local research farm (No.4 Dairy, Dexcel, Hamilton, New Zealand). Dexcel is "the research and extension arm of New Zealand's dairy industry" and is fully owned and funded by New Zealand farmers (Dexcel, 2003).

The unique feature about the farm was that it contained New Zealand's only operational automatic milking system – a Fullwood Merlin automated milking system supplied by Sensortec, a research and design company working in collaboration with Dexcel. The farm (henceforth referred to as the Greenfield site) is the trial site where Dexcel is performing research on the suitability of automated milking systems in a pasture-based farming system, such as that in New Zealand.

The milk-like substance used in these experiments was IntraLipid, an intravenously administerable nutritional supplement. It was obtained from nearby medical institutions. The important physical characteristics of IntraLipid will be discussed in a subsequent section.

5.3.1 The Fullwood Merlin Automated Milking System

The automated milking system (Merlin, Fullwood Ltd., Ellesmere, England) shown in Figure 5-12 consists of a stall for the cow to stand in, a robotic milking arm that holds the cups and udder cleaning brushes, a controller unit containing the control electronics, and a milk distribution system that includes a milk cooler and the pipework to the bulk storage tank.

Figure 5-12: The Fullwood Merlin automatic milking system, installed at the Dexcel No. 4 research farm.

The robotic arm also houses a laser-rangefinder that uses a scanning infrared laser to find the teats. The laser is mounted in a small turret on the arm, and is protected against contact with the cow. Figure 5-13 shows the robotic arm and its components while Figure 5-14 shows the location of the Merlin at the Greenfield site.

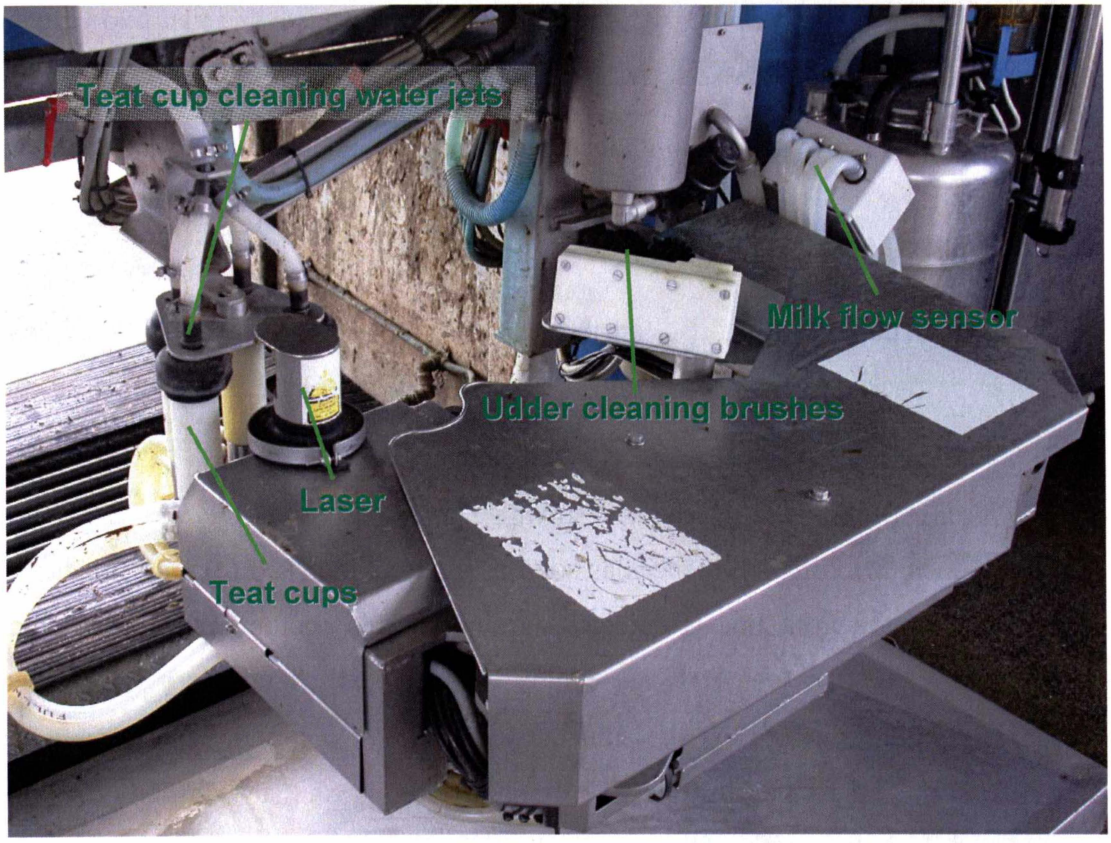

Figure 5-13: The robot arm on the Merlin milking system.

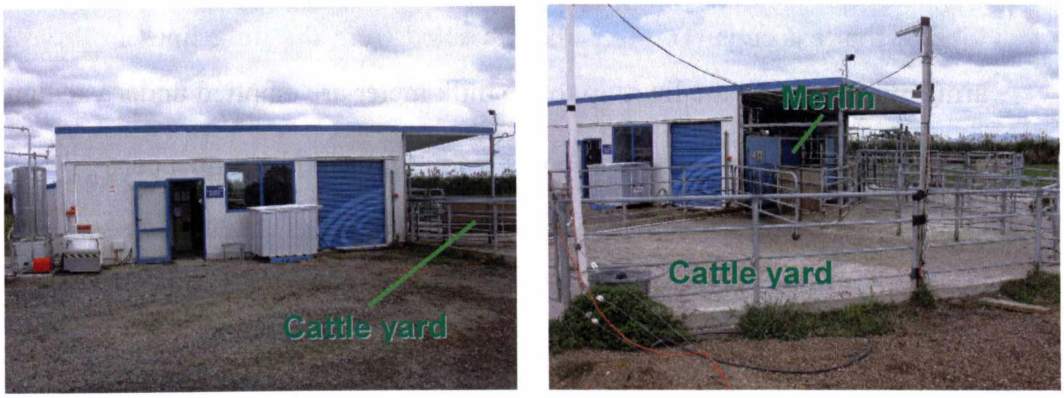

Figure 5-14: The Merlin building, side view (left) and including cattle yard (right).

The basic operation of the Merlin is (refer to Figure 5-15):

1. A cow approaches the Merlin building along the race (a). Cows wait in the cattle yard until the Merlin stall is available (b).
2. A cow enters the Merlin stall (c).
3. The Merlin identifies the cow via the use of a radio transponder attached to one of the cow's front leg. The transponder contains a pedometer, allowing the monitoring of the cow's activity. The gates to the stall close.
4. The robotic arm swings in under the cow and the udder cleaning cycle begins. Small rotary brushes lightly scrub the teats. When this is finished, the brushes are cleaned and disinfected.
5. The vacuum pump starts, and the teat location process begins (d). The laser scans back and forth, searching for the four teats. Once they are found, the cups are attached with the rear ones first, followed by the front ones.
6. When all cups are attached, a small jet of water rinses the udder cleaning brushes. Milking commences as soon as a cup is attached (e), and finishes as soon as the milk line is detected as empty. This occurs per-quarter, which means that the teat cups are removed individually, and there is no over-milking. Should the cups not attach satisfactorily, the cow may be rejected and the exit gate to the stall opens letting the cow out. She is diverted back to the yard ready for another attempt at milking by the robot.
7. At the completion of milking, teat spray is applied to the cow's udder and the exit gate opens. The robot arm retracts, and the teat cup cleaning jets rinse the tops of the teat cups (f). Pre milk is ejected from the milk lines in the robot arm, and the rest of the lines up to the milk meter are emptied under vacuum.
8. The entry gate opens, and the robot is ready to repeat the sequence.

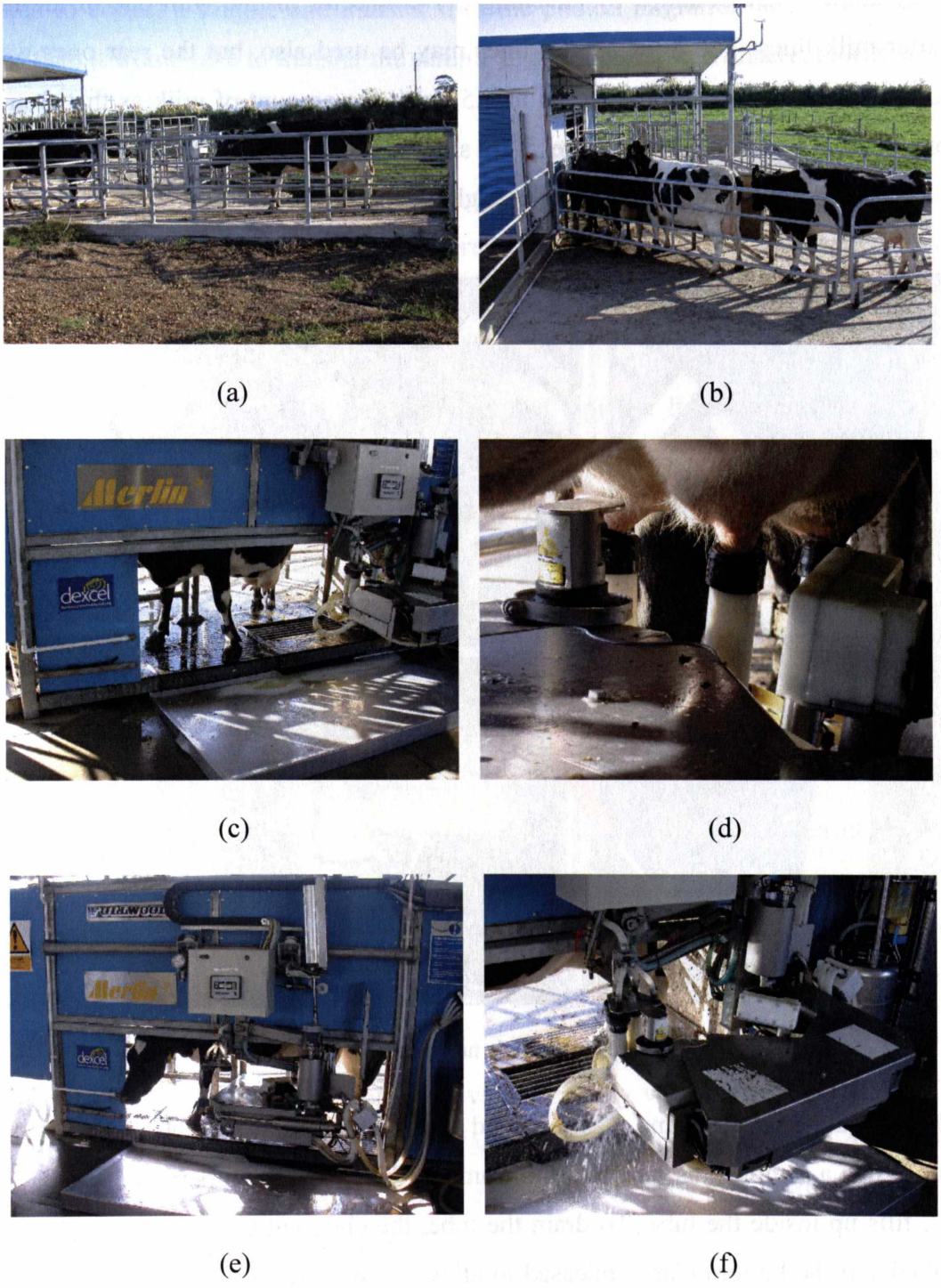

Figure 5-15: Merlin Operation. (a): Cow enters yard. (b): Cows waiting at Merlin entrance. (c): Cow enters stall. (d): Merlin attaches cups. (e): Cow being milked in Merlin. (f): Post-milking cleaning cycle.

Milk samples were obtained by attaching a T-connector in-line with one of the rear quarter milk lines. The front quarter lines may be used also, but the rear ones were chosen because they can produce up to 1.5 times the amount of milk as that from a front quarter (Eden, 2001). Figure 5-16 shows more detail on where the sample collection tube was fitted on the Merlin (highlighted red for clarity).

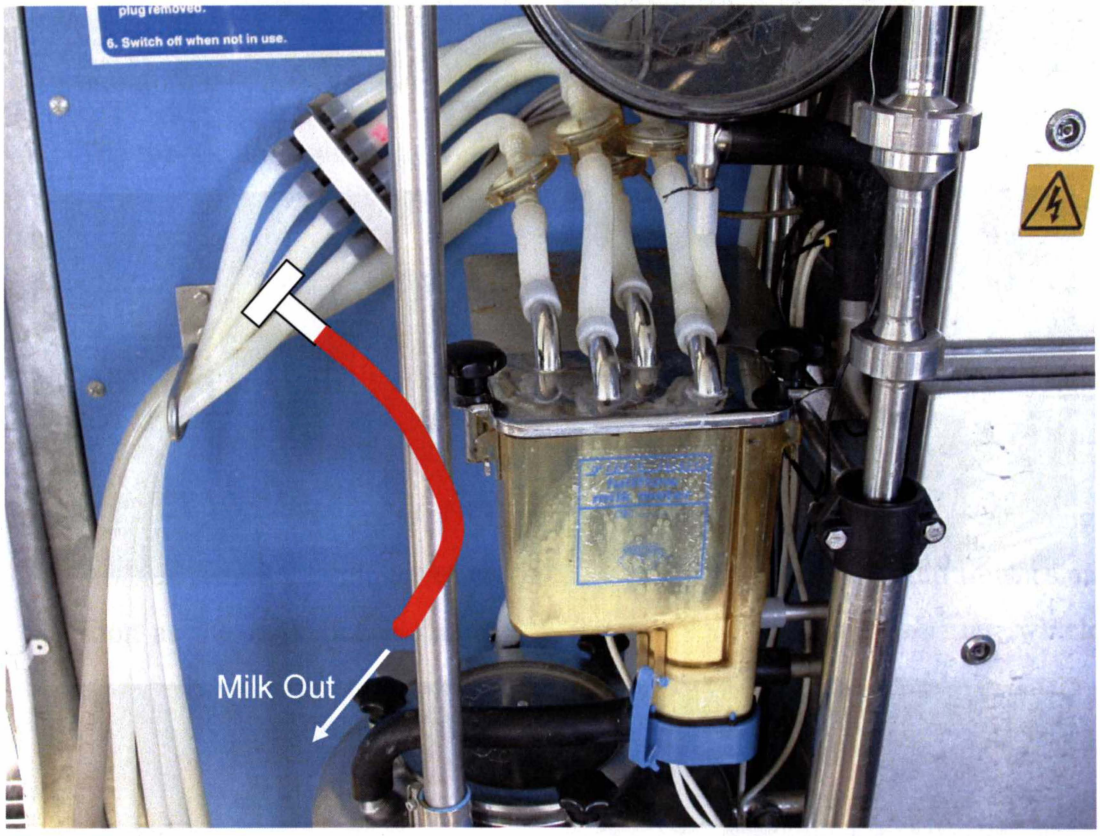

Figure 5-16: Sample tube placement detail.

A hand-operated snap clamp was mounted at the start and at the end of the sample tube. When a sample was required, the clamp at the end of the tube was applied, and milk fills up inside the tube. To drain the tube, the clamp at the top of the tube was applied and the bottom clamp released to allow the milk to flow out. Approximately 70 mL of milk could be collected per tube filling.

For the photon migration measurements, approximately 200 mL of milk was required, which meant that three fillings of the tube were required to fill up the sample container. The milk could still be considered "fresh" upon analysis as the total time required for three fillings was approximately one minute, and the transit time from collecting jar to sample container was approximately ten seconds. Certainly, the time

taken to collect a sample and transfer it to the photon migration instrument was far less than it would take to transfer the sample to a laboratory in a different location.

5.3.2 The Reference Sample

One of the requirements for photon migration measurements in milk was a reference sample. A desired quality of the reference was that its reduced-scattering and absorption coefficients were similar to that of milk.

An example of such a substance is Intralipid. This is an intravenously administered nutritional supplement made by Pharmacia and Upjohn. It has been found to be a suitable phantom for tissues by several researchers (Madsen *et al.*, 1991; Mourant *et al.*, 1997). Other alternatives exist, such as Abbott Laboratories' Liposyn as used by Cerussi (1999). Intralipid was chosen as a milk phantom as it was readily available. Its optical properties are also well known.

The Intralipid obtained was the variety known as Intralipid-20%. It was a 20 percent suspension of lipids in an aqueous substrate. There are other percentages of Intralipid available too, such as Intralipid-10% as used by van Stavreven *et al.* (1991).

The reduced-scattering coefficient of the Intralipid-20% was measured to be $420 \pm 10\ cm^{-1}$, which was at least ten times the value that we have previously measured for milk. This was measured with the photon migration instrument, after its initial testing and validation, but before the use of the IntraLipid in any experimental work.

Since the reduced-scattering coefficient varies linearly with the concentration of the particles in solution (as calculated with Mie theory), the Intralipid was diluted with distilled water to one-tenth of its initial concentration. This highly diluted Intralipid could be referred to as Intralipid-2%.

5.4 Summary

In this chapter, all the equipment used in this work was described as well as the samples and their sources. There were two areas of measurement – photon migration measurements to determine the optical coefficients of milk and *fluorescence* photon migration measurements to determine the concentration of a fluorophore in milk.

The samples fall into three categories – homogenised (standardised) milk, raw milk and milk phantoms. Usint these three types of samples and the two different measurement techniques formed the basis of the research.

6 Experimental Work

6.1 Introduction

In the previous chapters of this thesis, the theory behind the nature of milk, photon migration (in particular, the diffusion equation), and ways of applying photon migration measurements to milk were examined. With that information, it was possible to start taking measurements with milk. It is stated in chapter 4 that diffusion theory is suitable for these kinds of measurements.

Milk fat content, protein content, and somatic cell count are the quantities of interest. Fat and protein can, in theory, be measured with greater ease than somatic cell count. It is known that the fat and most of the protein in milk exists in the form of micelles or globules, and therefore the reduced-scattering coefficient should be related to those quantities. For somatic cell count however, an indirect method such as a form of fluorescence spectroscopy needs to be used to quantify it.

The measurement of fat content in milk was examined first. The objective was to be able to measure the fat content of raw milk straight from the cow. However, before these measurements were made, the photon migration instrument was tested to ensure that it was performing as expected. Section 6.2 covers the numerical simulations and the calibration of the photon migration instrument.

Section 6.3 describes the experimental work with homogenised milk. Since homogenised milk is much more uniform and predictable a medium than raw milk (as mentioned in chapter 2), this was the ideal way to initially test the photon migration instrument with real milk.

Section 6.4 covers experimentation with raw milk at the farm and away from it. This was mostly concerned with milk component measurements, and showed the photon migration instrument being used for the investigation of the properties of raw cow's milk.

Section 6.5 is about the detection of somatic cells in milk. These measurements were obtained in a different way to the previous measurements as they used fluorescence diffusion theory, and the fluorescence-measurement configuration of the photon migration instrument.

6.2 Simulation and Calibration

6.2.1 Simulation

Aim

An investigation of the expected results from the photon migration instrument was initially needed. That was important in order to know whether the instrument was returning results that agreed with diffusion theory. One of the ways this was done was to perform a numerical simulation with the diffusion equations. This allowed the determination, in a stepwise fashion, of how the solution to the diffusion equation would progress. The observed results should show a logarithmically decreasing amplitude and a linearly increasing phase.

Method

It was mentioned in chapter 4 that the diffusion equation is a second-order partial differential equation. These equations can be solved numerically using the Crank-Nicolson iterative method. This is an *implicit forward-time centered-space (FTCS)* method that is unconditionally stable and also accurate, which makes it a suitable method for use in this situation.

The source code for the simulation (*crankd.m,* shown in the Appendix 8.1) was written in the Matlab programming language and executed on a standard IBM PC compatible computer with the initial conditions being a background absorption coefficient of 0.02 cm^{-1} and a background reduced-scattering coefficient of 30 cm^{-1}. These were values that were used by Cerussi (1999) in his work.

The code was written to simulate a photon migration instrument operating in a one-dimensional infinite medium. Sampling points were at 2.0, 2.5 and 3.0 cm from the light source. The three points were equivalent to three pickup fibres inserted at those distances from the source. This configuration was similar to those in many other multi-distance photon migration instruments and should show results that are similar (Patterson & Pogue, 1994; Dam *et al.*, 2001; Cerussi *et al.*, 1996).

Samples from the 0 cm sampling point (the source) showed the input waveform. The input was a sinusoidally modulated point source with an intensity of 8.28×10^{16}

photons sec^{-1}. The initial amplitude of the point source was zero, but this did not affect the steady-state results.

Results

The output from the Matlab code is shown in Figure 6-1:

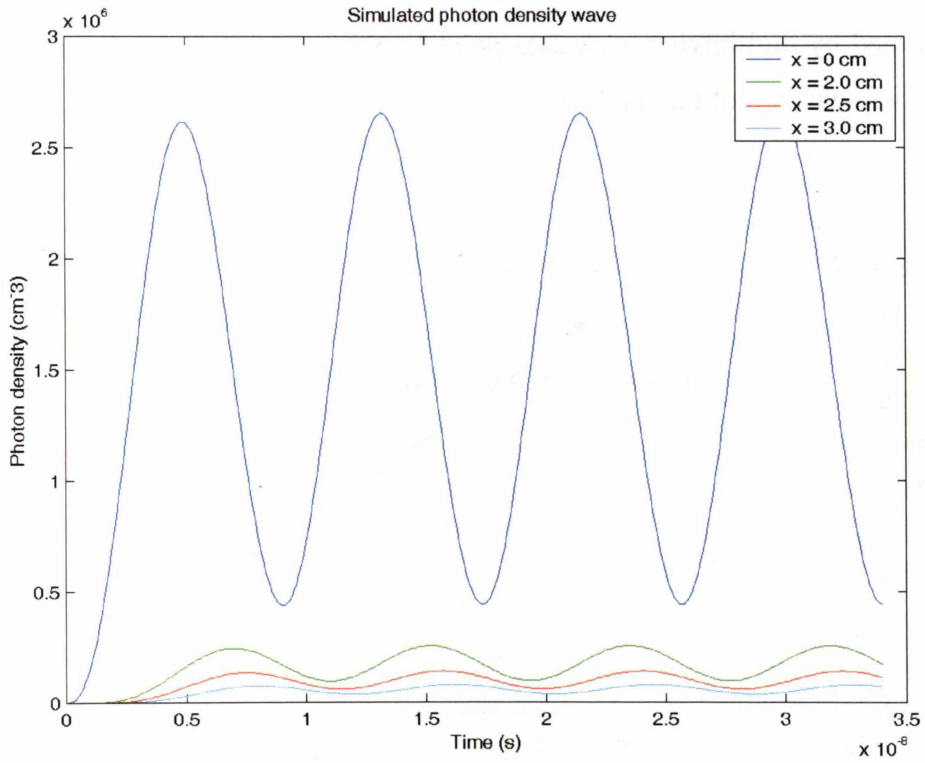

Figure 6-1: Matlab code *crankd.m* output.

The amplitude change at the different distances from the source was clearly evident. There was a significant (up to 10 times) decrease from the initial source amplitude to the amplitude at only 2 cm away. From equation 5-4c, it is evident that the amplitudes of the photon density waves should decrease in a logarithmic fashion. The numerical values are listed in Table 6-1:

Distance from source (cm)	Photon density (cm^{-3})
0	1.1065×10^6
2.0	7.9438×10^4
2.5	4.1014×10^4
3.0	2.1236×10^4

Table 6-1: Simulated photon density wave amplitudes.

These results showed a sinusoidally modulated wave that gradually decreases in intensity as the detector was moved further from the source. Figure 6-2 shows an analysis of the amplitude figures.

According to the theory shown in equation 5-5a, the results should have shown that the amplitude decreases logarithmically, and with minor manipulation, can be shown as a linear decrease. This trend is evident and is shown in Figure 6-2, with the results transformed by multiplying each data point by the source-detector distance and then taking the logarithm of the product.

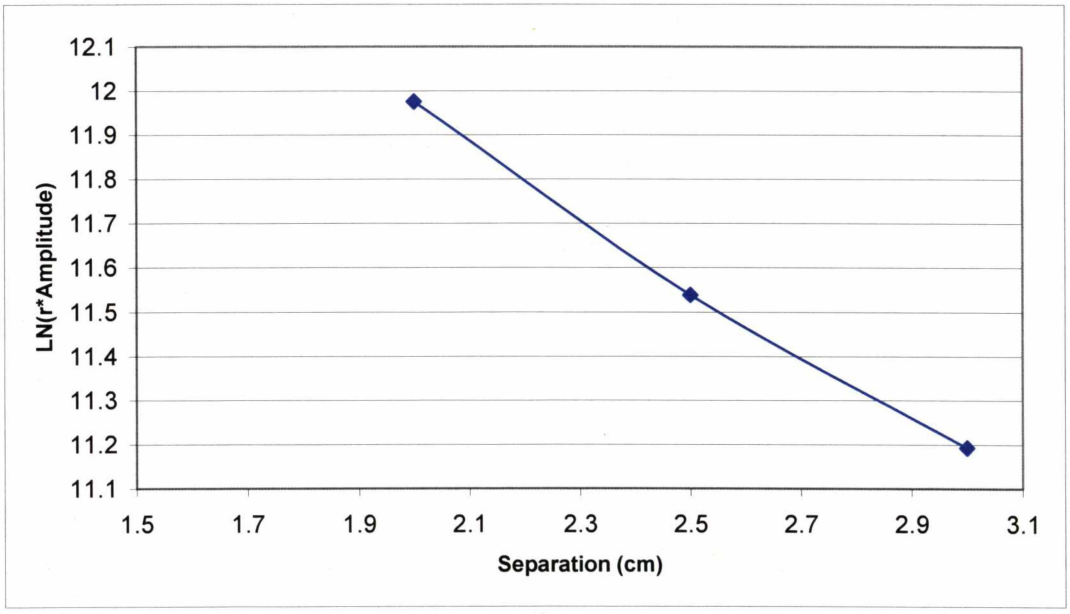

Figure 6-2: Amplitude versus source-detector separation with the data transformed.

The phase of the photon density wave is shown in Table 6-2:

Distance from source (cm)	Phase lag (degrees)
0	0
2.0	86.5
2.5	111.4
3.0	134.1

Table 6-2: Simulated photon density wave phase readings.

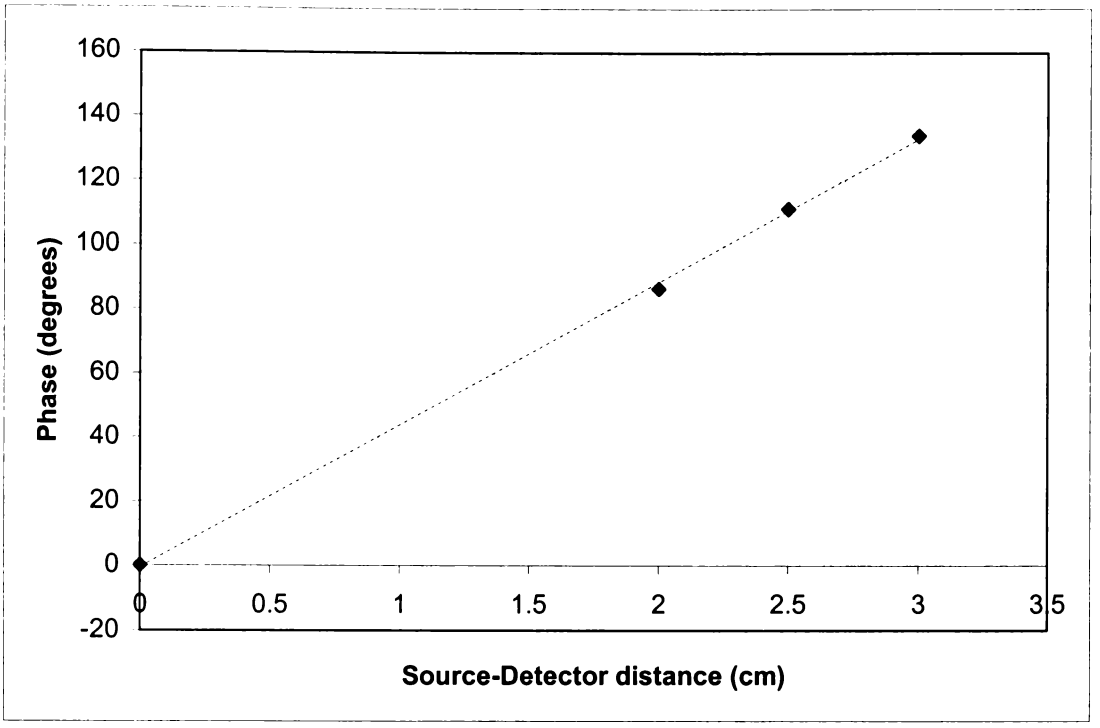

Figure 6-3: Phase versus source-detector separation.

According to equation 5-5b, the results should also exhibit a linear trend, which is observed in Figure 6-3. The trend line should pass through zero, and that can also be seen.

Both the amplitude and phase data shown here are indicative of what will be detected with a real photon migration instrument. However, this does not mean that the figures seen in these results will bear any semblance to the data that a real instrument will return – only the gradients of the phase and amplitude readings will bear that kind of similarity. In any case, it is not important since absolute values are not used to calculate the absorption and reduced-scattering coefficients.

6.2.2 Calibration with beads and Mie theory

Aim

With the simulations completed, tests with the real photon migration instrument were then done in order to answer some important questions about its performance.

1. What exactly is the instrument measuring?

2. Will the results the instrument is expected to return be correct under the conditions in which it is operated?
3. Are the results from the instrument agreeable to theory and other forms of measurement?

Without resolving those three issues, it was not possible to consider the photon migration instrument seriously as a measuring device.

Method

In chapter 4, it is clear that the expected results that the photon migration instrument will return are the reduced-scattering coefficient and the absorption coefficient, both of which have units of cm^{-1}. Both quantities are a measure of the number of absorption or scattering events per centimetre.

Mie theory can give an indication of the scattering coefficient μ_s and the scattering anisotropy (g). It is also stated in section 4.2.3 that $\mu_s' = \mu_s(1-g)$. Therefore, it was possible to use Mie theory to confirm the results that the photon migration instrument returned, since the size parameter, and the refractive index of the particle and medium were all available.

The scattering medium used was a suspension of 5.4 μm polymethyl methacrylate / styrene (PMMA/S) spheres (part number BB01N, Bangs Laboratories Inc., Fishers, Indiana) in distilled water at a concentration is 1.27×10^8 spheres cm^{-3}. Given that the refractive index of PMMA/S is 1.54 and the refractive index of distilled water is 1.333, the reduced-scattering coefficient of this mixture was calculated at a specified wavelength, which in this case was 670 nm.

Using equations 4-6b, 4-6c, and 4-7 to calculate the value of μ_s', it was found that:

$Q_{sca} = 2.596$

$g = 0.913$

$$\mu_s' = \frac{3}{2}\frac{Q_{scat}(n,x,\lambda)(1-g)\phi}{x} = \frac{3}{2}\frac{2.596\cdot(1-0.914)\cdot 0.0106}{5.4\times10^{-4}} = 6.57$$

In order to verify these numbers, photon migration software from the University of Pennsylvania (Nishimura *et al.*, 1996) was compiled and executed with the same parameters. Displayed in Figure 6-4 is the output from the software:

```
************************************************************
                  Photon Migration Imaging
     Version 2.1 (C) 1993, '94, '95
        Compiled: 14:06:57 May  2 2002
************************************************************

INPUT FILE :mie1.pmi
Lambda 670e-7
Mie 1.333000e+00 1.540000e+00 5.400000e+00 1.061100e-02
musp = 6.577721e+01 cm^{-1}        l* = 1.520283e-01 cm

THE END -    0.03 seconds total CPU time
```

Figure 6-4: PMI software output.

The reduced-scattering coefficient returned here (musp) was very close to that shown in the calculations.

The measured value should be close to that number. The results shown are those for the latest version of the photon migration instrument. This experiment has been carried out for previous configurations as well, but the most important result was for the configuration that has been used for the bulk of the photon migration work.

Configuration of the Photon Migration Instrument

In order to get reference results and observe the photon density wave passing each of the points, the photon migration instrument was configured in a slightly different manner. Firstly, the network analyser was used only as a 60 MHz sine-wave signal generator (the input was left disconnected). Secondly, a 5 Gsample s^{-1} oscilloscope (TDS-684C, Tektronix, Beaverton, USA) was connected at the output of the photomultiplier amplifier. Figure 6-5 shows a block diagram of this setup.

The laser diode used for this experiment had a nominal output wavelength of 670 nm (verified within 3 nm by measurement with a portable spectrometer), and was run with a bias current of 30 mA. The photomultiplier voltage was set to 750 V.

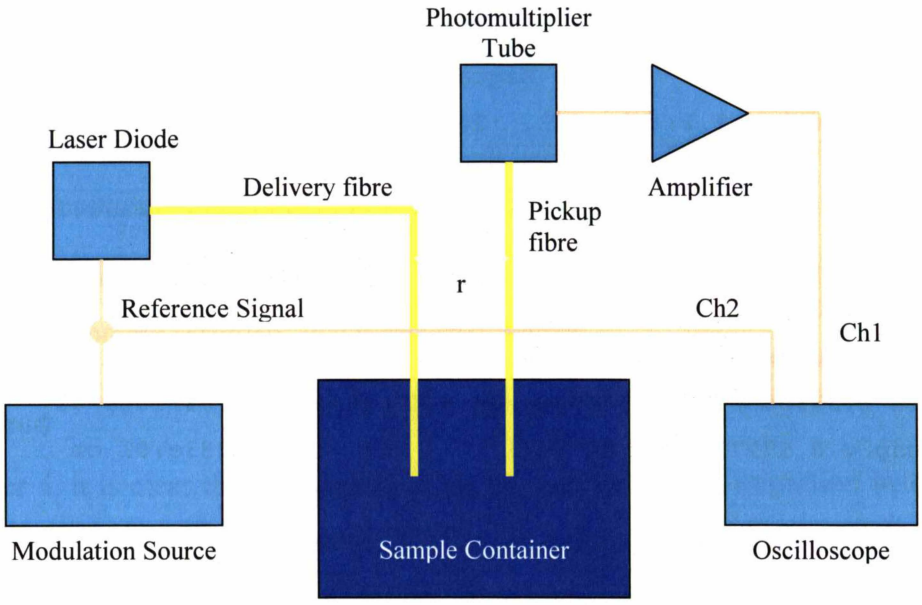

Figure 6-5: Alternative photon migration instrument configuration.

This configuration allowed the examinination of the shape of the photon density waves while taking the required phase and amplitude measurements at different source-detector distances. A point to note with this configuration is that the source-detector distance is fully variable, due to the need to take readings in sample containers of different volumes.

Results and Discussion

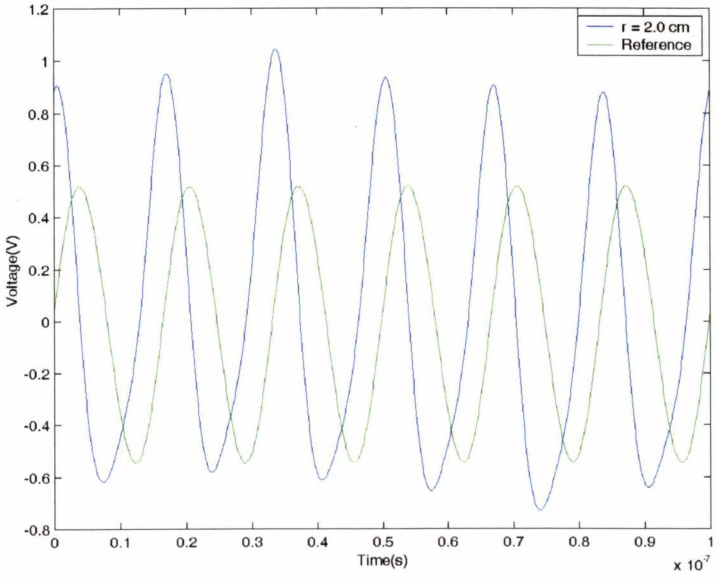

Figure 6-6: Voltage versus time for source-detector separation of 2.0 cm in bead suspension.

Figure 6-6 shows the data recorded from the oscilloscope at the 2.0 cm source-detector distance. The voltage of the blue trace is representative of the AC amplitude of the photon density wave light signal on the photomultiplier tube. The green trace is a reference signal from the network analyser and is shown only as a visual aid for comparing the phase lag. The displayed wave was sinusoidal in shape, as predicted. Figure 6-7 shows the same data, but for a 3.0 cm source-detector separation.

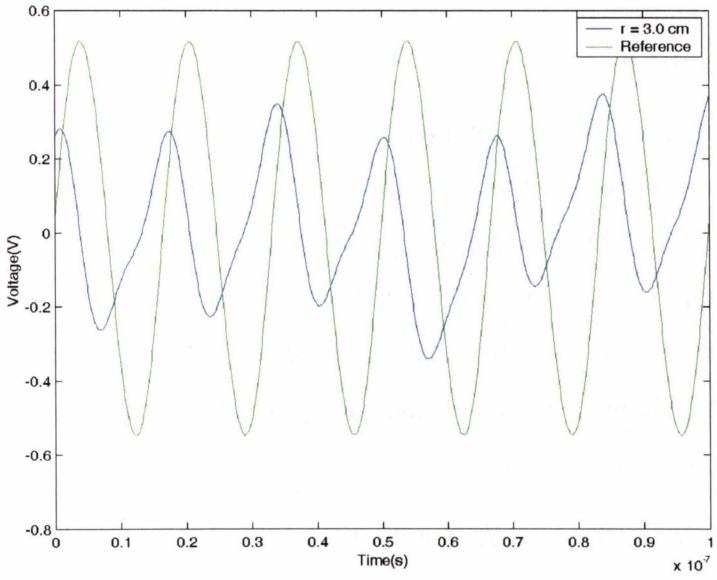

Figure 6-7: Voltage versus time for source-detector separation of 3.0 cm in bead suspension.

Shown in Figure 6-7 is the detected photon density wave for the 3.0 cm source-detector separation. It was quite different to that for the 2.0 cm source-detector separation case, with the most notable feature being the distortion of the sinusoidal shape. This distortion (or any DC offset) did not cause any difficulties with the measurements, as a Fourier transform was used to help eliminate any unwanted frequency components. Nevertheless, it was evident that the wave still had a frequency of 60 MHz.

From these results the absorption and reduced-scattering coefficients were calculated. The measured phase and amplitude gradients were 8.71 degrees cm^{-1} and -1.01 V cm^{-1}. Substituting these values into equations 5-6a and 5-6b and calculating the error yielded:

μ_s' $= 6.1 \pm 0.9\ cm^{-1}$

μ_a $= 0.152 \pm 0.005 cm^{-1}$

These values were close to those calculated by the PMI software and agreed within experimental error.

It would have been preferable to perform this experiment with several different sizes of microsphere, in order to obtain a calibration curve. However, this was not possible due to the high costs involved.

6.3 Experiments with homogenised milk

6.3.1 Introduction

In the last section, it was shown that the theory and concepts behind the photon migration instrument were sound, by the use of computer simulations and by the recovery of the optical coefficients of a highly controlled medium. In this section, the results are shown from testing the photon migration instrument with homogenised milk and cream. It was expected that in these experiments, the photon migration instrument could show a trend of increasing reduced-scattering coefficient with increasing milk fat concentration.

All the conclusions in these experiments were biased towards choosing the optimal configuration of the photon migration for on-farm, on-line measurements.

6.3.2 Initial measurements with homogenised milk

Use of the Infinite Medium boundary conditions with small containers

One issue that needed to be addressed is the volume required for the sample. Cerussi (1999) used a volume of at least 1 L for fluorescence measurements and also for normal photon migration measurements. However for practical purposes, using such large volumes can cause problems, as it would limit the speed at which samples can be taken when the instrument is used in a milking situation. This limits the usefulness of the instrument especially if many readings are taken. Therefore, a verification of whether a smaller sample of milk could be used satisfactorily was required.

Satisfactory here means results that are either similar in absolute value (within one standard deviation) or share a simple relationship with results of a larger volume of the same sample taken in a larger container. Repeated measurements in the different containers should fall within one standard deviation.

It has been shown in chapter 4 that having the source-detector distance r too small will cause the results to be inaccurate. This would place a lower limit on sample container dimensions (and hence, volume) if the diffusion approximation with the infinite-medium boundary conditions were to be used. A container that was too small would place boundaries close to the source and detector points. This would not allow the photons to reach the point of full isotropic scattering. The effect of this would be to distort the recorded photon density as photons leak out past the boundary (or container wall) and are not scattered back in.

For a container that is approximately spherical or cubical, a minimum volume of 200 mL should have acceptable dimensions. It should be noted that the distance from the source fibre to the detector fibres and the container walls should not be below r_{min} as shown in Figure 6-8. Similarly, the detector fibres should not be allowed to get too close to the container walls. This is because one of the conditions for the use of the diffusion equation is that the scattering must be isotropic. A crucial piece of knowledge is at which distance from the source fibre the scattering becomes isotropic. It is easy to see that the light distribution from the source fibre is not isotropic, and therefore the detector fibres must be a certain distance away from it. That "certain distance" can be considered as a spherical volume around the tip of the source fibre, where the medium must be homogeneous with no detector fibres in it. Similarly, an identical distance must be kept from the container walls.

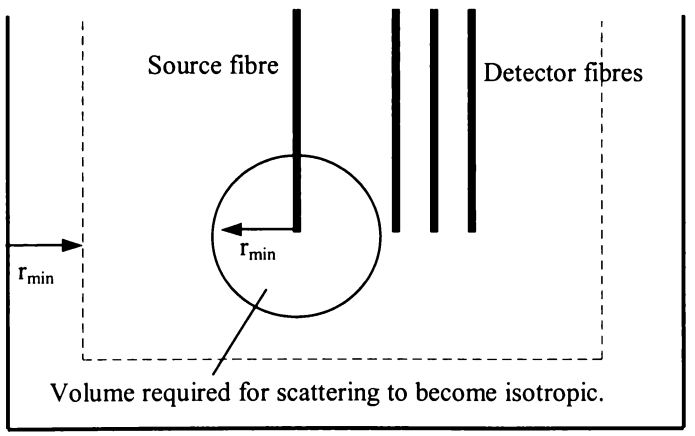

Figure 6-8: Minimum distance from sources and boundaries that must be observed.

The reduced-scattering coefficient represents the length scale after which the photon's initial trajectory no longer has any bearing on its current trajectory. The value r_{min} in

Figure 6-8 could be approximated by the reciprocal of the value of the reduced-scattering coefficient for the medium. For the standard homogenised milk used previously, r_{min} would be 1/36 cm, or 0.2 mm. However, that distance was increased by two orders of magnitude, up to 20 mm. That ensured that the photons had ample space for sufficient randomisation in direction.

Method

Similarly shaped rectangular sample containers of volumes 8 L, 4 L, 1 L, 500 mL and 250 mL were filled with the appropriate volume of standard homogenised milk. Care was taken to ensure that the photon migration instrument was configured so that the source and detector fibres were not placed near boundaries. This is so as not to violate the limitations shown in Figure 6-8. The milk temperature was kept at 20 °C.

The photon migration instrument was configured to have the RF network analyser as its signal source. A mounting system for the optical fibres was made so that the source-detector distance could be smoothly altered. This allowed the tracking of exactly how the phase and amplitude changed over the different source-detector distances used in the measurement.

The chosen source-detector distances were from 10 mm to 30 mm in 5 mm increments. Averaging on the RF network analyser was enabled (64 sample averaging) and the input bandwidth was set to 1200 Hz. The RF network analyser was set up for a frequency sweep from 50 to 100 MHz. The chosen laser diode wavelength was 651 nm, and its output power set to 15 mW (from a maximum of 35 mW).

Ten readings were taken per sample container, and the results averaged. The coefficient of variation was calculated, along with the absolute error for both the absorption and reduced-scattering coefficients. The absolute error was calculated as shown in section 5.1.1.

Results and Discussion

The results for all volumes tested are shown in Figure 6-9 and Figure 6-10.

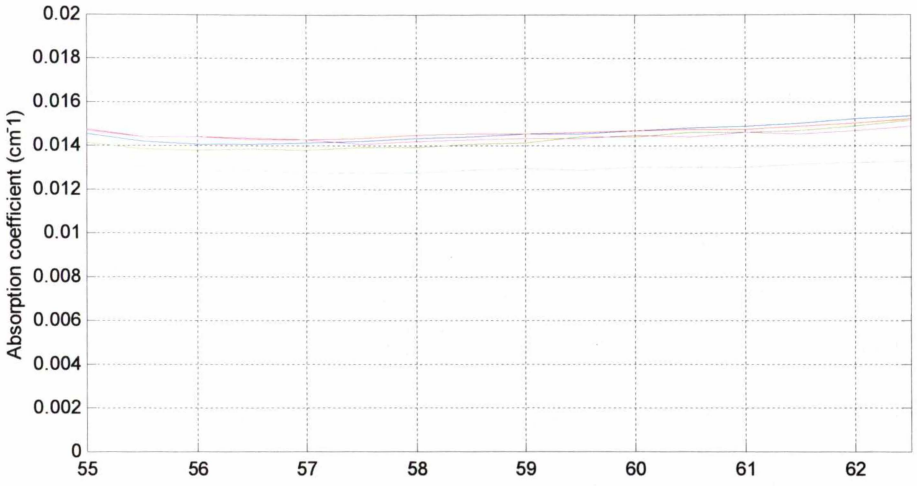

(a)

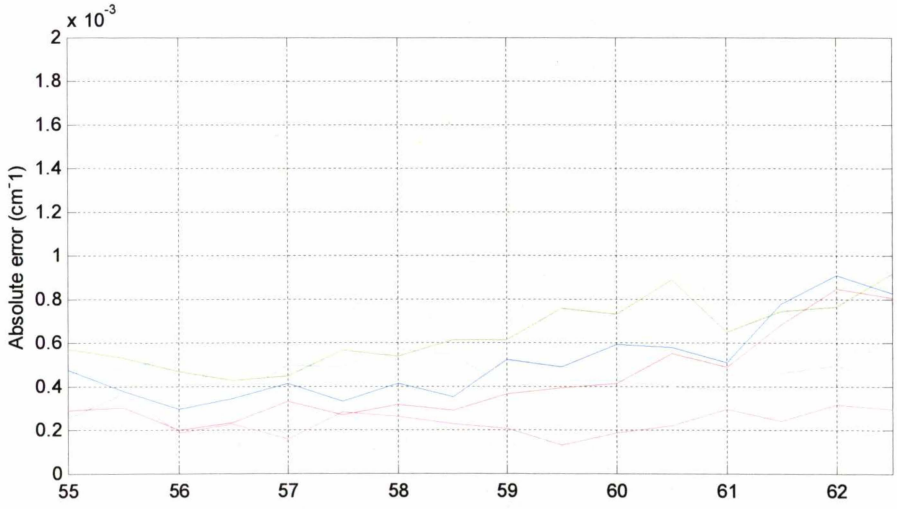

(b)

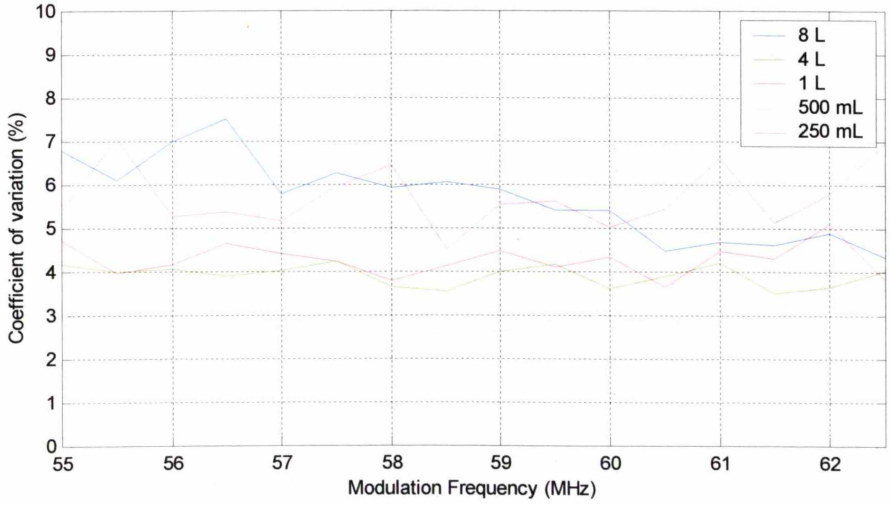

(c)

Figure 6-9: Absorption coefficient and error figures for different container volumes.

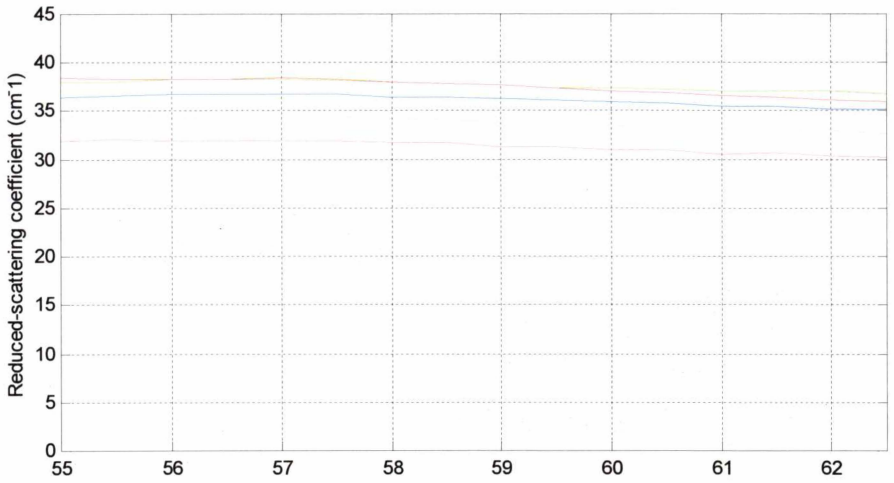

(a)

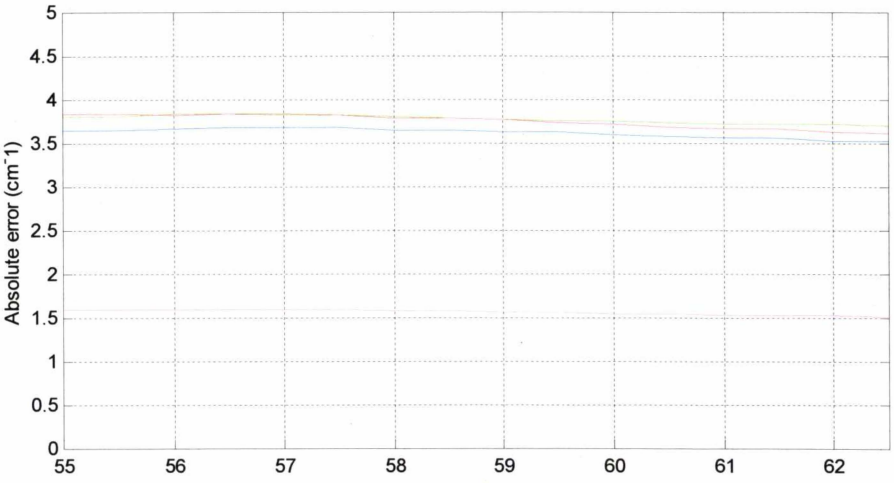

(b)

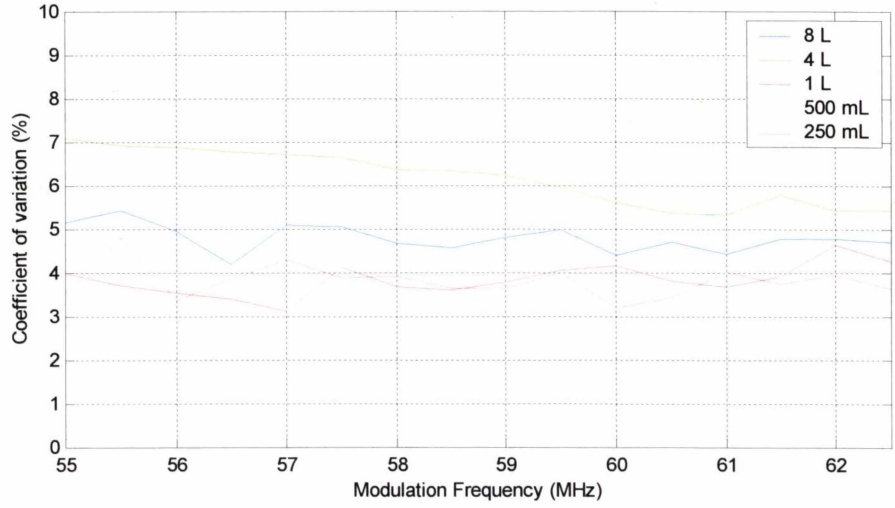

(c)

Figure 6-10: Reduced-scattering coefficient and error figures for different container sizes.

It should be noted that in the initial setup of the equipment, a reasonably large amount of interference was present. The source of that interference was unknown, but it affected the results from the instrument at certain frequency ranges. For that reason, only the results from 55 to 62.5 MHz will be discussed in any detail.

Another point to note is that only six measurements were made for the 250 mL container instead of the ten that the other containers had. This did not adversely affect the accuracy or precision of the readings compared to the others.

In the results, we see that the absorption and reduced-scattering coefficients were relatively unchanged over this small frequency range. Towards the ends of the range however, the effects of the interference were visible. In theory, the absorption and reduced-scattering coefficients should have remained unchanged for all modulation frequencies. While this is not observed in this set of results due to the interference, it was demonstrated in subsequent experiments.

Figure 6-9c and Figure 6-10c show the calculated coefficients of variation for the absorption coefficient and the reduced-scattering coefficient. The relatively high coefficients of variation of between 4% and 7% for the readings indicated that the instrument required some improved electrical shielding around the cables.

Collating these results and averaging the results over all frequencies gives:

Container volume	**Absorption coefficient (cm^{-1})**
8L container	0.0145 ± 0.0005
4L container	0.0142 ± 0.0006
1L container	0.0146 ± 0.0004
500 mL container	0.0130 ± 0.0005
250 mL container	0.0144 ± 0.0002
Container volume	**Reduced-scattering coefficient (cm^{-1})**
8L container	36 ± 4
4L container	37 ± 4
1L container	37 ± 4
500 mL container	34 ± 2
250 mL container	31 ± 2

Table 6-3: Results for all containers.

Given the results in Table 6-3, it was clear that changing the volume of the container from 1 L to 8 L had no significant effect on the absorption or the reduced-scattering coefficients of homogenised milk. The small differences in results between the different sized containers fall within the error of each of the measurements. Therefore, it can be surmised that a 1 L container of the same shape as an 8L container gives identical results.

The coefficients of variation for both the absorption and reduced-scattering coefficients fell inside the error figures as well. This showed that the instrument was capable of returning consistent results.

There is some uncertainty as to whether the instrument was recording an accurate value for the reduced-scattering coefficient when using the 500 mL and 250 mL containers. The reduced-scattering coefficients for those containers were different to those given by the larger 1 L, 4 L and 8 L containers. While it was stated that the difference in time of measurement between the larger and smaller containers might cause a slight change in the results, only the 500 mL absorption coefficient and both the 250 mL and 500 mL reduced-scattering coefficients are significantly affected.

The change in the absorption coefficient was not explainable apart from operator error. It was of the same size as the deviations in reduced-scattering coefficient. Thus it was significant, but at that point, of less importance than the change in the reduced-scattering coefficient. This is due to the nature of one of the more important milk components we wish to quantify – milk fat. Fat content is strongly related to the reduced-scattering coefficient but has little relationship with the absorption coefficient under these circumstances.

It was considered useful to look at the reduced-scattering coefficient more closely. Figure 6-11 shows a plot of the reduced-scattering coefficient against container volume. Since the 8 L, 4 L and 1 L containers can be considered identical with regards to the coefficients returned, only the 250 mL, 500 mL and 1 L containers were analysed.

The data in Figure 6-11 is intended just to show if any trend exists between the container size and the reduced-scattering coefficient. Any trend observed will only be of interest for calibration purposes.

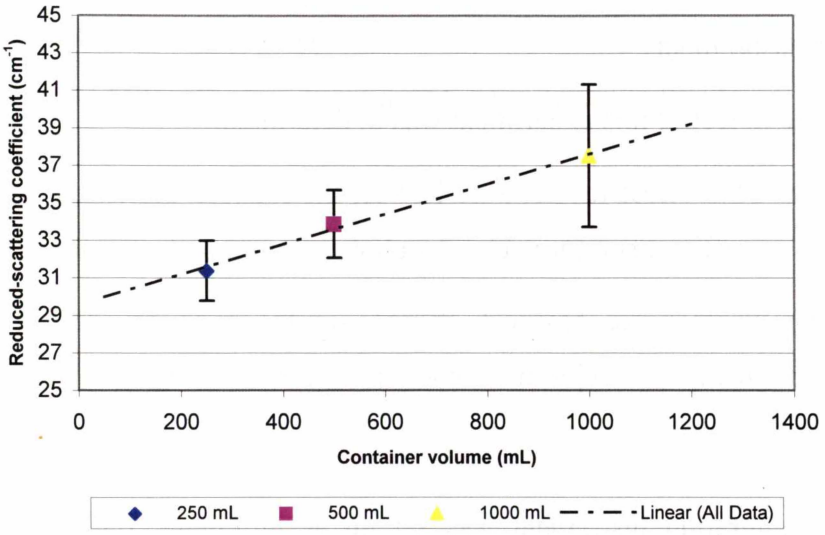

Figure 6-11: 250 mL, 500 mL and 1 L containers – reduced-scattering coefficient.

There appeared to be a linear trend between container size and the reduced-scattering coefficient. Due to the lack of data points, it was impossible to say that for certain. However, there is no evidence that points to the contrary.

With these results, it was determined that the use of a 250 mL container was acceptable. The reduced-scattering coefficient returned from the 250 mL container required scaling in order to make it correct, but that could removed completely with calibration. Using the 1L container would remove the uncertainty, but would present problems for on-farm results since the sample container would require four times more time to fill, and 1L of milk per measurement which is not practical from the application.

6.3.3 Temperature effects

Introduction and Aim

One effect worth considering was how the temperature of the sample affected the absorption and reduced-scattering coefficients. It was possible that the fat globules in milk behaved in different ways at different temperatures. One possibility is that they may have clumped at lower temperatures. It was also possible that at different temperatures, the casein micelles may have started to affect the reduced-scattering coefficient, thus reducing its dependence on the milk fat content. However, if that behaviour can be characterised, it can be compensated for in the instrument provided

that temperature measurements of the milk are taken at the same time as the photon migration measurements.

Therefore, the object of this experiment was to determine:

a) what effect temperature had on the reduced-scattering and absorption coefficients returned by the photon migration instrument.

b) whether the physical changes in the milk caused by temperature changes are reproducible and reversible.

Method

The photon migration instrument was set up as in Figure 5-3. The RF network analyser was used as the modulation source with the frequency range set from 60 to 65 MHz. The measurements were taken using the 250 mL container shown in Figure 5-10. A digital thermometer, which was built into the sample container, was used to track the sample temperature.

The sample was fresh standard homogenised milk tested within ten minutes of removal from the refrigerator. The milk for this experiment had most of its shelf storage life remaining, whereas that used in the previous experiments was close to the end of its shelf storage life. The temperature range studied was from 9 °C up to 27 °C (the range expected for milk after leaving the milking machine), in two stages. The first stage involved letting the milk warm up naturally by leaving it in a room-temperature environment and allowing it to heat up. Room temperature at the time of the experiment was 23 °C. Stirring was not required, since the milk was homogenised.

At 20 °C, the milk was artificially heated by placing a small sealed vial of hot water into the sample container and waiting until the milk reached a maximum temperature, which in this case was 27 °C. The milk was stirred during this time. Further readings were taken until the milk cooled down to room temperature.

Results

Figure 6-12 and Figure 6-13 show the relationship between temperature and the absorption coefficient and the reduced-scattering coefficient. One particularly noticeable feature is that the reduced-scattering coefficient is significantly larger than for the previous samples. This is attributed to the shorter shelf storage time of the milk.

The readings above 20 °C appeared not to follow the trend that the other readings did. In particular, they had a larger spread, and for the absorption coefficient readings, they seemed to not follow the trends exhibited in the previous results.

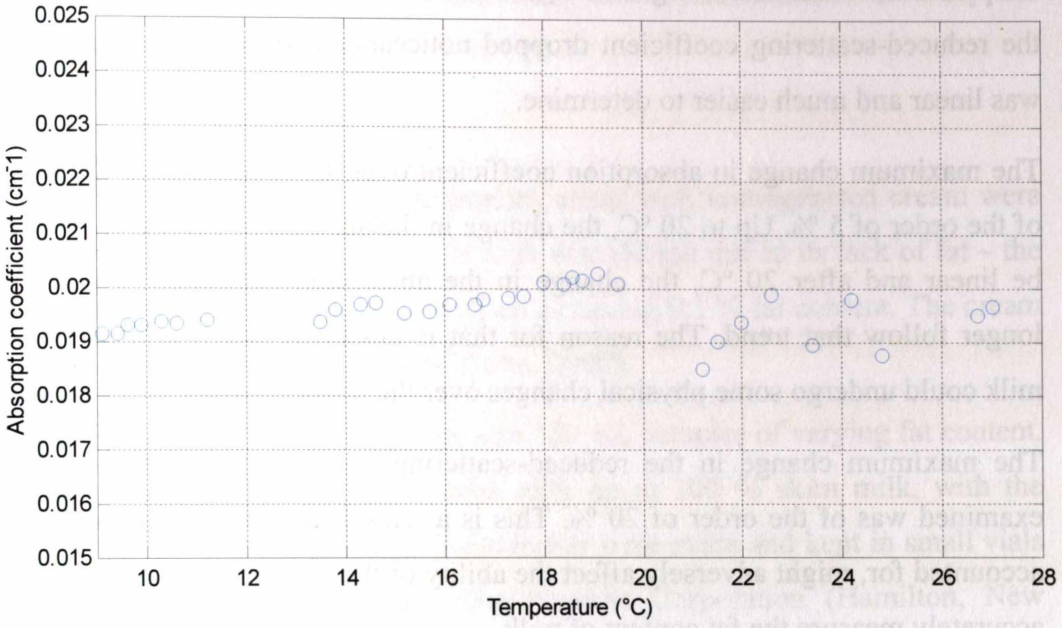

Figure 6-12: Plot of absorption coefficient versus temperature.

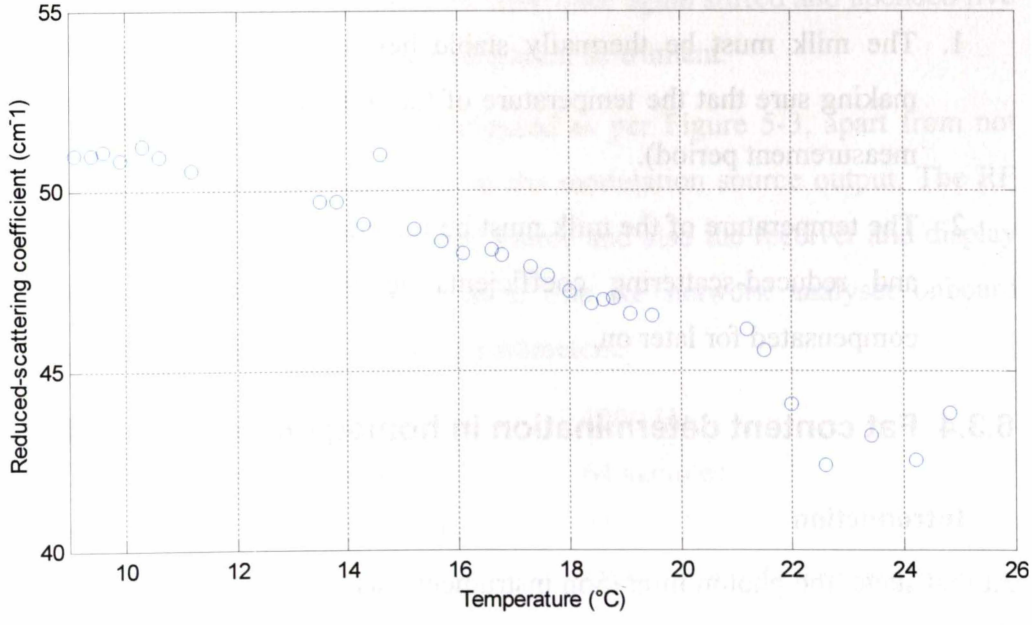

Figure 6-13: Plot of reduced-scattering coefficient versus temperature.

Discussion

Two conclusions were drawn from the experiments illustrated in Figure 6-12 and Figure 6-13. The first was that the absorption coefficient changed slightly with temperature, and that the slight change was difficult to define. The second was that the reduced-scattering coefficient dropped noticeably with temperature. The change was linear and much easier to determine.

The maximum change in absorption coefficient over the temperatures examined was of the order of 5 %. Up to 20 °C, the change in the absorption coefficient appeared to be linear and after 20 °C, the change in the absorption coefficient appeared to no longer follow that trend. The reason for that is unknown, but it is possible that the milk could undergo some physical changes over the temperature range examined.

The maximum change in the reduced-scattering coefficient over the temperatures examined was of the order of 20 %. This is a reasonably large deviation, and if not accounted for, might adversely affect the ability of the photon migration instrument to accurately measure the fat content of milk.

Therefore, the main conclusion from this experiment was that for subsequent work with milk fat measurement using the photon migration instrument, one of two procedures must be followed:

1. The milk must be thermally stable before making measurements (that is, making sure that the temperature of the milk does not change much over the measurement period).
2. The temperature of the milk must be recorded while measuring the absorption and reduced-scattering coefficients so that temperature effects can be compensated for later on.

6.3.4 Fat content determination in homogenised milk and cream

Introduction

At that stage, the photon migration instrument was considered to reliably measure the absorption and the reduced-scattering coefficient or a quantity linearly related to it (the emphasis here being on the reduced-scattering coefficient). With that information, realistic fat content measurements with homogenised milk and cream could be done.

Aim

The objective of this experiment was to show whether the photon migration instrument was able to measure milk fat, protein or somatic cell count in milk reliably. We expected to find (at least for fat) some linear trends. Measurement accuracy and precision were determined.

Method

Fresh skim milk obtained from a supermarket, along with homogenised cream were the samples for this experiment. The skim milk was chosen due to its lack of fat – the particular brand (Anchor) chosen is advertised as having 0.1 % fat content. The cream was assumed to have a 40 % fat content (Gunn, 2000).

The milk and cream were mixed together into 250 mL samples of varying fat content. The samples contained from 67.5 % skim milk up to 100 % skim milk, with the remainder of the sample being cream. Subsamples were made and kept in small vials ready for transport to the Livestock Improvement Corporation (Hamilton, New Zealand) milk testing laboratories for the determination of fat content using a commercial milk analyser.

The samples were thoroughly stirred and allowed to come to room temperature. Before any readings were taken, the samples were once again stirred and upended five times before being poured into the photon migration instrument.

The photon migration instrument was configured as per Figure 5-3, apart from not having the semi-rigid microwave cable from the modulation source output. The RF network analyser was the modulation signal source and also the receiver and display for the signal from the photomultiplier tube. The RF network analyser onboard settings were configured with the following parameters:

Bandwidth:	1200 Hz
Sample averaging:	64 samples
Number of data points:	21
Frequency:	60 MHz (single frequency)
RF power:	8.6 dBm
Source-Detector distances:	1.0 cm, 1.5 cm and 2.0 cm

Ten readings were taken from each sample. The average value was recorded and the absolute errors calculated. The RF network analyser was set to work at a single frequency in this experiment in order to help limit source-receiver cross talk by limiting the number of modulation frequencies used.

Results

The results of the photon migration instrument are shown in Figure 6-14 to Figure 6-19. Comparisons between the absorption and reduced-scattering coefficients against fat, protein and somatic cell count are shown. Figure 6-14 and Figure 6-15 are the plots of the reduced-scattering and absorption coefficients versus milk fat. Figure 6-16 and Figure 6-17 are the same for milk protein. Finally, Figure 6-18 and Figure 6-19 plot the reduced-scattering and absorption coefficients against the somatic cell count.

For Figure 6-14, comparing the reduced-scattering coefficient to the milk fat content showed a clear trend. This was expected, since as the fat content of the milk increased, the number of fat globules suspended in the milk increased too. It was also expected that the fat globules of the cream were of a uniform size since it was homogenised cream that was added to skim milk. That resulted in an increase in the reduced-scattering coefficient, as the number of scattering events per distance that a photon travels increased.

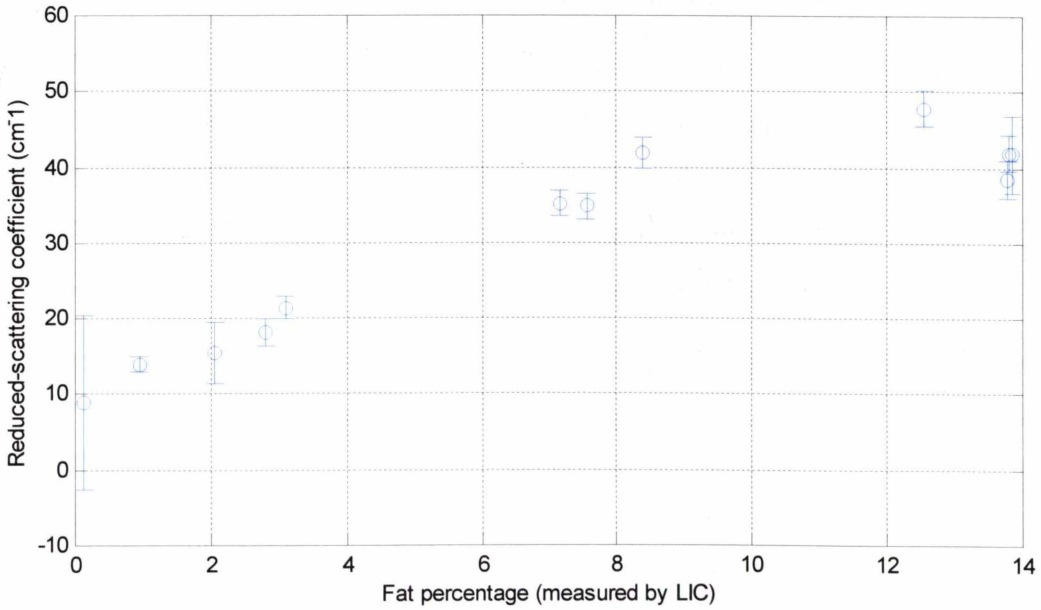

Figure 6-14: Reduced-scattering coefficient against measured fat percentage.

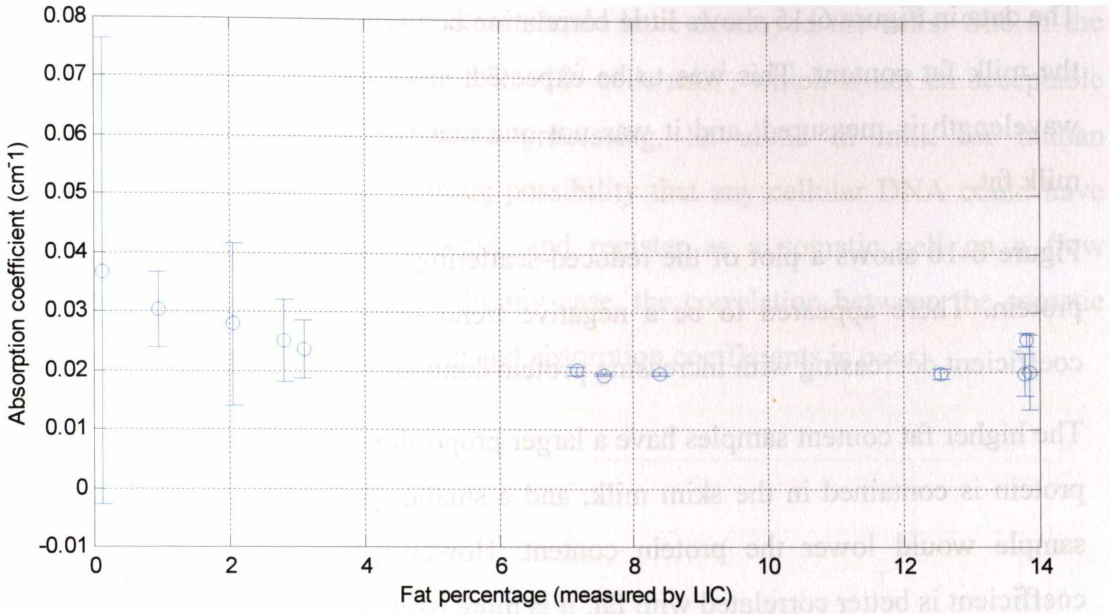

Figure 6-15: Absorption coefficient against measured fat percentage.

However, there was some unexpected behaviour in the reduced-scattering coefficient versus fat percentage results. Figure 6-14 shows that when the milk fat content exceeded 8.5%, the data no longer followed the trend set by the data representing milk fat content below 8.5%. This was explained by the fact that high fat milk is a strong light attenuator due to its greater scattering properties. That caused the signal at the 2.0 cm source-detector distance to be very weak and unreliable. The result is that some of the measurements may have a significant error in the amplitude gradients.

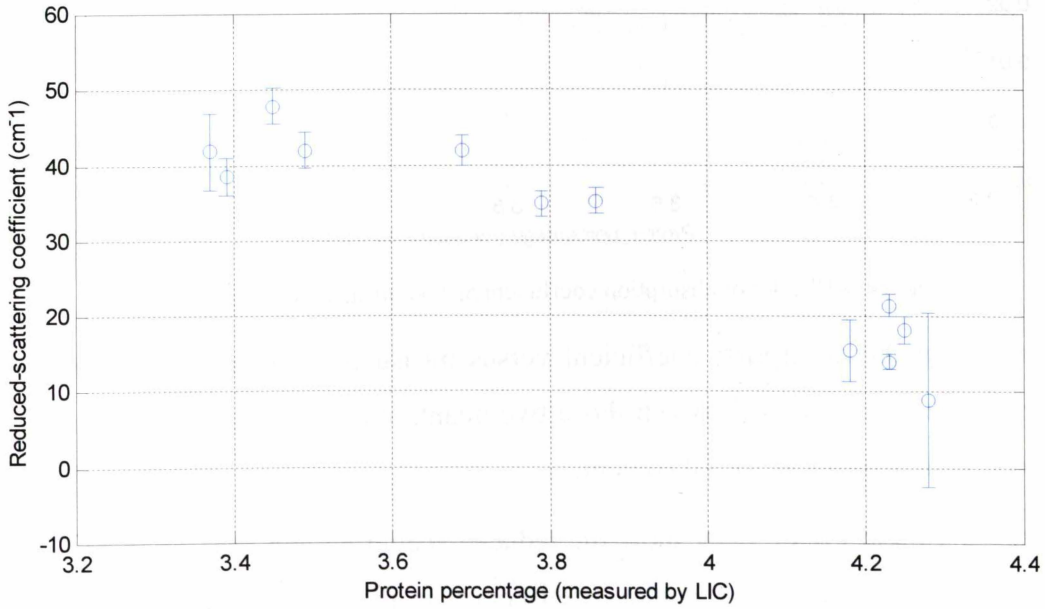

Figure 6-16: Plot of reduced-scattering coefficient against measured protein percentage.

The data in Figure 6-15 shows little correlation between the absorption coefficient and the milk fat content. This was to be expected, since the absorption at only a single wavelength is measured, and it was not one that was known to correlate well with milk fat.

Figure 6-16 shows a plot of the reduced-scattering coefficient versus measured milk protein. There appeared to be a negative trend there, with the reduced-scattering coefficient decreasing with increasing protein content.

The higher fat content samples have a larger proportion of cream in them. Most of the protein is contained in the skim milk, and a smaller proportion of skim milk in the sample would lower the protein content. However, since the reduced-scattering coefficient is better correlated with fat, it is more likely to track the cream content, not the protein content.

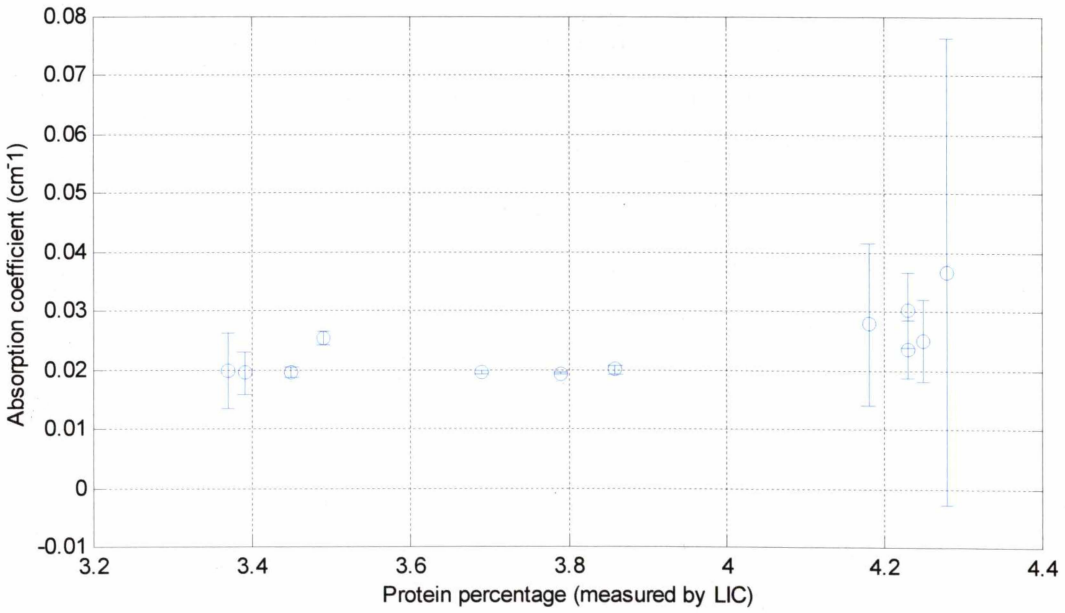

Figure 6-17: Plot of absorption coefficient against measured protein percentage.

The plot of the absorption coefficient versus measured protein in Figure 6-17 also showed little correlation between those two quantities. That was also to be expected, for the same reasons as for fat content.

Figure 6-18 and Figure 6-19 show the reduced-scattering and absorption coefficients respectively plotted against somatic cell count. In theory, there should have been a minimal somatic cell count in homogenised milk and cream. The fact that there was an appreciable somatic cell count in fresh homogenised milk is rather interesting in

itself since the homogenisation process should have destroyed the cells. One of the samples had a somatic cell count of 7×10^5 cells mL^{-1}, which is not an acceptable somatic cell count for milk before processing, let alone in milk for human consumption. However, is is a strong possibility that any cellular DNA could have survived the homogenisation process, and register as a somatic cell on a flow cytometer such as the Fossomatic. In any case, the correlation between the somatic cell count and the reduced-scattering and absorption coefficients is poor.

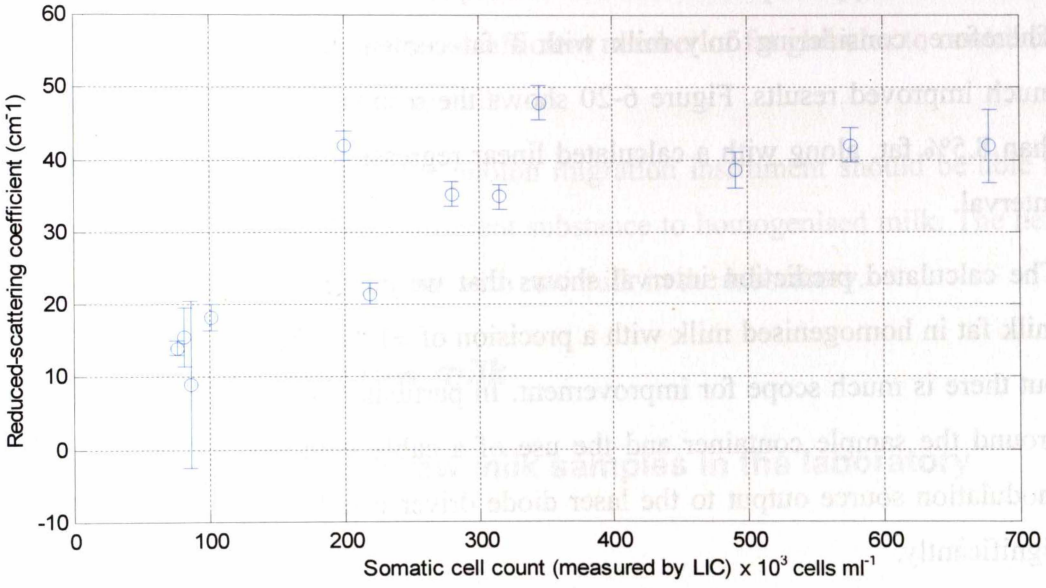

Figure 6-18: Plot of reduced-scattering coefficient against somatic cell count.

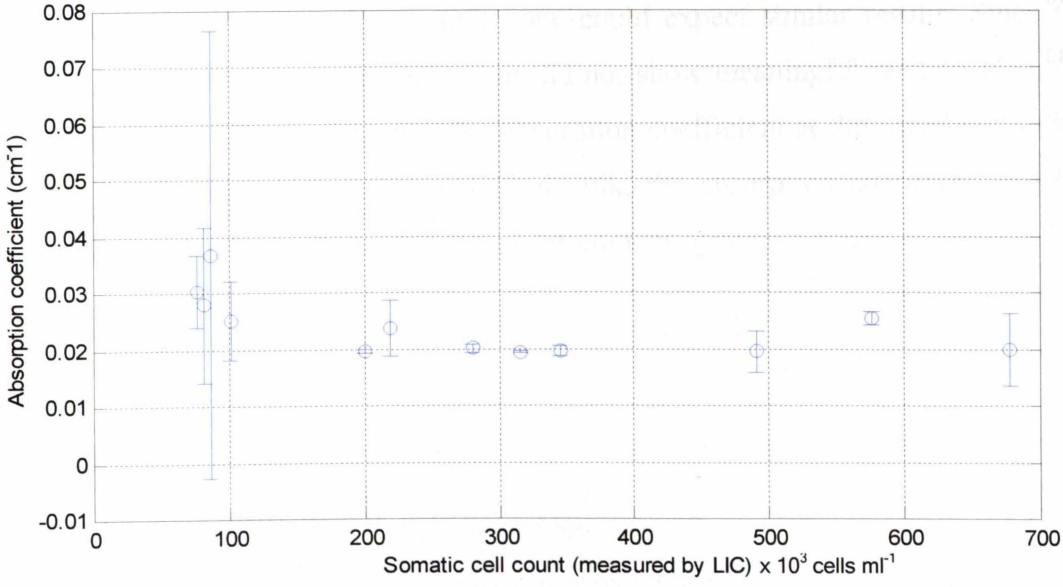

Figure 6-19: Plot of absorption coefficient against somatic cell count.

Discussion

The only data that appears to have a meaningful correlation is the fat versus reduced-scattering coefficient data. All the other comparisons either had a poor correlation, or could be explained away (protein versus reduced-scattering coefficient). Note that with the fat versus reduced-scattering coefficient data, reduced-scattering coefficient values for any milk with fat content above 8.5% deviated from the observed trend. This was due to the high light attenuation from high-fat samples degrading the signal at the furthest (2.0 cm distance) pickup fibre.

Therefore, considering only milk with a fat content lower than 8.5% should give much improved results. Figure 6-20 shows the results of all milk samples with less than 8.5% fat, along with a calculated linear regression model and a 90% prediction interval.

The calculated prediction interval shows that we can expect to be able to measure milk fat in homogenised milk with a precision of ±1 %. That is not a good precision, but there is much scope for improvement. In particular, the addition of a light shield around the sample container and the use of a cable with less RF leakage from the modulation source output to the laser diode driver could help to improve the results significantly.

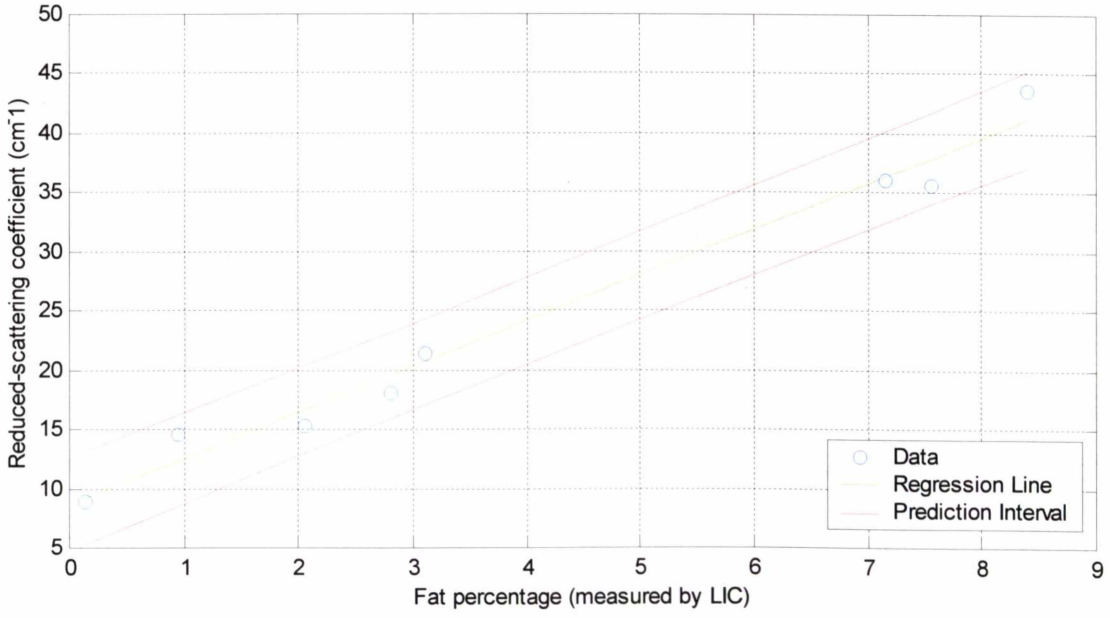

Figure 6-20: Fat data for samples with measured fat content under 8%. Regression model and 90% prediction interval data shown.

Note that the regression line does not pass through zero. This was explained by the fact that when there is no fat in the milk, there is still scattering caused by the casein micelles. Recall that the skim milk has 0.1% fat content, but still looks quite white (under daylight), but with a noticeably blue tinge which is consistent with the increased Rayleigh scattering from the smaller casein micelles.

Therefore, it was safe to say that the photon migration instrument was usable as a moderately precise indicator of milk fat content, but not of protein content or somatic cell count. However, the effects of the protein as the milk samples approached 0% fat were evident, as there were no longer a sufficient number of fat globules to contribute to the scattering characteristics of the milk.

With a few more improvements, the photon migration instrument should be able to handle raw milk, which is quite a different substance to homogenised milk. The next section discusses the first experiments with raw milk in the laboratory.

6.4 Experiments with raw milk

6.4.1 Fat determination of raw milk samples in the laboratory

Introduction

In the previous experiment, one can observe a clear trend between the reduced-scattering coefficient and the fat content of a homogenised milk sample. Thus if this procedure was repeated with raw milk, one could expect similar results. Since the results for protein and somatic cell count did not show meaningful relationships, the fat content was the primary target. The absorption coefficient at the wavelength used can also be ignored since in homogenised milk, the absorption coefficient did not have any strong relationship with any of fat content, protein content or somatic cell count.

Aim

The object of this experiment was to make measurements on raw milk using the photon migration instrument to determine the reduced-scattering coefficient and relate it to the measured fat content. Once that was done, we could then determine whether a similar trend for the reduced-scattering coefficient existed for raw milk, of which the physical composition is somewhat different.

Method

The photon migration instrument had further modifications in that a semi-rigid microwave cable had been installed from the modulation source out to the laser diode driver. This significantly decreased the amount of source-receiver cross talk and allowed the use of a modulation frequency range once again, as opposed to a single modulation frequency. Since these modifications did not alter the operating principle of the instrument and therefore did not invalidate the trends already observed, the previous experiment did not need to be redone.

Otherwise, the photon migration instrument was set up as in Figure 5-3, with the following settings applied to the RF network analyser:

Bandwidth:	1200 Hz
Sample averaging:	64 samples
Number of data points:	21
Frequency:	60 - 80 MHz
RF power:	8.6 dBm
Source-Detector distances:	1.5 cm, 2.0 cm and 2.5 cm

The source-detector distances were increased slightly (1.5 cm, 2.0 cm and 2.5 cm) to account for the lower light attenuation of raw milk compared to homogenised milk. Milk obtained from the Merlin automated milking system was transported back to the photon migration instrument in the laboratory. The milk was measured by the photon migration instrument within twenty-four hours of its collection from the cow. Before measurement, the milk was stored in a refrigerator at 4°C and then the bottle containing the milk was inverted several times to evenly distribute the fat throughout the milk. Ten readings per sample were taken, and the average was presented.

Results and Discussion

Figure 6-21 shows a poor relationship between measured fat content and the reduced-scattering coefficient. That was not attributable to any source-receiver cross talk in this experiment, as a semi-rigid microwave coaxial cable was used to deliver the modulation source to the laser diode driver.

One more point to note is that for each sample, the reduced-scattering coefficient for different modulation frequencies differed significantly, in excess of 10% from the average in all cases. According to diffusion theory, the reduced-scattering coefficient

should not have changed with modulation frequency. From this, the following questions must be asked – was the poor correlation an indication of a problem with the method (throry and implementation), or simply a problem with the tuning or set-

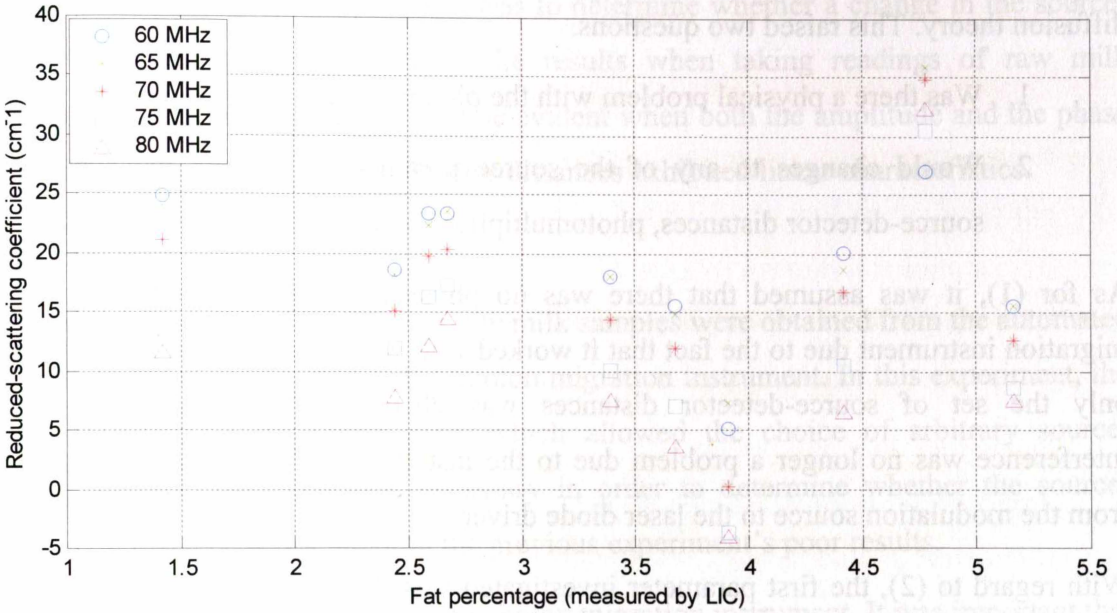

up of the instrument?

Figure 6-21: Sample set 2 – plot of fat content against reduced-scattering coefficient.

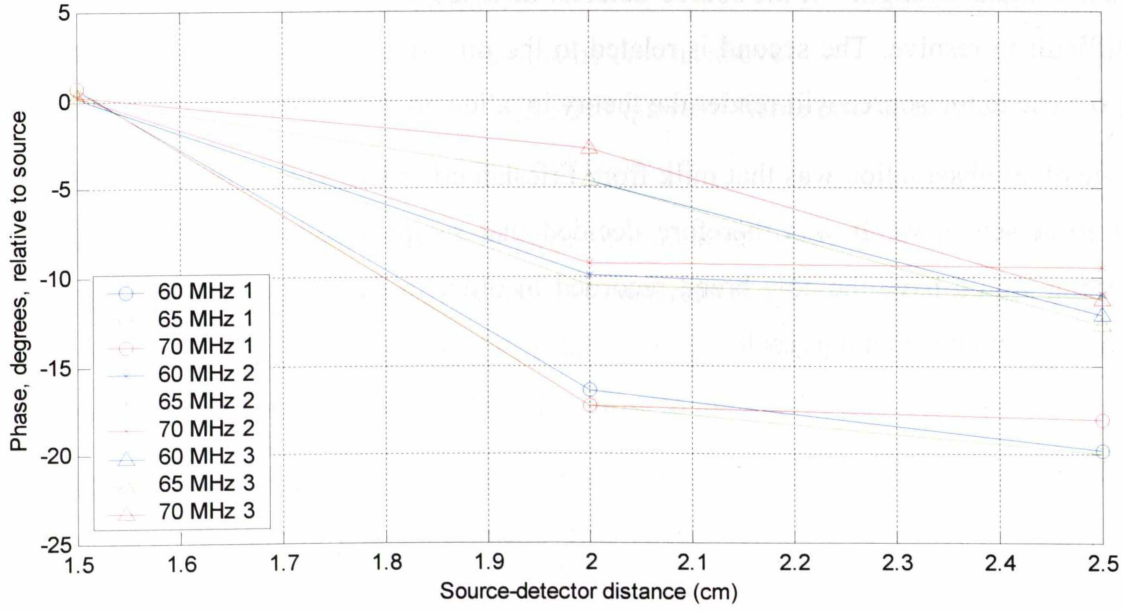

Figure 6-22: Phase readings for the three source-detector distances of three of the measurements.

The answers to those questions lay in a closer examination of the raw data returned from the photon migration instrument. Figure 6-22 shows the phase data for some of the readings taken. Clearly the phase did not decrease linearly, as predicted by diffusion theory. This raised two questions.

1. Was there a physical problem with the photon migration instrument?
2. Would changes to any of the source parameters (incident wavelength, source-detector distances, photomultiplier voltage, etc.) improve results?

As for (1), it was assumed that there was no physical problem with the photon migration instrument due to the fact that it worked well with homogenised milk, since only the set of source-detector distances was changed. Also, source-receiver interference was no longer a problem due to the installation of the semi-rigid cable from the modulation source to the laser diode driver.

With regard to (2), the first parameter investigated was the source-detector distance. Since these distances were increased from when the measurements were made with homogenised milk in order to compensate for the lower extinction from raw milk (with the immediately observable effect being a greater apparent transparency), it is a reasonable assumption that the small increase in distances was insufficient. There are two factors that must be balanced with the choice of source-detector distance. The first is signal strength – if the source-detector distance is too great, the signal becomes difficult to resolve. The second is related to the diffusion theory – distances that are too close to the source will render the theory invalid and the results useless.

One other observation was that milk from Friesian cows was visibly different to milk from Jersey cows. It was therefore decided that samples collected for subsequent testing would have the cow breed recorded in order to determine what effects cow breed would have on the results.

6.4.2 Adjustments to the photon migration instrument for raw milk measurements

Aim

The main point of this experiment was to determine whether a change in the source-detector distance would improve the results when taking readings of raw milk samples. This improvement would be evident when both the amplitude and the phase readings for the three source-detector distances exhibited linear characteristics.

Method

In order to test this, five different raw milk samples were obtained from the automated milking system and tested in the photon migration instrument. In this experiment, the variable-distance head was used, which allowed the choice of arbitrary source-detector distances. This was necessary in order to determine whether the source-detector distance was a factor in the previous experiment's poor results.

No other changes were made to the photon migration instrument. It was important that the photon migration instrument remained as similar as possible to the configuration used for the previous set of raw milk readings.

The five different milk samples were from:

- Bulk tank.
- Friesian cow, left rear quarter.
- Friesian cow, right rear quarter (same cow as above).
- Friesian cow, mixed left and right rear quarters (same cow as above).
- Jersey cow, mixed left and rear right quarters.

The two individual Friesian quarters gave an indication of the difference that can be expected between quarters on the same cow, whereas the mixed left and right quarter samples from the Jersey and the Friesian cow gave an indication of differences between breeds. Samples were collected as close to the start of milking as possible.

A series of source-detector distances from 1.0 cm up to 4.0 cm using 0.25 cm intervals were used in this experiment. This should have covered all the ranges of source-detector distances that could be used for milk analysis with the photon migration instrument.

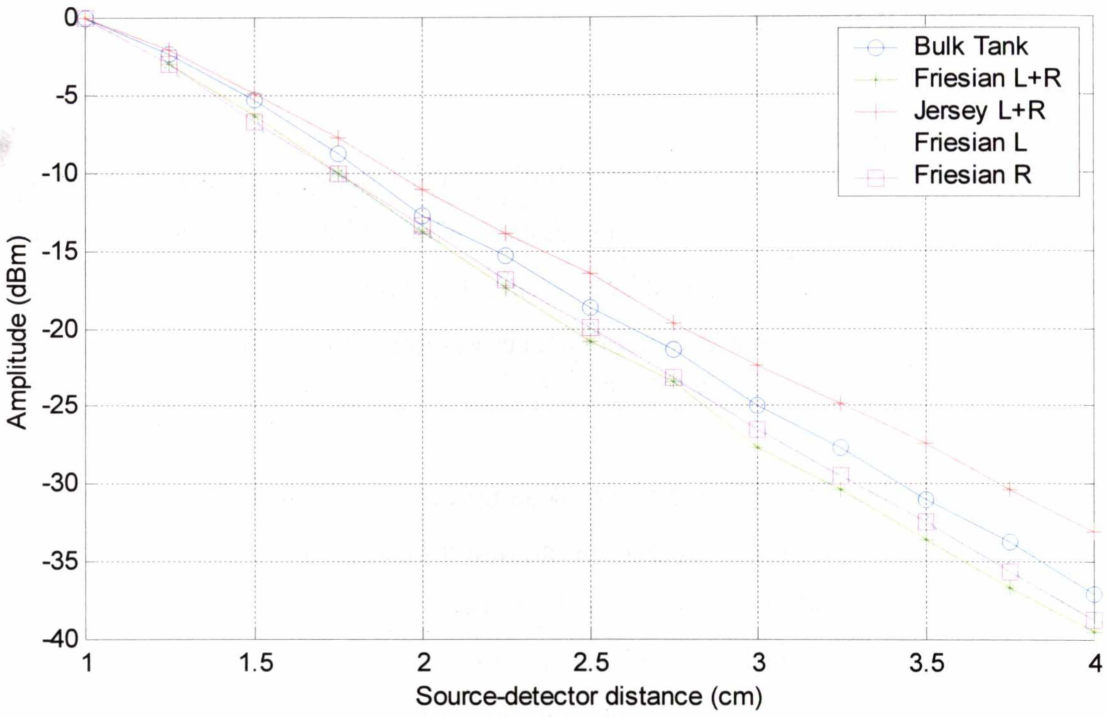

Figure 6-23: Amplitude measurements of various raw milk samples

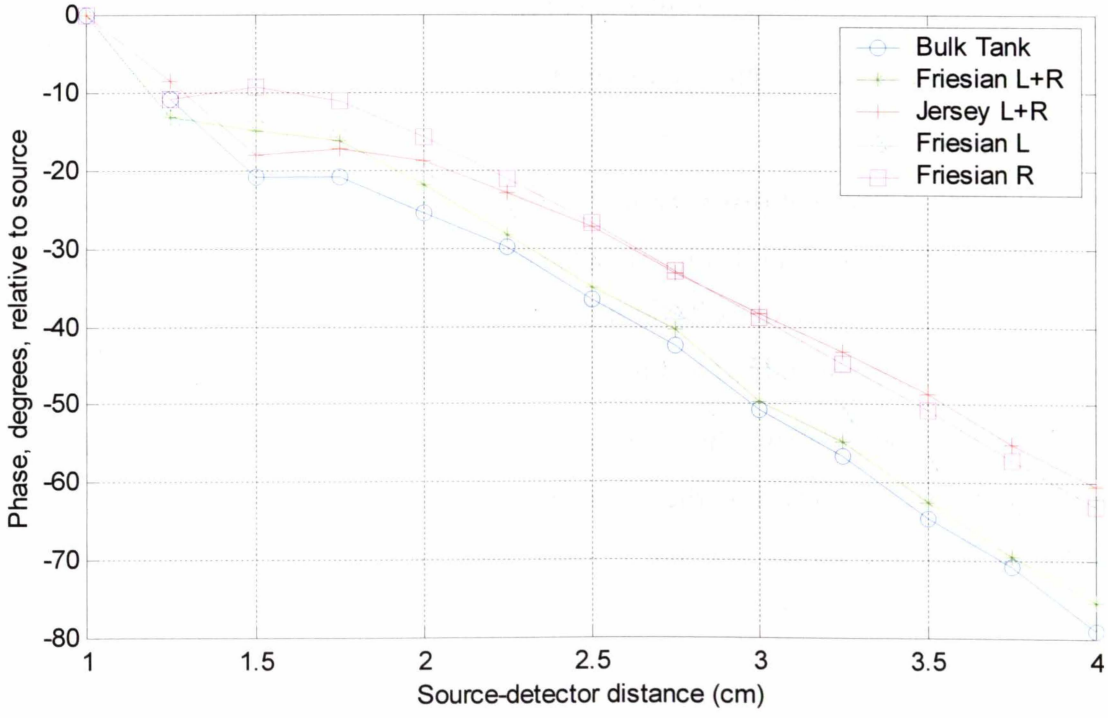

Figure 6-24: Phase measurements of various milk samples.

Results and Discussion

Figure 6-23 contains the amplitude data and Figure 6-24 contains the phase data. It was clear that there was a marked difference in linearity between the phase and amplitude figures. The amplitudes decreased fairly steadily with increasing source-detector distance, however the phases did not. The readings for distances up to 2.0 cm clearly did not follow a linear trend. From 2.0 cm onwards, the trend was linear.

Recalling the hypothesis in the last section regarding the reduced-scattering coefficient of raw milk compared to homogenised milk, it was fairly straightforward to see why that could be valid. If the raw milk is more watery, it must have scattered light less. Therefore, the minimum distance from the source to the detector, and the minimum distance from the source and detector to the container walls would be larger for raw milk than homogenised milk.

In light of these results, the 2.0 cm point indicated in the phase results was set as the indicator of the new minimum source-detector distance. The sample container's dimensions were large enough that only the source-detector distances needed to be changed. Thus, from these results, the new source-detector distances chosen for the photon migration instrument were 2.0, 2.5 and 3.0 cm.

Additional testing of the suitability of the new source-detector distances

The new source-detector distances needed verification as to their suitability for measurements on raw milk. This was achieved by measuring a set of samples with the photon migration instrument, using the new set of source-detector distances.

The milk samples in this case were the same as the set used to determine the new source-detector distances. A sufficient amount of milk had been collected to ensure that there would be enough for this verification. In addition, less than twenty-four hours had elapsed since the collection of the milk, and a sub-sample had been sent to the LIC testing laboratories earlier.

Figure 6-25 shows the plot of measured fat content versus the reduced-scattering coefficient as measured by the photon migration instrument set up with the new source-detector distances.

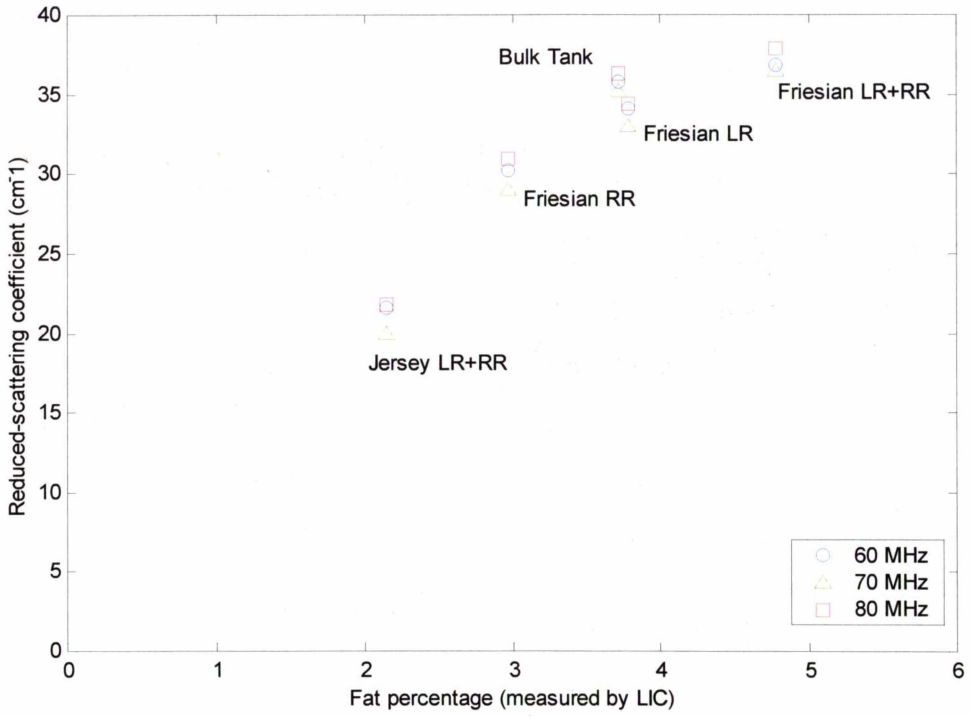

Figure 6-25: Reduced-scattering coefficient versus measured fat percentage with the new source-detector distances. RR = right rear quarter, LR = left rear quarter.

The results showed an increasing trend, although it did not appear as good or as linear as the one for homogenised milk. The reduced-scattering coefficient rose with milk fat percentage in a more predictable way than in the previous raw milk experiment.

However, one small question remained. Note that in the graph, the measured fat values for the bulk tank milk and the Friesian cow left rear quarter sample were close. Their reduced-scattering coefficients were also close. The question then, was whether it was possible to improve the correlation.

Recall that there were two questions regarding the previous poor performance of the photon migration instrument when used with raw milk. The results in Figure 6-25 now brought up a third question – was there a possibility that the characteristics of the raw milk could affect the precision of the photon migration instrument?

Two facts about the fat globules in milk are well known – firstly that they are the dominant particle and secondly, that they do not have a uniform size, but a size distribution. That was important as the size distribution of the fat globules should have affected the reduced-scattering coefficient. Thus, if equation 4-7 is modified to include the particle size distribution, one obtains:

$$\mu_s'(\lambda) = \int_0^{\infty} \frac{3}{2} \frac{Q_{scat}(n,x,\lambda)}{x} (1 - g(n,x,\lambda)) \phi f(x)\, dx \qquad [6\text{-}1]$$

The only difference is the *f(x)* term. That is the particle size distribution, normalised to unity for all $x > 0$. If a suitable function to describe *f(x)* could be found, then the precision of the correlation between the reduced-scattering coefficient and the fat content of the milk could be improved.

6.4.3 Determination of the particle size in raw cow's milk

Introduction and Aim

In order to determine the particle size distribution of raw cow's milk, a *f(x)* for equation 6-1 that described the particle size distribution of cow's milk needed to be found. One way to do this was to take reduced-scattering coefficient measurements of a milk sample at multiple wavelengths (Richter *et al.*, 1998).

This process could be aided by supplying a function that approximates the size distribution. From there, the parameters for the function that fit the actual size distribution need to be found. One point to note is that supplying the distribution function places a large restriction on the types of particle size distributions that can be accurately represented. However, work has been done on finding an arbitrary *f(x)* to enable the recovery of the particle size distribution for any particulate suspension that can be measured with a photon migration instrument (Jiang *et al.*, 1997). This method works well for a Weibull distribution (typical for particulate suspensions), but uses measurements with 15 different wavelengths to achieve sufficient accuracy.

As for a *f(x)* that can satisfactorily approximate the particle size distribution of raw milk, one can start with a simple normalised Gaussian, as 90% of the milk fat is represented by globules in the 3-5 mm diameter range. At this stage, only attempting to determine whether particle sizing is practical with the equipment available is sufficient, since it is quite likely that the particle size distribution for every single milk sample measured is required. However, it may be possible that a simple mean particle size (inside the 3-5 μm limit) determination is sufficient.

Aim

The objective of this experiment was to determine the parameters for the Gaussian that will describe the particle size distribution of the raw milk fat globules. Those parameters are the mean diameter and the spread of particle sizes around the mean. Another important parameter to recover is the volume fraction.

Method

In order to recover the Gaussian parameters and the volume fraction, several reduced-scattering coefficient readings were required per sample, using different wavelengths of light. The more wavelengths used, the more accurate the determination will be, as the algorithm used to find these parameters involves the minimisation of the function:

$$\chi^2 = \sum_{j=\lambda_1}^{\lambda_m} \left[\left(\mu_s'\right)_j^o - \left(\mu_s'\right)_j^c \right]^2 \qquad [6\text{-}2]$$

where $\left(\mu_s'\right)_j^o$ is the experimentally observed reduced-scattering coefficient and $\left(\mu_s'\right)_j^c$ is the reduced-scattering coefficient calculated using equation 6-1 and the current guess for *f(x)*. Since *f(x)* is a Gaussian, there is also an additional parameter *a*, which is the spread or width of the curve.

Matlab contains a simplex minimisation method as one of its standard tools. This exists in the form of a Matlab command, *fminsearch*. The code written for the recovery of the Gaussian parameters and the volume fraction uses this function. The source listing for this code is shown in the Appendix 8.2-8.6.

The algorithm was tested on simulated data before any measurements were made. Equation 6-1 supplied the calculated values, and the "observed" values were generated using the University of Pennsylvania photon migration software (Nishimura *et al.*, 1996). The "observed" values generated by the photon migration software were for a milk sample with a mean diameter of 3.5 microns, a standard deviation of 1.0 microns and a volume fraction of 0.03. The wavelengths used in this simulation were 635 nm, 651 nm, 670 nm and 780 nm.

Results

Figure 6-26 shows the results of the simulation with a range of values. The objective of the simulation was to find a minimum value of χ^2. That minimum value should

have coincided with the correct parameters for the Gaussian that describes the particle size distribution. That minimum point is difficult to see on Figure 6-26, so a close-up view around the minimum is shown in Figure 6-27.

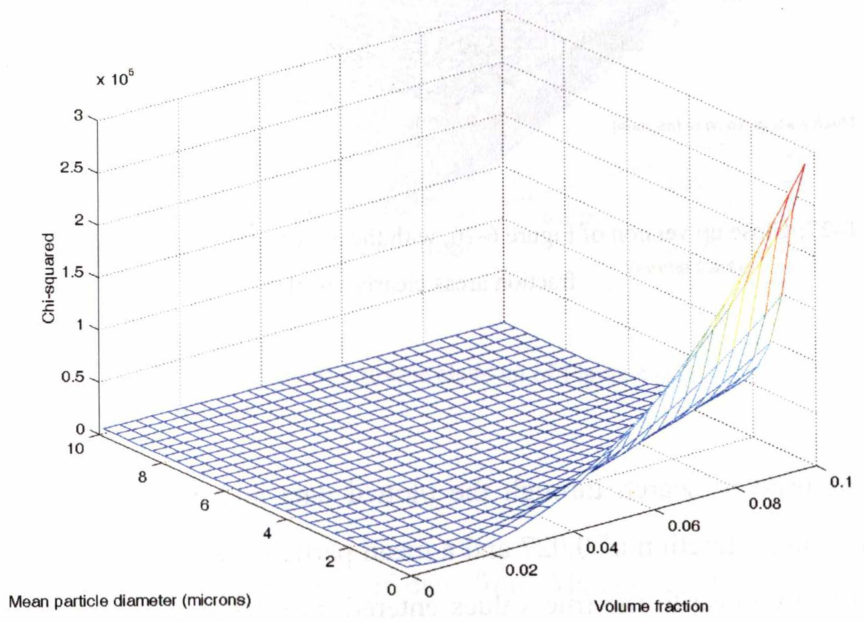

Figure 6-26: Difference between the calculated reduced-scattering coefficient and the "observed" reduced-scattering coefficient, plotted against mean particle size and volume fraction.

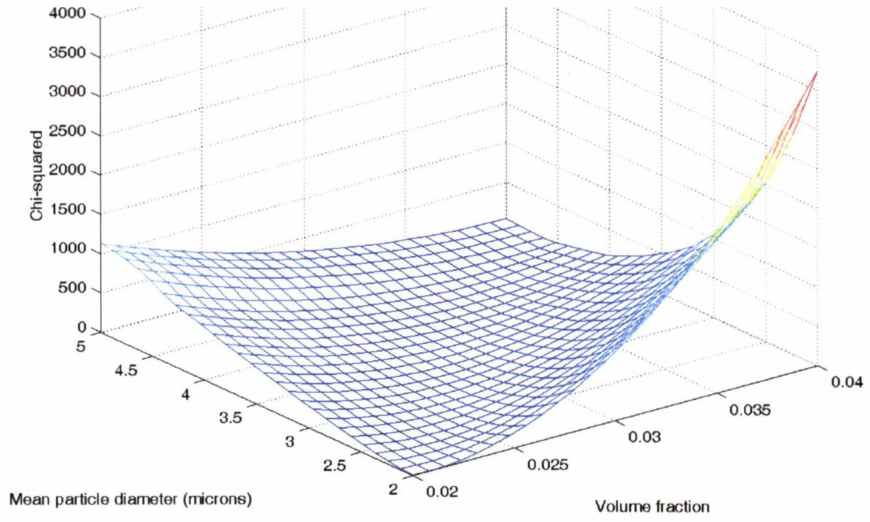

Figure 6-27: Close up version of Figure 6-26, with the 3.5 μm particle size and the 0.03 volume fraction areas clearly visible.

Matlab was used to search through the plotted data and retrieve the minimum. It returned a volume fraction of 0.027 and a mean particle size of 3.1 μm. Those values were reasonably close to the true values entered into the simulation. They were not exact because the reduced-scattering coefficient values from the photon migration software and the Matlab version of equation 6-1 were not in complete agreement. Increasing the resolution of the data (and therefore the plot) yielded a better result, as shown in Figure 6-28.

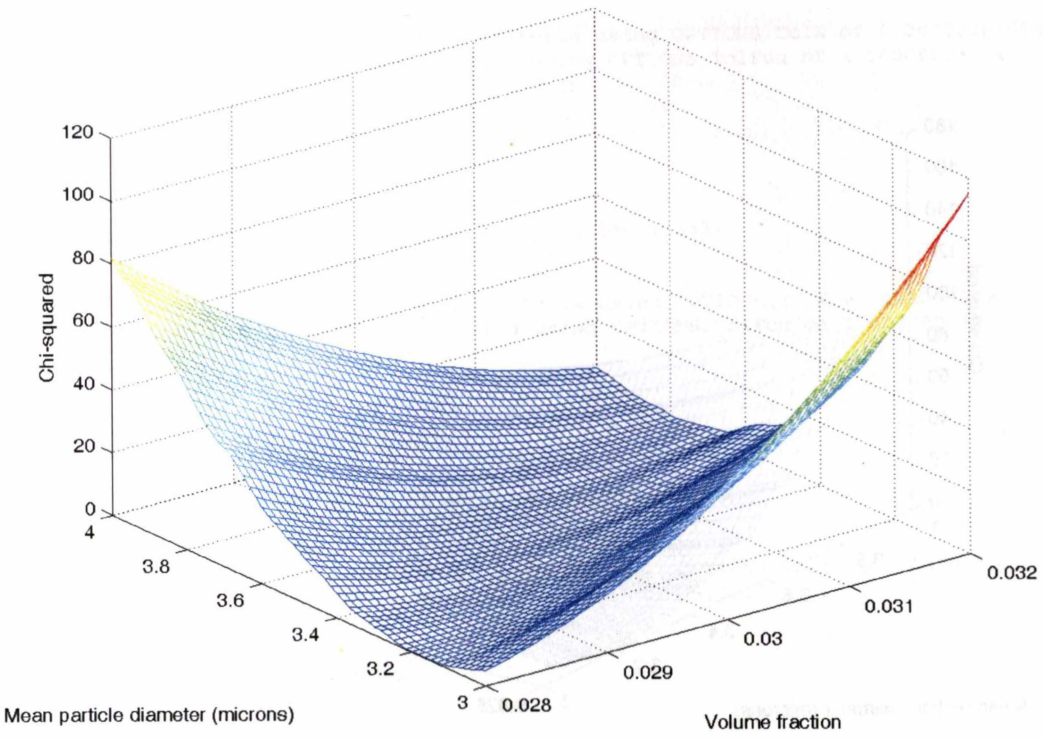

Figure 6-28: Extreme close-up of Figure 6-26.

The figures obtained from this set of data from Matlab are 3.5 μm and a volume fraction of 0.03. These are the same as the values that were originally entered into the simulation.

The resulting data shown from the numerical simulations represent a perfect situation. The photon migration instrument was unable to provide that kind of precision for reduced-scattering coefficient measurements. One way to overcome this was to use a greater number of wavelengths. However, that brought about another problem. As the difference between the observed reduced-scattering coefficients and the calculated reduced-scattering coefficients increased, an oscillation started to show up on the mean particle diameter axis. Figure 6-29 shows the same information as Figure 6-28, except that a new wavelength, 525 nm was added. The difference between the calculated 525 nm reduced-scattering coefficient and the "observed" reduced-scattering coefficient was greater than that for the other wavelengths.

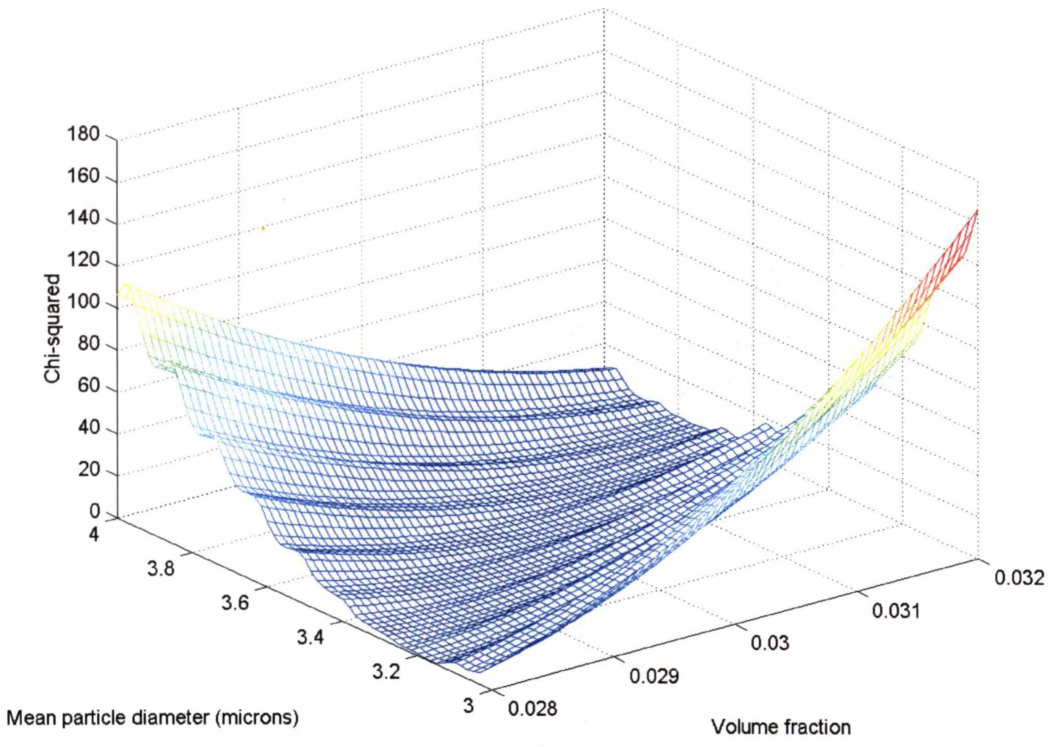

Figure 6-29: Extreme close-up of figure 6-25, but with the 525 nm simulation included.

The kind of results shown in Figure 6-29 is what we would be expecting from the photon migration instrument. That did not look so bad until a proper minimisation function, such as the *fminsearch* command mentioned previously was used. The ripples in the function, which were caused by numerical instabilities, caused a large number of local minima to appear. That had the effect of prematurely stopping most minimisation algorithms, leading to the reporting of incorrect results.

The results of using the Matlab *fminsearch* command depend very heavily on the initial guess chosen. Figure 6-26 and Figure 6-27 show clearly that in principle, the absolute minimum could easily be found. Here are three examples of the *fminsearch* command in use, with different initial guesses:

```
» fminsearch('minimi',[3,1,0.01],[],in_m,in_l,1.546,1.333)

Optimization terminated successfully:
 the current x satisfies the termination criteria using OPTIONS.TolX of 1.000000e-004
 and F(X) satisfies the convergence criteria using OPTIONS.TolFun of 1.000000e-004


ans =

    1.1091    1.2611    0.0147

» fminsearch('minimi',[3.5,1,0.03],[],in_m,in_l,1.546,1.333)

Optimization terminated successfully:
 the current x satisfies the termination criteria using OPTIONS.TolX of 1.000000e-004
 and F(X) satisfies the convergence criteria using OPTIONS.TolFun of 1.000000e-004


ans =

    3.4913    1.0292    0.0300

» fminsearch('minimi',[4.0,1,0.05],[],in_m,in_l,1.546,1.333)

Optimization terminated successfully:
 the current x satisfies the termination criteria using OPTIONS.TolX of 1.000000e-004
 and F(X) satisfies the convergence criteria using OPTIONS.TolFun of 1.000000e-004


ans =

    4.7156    1.0683    0.0378
```

For the second attempt with *fminsearch*, the returned result was close to the true result by using them as the initial guesses. Further experimentation with a larger number of figures showed that straying far from the real figures for the initial guess caused incorrect values to be returned from the minimisation. Tuning the minimisation parameters (as shown in the Matlab documentation for the *fminsearch* command) had little effect on the results. Changing the algorithm from a simplex search to a Levenberg-Marquardt algorithm did not improve the results either.

The problem with the particle sizing turned into a problem of unconstrained minimisation of a three-parameter function with many local minima, the three parameters being mean particle diameter, standard deviation of the particle diameter and the volume fraction. Problems of this nature are difficult to solve in general and are outside the scope of this thesis.

An additional problem encountered is the length of time required for the minimisation algorithm to run. These simulations were performed on an Intel Pentium-III 866 MHz desktop computer, and took approximately four minutes per run. This is not suitable for an on-line application in the near future. It would require at the minimum, a tenfold increase in the processing speed before the minimisation algorithm would be fast enough.

Therefore, we conclude from this set of simulations that particle sizing in milk is a difficult problem to perform in online applications. It requires much computing time and power, and therefore would be impractical for use in a live situation, such as in an automated milking system. Due to this, no further development on milk fat globule size distribution was performed.

6.4.4 Experiments with fresh raw milk at the automated milking system

Introduction and Aim

It is at this stage that the photon migration instrument was deemed ready to take measurements of fresh raw milk. Even though the particle size distribution of milk could not be measured, it was possible to collect useful data about raw milk samples. The main difference between this set of experiments and the previous set is that the photon migration instrument is located at the automated milking system site, not in a laboratory. Consequently, the environment was a lot less controlled and thus there were many more opportunities for interference of all kinds (mainly RF and stray light) to affect the readings.

The properties of milk that were being investigated in those experiments were:

1) The verification of how milk changes over the course of a single milking.
2) The correlation that the reduced-scattering coefficient has with milk fat content.

It is well known that the milk fat percentage changes during milking from a low fat percentage to a high fat percentage. It was therefore expected that the reduced-scattering coefficient would also change in a similar way. However, since it was not possible to measure the particle size distribution, the possibility was raised that the correlation between the reduced-scattering coefficient and the fat content could be poor. That being due to the fact that there is a likelihood that different cows will produce milk having fat globules with different size distributions.

Method

In order to answer the two questions posed, the photon migration instrument needed to be capable of recording the required multiple source-detector distance amplitudes and phases quickly. The cycle time for measurement using that photon migration instrument was about thirty seconds per sample, which proved sufficient since the average time required for milking was close to 5 minutes. The timings were only a rough estimate, but gave an indication that at least three measurements per milking were possible.

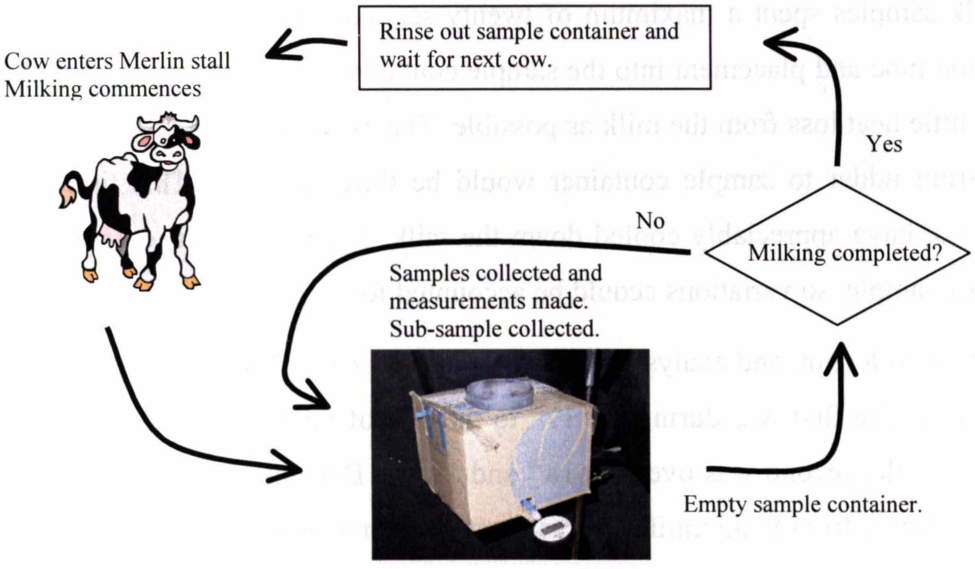

Figure 6-30: Experimental procedure.

The automated milking system has a feature where the mass of the milk delivered by the cow on her last milking is displayed on the control panel. This helped to give an estimate of how many measurements per cow could be taken. A cow that delivered 9-12 kg of milk could usually have three measurements taken whereas a cow that delivered 20 kg or more milk could usually have as many as five measurements taken.

The sample container was designed to connect to one of the milk lines coming from the robotic milking arm to the milk meter, shown in Figure 5-16. Its original design allowed it to be fitted in-line but due to technical difficulties arising from the extra flow distance introduced by the sample container and associated tubing causing the milk flow sensor to not function properly, the sample container was not fitted on line,

but instead placed within 1.5 m of the sampler tube connection point (refer to Figure 5-16 for details).

Figure 6-30 shows the procedure followed for collecting samples and taking readings. Milk was gathered from two sampler tubes (connected to the left rear and right rear quarter milk lines), poured into the sample container, and a single multiple-distance measurement was made for each sample. Approximately 210 mL of milk was used per sample, with a subsample taken and placed in a labelled vial for analysis at the LIC testing laboratories. A small number of these subsamples were duplicated and sent to the Dexcel testing laboratories for more precise analysis using near-infrared spectroscopy.

All milk samples spent a maximum of twenty seconds between collection from the collection tube and placement into the sample container. This was to ensure that there was as little heat loss from the milk as possible. The estimated time taken for the milk to go from udder to sample container would be thirty seconds. This time interval should not have appreciably cooled down the milk. Temperature readings were also taken per sample, so variations ccould be accounted for.

The actual collection and analysis of the samples was carried out over several days in two blocks. The first was during the 17th to the 20th of September 2002 after calving season, and the second was over the 18th and 19th of December 2002. Measurements were conducted from 9 am until 4 pm as most cows arrived to be milked at least once during those hours.

The settings on the photon migration instrument are:

Bandwidth:	1200 Hz
Averaging:	64 samples
Number of data points:	21
Frequency:	60 - 80 MHz
RF power:	8.6 dBm
Source-Detector distances:	2.0 cm, 2.5 cm and 3.0 cm

Results and Discussion

Over the two periods of gathering data, 115 measurements were made with milk from Jersey and Friesian cows. The herd at the automated milking system was strongly

dominated by Friesians (n = 95) and so the results had a high proportion of Friesian milk samples in them. The total number of Jersey samples was 20.

Very little RF interference below 80 MHz was observed over both the data-gathering periods. Some of the cows had trouble being milked by the robot, and therefore only one or two samples were taken from them.

The results are shown in Figure 6-31. Only the 65 MHz figures are shown, but all the modulation frequencies recorded show similar results but with the size of the spread around the mean being different. The 80 MHz data was less linear than the results from the 60 to 75 MHz modulation frequencies.

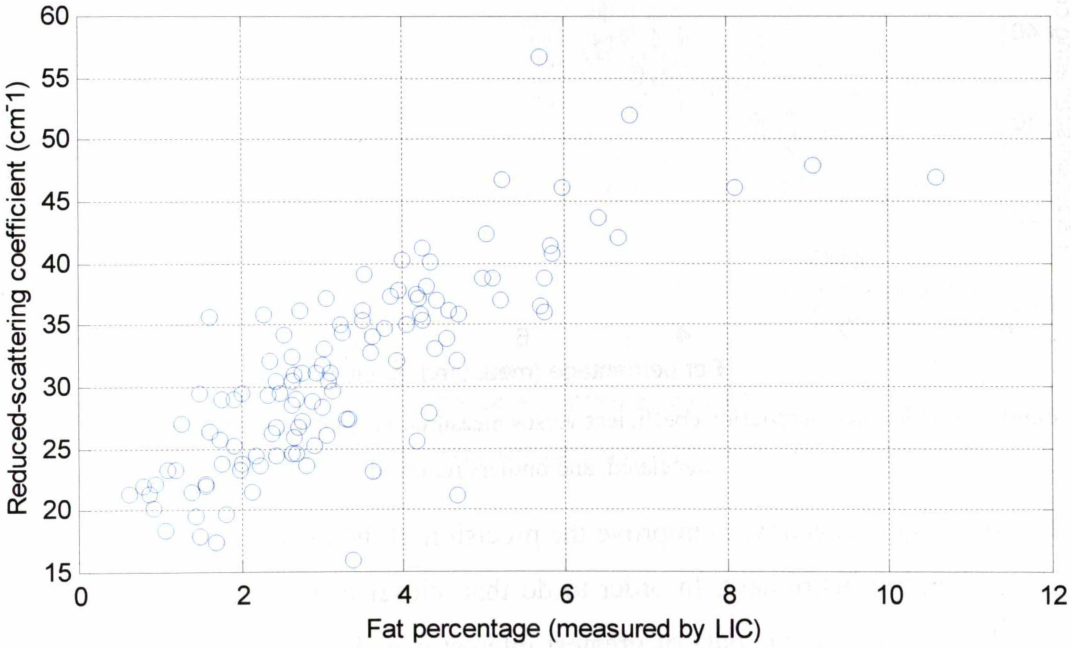

Figure 6-31: All reduced-scattering coefficient versus measured fat content data for raw milk.

There were a few outliers among the data points. Some were directly attributable to operator error during the sampling, such as neglecting to cover the top of the sample container (the light shield does not cover the top). A total of four samples were identified with these issues, and they were removed from the data. Figure 6-32 shows the reduced-scattering coefficient plotted against measured fat content again, but this time with the outliers removed and statistics calculated for the data.

Figure 6-32 shows the same data with a 90 % prediction interval plotted. That data shows a precision of ± 2 % for reduced-scattering coefficient measurements against

fat content. This kind of precision is insufficient for on-line measurement at the farm, even as an indicator.

Note the wide spread of reduced-scattering coefficients for each fat content value. This indicated that there was at least another factor (most likely particle size distribution) directly affecting the results.

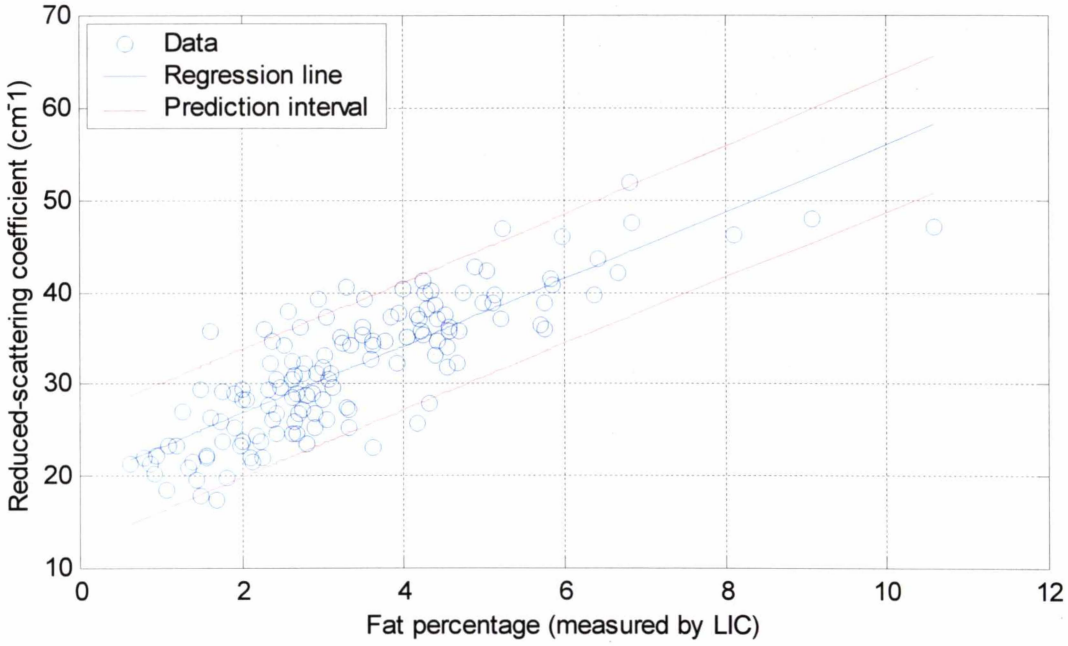

Figure 6-32: Reduced-scattering coefficient versus measured fat content. 90% prediction interval calculated, and outliers removed.

The next question was how to improve the precision of the measurements made by the photon migration instrument. In order to do that, closer examination of the data was required. In particular, the data of greatest interest was that regarding any correlation with the cow breed or the milk sample temperature when the measurement was made.

Figure 6-33 and Figure 6-34 show the reduced-scattering coefficient versus measured fat content for Friesian cows and Jersey cows respectively.

Separating the different breeds of cow showed that there was quite likely to be a difference between their milks, in terms of the size distribution of the fat globules. However, upon closer analysis, separating out the milk samples by breed yielded a noticeably high measurement precision. For Friesian cows, the fat content could be measured to a precision of ±1.6 % and for Jersey cows, the fat content could be measured with a precision of ± 1.4 %. The appearance of Figure 6-34, indicated that

there could be a possibility that the fat globules of the Jersey milk were more uniform across many cows than the fat globules of Friesian milk.

Having a different regression line for the two different breeds of cow improved the precision of the fat content determination using the photon migration instrument. However, the improvement in precision was still not yet enough for it to be used as a monitoring instrument.

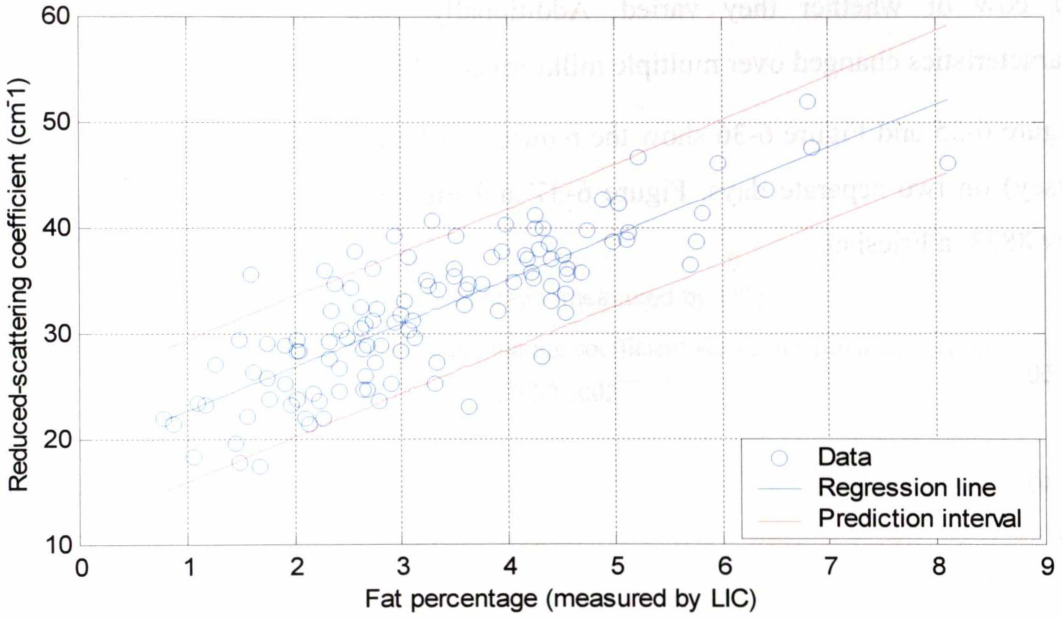

Figure 6-33: Reduced-scattering coefficient versus fat content for Friesian cows.

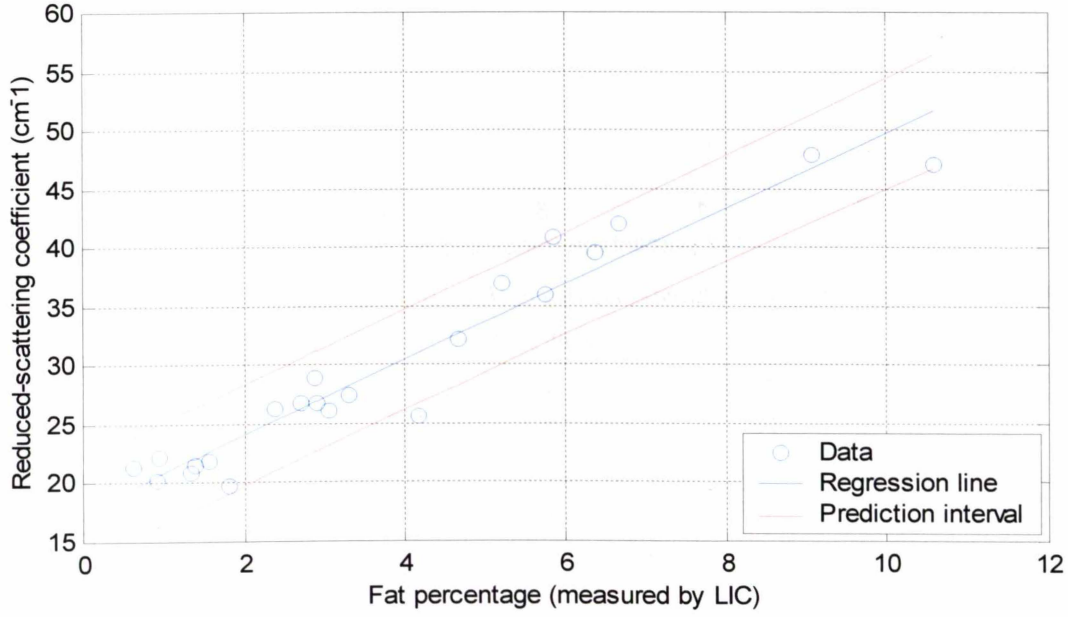

Figure 6-34: Reduced-scattering coefficient versus fat content for Jersey cows.

The data was then separated out into readings for individual milkings. That analysis give an indication of the nature of the fat globules per milking per cow, and whether it was consistent over multiple milkings. If we had found that for any single milking the reduced-scattering coefficient and the measured fat content had a linear relationship, then it would have been a reasonable assumption that the fat globule characteristics were consistent over a single milking. Since this also broke up the data down to a per-cow basis, it would also show whether the fat globule characteristics were constant per cow or whether they varied. Additionally, data on how the fat globule characteristics changed over multiple milkings could be viewed.

Figure 6-35 and Figure 6-36 show the reduced-scattering coefficient for cow 9517 (a Jersey) on two separate days. Figure 6-37 and Figure 6-38 show the same data for cow 8833, a Friesian.

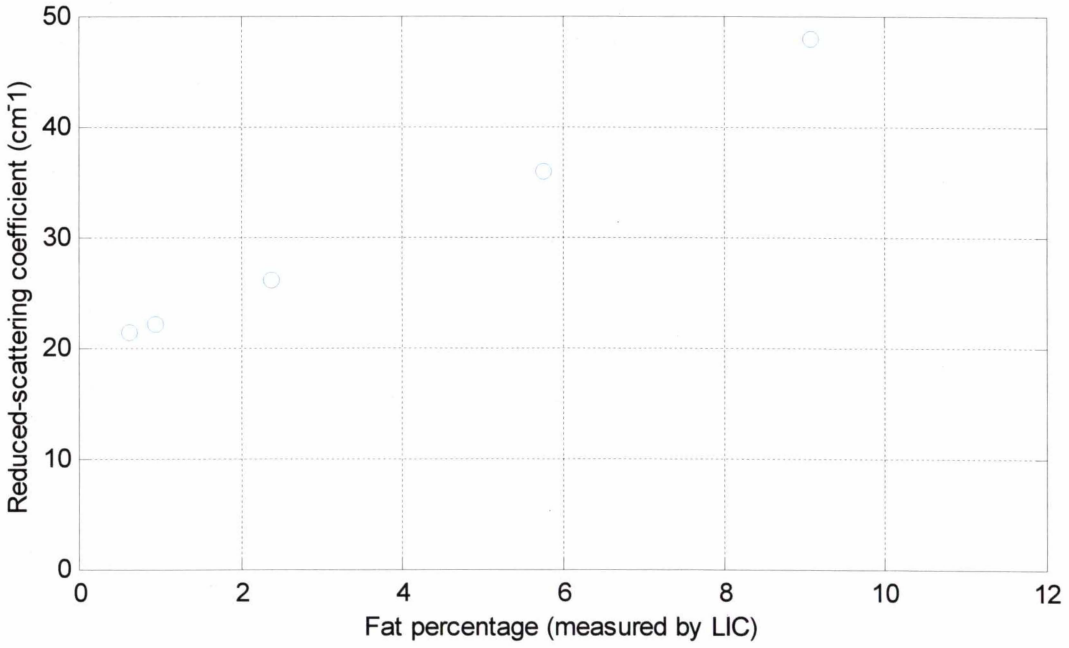

Figure 6-35: Jersey cow (9517) reduced-scattering coefficient versus measured fat percentage data - 19/09/2002

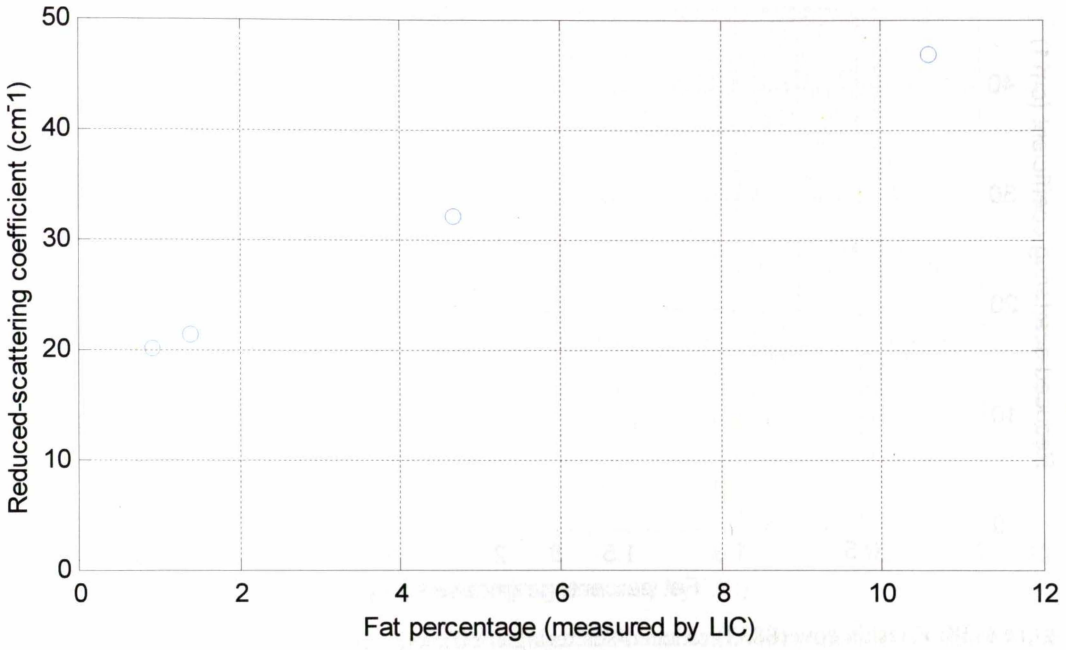

Figure 6-36: Jersey cow (9517) reduced-scattering coefficient versus measured fat percentage data - 20/09/2002

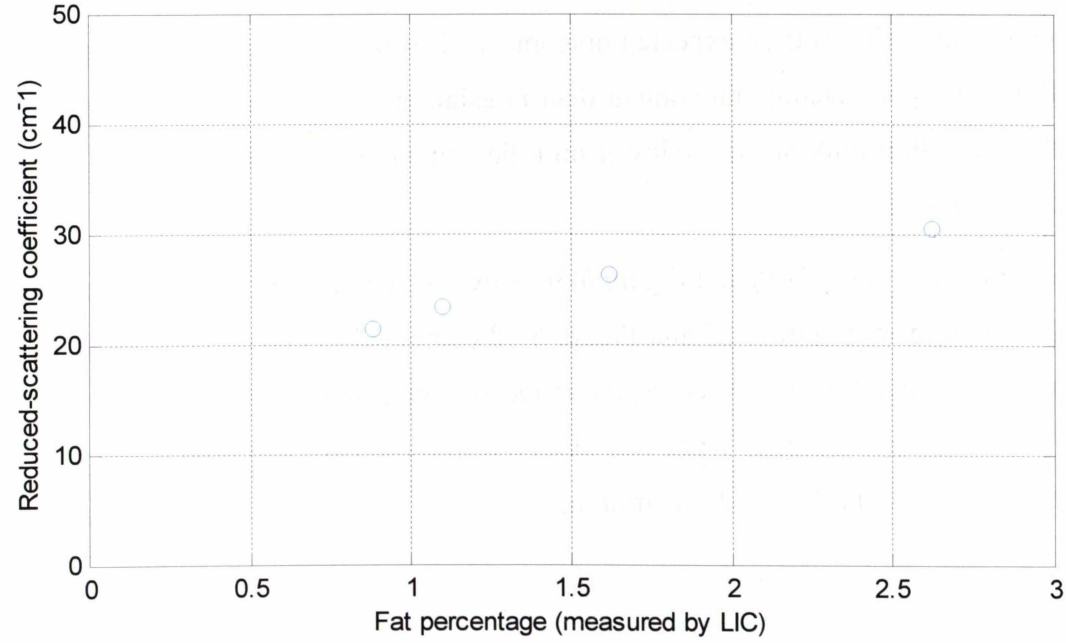

Figure 6-37: Friesian cow (8833) reduced-scattering coefficient versus measured fat percentage data - 19/09/2002

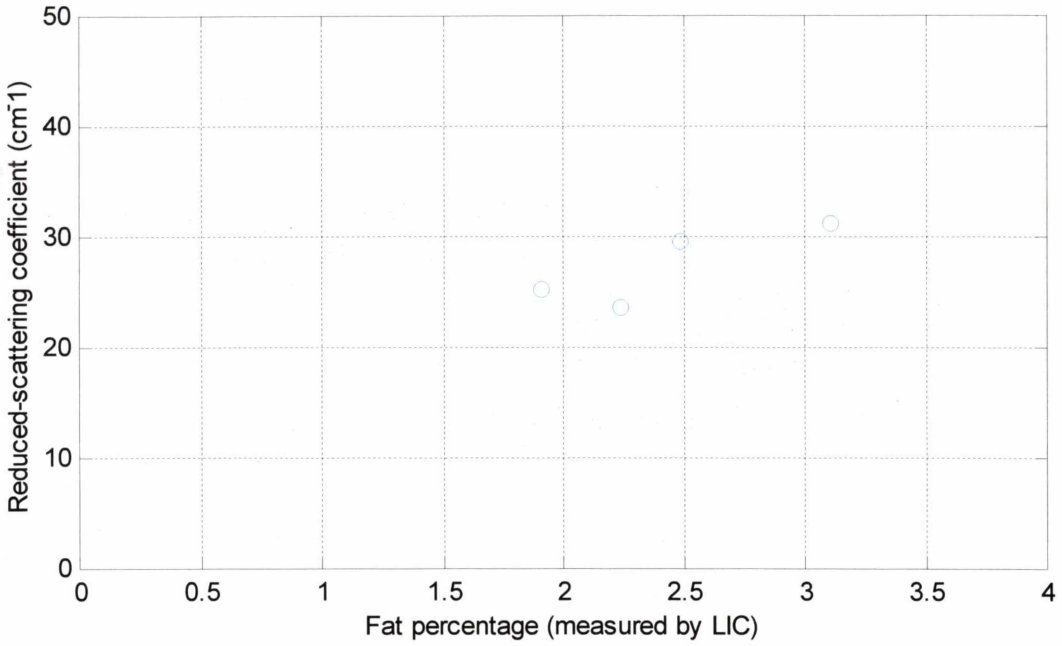

Figure 6-38: Friesian cow (8833) reduced-scattering coefficient versus measured fat percentage data - 20/09/2002

Positive trends in both the Jersey cow and Friesian cow data were visible. The Jersey cow data appeared to show a much tighter linear trend, as shown by Figure 6-34. Notice also that the range of fat percentages for Jersey milk were much larger than for Friesian milk. This was an expected outcome, as it was commonly known that Jersey milk has a higher average fat content than Friesian milk. It was also well known that both breeds start milking with a lower milk fat content and end milking with a higher milk fat content.

The data from Figure 6-35 and Figure 6-36 were then combined to create Figure 6-39, and the data from Figure 6-37 and Figure 6-38 combined to make Figure 6-40. Those figures show that for the two cows, the reduced-scattering coefficient could show the fat percentage per milking. What was observed in those two new figures was that the relationship held up over multiple milkings.

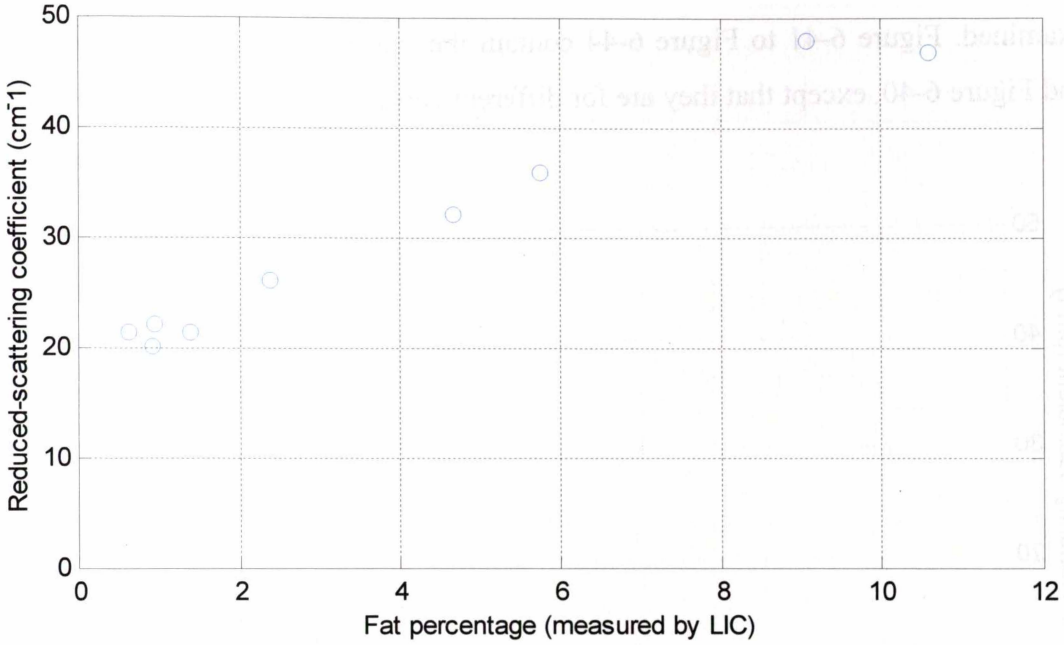

Figure 6-39: Jersey cow (9517) reduced-scattering coefficient versus measured fat percentage data - 19/09/2002 and 20/09/2002

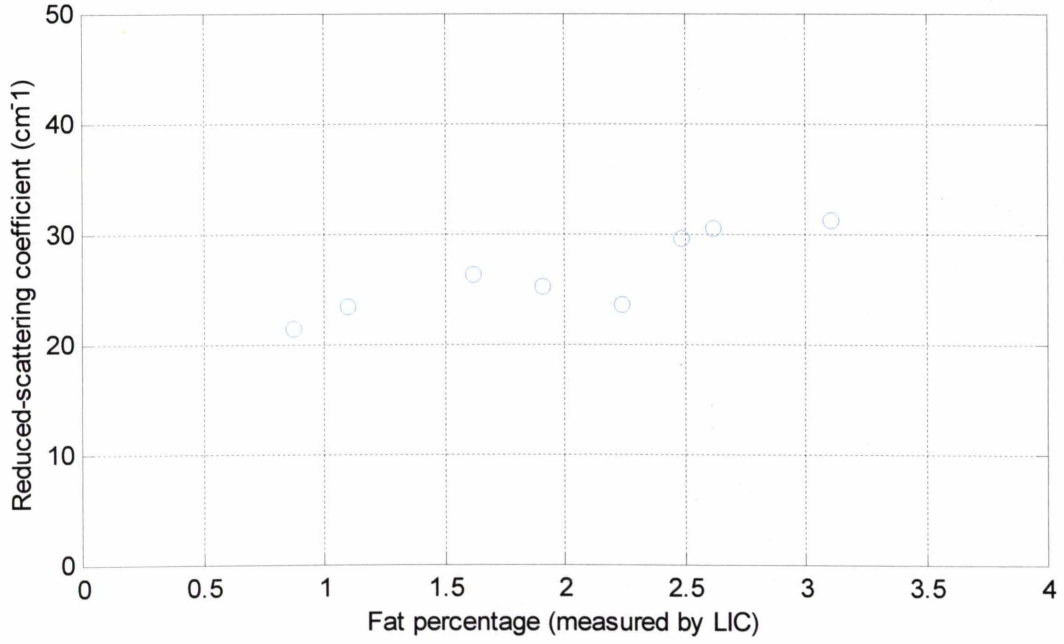

Figure 6-40: Friesian cow (8833) reduced-scattering coefficient versus measured fat percentage data – 19/09/2002 and 20/09/2002

The relationship between the reduced-scattering coefficient and the measured fat percentage appeared to be consistent over the two milkings on different days, for

these two cows. To confirm this suspicion, similar data from some other cows were examined. Figure 6-41 to Figure 6-44 contain the same type of data as Figure 6-39 and Figure 6-40, except that they are for different cows.

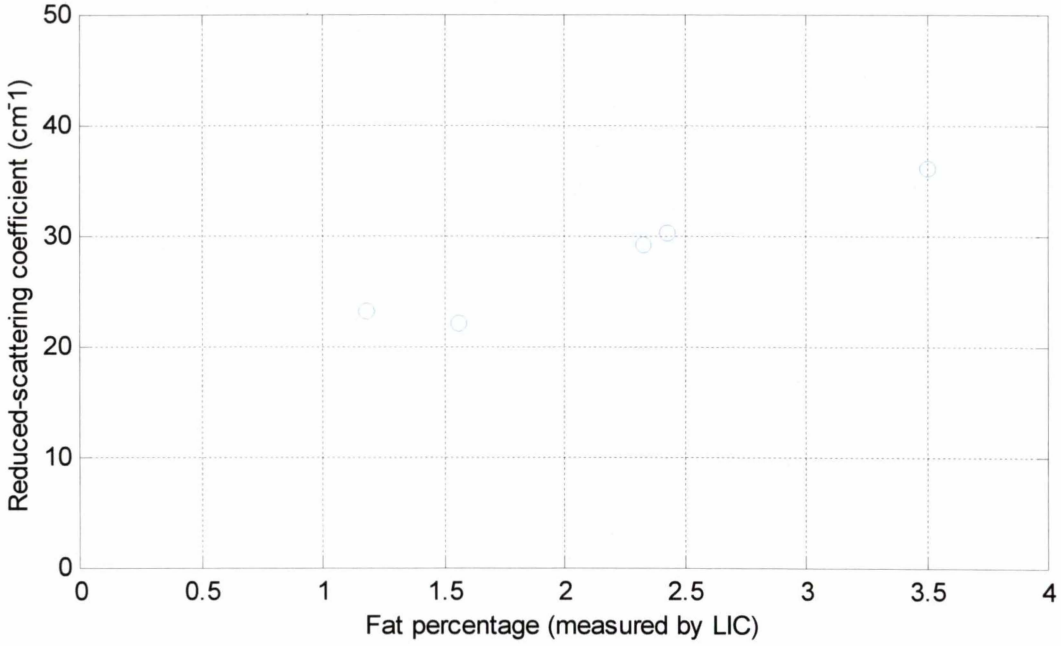

Figure 6-41: Jersey cow (7641) reduced-scattering coefficient versus measured fat percentage data - 19/09/2002 and 20/09/2002

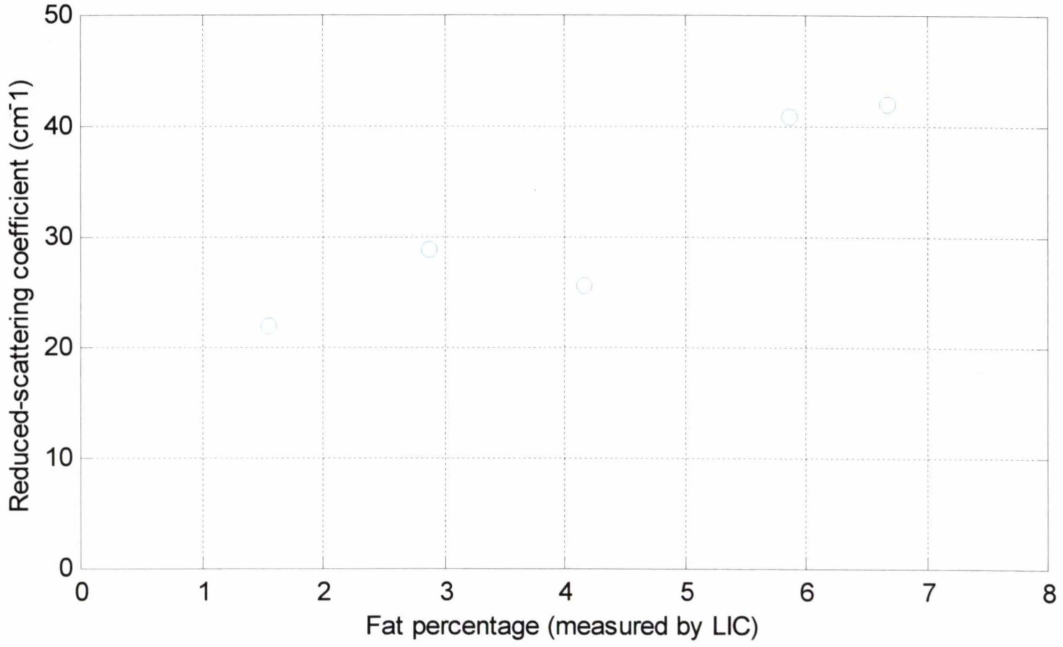

Figure 6-42: Friesian cow (8714) reduced-scattering coefficient versus measured fat percentage data – 18/09/2002, 19/09/2002 and 20/09/2002

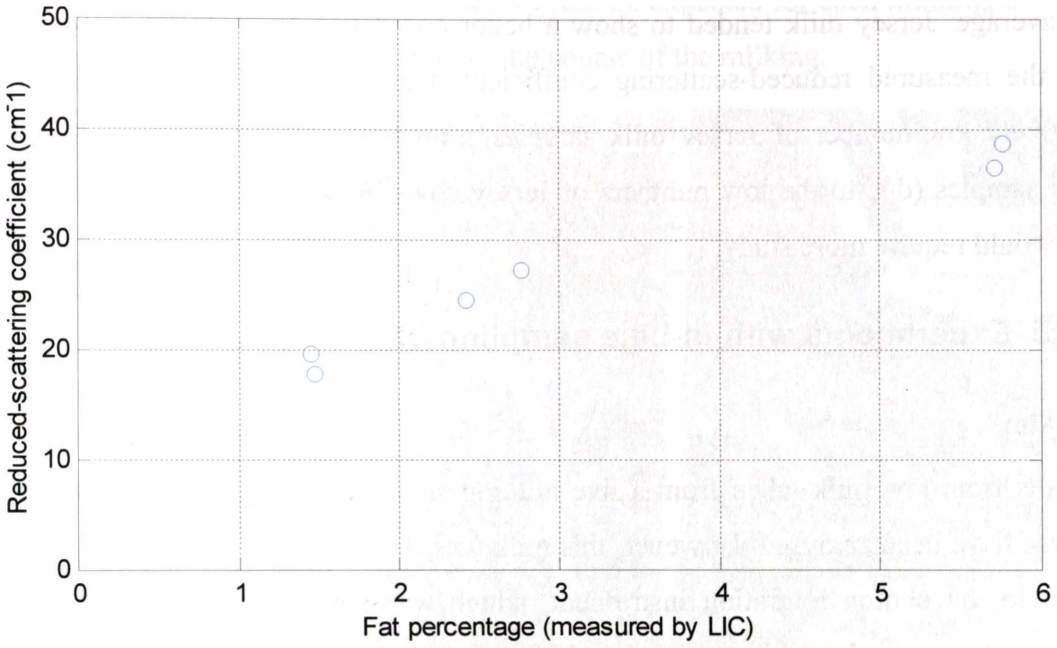

Figure 6-43: Friesian cow (9643) reduced-scattering coefficient versus measured fat percentage data – 18/09/2002 and 20/09/2002

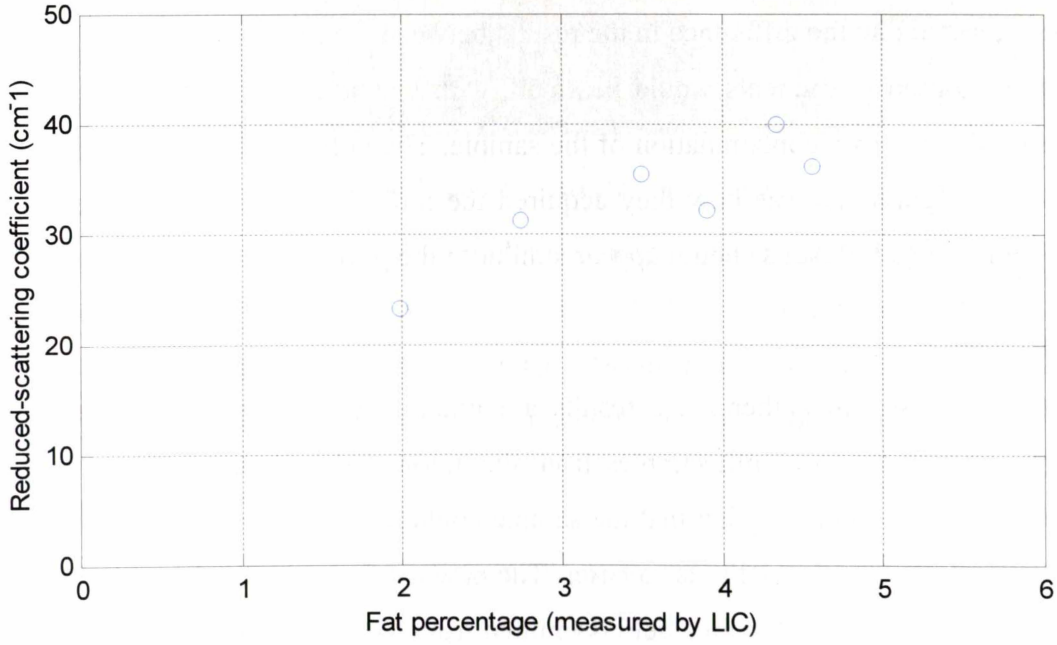

Figure 6-44: Friesian cow (1158) reduced-scattering coefficient versus measured fat percentage data – 19/09/2002 and 20/09/2002

The results from the four cows in Figure 6-41 to Figure 6-44 showed that there was a reasonably linear relationship between the reduced-scattering coefficient and the fat content in raw milk, when measured per cow. Applying the measurements on a per-

cow basis increased the precision from ± 2.0 % for all cows to ± 0.8 % for both Jersey cows and Friesian cows.

On average, Jersey milk tended to show a better correlation between fat percentage and the measured reduced-scattering coefficient than Friesian milk. However, the relatively low number of Jersey milk samples compared to the number of Friesian milk samples (due to the low numbers of Jersey cows in the herd tested) meant that this would require more study.

6.4.5 Experiments with In-Line sampling of fresh raw milk

Aim

Results from raw milk taken from a live milking situation at the automated milking system have been analysed. However, this milk was removed from the milk lines and taken to the photon migration instrument, which was situated close by. The next logical step was the ultimate goal, which was to install the photon migration instrument so that its sampling chamber was in-line – that is, all milk from the quarter being sampled was to flow through the photon migration instrument.

It was expected that the difference in the results between the two configurations of the photon migration instruments would be small, with maybe only a small decrease in precision due to cross-contamination of the sample. The only real difference between the two configurations was how they acquired the milk sample. In theory, the milk itself is unchanged. Results should appear similar to the previous experiments.

Method

The methods used to gather these results are much the same as for the previous experiment with the raw milk samples from the automated milking system with the notable difference being the fact that the sample container was now positioned in-line with the milk line for the right rear quarter. The new configuration is shown in Figure 6-45. Note though, that the light shield is omitted from the figure for clarity.

With the apparatus shown in Figure 6-45, milk could be diverted either through the sample container or along a bypass tube that allowed the milk to continue through without entering the sample container. The bypass option was used once it was determined that the end of milking would prematurely end the collection of a sufficient quantity of milk. The decision not to take another sample was based on the

estimated amount of milk remaining, by comparing the current milk yield with the previous milk yield and taking into account the amount of time already spent in milking. Typically, three measurements could be expected for each milking, allowing for rough profiling of fat content over the course of the milking.

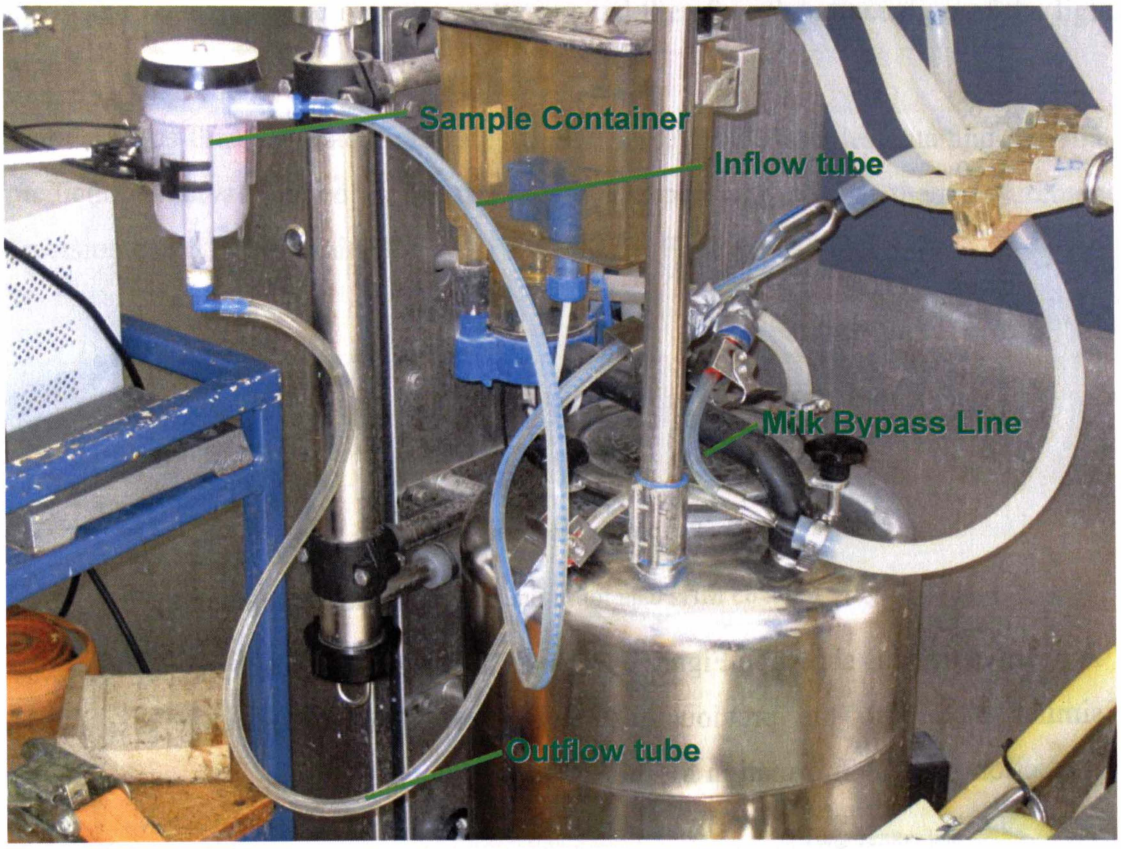

Figure 6-45: In-Line Photon Migration Apparatus (not showing light shield for clarity).

It was useful to note that allowing milk to go both via the bypass tube and through the sample container (both lines open) caused the milk in the sample container to empty more quickly, especially if the container was tipped horizontally. This was used to good effect as it managed to reduce the inter-sample time considerably.

Results and Discussion

The results from this set of measurements were expected to be similar to the results from the previous experiments, as mentioned. However, several individual cows from the herd that the milk was sampled from had recently calved, and had visible colostrum in the milk, which increased the extinction of light in the milk sample. Recently calved Jersey cows had the most noticeably thicker looking milk, and hence the milk that most affected the performance of the photon migration instrument. Therefore, the milk was not the same as for the previous off-line experiments.

What was expected then if the 65 MHz data is displayed as before, was a data set that showed a positive trend when plotted against measured fat content. Figure 6-46 shows this data, in the same style as Figure 6-31.

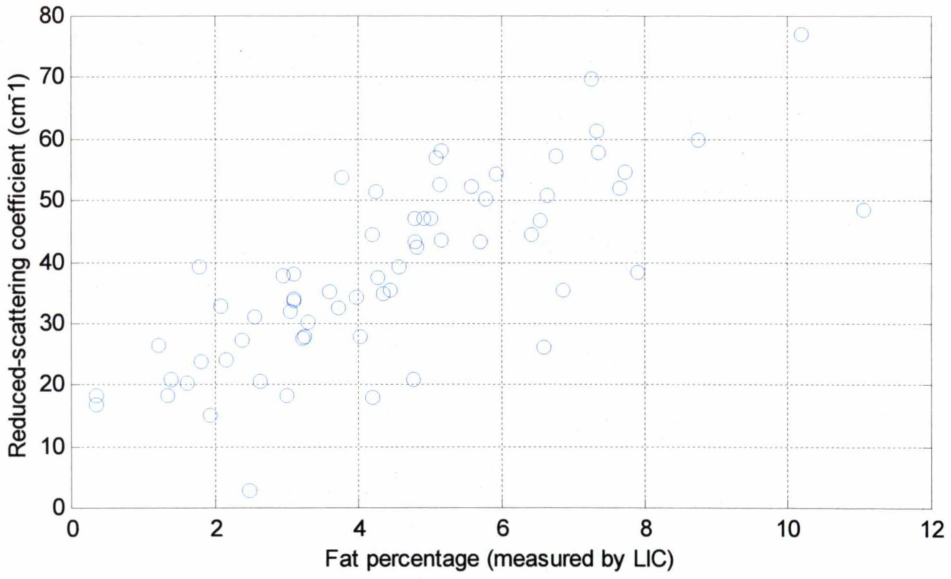

Figure 6-46: 65 MHz data for in-line photon migration instrument.

A positive trend is shown in Figure 6-31, with the data clearly well spread. This was a similar picture to the previous results on the automated milking system. The prediction interval information for this data set is shown in Figure 6-47.

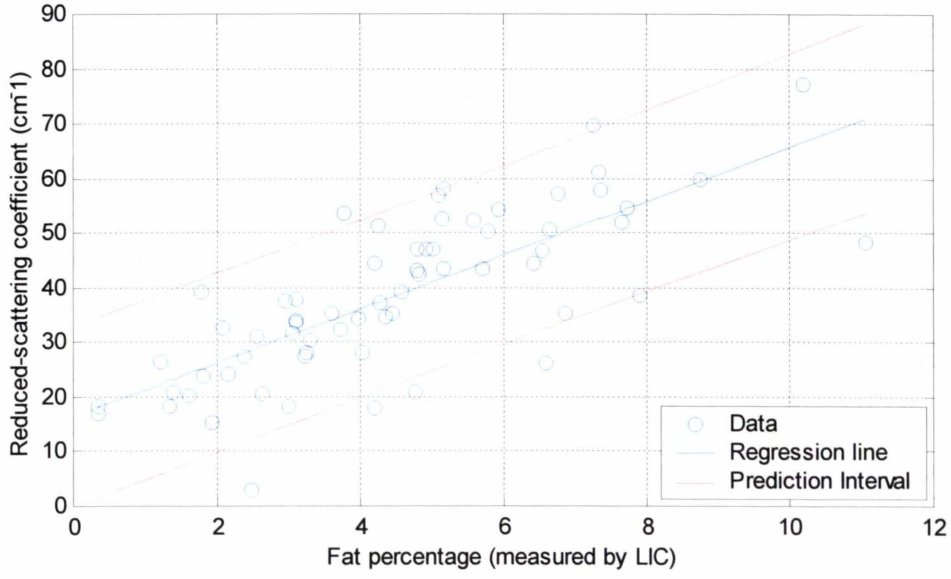

Figure 6-47: Reduced-scattering coefficient versus measured fat content. 90% prediction interval calculated, and outliers removed

The 90% prediction interval for this data showed that we could measure milk fat in-line to a precision of ± 2.4%. This was less precise than the offline measurement, but the number of recently calved cows that were producing colostrum could explain some of that variation. The presence of colostrum in the sample changed the nature of the milk markedly, increasing the scattering and therefore the attenuation of the light in the milk.

The data was then separated into Friesian and Jersey milk samples data and the 90% prediction interval plotted as per the previous experiment so that the measurement precision could be determined. This is shown in in Figures 6-48 and 6-49.

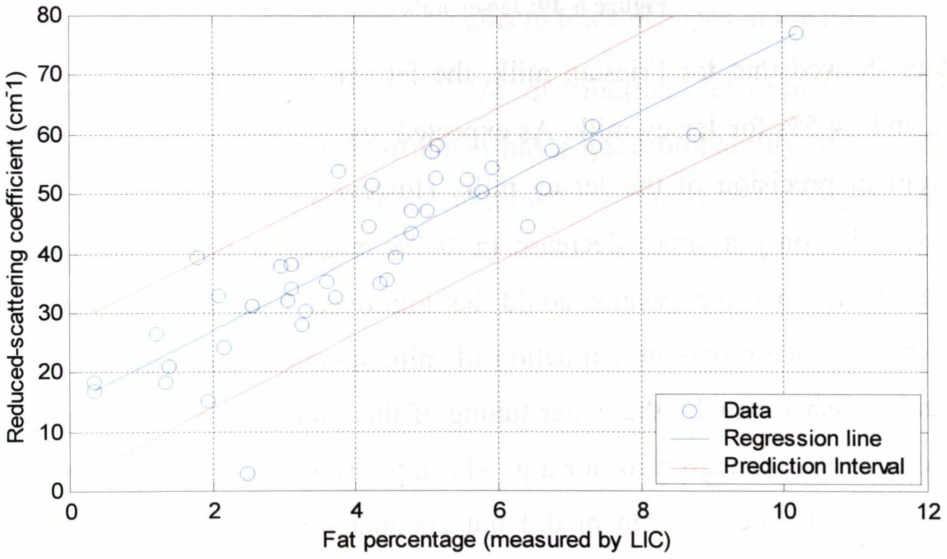

Figure 6-48: Friesian milk data, on-line.

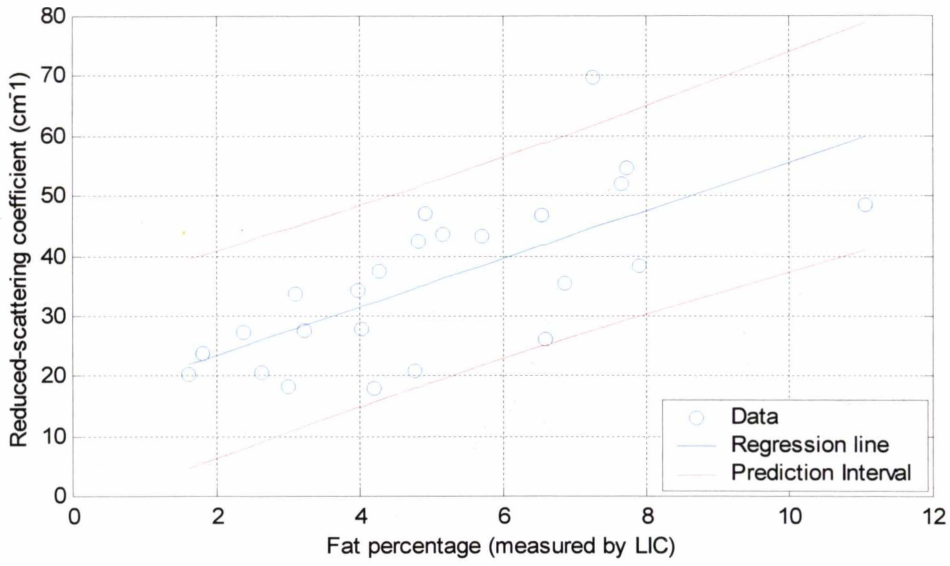

Figure 6-49: Jersey milk data, on-line.

The data showed that for Friesian milk, the fat can be predicted to an accuracy of ±2.2%, and ±4.5% for Jersey milk. As expected, the colostrum adversely affected the measurement precision of the Jersey milk. However, the Friesian milk behaved as expected, with only a small decrease (± 0.4% measured fat) in precision. It was theorised then, that the results could be improved with the implementation of measures to reduce cross-contamination of milk samples. One way that could have been accomplished was by the better tuning of the outlet rate of the sample chamber drain hole, so that enough milk for a good sample was retained with high milk flow. The previous off-line experiment did not encounter the same cross-contamination difficulties.

6.4.6 Conclusions

This was the *first* time that on-line data had been gathered from a live milking situation in a commercial dairy parlour using photon migration methods. It can be concluded that the photon migration instrument was able to measure fat percentage in raw milk to a precision of ± 2.0 % when no attempt is made to discriminate between individual cows and samples are sufficiently isolated from each other. However, if the data was sorted according to breed, the precision of the photon migration instrument in measuring fat content in raw milk increased to ± 1.6 % for Friesian milk and ± 1.4 % for Jersey milk. Splitting the data into records for individual cows showed yet another marked improvement in precision, approaching ± 0.8 % for some cows.

The increase in precision was most likely attributed to an increase in the consistency of the particle size distribution between milk samples. This increase in consistency would come from the increase in the consistency of the fat globule size distributions once the data had been separated by breed. Further separation of the samples into milk from individual cows further increased the consistency of the milk fat globule size distribution.

The measurement of the increase in the fat content of milk as milking progresses has been demonstrated successfully using the photon migration instrument. This could form the basis of long term studies to determine whether the reduced-scattering coefficient can be used to monitor other characteristics of milk, possibly to go as far as to keep track of cow health. At that point, one possibility would be to use the absorption coefficient at multiple wavelengths to track changes in the milk.

Once the shortcomings with particle size distribution determination have been overcome, the photon migration instrument has a good probability of being a useful tool in the real-time and long term monitoring of milk fat content, and other components, or even cow health.

6.5 Somatic cell count detection in raw milk

6.5.1 Introduction and principles of operation

The rapid and accurate detection of high levels of somatic cells in raw milk is a highly sought-after target for many instruments. However, due to their low concentration in milk, they are difficult to detect directly, since they are of the same order of magnitude in size as milk fat globules.

Most existing somatic cell detection methods use indirect means to detect the cells. This approach was also used in the experimental work described in this section. The particular property that we investigated that should correlate with milk somatic cell count, is the fluorescence of a dye that binds to a component of the somatic cell. The component is the cellular DNA, and the dye is ethidium bromide.

Fluorescence photon migration measurements with ethidium bromide with the purpose of determining somatic cell count in milk were first performed by Cerussi (1999). The idea of the experiment was to show that fluorescence lifetime spectroscopy with multiple fluorophores is possible. The results from that experiment were positive in that they showed that the fluorescence lifetime of the two ethidium bromide species (bound and non-bound) could be isolated, and a calibration could be made using the detected phase to determine the bound DNA, and hence the somatic cell count.

A single, high cell count milk sample was used, and diluted with Liposyn to obtain lower cell count milk samples. The original volume of the sample was one litre, and at all times, this volume remained constant. Subsequent samples were made by removing half of the volume of milk and replacing it with an equal volume of Liposyn. This halved the concentration of the somatic cells with every dilution.

The results showed that the measured phase of the fluorescence photon density wave had a definite positive relationship with the somatic cell count. However an exact relationship between the ratio of bound to free ethidium bromide and the somatic cell count could not be found, due to the unknown behaviour of ethidium bromide in the cellular environment. Also, this work was preliminary and indicative only. To transfer this work to an online solution, the techniques needed to be adapted to raw milk in an online situation.

The main goal of the experimental work carried out here was to obtain a calibration curve for somatic cell count using the fluorescence photon migration method. The secondary goal was to develop measurement equipment to measure the somatic cell count using this method, but capable of doing so in an on-farm situation.

An overview of the theory behind fluorescence photon migration based somatic cell count work was written by Cerussi (1999). We refer to his theoretical discourse, as we shall be using exactly the same theory in this work.

Somatic cell DNA and ethidium bromide properties

Bovine somatic cells are the chief source of DNA in the dairy cow's milk. Each bovine cell contains about 3.651×10^9 base pairs of DNA in the genome, compared to 3.4×10^9 base pairs for humans (Technical University of Denmark DTU, 2003). Since bovine cells are diploid, that number doubles to approximately 7.3×10^9 base pairs per cell available.

Consider the mastitic cow – there will be many somatic cells in the milk, contributing a considerable number of DNA base pairs to the total DNA count in the milk. However, there are also the bacteria that caused the mastitis. Their DNA will not contribute appreciably as they have one thousand times fewer DNA base pairs in their genome.

There should therefore be a correlation between the amount of DNA in the milk and the somatic cell count. As mentioned previously, one such way to detect the DNA is to dye it with ethidium bromide.

Ethidium bromide is a common and relatively inexpensive fluorescent DNA marker. It binds by *intercalating* with the DNA (Haugland, 1996), or inserting itself into the DNA structure. This process often distorts the double helix structure of the DNA, which is usually undesirable for living cells. The binding properties of ethidium bromide have been well studied (Bugs & Cornelio, 2001; Cosa *et al.*, 2001). Ethidium bromide binds tightly to double-stranded RNA and DNA. Upon binding, its fluorescence characteristics change markedly. Table 6-4 lists the optical properties of interest for ethidium bromide.

Parameter	Free	Bound
absorption peak (nm)	480	518
emission peak (nm)	620	605
quantum efficiency at absorption peak	5.6	5.6
quantum efficiency at 600 nm	~ 0.01	~ 0.05
fluorescence quantum yield (%)	~ 8	~ 100
fluorescence lifetime (ns)	1.73 ± 1	22 ± 2

Table 6-4: Optical properties of ethidium bromide (Byrne & de Mello, 1997)

Principles of operation

The main contrast mechanism is the change in the fluorescence lifetime between bound and free, which is an order of magnitude. This allows one to easily discern one form from another by choice of a suitable modulation frequency. Calculating the $\omega\tau \sim 1$ frequencies for both the fluorescence lifetimes yields 7.2 MHz for the bound state and 92 MHz for the free state. If a frequency is chosen that is close to 7.2 MHz, it will be highly sensitive to the delay caused by the bound state, while being relatively insensitive to the delay caused by the free state. However, there is one point of caution. Cerussi (1999) noticed that the binding of the ethidium bromide to non-DNA cellular components shortened the lifetime of the ethidium bromide to 17 ns. To compensate for this, a slightly higher modulation frequency must be chosen.

The number of DNA base pairs that are available per cell is a known quantity, but what is not yet known is how many of them are available to bind to ethidium bromide. Waring (1965) showed that the bound fraction of ethidium bromide to calf thymus DNA is about 0.22. This reduces the number of free DNA base pairs available for the ethidium bromide as binding sites to approximately one fifth of its original number.

That simple estimate still is not an accurate gauge of the number of DNA base pairs available to bind to the ethidium bromide. Cellular DNA is normally found in a tightly wound state. This will hide many base pairs from any binding by ethidium bromide. As mentioned previously, ethidium bromide will also bind to non-DNA cellular components too. Also, even though bacterial DNA has been considered to be insignificant compared to the amount of bovine DNA present, it is still certainly there, and available to take up ethidium bromide. Altogether, the conclusion that is reached

is that it is impossible to accurately predict the number of binding sites available. Therefore, calibration is required to obtain a correlation between bound DNA and the somatic cell count.

Binding affinity

A model the binding of ethidium bromide to the bovine cellular DNA is now required. This can be done by considering three different quantities.

- Unbound ethidium bromide (G)
- Bound ethidium bromide / DNA complex (C)
- Unbound DNA (R)

(Cerussi, 1999) derives an expression that describes the binding of ethidium bromide to DNA. It is written in the same form as a reversible chemical reaction.

$$R + G \underset{K_d}{\overset{K_a}{\rightleftharpoons}} C \qquad [6\text{-}3]$$

where K_a is the association coefficient and K_d is the dissociation coefficient. The association coefficient describes the affinity for the forward reaction (from separate R and G into the complex, C), and the dissociation coefficient describes the affinity for the reverse reaction. Thus, the higher the K_a the more likely the reaction is to favour the complex C (and hence the tighter the binding), while the higher the K_d the looser the binding, and the more likely it is for the complex C to dissociate into R and G. Both K_a and K_d have units of Molar. Equation 6-4 shows the derivation of K_a and K_d.

$$K_a = \frac{[C]}{[R][G]} = \frac{1}{K_d} \qquad [6\text{-}4]$$

For DNA in soution, the K_d for ethidium bromide is 0.7 μM, suggesting that the binding is strong if the ethidium bromide concentration is in the μM range. We can also assume that different binding sites do not interact with each other (Waring, 1965).

Equation 6-4 can be solved for [C]. With a given amount of unbound ethidium bromide G_0, the amount of it available G as the complex C forms will be $G = G_0 - C$.

The number of remaining binding sites is $R = R_0 - C$. Inserting these relationships into equation 6-4 and solving for [C] gives:

$$[C] = \frac{1}{2}\left([R_0] + [G_0] + K_d - \sqrt{([R_0] + [G_0] + K_d)^2 - 4[R_0][G_0]} \right) \qquad [6\text{-}5]$$

Figure 6-50 shows this relationship.

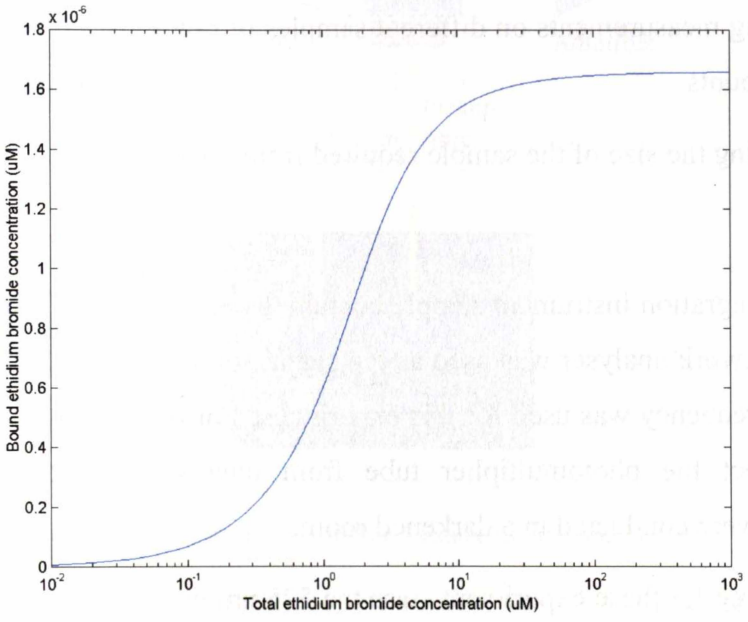

Figure 6-50: Ethidium bromide binding characteristics. K_d = 0.7 μM, with 10^6 cells per mL and 10^9 binding sites per cell.

This relationship shows that after the ethidium bromide concentration exceeds 10 μM, the amount of bound ethidium bromide compared to the total amount of ethidium bromide becomes almost constant. That is due to all the binding sites being occupied by the ethidium bromide. Care must be taken during experiments to make sure that the ethidium bromide concentration is sufficient to fill as many binding sites as possible, but not too high or the ability to detect the bound ethidium bromide will decrease. Recall that the emission phases for multiple fluorophores in solution add as phasors. Therefore, if there are roughly equal proportions of both the bound and unbound ethidium bromide and there are no more binding sites available, the addition of any more ethidium bromide will cause the phase contribution from the bound ethidium bromide to lose significance.

6.5.2 Experiments on raw cow's milk

Aim

The purpose of this experiment was to test whether there was a relationship between somatic cell count and measured phase lag in raw milk. These are proof-of-concept types of measurements, and extend on Cerussi's work by

1. making measurements on different samples of raw milk with different somatic cell counts
2. reducing the size of the sample required from 1 L to 100 mL.

Method

The photon migration instrument sample container was set up as discussed in chapter 5. The RF network analyser was used as the signal source and receiver. Only a single modulation frequency was used for this experiment. For optimal signal-to-noise ratio, and to protect the photomultiplier tube from overexposure to stray light, the experiments were conducted in a darkened room.

The light source for these experiments was the 525 nm ultra-bright LED as there were no available laser diodes of that wavelength. A frequency-doubled Nd-YAG laser was considered, but the bulk of such a device would cause problems in future designs. Since the modulation frequency dropped from 60-80 MHz down to 10 MHz, a commonly available LED was used as our excitation source. In order to drive it properly though, the RF network analyser supplying the modulation frequency was set to its highest output power of 23 dBm, into 50 ohms. This modulation resulted in a ± 45 mA sine wave that was used to modulate a 35 mA DC bias current to the LED. Also, since the LED was being driven with more current than in its specifications, the temperature controller of the laser diode driver was set to lower the temperature inside the laser diode driver module down to 15 °C to help keep the junction temperature of the LED down. Figure 6-51 shows the configuration of the photon migration instrument for fluorescence lifetime measurements.

The sample container was a 100 mL plastic sample vial with transparent sides and a 25 mm bottom radius. The 1 L volume that was used in previous experimentation in this area was not used in this experiment. This is because at the edge of the container, there was no detectable excitation light and thus no contribution to the fluorescence at

that point. Therefore, an upper limit to the radius of the container from the light source could be determined. With no detectable light at the container boundaries, there could be no boundary effects on the results measured.

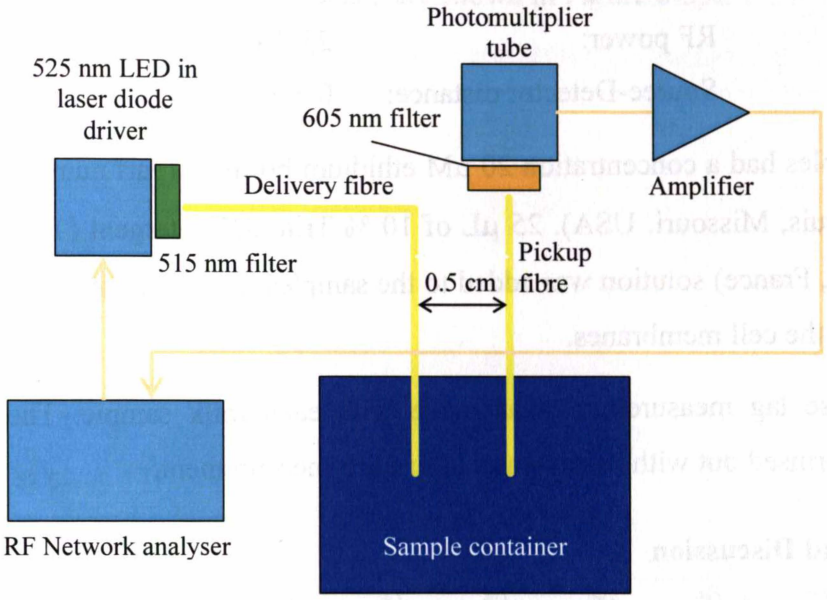

Figure 6-51: Photon migration instrument in fluorescence lifetime measurement configuration.

A 515 nm bandpass interference filter (part number 03-FIL-204, Melles-Griot, USA) was placed in front of the output lens of the laser diode driver. Correspondingly, a 605 nm filter was placed before the photomultiplier, ensuring that only fluorescence signals could be detected.

The milk samples used in this experiment were obtained from the automated milking system. Subsamples were sent to the LIC testing laboratories for somatic cell count determination. Three milk samples were from healthy cows, exhibiting a range of SCC readings from 5.4×10^4 cells mL^{-1} to 7.7×10^4 cells mL^{-1}. One sample had a cell count of 7.9×10^5 cells mL^{-1}. The remaining three samples were linear dilutions (100 %, 60 % and 30 %) of milk from a cow with clinical mastitis. The SCC reading from this sample was 9.9×10^6 cells mL^{-1}. The high cell count milk was diluted with known low cell count milk to form the linear dilutions.

The settings on the RF network analyser for this experiment were:

Bandwidth:	15 Hz
Averaging:	64 samples
Number of data points:	5
Frequency:	10 MHz
RF power:	23 dBm
Source-Detector distance:	0.5 cm

All milk samples had a concentration 20 μM ethidium bromide (part number E-1510, Sigma, St. Louis, Missouri, USA). 25 μL of 10 % Triton-X detergent (Triton X100, Prolabo, Paris, France) solution was added to the samples to aid the ethidium bromide in penetrating the cell membranes.

A single phase lag measurement was made with each milk sample. The sample container was rinsed out with warm water after each measurement.

Results and Discussion

Figure 6-52 shows the measured relationship between the somatic cell count and the measured phase lag. The error bars are from the quoted phase measurement error of the network analyser.

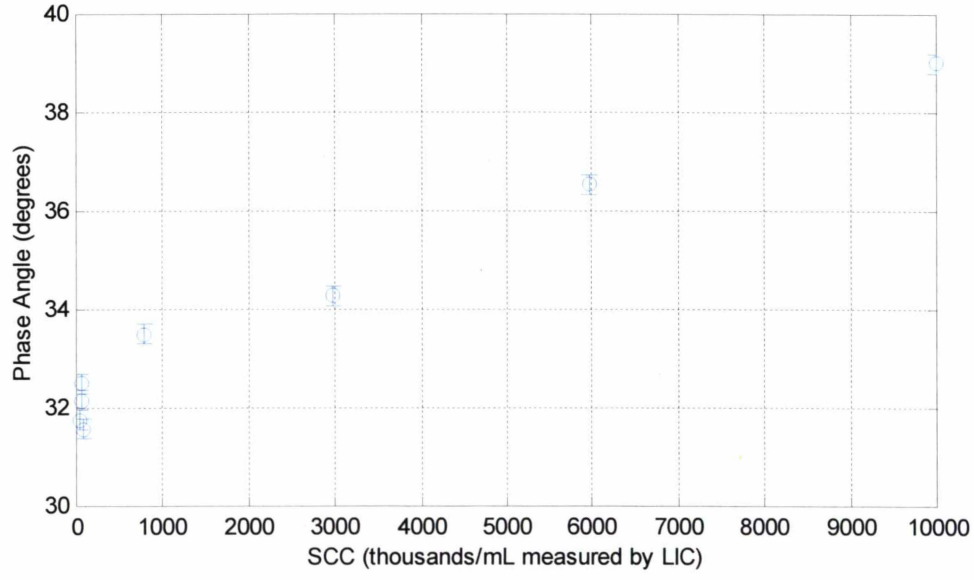

Figure 6-52: Phase lag versus somatic cell count.

A cell count of 10^7 cells mL^{-1} is assumed for this milk sample. The data in Figure 6-52 show a linear trend. However, that was only for the higher cell count milk. The phase lag from the milk with lower cell counts did not seem to change much – in fact,

it clustered around the 32 degree mark. That was not expected behaviour. Ten more milk samples of known low cell count were obtained, and another set of measurements made, using exactly the same method as for the original samples, except with no dilutions. The results are shown in Figure 6-53.

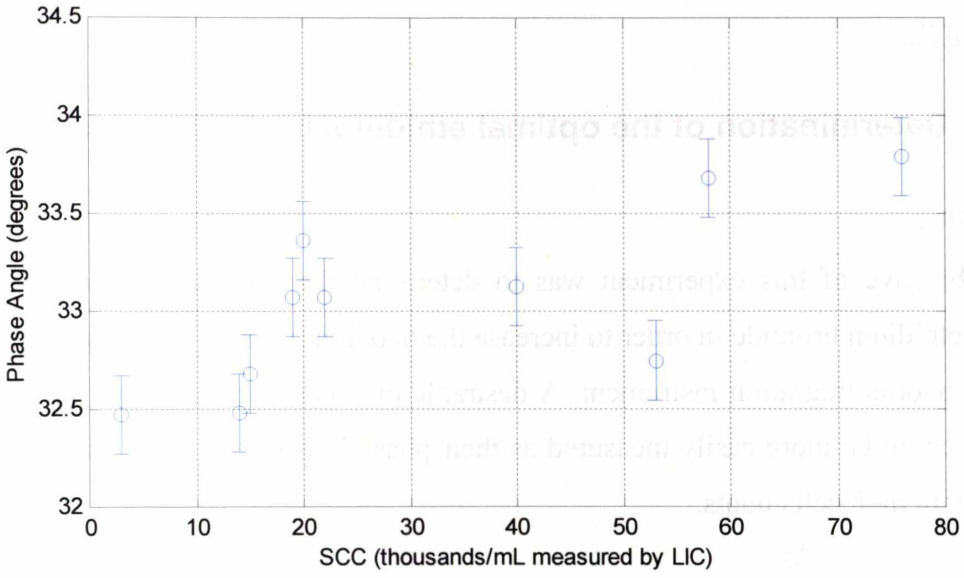

Figure 6-53: Low cell count milk phase lag versus measured somatic cell count.

The results for the second set of measurements were not as clear as those for higher cell counts. There is the possibility of a trend, but the scatter is too large for any measure of confidence. Certainly, even with these low cell counts, the phase lag is far too high. The phase lag for purely unbound ethidium bromide should be close to 7 ° at 10 MHz, as shown in section 6.5.1.

The maximum variation of this instrument was quite low, being only at best 8 ° at 10 MHz. Since the phase lag ought to be less for low cell counts, one possibility is that there was insufficient ethidium bromide added to the milk, and thus all of it was being bound, causing a higher-than-usual phase lag. That possibility was unlikely as the same amount of ethidium bromide added to milk with a high cell count had a far greater phase lag.

Another possibility is that the ethidium bromide is being inhibited by something in the milk. The first possible cause that was to be investigated however, was whether the concentration of ethidium bromide was incorrect, causing either an oversupply of available binding sites, or an oversupply of unbound ethidium bromide.

The results showed that somatic cell count can be measured with a lower limit of about 4×10^5 cells mL^{-1}, and up to 1×10^7 mL^{-1}. This is suitable for the detection of clinical mastitis and would detect some incidences of subclinical mastitis. However, a lower limit of detection of 4×10^5 cells mL^{-1} is only just adequate as the upper limit before penalties for somatic cell count for bulk tank milk in New Zealand is 4×10^5 cells mL^{-1}.

6.5.3 Determination of the optimal ethidium bromide concentration

Aim

The objective of this experiment was to determine the optimum concentration of added ethidium bromide in order to increase the maximum variation in phase returned by the photon migration instrument. A desirable outcome was that milks of low cell counts could be more easily measured as their phase lags would be much lower than those with high cell counts.

Method

The photon migration instrument was set up as per the experiment described in section 6.5.2. A 1 L milk sample (cell count measured by LIC as 4.5×10^5 cells mL^{-1}) was obtained from the automated milking system and divided into 10 subsamples of 100 mL each. To each of the samples, 25 μL of 10 % Triton-X was added, before adding the ethidium bromide. Each sample received a gradually increasing amount of ethidium bromide, ranging from 0.02 μM to 300 μM in logarithmic base-10 steps.

An IntraLipid suspension was used to set the zero point on the phase readings from the RF network analyser, as IntraLipid has no DNA content. The phase lag from the IntraLipid plus ethidium bromide was the same as the phase lag for water plus ethidium bromide. This made it a suitable medium for calibrating the photon migration instrument.

A single phase lag measurement was made for each of the subsamples. The sample container was rinsed out with warm water after each measurement.

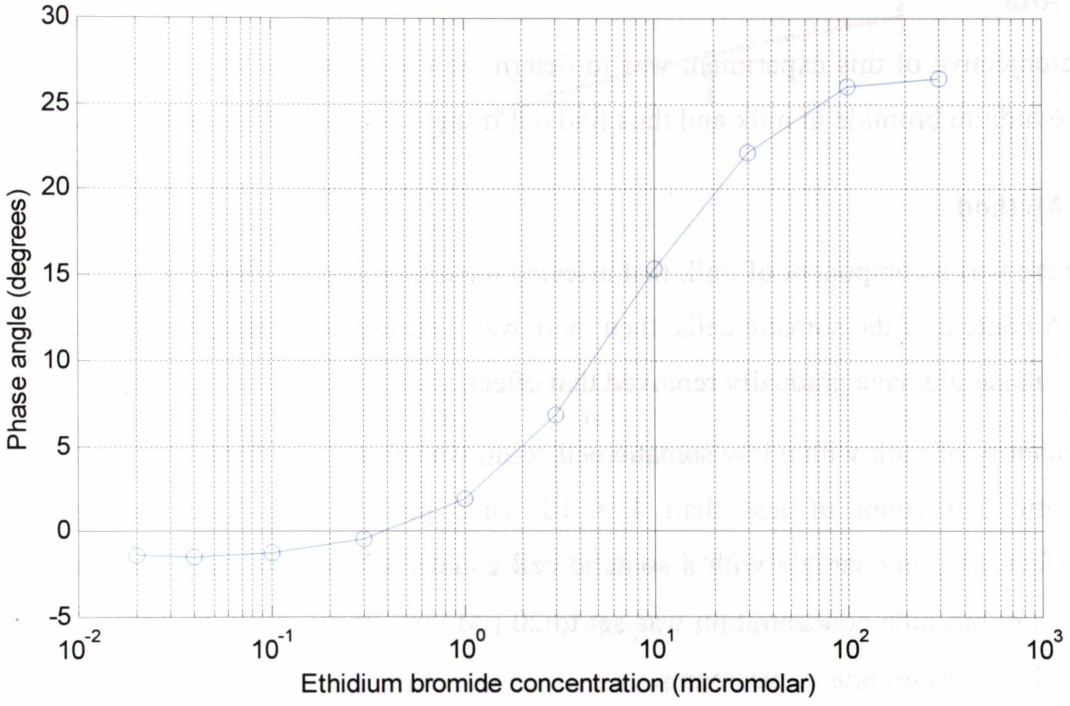

Figure 6-54: Phase angle versus ethidium bromide concentration.

The results plotted in Figure 6-54 show that by lowering the ethidium bromide concentration, the phase lag can be brought towards zero. This is counterintuitive, as when the proportion of unbound ethidium bromide increases, the contribution of the short-lifetime phase should also increase, thus bringing the overall phase measured down towards the 7° phase lag that unbound ethidium bromide should show with a 10 MHz modulation frequency.

It is not certain what caused the anomalous results. However, it was likely that the desired outcome (a lower phase for a lower somatic cell count) could have been achieved by lowering the ethidium bromide concentration.

The next step was to find out whether there was something in the milk that was either binding with the ethidium bromide (and is not DNA), or inhibiting its activity.

6.5.4 The fluorescence behaviour of ethidium bromide in milk that is being progressively diluted

Aim

The objective of this experiment was to determine the behaviour of the phase lag of the ethidium bromide in milk and thus find out if there was something affecting it.

Method

If there was a component of milk that affected the binding of ethidium bromide to the DNA content of the somatic cells, then there was a strong possibility that the dilution of milk should have gradually removed that effect.

A quantity of milk with a low somatic cell count was obtained. Since anything with a somatic cell count of less than 4×10^5 cells per mL could not be resolved satisfactorily, any sample with a somatic cell count less than that was suitable. The ethidium bromide concentration was set to 20 μM, and 25 μL of 10 % Triton-X was added, as per previous experiments.

Seven samples were made, with milk content from 10 % up to 100 %, with the remainder of the sample being distilled water. Samples were poured (in turn) into the sample container and the phase lag from the bound ethidium bromide recorded. Afterwards, the sample was discarded and the sample container rinsed out with warm water.

Note that here, the phase lag of unbound ethidium bromide in water is defined as zero degrees – that is, the offset from our phase measurements was removed.

The RF network analyser settings for this experiment are:

Bandwidth:	15 Hz
Averaging:	64 samples
Number of data points:	5
Frequency:	10 MHz
RF power:	23 dBm
Source-Detector distance:	0.5 cm

Results and Discussion

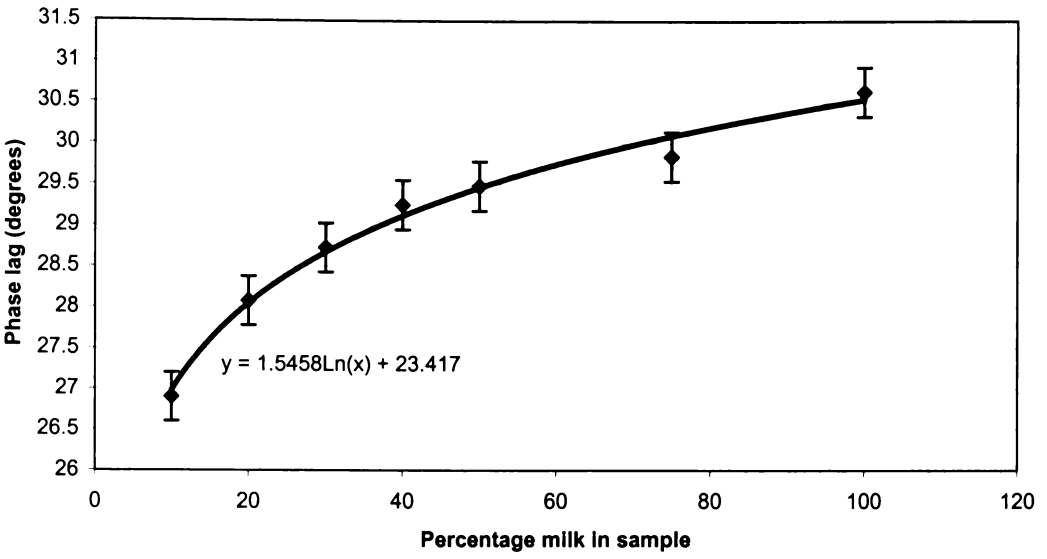

Figure 6-55: Phase lag results – milk diluted with water.

The results for gradual dilution of the milk sample with distilled water are shown in Figure 6-55. There was a definite decrease in the phase lag as the milk was diluted. However, this decrease was quite small until the proportion of milk in the sample was quite low. At 10 % milk content, the phase lag was still 27 degrees. The phase lag at 0 % milk (100 % water) was defined to be zero. This result led to the hypothesis that there was a substance in milk that interfered with the binding of ethidium bromide to DNA. If that was the case, then a way to calibrate for it was required.

6.5.5 Raw milk and IntraLipid dilutions

Introduction and Aim

The objective of this experiment was to once again characterise the fluorescence phase lag of a raw milk sample that had been diluted. This time however, the samples were diluted with IntraLipid that had been itself diluted so that it matched the average reduced-scattering coefficient of raw milk (about 30 cm^{-1}). This experiment also took into account the findings from the experiment in section 6.5.3 in that a range of lower concentrations of ethidium bromide were tested. This experiment was an extended version of the experiment that Cerussi (1999) performed, and the results here should have been similar.

Method

This experiment required the use of high cell count milk. Two samples were obtained. The first sample had a cell count of 6×10^5 cells mL^{-1} and the second had a cell count of 7×10^5 cells mL^{-1}. Each milk sample was divided into three subsamples to which a different amount of ethidium bromide was added. The ethidium bromide concentrations in the three samples were 1 μM, 3 μM and 10 μM. These concentrations were the ones that lower the phase lag for lower cell count milks. Six subsamples were made in total from both milk samples.

The phase lag of the photon migration instrument was set to zero with an IntraLipid and ethidium bromide control sample. This was done before each subsample was measured. All of the subsamples were treated with 25 μL of 10 % Triton-X solution.

Each subsample was poured into the sample container and a phase reading obtained. Following this, the subsample was evacuated into another container and half of its contents were removed, and substituted with the same volume of IntraLipid. Additional ethidium bromide was added to the subsample to make up for the amount lost with the removal of half of the subsample. Then, the subsample was put back into the sample container and another phase reading obtained.

This process was repeated eight times for each subsample, giving a range of dilutions from not diluted up to 1/128 of the original subsample. Each successive dilution halved the concentration of milk (and somatic cells / DNA) in the subsample.

Results and Discussion

Figure 6-56 and Figure 6-57 show the phase lag readings for both the 6×10^5 cells mL^{-1} and the 7×10^5 cells mL^{-1} samples respectively. The readings for both milk samples were not as expected. The most unexpected result shown by both milks was the curving of the phase lag graphs where the milk was the least diluted.

If there were an inhibitory substance in the milk, then this would have explained the results. So if it was assumed that there was a certain quantity of inhibitor in the milk in the beginning, then upon the first addition of the ethidium bromide, a certain quantity of inhibitor proportional to the amount of ethidium bromide added would have been used up. That is assuming that this inhibitor was used up in a non-reversible way. At each dilution, half the inhibitor would have been poured out and a

fresh amount of ethidium bromide (half the amount originally injected) would have been mixed in. Therefore the amount of inhibitor would gradually decrease, while the ethidium bromide concentration would remain constant. Notice that in both Figure 6-56 and Figure 6-57, the 10 μM ethidium bromide data was the most linear, followed by the 3 μM data. This was consistent with there being an ethidium bromide inhibiting agent.

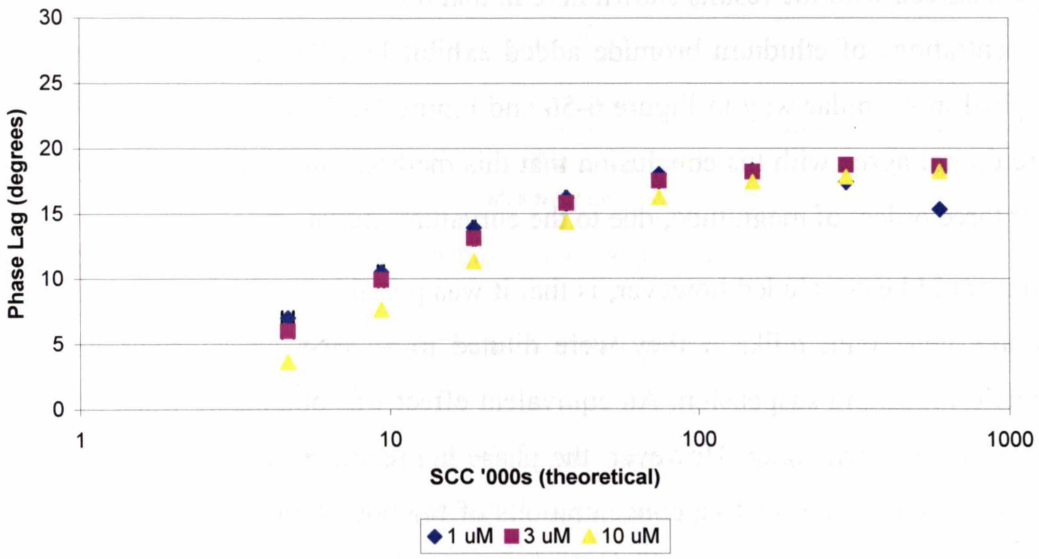

Figure 6-56: Phase lag versus somatic cell count for various dilutions of milk with 6×10^5 cells mL^{-1}.

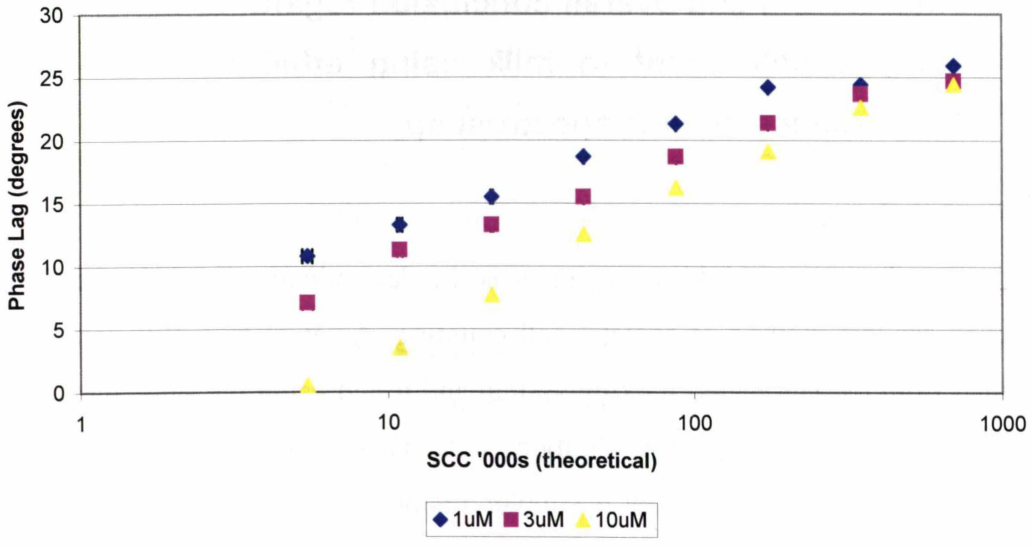

Figure 6-57: Phase lag versus somatic cell count for various dilutions of milk with 7×10^5 cells mL^{-1}.

After the third dilution, the data started to show a more linear trend. A sample that had milk with a high enough somatic cell count would have had a phase lag result that

followed a linear trend if the ethidium bromide concentration in that sample had been high enough.

The results generated by Cerussi (1999) showed a linear trend with the phase lag versus the logarithm of the somatic cell count. The milk sample he used had an initial cell count of 2.2×10^6 cells mL^{-1} and had an ethidium bromide concentration of approximately 20 μM. His results did not show the same curvature when graphed, which agreed with the results shown here in that phase readings with milk with higher concentrations of ethidium bromide added exhibit less flattening and curving when graphed in a similar way to Figure 6-56 and Figure 6-57. However the results shown here do not agree with his conclusion that this method can resolve somatic cell count over three orders of magnitude, due to the curvature shown.

What could be concluded however, is that it was possible to obtain reasonable results for low cell count milks if they were diluted to at least 1/8 concentration with a suitable IntraLipid suspension. An equivalent effect was obtainable when diluting the milk with distilled water. However, the phase lag readings would then be dependent on two factors – the relative concentrations of the bound and free ethidium bromide and the reduced-scattering coefficient of the sample, which would decrease linearly with dilution.

6.5.6 Final testing and overall conclusion regarding the testing for somatic cell count in milk using ethidium bromide and fluorescence lifetime spectroscopy

Final testing

The expected outcome of this experiment is the determination of the lower limit of detection for this method of somatic cell counting. A set of five milk samples was obtained from the automated milking system and tested using the same method as in section 6.5.5. However, only four dilutions were made, as it was at the third dilution where the results start to follow a simpler relationship. The results are shown in Figure 6-58.

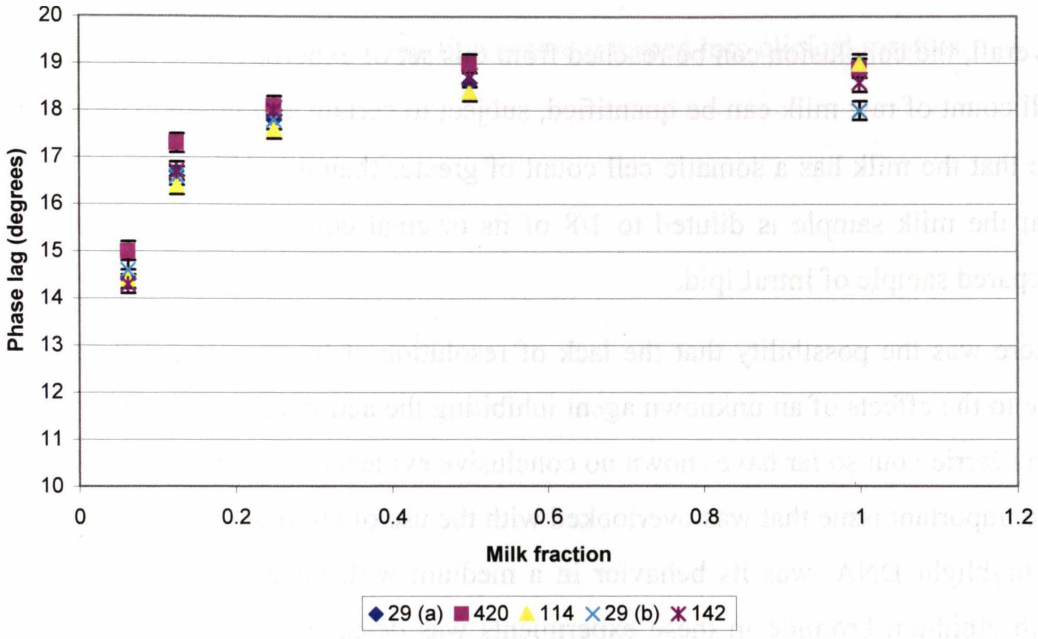

Figure 6-58: Phase lag of diluted milk samples. Graph legend is the cell count of the milk ($\times 10^3$ cells mL^{-1}) as measured by LIC.

The milk with the highest cell count of all the samples available at the time had a measured cell count of 4.2×10^5 cells mL^{-1}. As it was the highest cell count milk that was available at the time (and for the foreseeable future), the experiments focused on those results.

Notice that the highest cell count milk consistently reads with the highest phase. This difference in readings is clearly outside the error bars, indicating that it is most likely a proper change, not a measurement artifact. It can be concluded from this that the lower limit of detection of somatic cell count using ethidium bromide as a DNA stain and fluorescence lifetime as the contrast factor lies in the range between 3×10^5 cells mL^{-1} and 4×10^5 cells mL^{-1}.

There was still the factor of the ethidium bromide inhibiting agent. The data shown here was consistent with that explanation. A further two informal tests were carried out to see if the inhibiting factor was a related to alkaline pH or added Triton-X concentration, with both of them coming up with a negligible correlation. Acid pH was not tested as milk starts to curdle at around pH 5.5, and that is certainly not a natural condition.

Discussion and conclusion of the ethidium bromide fluorescence experiments

Overall, the conclusion can be reached from this set of experiments is that the somatic cell count of raw milk can be quantified, subject to certain conditions. The conditions are that the milk has a somatic cell count of greater than 4×10^5 cells mL^{-1} and also that the milk sample is diluted to 1/8 of its original concentration with a specially prepared sample of IntraLipid.

There was the possibility that the lack of resolution at low somatic cell counts was due to the effects of an unknown agent inhibiting the action of ethidium bromide. The tests carried out so far have shown no conclusive evidence of such an agent. However, one important issue that was overlooked with the use of ethidium bromide in raw milk to highlight DNA, was its behavior in a medium with micelles. The DNA binding with ethidium bromide in these experiments was designed around the behaviour of ethidium bromide in water. While milk is mostly water, there is a significant amount of fat and protein suspended in the form of globules and micelles. Pal *et al.* (2000) state that the emission intensity of ethidium bromide is low in highly polar solvents such as water, but can increase nearly five-fold in a non-polar medium. One possibility for this in milk, is the uptake of ethidium bromide by fat globules, thus strongly enhancing the fluorescence output. Note that the fluorescence photon migration instrument *does not* distinguish between the two different emission wavelengths. Pal *et al.* (2000) also note that anionic solvents can increase the emission lifetime such as when ethidium bromide is taken up by a fat globule. This would have introduced an unexpected phase delay, which would increase the lower measurement limit for somatic cell count with the fluorescence photon migration instrument. This effect is indeed what was observed, and thus needed to be eliminated to improve the performance of the instrument.

The rather high figure for the lower detection limit hampered the usefulness of the fluorescence photon migration instrument as a somatic cell counter due to the similarity of the lower detection limit to the maximum permitted bulk tank somatic cell count imposed by most dairying industries around the world. However, since cows with greater than 10^6 cells mL^{-1} are usually considered to have clinical mastitis, the instrument could be used to detect cows with subclinical mastitis. A single cow with subclinical mastitis and a cell count between 4×10^5 and 10^6 cells mL^{-1} would

not affect the bulk tank count much, but could easily be detected on her own, enabling early treatment of the subclinical mastitis before it turned into clinical mastitis.

7 Conclusion and Future Work

7.1 Conclusion

The aims of this thesis were to:

1. determine the extent with which photon migration measurement techniques can yield useful information about milk composition and
2. determine whether these techniques can be applied to an online situation.

In order to achieve this, the properties of milk were reviewed, and then a suitable mathematical model was selected to describe it.

The model selected for the description of light transport in milk was the diffusion approximation to the Boltzmann transport equation. This was found to be a commonly used mathematical model for highly scattering media. It was appropriate for use with milk as it had been used with other highly scattering media. It was also relatively straightforward to implement. The limitations of using the diffusion approximation were avoidable in milk, by choosing the correct physical configuration of the sample container. The experiments showed also that there was no absolute requirement to follow the same types of geometries as prior experiments had used.

The application of the diffusion approximation to milk fell into two main areas. The first, being the measurement of the fat content in homogenised and raw milk, and the second being the measurement of the somatic cell count of raw milk. It was not possible to measure other components such as total protein, casein or lactose due to the lack of response of the photon migration instrument to those quantities.

The measurement of the fat content of raw milk was a direct application of the diffusion theory since the reduced-scattering coefficient of the milk should correlate with the fat content. The experiments regarding this area showed that there was a positive correlation, and therefore the reduced-scattering coefficient could be used as an indicator of the fat content in both homogenised and raw milk. The results of these experiments were unique in that this was the first time that photon migration measurement methods have been used in an on-line situation – that is, with the milk being measured non-invasively *while it is still in the milking machine system.*

The application of the diffusion approximation to somatic cell count in raw milk required a small extension to the theory. The light source that was to be measured was no longer the light distribution from a single fibre, but was a solution of the diffusion equation at the excitation wavelength. That meant that photon density waves from the source fibre became the source term for the photon density wave from the fluorophores distributed throughout the medium.

Measuring the somatic cell count in milk using this modified equation was straightforward once the choice of the measurement quantity (contrast factor) was determined. The fluorescence lifetime was used in the experiments in this thesis, as that is one of the most striking features of the dye used, ethidium bromide. The dye binds to the DNA in somatic cells. The fluorescence lifetime for the bound dye is an order of magnitude longer than for the non-bound dye.

The measurements that were made indicated that ethidium bromide and raw milk combined with the fluorescence photon migration instrument could quantitatively measure the somatic cell count in milk. However the lower limit of detection was too high for it to be a useful on-farm instrument. The fact that the binding and fluorescence lifetime of ethidium bromide was affected by non-cellular components in milk (namely fat globules and casein micelles) gave much room for exploration with regard to improving these results.

Therefore, two areas have been identified that can be readily measured using photon migration techniques - fat content and somatic cell count. It has been demonstrated that these techniques can obtain that information but with a lower precision than desired. It has also been shown that these techniques can be applied online, especially in the case of the fat measurements. However, there was no reason why the somatic cell count measurements could not be also performed online. Those results fulfilled the aims of this thesis, which were stated at the beginning of this chapter. The extent with which photon migration measurements can be used for milk composition analysis has been examined. Along with this, photon migration measurement techniques have been successfully applied to an in-line milking situation where the milk can be analysed non-invasively and non-destructively.

The milk fat measurement data was presented at the 2004 New Zealand Non-Destructive Testing Association Conference in Palmerston North (Khoo *et al.* 2004a)

and the somatic cell count data was presented at the 2004 International Conference on Experimental Mechanics in Singapore (Khoo *et al.* 2004b)

In conclusion, the use of photon migration theory in the form of the diffusion approximation could be a useful tool in the analysis of milk components. In the form examined in this thesis, it was shown to require further refinement due to the lack of precision in the fat measurements, the high lower limit of detection for the somatic cell count and the non-responsiveness to protein content. Further improvements must be made before the instrument can realise its full potential.

7.2 Future work

The full potential of the photon migration instrument is quite broad indeed. It is a conceptually straightforward operation to modify the instrument for use as a multi-component analyser for milk. In theory, it is capable of measuring fat content, protein content and somatic cell count – the three main quantities that are measured for in milk. What will be examined now is the work required in order to achieve this potential.

7.2.1 Increasing the precision of the fat content measurement

The main problem with the fat content measurement is that the particle size distribution cannot be quickly and accurately measured. Currently, particle size distribution measurements require the milk to undergo several individual readings in the photon migration instrument (at different wavelengths), with all the readings processed later on to obtain the size distribution. The processing required is quite intensive, and would need quite a powerful computational device.

If a fast way of getting an approximate particle size distribution were available, the precision of the fat measurements would increase. A side effect of being able to measure the particle size distribution would be the ability to monitor damage to the fat globules and possibly devise a correlation with the free-fatty acid content of milk. Free fatty acids cause the rancid odour in milk and in some countries, regulations are being put in place to ensure minimal amounts of these odoriferous substances are in milk destined for processing.

7.2.2 Lowering the detection limit for somatic cell count

Finding out the nature of the ethidium bromide inhibitor is one way of lowering the detection limit. With that information, the instrument can be calibrated, or else a process to neutralise the inhibitor could be devised and inserted into the measurement method. One way of doing that is to completely lyse the somatic cells in milk with a high concentration of detergent as with the California Mastitis Test. This will release the DNA in the somatic cells, allowing easier interaction with ethidium bromide.

Another possibility for the future is to extend the work done on the dilutions with IntraLipid. There is a strong possibility that further experimentation with milks of varying cell count will yield a calibration against the phase lag from the ethidium bromide.

7.2.3 Detecting protein and other milk components

The absorption coefficient has been neglected for the most part in this work. Applying the same techniques that are used in spectroscopy and incorporating multiple light sources of different wavelengths will enable the use of the photon migration instrument as a spectrometer. A major advantage of using the photon migration instrument as a spectrometer is that the scattering properties of milk can be ignored or accounted for by use of the reduced-scattering coefficient.

Protein content in milk is usually measured using near infrared spectroscopy. The determination of the content is usually from a ratio of intensities of two or more different wavelengths. However, the main difficulty is the acquisition of light sources of the correct wavelength that have a sufficient modulation depth at the modulation frequencies the photon migration instrument uses.

Implementing a multiple-wavelength system like this would vastly increase the usefulness of the photon migration instrument as a diagnostic and monitoring tool, especially when applied online.

8 Appendix - Matlab source code

8.1 Matlab Code crankd.m

```
% crankd.m - program to solve the diffusion equation using the Crank-
Nicolson
%            algorithm.

clear;
help crankd.m
N = 321;                          % number of grid points
L = 10;                           % length of system, from -N/2 to N/2
h = L/(N-1);                      % grid size
tau = 1E-12;                      % time step (default is 1 picosecond)
nu = 2.26E10;                     % Speed of light in medium (cm/s)
pow = 8.2834E16;                  % Source intensity (photons/sec)
mu_s = 20;                        % reduced scattering coefficient
mu_a = 0.02;                      % absorption coefficient
D = 1/(3*mu_s + mu_a);            % diffusion coefficient

%%% Set up the Wellingtonian Operator Matrix (WOM) %%%
wel = zeros(N);
coeff = D ./ h.^2;
for m = 2:(N-1)
   wel(m,m-1) = coeff;
   wel(m,m) = -2 * coeff - mu_a;
   wel(m,m+1) = coeff;
end;
wel(1,1) = -2 * coeff;      % non-periodic boundary conditions.
wel(1,2) = 1 * coeff;
wel(N,N) = -2 * coeff;
wel(N,N-1) = 1 * coeff;

%%% Compute Crank-Nicolson matrix %%%

disp('Computing Crank-Nicolson matrix. Please wait.');
dCN = inv(eye(N) - 0.5*tau*nu*wel) * (0.5*tau*nu*wel + eye(N));

%%% Plotting variables set here %%%

xplot = (0:N-1)*h - L/2;          % Record the x scale for plots
iplot = 1;                        % Counter used to count plots
nstep = 34000;                    % Maximum number of iterations
nplots = 340;                     % Number of snapshots (plots) to take
plot_step = nstep/nplots;         % Number of time steps between plots
phase = zeros(9,nplots);
pfough = zeros(N,1);              % Active Variable
q = round(N/2);
r = round(1/h);
s = round(0.5/h);

%%% Main Loop. Have fun. %%%

disp('Entering Main Loop. Please fasten your seat belts.');
for istep = 1:nstep
   pfough(q) = pfough(q) + pow*tau*(sin(2*pi*6e7*istep*tau)).^2;
   pfough = dCN*pfough;
   if( rem(istep,plot_step) < 1 )    % Every plot_step steps
      if (rem (iplot,10) < 1)
```

```
         fprintf('%g ns\n',istep*tau/1E-9);
      end
      phase(1,iplot) = pfough(q);
      phase(2,iplot) = pfough(q + 2*r);
      phase(3,iplot) = pfough(q + round(2.5*r));
      phase(4,iplot) = pfough(q + 3*r);
      time(iplot) = istep*tau;
      %plot(xplot,pfough);
      %axis([-L/2 L/2 0 1e6]);
      pause(0.05);
      iplot = iplot + 1;
   end
end
plot(time,phase(1,:),time,phase(2,:),time,phase(3,:),time,phase(4,:))
;
a = phase(1,:);
b = phase(2,:); save 20a1.txt time a b -ASCII -DOUBLE
b = phase(3,:); save 30a1.txt time a b -ASCII -DOUBLE
b = phase(4,:); save 40a1.txt time a b -ASCII -DOUBLE
```

8.2 Matlab Code minplot.m

```
%minplot.m - code to plot a range of scattering coefficient
comparisons
clear;
in_l = [635 651 670 780];
in_m = [29.756 29.087 29.364 27.595];
xmin = 3;
xmax = 4;
ymin = 0.028;
ymax = 0.032;
npoints = 60;
s = 1; %volume fraction
m = 1;
for ex = xmin:(xmax-xmin)/npoints:xmax;
   n = 1;
   for why = ymin:(ymax-ymin)/npoints:ymax;
      data(m,n) = minimi([ex,1,why],in_m,in_l,1.546,1.333);
      n = n + 1;
   end;
   fprintf('m :%g \n',m);
   m = m + 1;
end;

x = xmin:(xmax-xmin)/npoints:xmax;
y = ymin:(ymax-ymin)/npoints:ymax;
mesh(y,x,data);
```

8.3 Matlab Code minimi.m

```
function out = minimi(stats, in_m, in_l, m, n)

% out = minimi(stats, in_m, in_l, m, n);
% Returns the chi-squared value as in that particle sizing paper.
%
% stats =   vector of different sizes to check out.
% in_m =    Vector of measured scattering coefficients
% in_l =    Vector of corresponding wavelengths (in a vacuum)
% m =       Refractive index of particles.
% n =       Refractive index of the surrounding medium.
%
% size =    Expected average size of the particles.
% spread =  Expected standard deviation of the particles.
% vol =     Expected volume fraction of particles.

[a num_readings]=size(in_m);

sum = 0;

for count = 1:num_readings;
   sum = sum + (in_m(count) - scat(stats, m, n, in_l(count))).^2;
end;
%fprintf('ChiSquared = %g\n',sum);
out = sum;
```

8.4 Matlab Code scat.m

```
function mus = scat(x,m,n,l);
% mus = scat(x,m,n,l)
%
% Given real-world input parameters, returns useful Mie scattering
numbers.
%
% requires: x =    [size, spread, volume]
%      m =    refractive index of particle
%      n =    refractive index of medium
%      l =    wavelength in vacuum in nanometres
%
% returns: [Qscat g mu_s]
%

d = x(1)/1e6;
l = l*1e-9/n;

k = (2*pi)/l;
ex = k*(d/2);

coeffs = mie(m/n,ex);
qscat = coeffs(5);
g = coeffs(8);

%fprintf('d = %g \t v = %g\n',x(1),x(2));
%mus = 0.01 * ((3/2)*(qscat*(1-g)))/d * x(3);
mus = 0.01 * (3/2) * (qscat/d) * (1-g) * x(3) * quad('gtest', x(1) -
5*x(2), x(1) + 5*x(2),[],[],x(1),x(2));
```

8.5 Matlab Code gtest.m

```
function y = gtest(x,a,b); % y = gtest(x,a,a2,b,b2);
%gtest(x,a,a2,b,b2);
%gtest - returns a double gaussian centered at a and a2, widths b and
b2
y = sqrt(1./(2*pi*b.^2)).*exp(-((x - a).^2)./(2*b^2));   % gaussian
%y1 = exp(-((x - a).^2)./(2*b^2));  % non-normalised gaussian
%y1 = (c/b).*((x-a)/b).^(c-a).*exp(-((x-a)/b).^c); % weibull
%y2 = sqrt(1./(2*pi*b2.^2)).*exp(-((x - a2).^2)./(2*b2^2)); %
gaussian
```

8.6 Matlab Code minfind.m

```
% minfind - two-step program to find the minimum of this sum of
squares function.

clear;
%in_l = input('Wavelengths vector :');
%in_m = input('Measured scattering coefficients vector :')

in_l = [525 635 651 670 780];
in_m = [27.803 27.482 27.513 27.205 26.214];

xmin = 0.1;
xmax = 15;
ymin = 0.0001;
ymax = 0.15;
npts = 10;
nextsize = 500;

for finecount = 1:4:5;
   sizediff = 1;
   npoints = finecount * 10;
   while sizediff > 0.05;
      m = 1;
      for ex = xmin:(xmax-xmin)/npoints:xmax;
         n = 1;
         for why = ymin:(ymax-ymin)/npoints:ymax;
            data(m,n) = minimi([ex,why],in_m,in_l,1.546,1.333);
            n = n + 1;
         end;
         fprintf('iteration percentage complete :%g
\r',(m/npoints)*100);
         m = m + 1;
      end;

      x = xmin:(xmax-xmin)/npoints:xmax;
      y = ymin:(ymax-ymin)/npoints:ymax;
      mesh(y,x,data);

      [mincols cols] = min(data);
      [minval d] = min(mincols);
      minval2 = data(cols(d),d);
      if minval ~= minval2 disp('Minimal values do not match!'); end;

      oldnextsize = nextsize;
      nextsize = x(cols(d));
      nextvol = y(d);
      sizediff = abs(nextsize-oldnextsize);

      xmin = nextsize - (nextsize/4);
      xmax = nextsize + (nextsize/4);
      ymin = nextvol - (nextvol/4);
      ymax = nextvol + (nextvol/4);
      fprintf('Current guess - size = %g and volume fraction =
%g\n',nextsize,nextvol);
      if npoints > 10 sizediff = 0; end;
   end;
end;
fprintf('particle size = %g microns\n',nextsize);
```

```
fprintf('volume fraction = %g\n',nextvol);
```

9 List of References

Agilent Technologies, 2000. *Agilent 8712ET and 8714ET RF Network Analyzers User's Guide*. pp.9-24-9-25.

Alexandrakis, G., Busch, D. R., Faris, G. W., & Patterson, M. S., 2001. *Determination of the optical properties of two-layer turbid media by use of a frequency-domain hybrid Monte carlo diffusion model.* Applied Optics, 40, pp. 3810-3821.

Alexandrakis, G., Farrell, T. J., & Patterson, M. S., 2000. *Monte Carlo diffusion hybrid model for photon migration in a two-layer turbid medium in the frequency domain.* Applied Optics, 39, pp. 2235-2244.

Alfano, R. R., Pradhan, A., & Tang, G. C., 1989. *Optical spectroscopic diagnosis of cancer and normal breast tissues.* Journal of the Optical Society of America B, 6, pp. 1015-1023.

Aronson, R. & Corngold, N., 1999. *Photon diffusion coefficient in an absorbing medium.* Journal of the Optical Society of America A, 16, pp. 1066-1071.

Arridge, S. R., Cope, M., & Delpy, D. T., 1992. *The theoretical basis for the determination of optical pathlengths in tissue: temporal and frequency analysis.* Physics in Medicine and Biology, 37, pp. 1531-1560.

Atherton, H. V. & Newlander, J. A., 1977. *Chemistry and Testing of Dairy Products.* The AVI Publishing Company Inc., Westport, Connecticut.

Blowey, R. & Edmondson, P., 1995. *Mastitis Control in Dairy Herds - An Illustrated and Practical Guide.* Farming Press, Tonbridge, UK.

Boas, D. A., Liu, H., O'Leary, M. A., Chance, B., & Yodh, A. G., 1995. *Photon migration within the P3 approximation.* SPIE, 2389, pp. 240-247.

Boas, D. A., O'Leary, M. A., Chance, B., & Yodh, A. G., 1997. *Detection and characterization of optical inhomogeneities with diffuse photon density waves: a signal-to-noise analysis*. Applied Optics, 36, pp. 75-92.

Bohren, C. F. & Huffman, D. R., 1983. *Absorption and scattering of light by small particles*. Wiley Interscience, New York.

Bugs, M. R. & Cornelio, M. L., 2001. *Analysis of the Ethidium Bromide Bound to DNA by Photoacoustic and FTIR Spectroscopy*. Photochemistry and Photobiology, 74, pp. 512-520.

Byrne, C. D. & de Mello, A. J., 1997. *Photophysics of ethidium bromide complexed to ct-DNA: a maximum entropy study*. Biophysical Chemistry, 70, pp. 173-184.

Cerussi, A. E., 1999. *Quantitative Frequency-Domain Fluorescence Spectroscopy in Tissues and Tissue-Like Media*. PhD Thesis, University of Illinois at Urbana-Champaign, IL, USA.

Cerussi, A. E., Fantini, S., Maier, J. S., Mantulin, W. W., & Gratton, E., 2001. *Chromophore detection by fluorescence spectroscopy in tissue-like phantoms*. SPIE, 2979, pp. 139-150.

Cerussi, A. E., Maier, J. S., Fantini, S., Franceschini, M. A., & Gratton, E., 1996. *The Frequency-Domain Multi-Distance Method in the Presence of Curved Boundaries*. In OSA TOPS on Biomedical Spectroscopy and Diagnostics, (pp. 92-97). Optical Society of America, USA.

Cerussi, A. E., Maier, J. S., Fantini, S., Franceschini, M. A., Mantulin, W. W., & Gratton, E., 1997. *Experimental verification of a theory for the time-resolved fluorescence spectroscopy of thick tissues*. Applied Optics, 36, pp. 116-124.

Cerussi, A. E. & Tromberg, B. J., 2003. *Photon Migration Spectroscopy Frequency-Domain Techniques*. In T.Vo-Dinh (Ed.), Biomedical Photonics Handbook, (pp. 22-1-22-17). CRC Press, Boca Raton, FL, USA.

Chance, B., Cope, M., Gratton, E., Ramanujam, N., & Tromberg, B. J., 1998. *Phase measurement of light absorption and scatter in human tissue.* Review of Scientific Instruments, 69, pp. 3457-3481.

Chen, B., Stamnes, K., & Stamnes, J. J., 2001. *Validity of the diffusion approximation in bio-optical imaging.* Applied Optics, 40, pp. 6356-6366.

Clements, M., 1998. *Bovine Mastitis: Products and Markets.* Animal Pharm Reports, PJB Publications Ltd., London, UK.

Coquoz, O., Svaasand, L. O., & Tromberg, B. J., 2001. *Optical property measurements of turbid media in a small-volume cuvette with frequency-domain photon migration.* Applied Optics, 40, pp. 6281-6291.

Cornell, D. G. & Pallansch, M. J., 1966. *Counting and Sizing Fat Globules Electronically.* Journal of Dairy Science, 49, pp. 1371-1375.

Cosa, G., Focsaneanu, K.-S., McLean, J. R. N., McNamee, J. P., & Scaiano, J. C., 2001 . *Photophysical Properties of Fluorescent DNA-dyes Bound to Single- and Double-stranded DNA in Aqueous Buffered Solution.* Photochemistry and Photobiology, 73, pp. 585-599.

Crofcheck, C. L., Payne, F. A., Gillette, K. S., Nokes, S. E., & Hicks, C. L., 2000. *Relating Milkfat in Cream to Fiber Optic Backscatter Measurements.* An ASAE Meeting Presentation, ASAE, St. Joseph, MI, USA.

Dam, J. S., Pedersen, C. B., Dalgaard, T., Fabricius, P. E., Aruna, P., & Andersson-Engels, S., 2001 . *Fiber-optic probe for noninvasive real-time determination of tissue optical properties at multilpe wavelengths.* Applied Optics, 40, pp. 1155-1164.

Das, B. B., Yoo, K. M., & Alfano, R. R., 1993. *Ultrafast time-gates imaging in thick tissues: a step toward optical mammography.* Optics Letters, 18, pp. 1092-1094.

Dexcel, 2003. *About Dexcel.* http://www.dexcel.co.nz/about_dexcel.html. Accessed on 20-3-2003

Drezek, R., Dunn, A., & Richards-Kortum, R., 1999. *Light scattering from cells: finite difference time-domain simulations and goniometric measurements.* Applied Optics, 38, pp. 3651-3660.

Durduran, T., Yodh, A. G., Chance, B., & Boas, D. A., 1997. *Does the photon-diffusion coefficient depend on absorption?* Journal of the Optical Society of America A, 14, pp. 3358-3365.

Durkin, A. J., Jaikumar, S., Ramanujam, N., & Richards-Kortum, R., 1994. *Relation between fluorescence spectra of dilute and turbid samples.* Applied Optics, 33, pp. 414-423.

Eden, M. (2001). *Revving up rotary turnaround.* New Zealand Dairy Exporter, 13-14.

Fantini, S., Franceschini, M. A., Fishkin, J. B., Barbieri, B., & Gratton, E., 1994. *Quantitative determination of the absorption spectra of chromophores in strongly scattering media: a light-emitting-diode based technique.* Applied Optics, 33, pp. 5204-5213.

Fantini, S., Franceschini, M. A., & Gratton, E., 1997. *Effective source term in the diffusion equation for photon transport in turbid media.* Applied Optics, 36, pp. 156-163.

Femto Messtechnik GmbH, 1999. *DC-Path (BIAS-T) for fast Photodetectors.* http://www.femto.de/datasheet/ane03.pdf. Accessed on 23-6-2000.

Fishkin, J. B. & Gratton, E., 1993. *Propagation of photon-density waves in strongly scattering media containing an absorbing semi-infinite plane bounded by a straight edge.* Journal of the Optical Society of America A, 10, pp. 127-140.

Fishkin, J. B., Gratton, E., vandeVen, M. J., & Mantulin, W. W., 1991. *Diffusion of Intensity-Modulated Near-Infrared Light in Turbid Media.* SPIE, 1431 Time-Resolved Spectroscopy and Imaging of Tissues., pp. 122-135.

Foss Electric AS, 2003a. *Foss Milko-Scan FT6000 Fourier Transform Infra-Red Spectrometer.*

http://www.foss.dk/files/productfamilyfiles/MilcoScanFT6000.jpg. Accessed on 17-5-2003.

Foss Electric AS, 2003b. *Fossomatic 5000.* http://www.foss.dk/files/productfamilyfiles/fossomatic5000.jpg. Accessed on 17-6-2003.

Foss Electric AS, 2003c. *Fossomatic 5000 Technical Specifications.* http://www.foss.dk/c/p/solutions/products/showprodfamily.asp?prodfamilypkid=83&languageId=1&stepselect=5. Accessed on 17-6-2003.

Franceschini, M. A., Fantini, S., Paunescu, L. A., Maier, J. S., & Gratton, E., 1998. *Influence of a superficial layer in the quantitative spectroscopic study of strongly scattering media.* Applied Optics, 37, pp. 7447-7458.

Fung, L., Tuoc, T. K., & McCarthy, O., 1998. *Measurement of Milk Fat Globule Membrane Damage.* In Milk Quality Conference 1998, Palmerston North, New Zealand.

Gerken, M. & Faris, G. W., 1999. *Frequency-domain immersion technique for accurate optical property measurements of turbid media.* Optics Letters, 24, pp. 1726-1728.

Ghosh, N., Mohanty, S. K., Majumder, S. K., & Gupta, P. K., 2001. *Measurement of the optical transport properties of normal and malignant human breast tissue.* Applied Optics, 40, pp. 176-184.

Goulden, J. D. S., 1964. *Analysis of milk by infra-red absorption.* Journal of Dairy Research, 31, pp. 273-284.

Grappin, R. & Ribadeau-Dumas, B., 1992. *Analytical Methods for Milk Proteins.* In P.F.Fox (Ed.), Advanced Dairy Chemistry, Elsevier Applied Science,

Gunn, I.H., 2000. *Fat percentage in homogenised cream* (personal communication).

Hasegawa, Y., Yamada, Y., Tamura, M., & Nomura, Y., 1991. *Monte Carlo simulation of light transmission through living tissues.* Applied Optics, 30, pp. 4515-4521.

Haskell, R. C., Svaasand, L. O., Tsay, T., Feng, T., McAdams, M. S., & Tromberg, B. J., 1994. *Boundary Conditions for the Diffusion Equation in Raidative Transfer*. Journal of the Optical Society of America A, 11, pp. 2727-2741.

Haugaard, G. & Damm, M. G., 1961. *Photometric protein determination in skim milk.* Milchwissenschaft, 16, pp. 452-456.

Haugaard, G. & Pettinati, J. D., 1959. *Photometric Milk Fat Determination.* Journal of Dairy Science, 42, pp. 1255-1275.

Haugland, R. P., 1996. *Handbook of Fluorescent Probes and Research Chemicals.* Molecular Probes Inc., Eugene, Oregon

Henyey, L. G. & Greenstein, J. G., 1940. *Diffuse Radiation in the Galaxy.* Astrophysical Journal, 800, pp. 70-83.

Hielscher, A. H., Alcouffe, R. E., & Barbour, R. L., 1998. *Comparison of finite-difference transport and diffusion calculations for photon migration in homogeneous and heterogeneous tissues*. Physics in Medicine and Biology, 43, pp. 1285-1302.

International Dairy Federation, 2003. *List of IDF Standards*. http://www.fil-idf.org/StandardsEnglish.htm. Accessed on 30-1-2003.

Ishimaru, A., 1978. *Wave Propagation and Scattering in Random Media*. Academic Press Inc., San Diego, CA, USA.

Ishimaru, A., 1989. *Diffusion of light in turbid material*. Applied Optics, 26, pp. 2210-2215.

Jenness, R. & Patton, S., 1959. *Principles of Dairy Chemistry*. John Wiley & Sons Inc., New York, NY, USA.

Jensen, R. G., 1995. *Introduction*. In R.G.Jensen (Ed.), Handbook of Milk Composition, (pp. 1-3). Academic Press, San Diego, CA, USA.

Jensen, R. G. & Newberg, D. S., 1995. *Bovine Milk Lipids*. In Robert G.Jensen (Ed.), Handbook of Milk Composition, (pp. 543-573). Academic Press, San Diego

Jiang, H., 1998. *Frequency-domain fluorescent diffusion tomography: a finite-element-based algorithm and simulations.* Applied Optics, 37, pp. 5337-5343.

Jiang, H., Pierce, J., Kao, J., & Sevick-Muraca, E. M., 1997. *Measurement of particle-size distribution and volume fraction in concentrated suspensions with photon migration techniques.* Applied Optics, 36, pp. 3310-3318.

Kaltenbach, J. & Kaschke, M., 1993. *Frequency- and time-domain modeling of light transport in random media.* In Medical Optical Tomography: Functional Imaging and Monitoring, (pp. 65-86). SPIE Press, Bellingham, WA, USA.

Kamishikiryo-Yamashita, H., Oritani, Y., Takamura, H., & Matoba, T., 1994 . *Protein Content in Milk by Near-Infrared Spectroscopy.* Journal of Food Science, 59, pp. 313-315.

Keenan, T. W. & Patton, S., 1995. *The Milk Lipid Globule Membrane.* In Robert G.Jensen (Ed.), Handbook of Milk Composition, (pp. 5-44). Academic Press, San Diego

Keijzer, M., Star, W. M., & Storchi, P. R. M., 1988. *Optical Diffusion in Layered Media.* Applied Optics, 27, pp. 1820-1824.

Kernohan, E. A. & Lepherd, E. E., 1968. *Size distribution of fat globules in cow's milk during milking, measured with a Coulter counter.* Journal of Dairy Research, 36, pp. 177-182.

Khoo, G., Künnemeyer, R., & Claycomb, R. W., 2004a. *On-Line Raw Milk Component Analysis Using Photon-Migration Methods.* In, New Zealand Non-Destructive Testing Association, Palmerston North, New Zealand.

Khoo, G., Künnemeyer, R., & Claycomb, R. W., 2004b. *Fluorescence Photon Migration Techniques for the On-farm Measurement of Somatic Cell Count in Fresh Cow's Milk.* In, International Conference on Experimental Mechanics, Singapore.

Kim, A. & Ishimaru, A., 1998. *Optical diffusion of continuous-wave, pulsed, and density waves in scattering media and comparisons with radiative transfer.* Applied Optics, 37, pp. 5313-5319.

Kim, H., Hardy, J., Novak, G., Ramet, J. P., & Weber, F., 1984. *Standards and methods of analysis of the International Dairy Federation (IDF).* http://www.fao.org/DOCREP/003/X6537E/X6537E05.htm#ch5. Accessed on 30-1-2003.

Konev, S. V. & Kozunin, I. I., 1959. *Fluorescence Method for the Determination of Protein in Milk.* Dairy Science Abstracts, 23, pp. 103-105.

Kubelka, P., 1948. *New Contributions to the Optics of Intensely Light-Scattering Materials. Part I.* Journal of the Optical Society of America, 38, pp. 448-457.

Livestock Improvement Corporation, 2001. *Managing Mastitis - A practical guide for New Zealand dairy farmers.* Livestock Improvement Corporation, Hamilton, New Zealand.

Madsen, S. J., Anderson, E. R., Haskell, R. C., & Tromberg, B. J., 1994 . *Portable High-Bandwidth Frequency-Domain Photon Migration Instrument for Tissue Spectroscopy.* Optics Letters, 19, pp. 1934-1936.

Madsen, S. J., Patterson, M. S., & Wilson, B. C., 1991. *The use of India ink as an optical absorber in tissue-simulating phantoms.* Physics in Medicine and Biology, 37, pp. 985-993.

Maier, J. S., Walker, S. A., Fantini, S., Franceschini, M. A., & Gratton, E., 1994. *Possible correlation between blood glucose concentration and the reduced scattering coefficient of tissues in the near infrared.* Optics Letters, 19, pp. 2062-2064.

Martelli, F., Sassaroli, A., Yamada, Y., & Zaccanti, G., 2002. *Analytical approximate solutions of the time-domain diffusion equation in layered slabs.* Journal of the Optical Society of America A, 19, pp. 71-80.

Matheson, A. R. & Otten, P., 1999. *Automation of the Rose Gottlieb method for fat determination in dairy products using an expertsystem.* American Laboratory, March 1999, pp. 13-19.

Mobley, J. & Vo-Dinh, T., 2003. *Optical Properties of Tissue.* In T.Vo-Dinh (Ed.), Biomedical Photonics Handbook, (pp. 2-1-2-75). CRC Press, Boca Raton, FL, USA.

Mourant, J. R., Fusilier, T., Boyer, J., Johnson, T. M., & Bigio, I. J., 1997. *Predictions and mesaurements of scattering and absorption over broad wavelength ranges in tissue phantoms.* Applied Optics, 36, pp. 949-957.

Mur, G., 1981 . *Absorbing Boundary Conditions for the Finite-Difference Approximation of the Time-Domain Electromagnetic Field Equations.* IEEE Transactions on Electromagnetic Compatibility, EMC-23, pp. 377-382.

Nageswarao, G. & Derbyshire, J. B., 1969. *Studies on the mechanism of gel formation in the California mastitis test reaction.* Journal of Dairy Research, 36, pp. 359-370.

Nair, M. S., Ghosh, N., Raju, N. S., & Pradhan, A., 2002. *Determination of optical parameters of human breast tissue from spatially resolved fluorescence: a diffusion theory model.* Applied Optics, 41, pp. 4024-4035.

Neville, M. C. & Jensen, R. G., 1995. *The Physical Properties of Human and Bovine Milks.* In Robert G.Jensen (Ed.), Handbook of Milk Composition, (pp. 81-85). Academic Press, San Diego, CA, USA.

Ng-Kwai-Hang. & Moxley, J. E., 1987. *Factors affecting Differences in Milk Fat Test Obtained by Babcock, Rose-Gottlieb, and Infrared Methods and in Protein Test from Infrared Milk Analysis.* Journal of Dairy Science, 71, pp. 290-298.

Nielen, M., Deluyker, H., Schukken, H., & Brand, A., 1991. *Electrical Conductivity of Milk: Measurement, Modifiers, and Meta Analysis of Mastitis Detection Performance.* Journal of Dairy Science, 75, pp. 606-614.

Nilsson, A. M. K., Berg, R., & Andersson-Engels, S., 1995. *Measurements of the optical properties of tissue in conjunction with photodynamic therapy*. Applied Optics, 34, pp. 4609-4619.

Nishimura, G., Boas, D. A., & O'Leary, M. A. 1996. Photon Migration Imaging (Version 2.1) [Computer software]. University of Pennsylvania, Philadelphia, PA, USA.

Osborne, S. D., 1994. *Determination of the Fat and Protein Content of Fresh Cows Milk*. University of Waikato, Hamilton, New Zealand.

Paithankar, D. Y., Chen, A. U., Pogue, B. W., Patterson, M. S., & Sevick-Muraca, E. M., 1997. *Imaging of fluorescent yield and lifetime from multiply scattered light reemitted from random media*. Applied Optics, 36, pp. 2260-2272.

Pal, S. K., Mandal, D., & Bhattacharyya, K., 2000. *Photophysical Processes of Ethidium Bromide in Micelles and Reverse Micelles*. Journal of Physical Chemistry B, 102, pp. 11017-11023.

Patterson, M. S., Chance, B., & Wilson, B. C., 1989. *Time resolved feflectance and transmittance for the non-invasive measurement of tissue optical properties*. Applied Optics, 28, pp. 2331-2336.

Patterson, M. S., Madsen, S. J., Moulton, J. D., & Wilson, B. C., 1991a. *Diffusion Equation Representation of Photon Migration in Tissue*. IEEE 1991 Microwave Syposium Digest, BB-1, pp. 905-908.

Patterson, M. S. & Pogue, B. W., 1994. *Mathematical model for time-resolved and frequency-domain fluorescence spectroscopy in biological tissues*. Applied Optics, 33, pp. 1963-1974.

Patterson, M. S., Wilson, B. C., & Wyman, D. R., 1991b. *The Propagation of Optical Radiation in Tissue I.* Lasers in Medical Science, 6, pp. 155-168.

Patton, S., 1973. *Origin of the Milk Fat Globule*. Journal of the American Oil Chemists Society, 50, pp. 178-185.

Pogue, B. W., Geimer, S., McBride, T. O., Jiang, S., Österberg, U., & Paulsen, K. D., 2001. *Three-dimensional simulation of near-infrared diffusion in tissue: boundary condition and geometry analysis for finite-element image reconstruction.* Applied Optics, 40, pp. 588-600.

Ramanujam, N., Du, C., Ma, H. Y., & Chance, B., 1998. *Sources of phase noise in homodyne and heterodyne phase modulation devices used for tissue oximetry studies.* Review of Scientific Instruments, 69, pp. 3042-3054.

Richter, S. M., Shinde, R. R., Balgi, G. V., & Sevick-Muraca, E. M., 1998. *Particle sizing using Frequency Domain Photon Migration.* Particle Particle System Characteristics, 15, pp. 9-15.

Roy, R. & Sevick-Muraca, E. M., 2001. *Three-dimensional unconstrained and constrained image-reconstruction techniques applied to fluorescence, frequency-domain photon migration.* Applied Optics, 40, pp. 2206-2215.

Saleh, B. E. A. & Teich, M. C., 1991. *Fundamentals of Photonics.* John Wiley & Sons Inc., New York, NY, USA.

Schalm, O. W. & Noorlander, D. O., 1957. *Experiments and Observations Leading to Development of the California Mastitis Test.* Journal of the American Veterinary Medical Association, 130, pp. 199-204.

Sensortec Ltd., 2003. *Sensortec - Specialists in measuring biological components* (brochure). Sensortec Ltd., Hamilton, New Zealand.

Sevick-Muraca, E. M., Heintzelman, D. L., Lee, J., Troy, T. L., & Paithankar, D. Y., 1997. *Role of higher-order scattering in solutions to the forward and inverse optical-imaging problems in random media.* Applied Optics, 36, pp. 9058-9067.

Sevick-Muraca, E. M., Kuwana, E., Godavarty, A., Houston, J. P., Thompson, A. B., & Roy, R., 2003. *Near-Infrared Fluorescence Imaging and Spectroscopy in Random Media and Tissues.* In T.Vo-Dinh (Ed.), Biomedical Photonics Handbook, (pp. 33-1-33-66). CRC Press, Boca Raton, FL, USA.

Shinde, R. R., Balgi, G. V., Nail, A. L., & Sevick-Muraca, E. M., 1999. *Frequency-Domain Photon Migration Measurements for Quantitative Assessment of Powder Absorbance: A Novel Sensor of Blend Homogeneity*. Journal of Pharmaceutical Sciences, 88, pp. 959-966.

Sidersky, M. D., 1909. *L'homogénisation du lait*. In Compte rendu 4^{me} Congr. Intern. Laiterie, (pp. 281-292), Budapest.

Sjaunja, L. O. & Andersson, I., 1985. *Laboratory Experiments with a New Infrared (IR) Milk Analyzer, the Milko-Scan 605*. Acta Agriculturæ Scandinavica, 35, pp. 345-352.

Sjaunja, L. O. & Schaar, J., 1984. *Determination of casein in milk by infrared spectrophotometry*. Milchwissenschaft, 39, pp. 288-289.

Slattery, C. W., 1976. *Casein Micelle Structure; An Examination of Models*. Journal of Dairy Science, 59, pp. 1547-1555.

Spott, T. & Svaasand, L. O., 2000. *Collimated light sources in the diffusion approximation*. Applied Optics, 39, pp. 6453-6465.

Star, W. M., 1989. *Comparing the P3-Approximation with Diffusion Theory and with Monte Carlo Calculations od Light Propagation in a Slab Geometry*. SPIE Institute Series, IS5, pp. 147-154.

Swaisgood, H. E., 1995. *Protein and Amino Acid Composition of Bovine Milk*. In Robert G.Jensen (Ed.), Handbook of Milk Composition, (pp. 464-468). Academic Press, San Diego, CA, USA.

Taflove, A. & Brodwin, M. E., 1975. *Numerical Solution of Steady-State Electromagnetic Scattering Problems using the Time-Dependent Maxwell's Equations*. IEEE Transactions on Microwave Theory and Techniques, MTT-23, pp. 623-630.

Taponen, J. & Myllys, V., 1995. *The Economic Impact of Mastitis*. In M.Sandholm, T. Honkanen-Buzalski, L. Kaartinen, & S. Pyörälä (Eds.), The Bovine Udder

and Mastitis, (pp. 261-264). University of Helsinki Faculty of Veterinary Medicine, Helsinki, Finland.

Technical University of Denmark DTU, 2003. *Database Of Genome Sizes.* http://www.cbs.dtu.dk/databases/DOGS/index.html. Accessed on 25-5-2003.

Thompson, D. I. & Postle, D. S., 1964. *The Wisconsin Mastitis Test - An Indirect Estimation of Leucocytes in Milk.* Journal of milk food technology, 27, pp. 271-275.

Tonon, C., Rozé, C., Girasole, T., & Dinguirard, M., 2001. *Four-flux model for a multilayer, plane absorbing and scattering medium: application to the optical degradation of white paint in a space environment.* Applied Optics, 40, pp. 3718-3725.

Tracy, P. H., 1941. *Some technical problems related to the processing of homogenised milk.* International Association of Milk Dealers, 22, pp. 537-580.

Trout, G. M., 1950a. *An Introduction to Homogenised Milk.* In Homogenised Milk - a review and guide, (pp. 1-28). Michigan State College Press, East Lansing, MI, USA.

Trout, G. M., 1950b. *Effect of Homogenization on the Fat and Proteins of Milk.* In Homogenised Milk - a Review and Guide, (pp. 47-59). Michigan State College Press, East Lansing, MI, USA.

Trout, G. M., 1950c. *Effect of Homogenization on the Physical and Chemical properties of Milk.* In Homogenised Milk - a Review and Guide, (pp. 29-46). Michigan State College Press, East Lansing, MI, USA.

Tsenkova, R. N., Atanassova, S., Itoh, K., Ozaki, Y., & Toyoda, K., 2000. *Near infrared spectroscopy for biomonitoring: Cow milk composition measurement in a spectral region from 1,100 to 2,400 nanometers.* Journal of Animal Science, 78, pp. 515-522.

Tsenkova, R. N., Yordanov, K. I., Itoh, K., Shinde, Y., & Nishibu, J., 1994. *Near-Infrared spectroscopy of Individual Cow Milk as a means for Automated*

Monitoring of Udder Health and Milk Quality. In NMC 33rd Annual Meeting Proceedings, (pp. 202-211). National Mastitis Council,

Tsuchiya, Y. & Urakami, T., 1996. *Non-invasive spectroscopy of variously shaped turbid media like human tissue based on the microscopic Beer-Lambert law.* In OSA TOPS on Biomedical Spectroscopy and Diagnostics, (pp. 98-100). Optical Society of America, Orlando, FL, USA.

Tuchin, V., 2000. *Tissue Optics.* SPIE Press, Bellingham, WA, USA.

Umashankar, K. & Taflove, A., 1982. *A Novel Method to Analyze Electromagnetic Scattering of Complex Objects.* IEEE Transactions on Electromagnetic Compatibility, EMC-24, pp. 397-405.

Van de Hulst, H. C., 1957. *Light Scattering by Small Particles.* Wiley Interscience, New York, NY, USA.

van Stavreven, H. J., Moes, C. J. M., van Marle, J., Prahl, S. A., & van Gemert, M. J. C., 1991. *Light scattering in Intralipid-10% in the wavelength range of 400-1100 nm.* Applied Optics, 30, pp. 4507-4514.

Vargas, W. E., 1998. *Generalized four-flux radiative transfer model.* Applied Optics, 37, pp. 2615-2623.

Wabnitz, H. & Rinneberg, H., 1997. *Imaging in turbid media by photon density waves: spatial resolution and scaling relations.* Applied Optics, 36, pp. 64-74.

Walstra, P., 1965. *Light scattering by milk fat globules.* The Netherlands Milk and Dairy Journal, 19, pp. 93-109.

Waring, M. J., 1965. *Complex Formation between Ethidium Bromide and Nucleic Acids.* Journal of Molecular Biology, 13, pp. 269-282.

Whittlestone, W., 1962. *The size distribution of fat globules in cow's milk throughout milking.* The Australian Journal of Dairy Technology, April-June, pp. 108-111.

Whittlestone, W. & Allen, D., 1966. *An automatic viscometer for the measurement of the California mastitis reaction.* The Australian Journal of Dairy Technology, 21, pp. 138-139.

Whyte, D. S., 1998. *Investigation of Milk Mass Metering Techniques.* MSc(Tech) Thesis, University of Waikato,

Whyte, D. S., Claycomb, R. W., & Mein, G. A., 2002. *On-Line Mastitis Sensing.* In 2nd Panamerican Congress on Milk Quality and Mastitis Control, (pp. 155). Instituto Fernando Costa, São Paulo, Brazil.

Wiegner, G., 1914. *Ueber die Aenderung einiger Physikalischer Eigenschaften der Kuhmilch mit der Zerteilung ihrer dispersen Phasen.* Kolloid Zeitschrift, 15, pp. 105-123.

Work and Income New Zealand, 2000. *Regional Plan for Waikato 2000/2001.*

Yee, K. S., 1966. *Numerical solution of initial boundary value problems involving Maxwell's Equations in Isotropic Media.* IEEE Transactions on Antennas and Propagation, AP-14, pp. 302-307.

Yoo, K. M., Liu, F., & Alfano, R. R., 1990. *When does the diffusion approximation fail to describe photon transport in random media?* Physical Review Letters, 64, pp. 2647-2650.

Yoon, G., Prahl, S. A., & Welch, A. J., 1989. *Accuracies of the diffusion approximation and its similarity relations for laser irradiated biological media.* Applied Optics, 28, pp. 2250-2255.

Zhang, H., Urakami, T., Tsuchiya, Y., Lu, Z., & Hiruma, T., 1999. *Time Integrated Spectroscopy of Turbid Media Based on the Microscopic Beer-Lambert Law: Application to Small-Size Phantoms Having Different Boundary Conditions.* Journal of Biomedical Optics, 4, pp. 183-190.

Zijp, J. R. & ten Bosch, J. J., 1997. *Anisotropy of volume-backscattered light.* Applied Optics, 36, pp. 1671-1680.